GEOMAR
Research Center
for Marine Geosciences
Christian-Albrechts-University
in Kiel

HYDGAS

Quantification of gas hydrates and gas in the sediment of the Cascadia accretionary wedge using seismic methods

Seismische Quantifizierung von Gashydraten im Sediment der Cascadia-Subduktionszone

FS SONNE
FAHRTBERICHT SO-150
CRUISE REPORT SO-150

17.09.2000 - 27.10.2000

Edited by
Dirk Klaeschen, Achim Kopf, Matthew Arsenault, and Jörg Bialas
with contributions of cruise participants

KIEL 2001

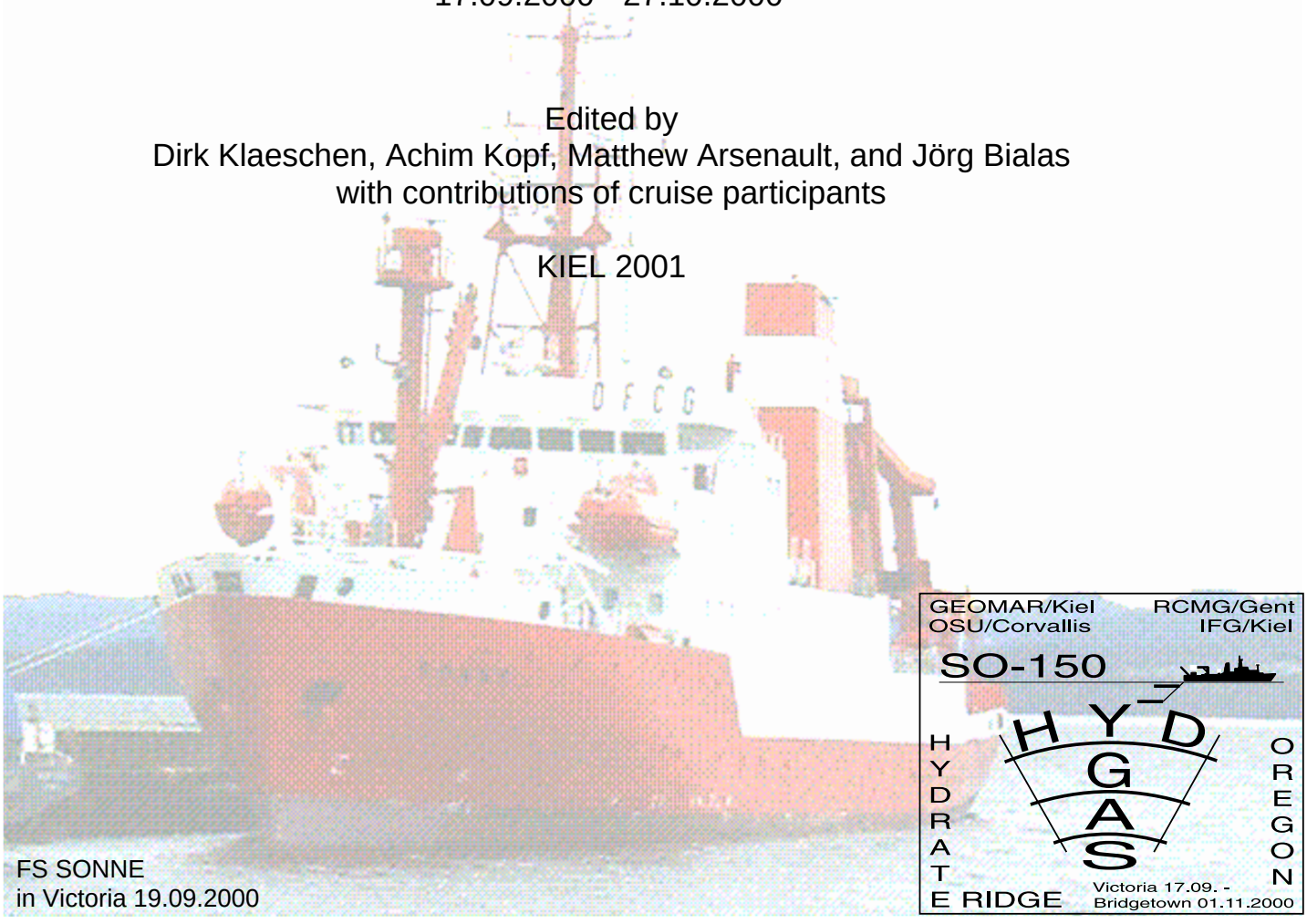

FS SONNE
in Victoria 19.09.2000

Redaktion dieses Reports:
Dirk Klaeschen, Achim Kopf,
Matthew Arsenault und Jörg Bialas

Editor of this issue:
Dirk Klaeschen, Achim Kopf,
Matthew Arsenault, and Jörg Bialas

GEOMAR
Forschungszentrum
für marine Geowissenschaften
D – 24148 Kiel
Tel. (0431) 600-2555, 600-2505

GEOMAR
Research Center
for Marine Geosciences
D – 24148 Kiel
Tel. (0431) 600-2555, 600-2505

TABLE OF CONTENTS

1.1 ZUSAMMENFASSUNG

Die Zirkulation von Gasen und Fluiden sowie das massive Auftreten von Gashydraten im Bereich aktiver Plattenränder und ihre Rolle im globalen Stoffhaushalt sind wichtige Gesichtspunkte moderner geowissenschaftlicher Grundlagenforschung, die in den letzten zwei Jahrzehnten mit unterschiedlichen Methoden untersucht wurden. Das Forschungsvorhaben HYDGAS stellt sich als Hauptziel, während der Schiffsexpedition *Sonne SO-150* Gashydrate im Sediment mit Hilfe von seismischen Messungen zu erfassen. Gashydrate, oder Clathrate, sind eisähnliche Feststoffe aus verschiedenen Gasen (vornehmlich Methan) und Wasser, die unterhalb des Ozeanbodens im Sediment vorkommen. Ihr weltweites Vorkommen übersteigt nach Schätzungen bei weitem die Vorräte anderer Energieträger (Erdöl, Erdgas), sodaß der Erforschung von Gashydrat neben wissenschaftlicher auch ökonomische und ökologische Bedeutung zukommt. Der Kontinentalrand vor Oregon, wo die Juan-de-Fuca-Platte der Nordamerikanischen Platte unterschoben wird, ist eines der reichsten und gleichsam bestuntersuchtesten Gashydratvorkommen auf der Erde. Im oberhalb der Subduktionszone akkumulierten Sediment, dem sog. Cascadia-Akkretionskeil, sind massive Gashydrate, begleitende chemische Anomalien (Salzlaken) und chemische Umwandlungsprodukte (verschiedene authigene Karbonatformen) sowie charakteristische Faunenvergesellschaftungen gut dokumentiert. Neben dem prinzipiellen Verständnis des Systems war es Ziel der HYDGAS-Expedition, über quantitative Ansätze das Volumen der vorhandenen Gashydrate besser zu bestimmen.

Die während der Fahrt *Sonne SO-150* durchgeführten Arbeiten dienten der räumlichen Verteilung, Identifizierung und Quantifizierung der Hydratvorkommen in der Cascadia-Subduktionszone entlang des Hydratrückens, einer untermeerischen Gebirgsstruktur in nur etwa 800 m Wassertiefe. Das Vorhaben ist in einer Linie zu sehen mit den erfolgreichen Untersuchungen der Sonne-Expeditionen *SO-108, -109, -110*, der Tiefseebohrung ODP *Site 892*, sowie des TECFLUX-Programms (mit zahlreichen erfolgreichen Tauchboot- und Robotereinsätzen) zu sehen. Enge Kooperation mit der Arbeitsgruppe um A. Trehu, OSU, COAS Corvallis, ergänzt die deutschen Expeditionen um die jüngsten Erkenntnise amerikanischer Kollegen. Erst die Kombination von geologischen, geochemischen, biologischen und hydrographischen Untersuchungen mit den gesammelten geophysikalischen Daten in einem kleinregionalen Arbeitsgebiet eröffnet die einmalige Gelegenheit, das Grundlagenwissen zu vertiefen und damit verbunden das genaue Volumen und die Klimarelevanz der Gashydratvorkommen für die Zukunft besser abzuschätzen.

Insgesamt fünf Auslagen von Ozeanbodenhydrophonen (OBHs) und Ozeanbodenseismometern (OBSs) am Merresboden (räumlicher Abstand der einzelnen OBH/OBS ca. 200 m) um eine abgeteufte (ODP Leg 146 Site 892) und zwei geplante Bohrlokationen (ODP Leg 204, in Herbst 2002) stellen die Basis des seismischen Experiments dar. Mit fünf Quellen unterschiedlicher Frequenz (5 Hz bis 2 kHz) und drei verschiedenen Streamertypen, oberflächen und tiefgeschleppte Systeme, wurden insgesamt 1490 km reflexionsseismischer Profile akquiriert. Engabständige Profilnetze sowie Parasound als auch Hydrosweep-Aufnahmen gepaart mit den obengenannten Experimenten werden in der Folge erlauben, Hydrat- und Gasvorkommen qualitativ wie quantitativ besser zu erfassen.

1.2 SUMMARY

The circulation of gases and aqueous fluids, as well as the abundance of gas hydrates in convergent margin scenarios, play a significant role in global mass balances. Hence, the study of these processes with various techniques has become a major objective in geosciences research during the previous decade. The main focus of the research expedition HYDGAS during cruise *Sonne SO-150* was the qualification and quantification of massive gas hydrates in the sediment using seismic methods. Gas hydrates, or clathrates, are ice-like crystals of gases (predominantly methane) and water, which occur in various forms in subseafloor sediments. According to global estimates, the carbon fixed in such gas hydrates exceeds by far the amount of presently discovered oil and gas occurrences. Thus, gas hydrate research is of both scientific, economic, and environmental importance.
The continental margin off Oregon, where the Juan de Fuca Plate is subducted beneath the North American continental plate, is a well studied area which is characterized by its wealth of clathrates and hydrate-related deposits. Within the accumulated sediment of the upper subduction zone, the so called Cascadia accretionary prism, massive gashydrates and associated chemical anomalies (brines), their chemical oxidization products (authigenic carbonate), and typical fauna assemblages related to methane-rich fluids have been previously reported. Apart from shedding more light on the principal understanding of gas hydrate environments, the main aim of the HYDGAS expedition is an estimate of gas hydrate quantities, their potential economic relevance in the future, and the risk of environmental hazards (submarine slides, release of greenhouse gases into the atmosphere) from gas hydrate dissociation.

During cruise *Sonne SO-150* , improved geophysical methods were used to identify and quantify the spatial variation of gas hydrates across Hydrate Ridge. Narrowly spaced receivers on the seafloor (approximately 200 m apart), shallow and deep towed systems, and a broad range of source frequencies (5 Hz to 2 kHz) were used to guarantee pristine data quality. Here, special attention will be given to parameters which will assist in gas hydrate identification and quantification. The new geophysical data will be compared and calibrated using the results from direct measurements on recovered core as well as along the borehole wall (downhole logging) at ODP *Site 892*. Calibration of the geophysical information will allow us to optimize data processing and interpretation. The results from cruise *Sonne SO-150* will significantly broaden the understanding of seismic signals in hydrate-bearing sediments, and thus will add a quantitative component to the overall gas hydrate research.

Five receiver assemblages in three locations, at Site 892 (ODP Leg 146) and at two future ODP drillsites (ODP Leg 204, scheduled for autumn 2002), provided a wealth of data from 5 different sources used. During intervals of data retrieval and OBH/OBS refitting, a total of 1490 km of seismic reflection profiles were acquired using five different source (broad frequency range) and three different streamer (surface and deep tow) configurations. The narrowly spaced grid of seismic reflexion and Parasound lines permits us to tie in the results from the receiver experiments for quantitative estimates.

2. INTRODUCTION TO THE HYDGAS PROJECT

2.1 THE OBJECTIVES OF HYDGAS

(D. Klaeschen, A. Kopf, J. Bialas)

Fluid circulation and gas hydrate processes are of increasing global importance in the study of the geology of active convergent margins. Numerous studies in the upper parts of several subduction zones (Aleutians, Costa Rica, Cascadia) have characterized fluid budgets in detail (Wallmann et al., 1997; Suess et al., 1999). Gas hydrate reactions as a function of the dynamics of their stability field were a main focus (Suess et al., 1999; Kopf et al., 2000). Combined geological, geochemical, biological and hydrological studies in the Hydrate Ridge area has recently allowed us to deepen the knowledge of the complex interactions in such a gas hydrate environment. Hence, HYDGAS has to be seen in a series of investigations like R/V Sonne-cruises SO-108, -109, -110 (Flueh and Fisher, 1996; Herzig et al., 1997; Suess and Bohrmann, 1997), deep sea drilling Site 892 by the Ocean Drilling Program (Westbrook et al., 1994), as well as almost a dozen cruises within the international TECFLUX-programme (including the successful use of submersibles and remotely controlled seafloor vehicles for sampling; e.g., Bohrmann et al., 1999).

Hydrate Ridge is the second highest topographic elevation landward of the deformation front of the Cascadia accretionary complex, off the Oregon continental margin (MacKay et al., 1995). Its seafloor topography was mapped in detail during cruise SO110. The ridge has accumulated mainly Pliocene sediments from the downgoing Juan de Fuca Plate (Figs. 2.1.1 and 2.1.2), which are imbricated against their abutment, the Coast Range mountain chain on land. Gas hydrate occurrence was inferred from seismic data showing prominent BSRs (MacKay et al., 1992, 1994), and from authigenic carbonate precipitates of a characteristic chemical signature (Ritger et al., 1987; Carson et al., 1990). Later, deep sea drilling ODP Leg 146 on Hydrate Ridge recovered gas hydrate and overpressured sediment (from its dissociation in the core liner after pressure release) for the first time in the area (Westbrook et al., 1994). The abundant carbonate precipitates found within the cores of clayey sediment are relics of ancient pore water having been oxidized by sulfate reducing bacteria. Fluid as well as gas vents have subsequently been mapped and sampled (Herzig et al., 1997; Suess and Bohrmann, 1997; Suess et al., 1999), and have been found most abundant on the Hydrate Ridge (away from the deformation front). Large amounts of massive gas hydrates and a wealth of authigenic carbonate phases were also taken, and a close interrelationship between the two could be established (Bohrmann et al., 1998; Greinert et al., 2000). Isotope signatures are normal marine, thermogenic, and sometimes hint towards gas hydrate cage water. However, authigenic carbonates from deep drilling yielded isotope signatures indicative of a distinct "deep" origin of the parent fluid (Sample and Kopf, 1995). Hence, it is concluded that the toe of the prism is dominated by deep seated fluids migrating along the décollement, while the second ridge (Hydrate Ridge) shows mostly precipitation from seawater and gas hydrate water (Deyhle et al., in press). Flowmeter data and submersible observations indicate that some of the gas hydrates are at the extent of their stability field (Linke et al., 1999). Indeed, gas bubbling from either instantaneous gas hydrate destabilization or efflux of free gas from the pore space frequently occurs at low tide as a function of the decrease in hydrostatic head. The HYDGAS experiments thus aimed mainly to distinguish by geophysical means how much free gas and how much gas hydrate occur within the sediment. In a second step, such quantitative estimates could be refined to models concerning gas hydrate dynamics.

Estimating the depth and thickness of gas hydrate layers at Hydrate Ridge is a geophysically challenging endeavour. It follows three overarching objectives:

- To estimate the amount of gas hydrate against an economic background;
- To assess an environmental hazard from dissociation and release of radiatively active gases (greenhouse climate) from hydrate dissociation; and

- To understand the dynamics of gas hydrate processes and their geodynamic controls (slope stability through change in physical properties of hydrate-bearing sediments; see Zhang et al., 1999), possible self-regulating processes, etc.

Each of these points potentially has important implications to events known in Earth's history and regarding future research and prevention of hazards.
It has been proposed to closely study and spatial and depth-related gas hydrate characteristics using improved seismic acquisition and processing techniques. The geophysical data can be immediately calibrated against geological information from sediment drillcores recovered from ODP Site 892 (Westbrook et al., 1994). In addition, some downhole logging information is also available from this borehole (e.g. Jarrard et al., 1995; Moore et al., 1995). Data to be used for calibration are Vp and density-log from MST, lithologic description and physical properties on discrete samples (Westbrook et al., 1994). In the near future, another evaluation of the geophysical information will be tied into the anticipated results from an ODP follow on cruise, Leg 204 in autumn 2002.

In order to achieve these goals, a narrowly spaced grid of high resolution seismic reflection lines together with 3D seismic experiments was developed. Both the sources and receivers covered wide frequency ranges. The receivers were placed in key locations where lithologic and geophysical evidence has been collected (ODP Leg 146), or is soon to be investigated (Leg 204). The resulting spatial distribution and variation of the BSRs will allow us to understand fluid flow paths and pockets of free gas in the study area.

When regarding the geophysical acquisition in more detail, it is apparent that aperture and azimuth distribution of multi channel seismic data is insufficient for gas hydrate studies. Hence, combined employment of OBH/OBSs (Ocean Bottom Hydrophones and Seismometers) together with deep tow sources and receivers, lowers the Fresnel zone and improves spatial and temporal resolution (Fig. 2.1.3). It is believed that the occurrence of gas hydrate in the sediment causes a gradual increase in p-wave velocity, so that zones with velocity gradients can be detected and mesured by OBH/OBS techniques. OBSs offer the advantage of registering the entire 3D elastic wave field, which then can be used for modelling and inversion techniques. With a narrowly spaced profile of OBH/OBS positions, an OBC (ocean bottom cable) simulation can ensure high spatial resolution of the data. Characterization of gas hydrate occurrences as well as the properties of the surrounding lithologies is achieved by true amplitude (TA) migration followed by amplitude versus angle (AVA) inversion. Changes in Vp (p-wave velocity), Vs (shear wave velocity), and density at the BSR can be monitored as a function of the varying angles and amplitudes. The analyses are focused on the area of existing MCS data (OR89 survey; see MacKay et al., 1995; Trehu et al., 1999), and utilize borehole information from previous ODP Site 892 drilling (see below). Modelling calculations support the relation the seismic properties to porosity and its occupancy by gas hydrates and gas (Clennell et al., 1999; Henry et al., 1999).

In summary, the following approaches address quantiative aspects of gas hydrate and gas occurrences, and fluid migration paths:
- Mapping of the spatial and depth-related BSR occurrence and signature
  (surface and deep tow streamers, broad frequency range, MCS-OR89)
- Identification of the amounts of gas and gas hydrate in the sediment
  (seismic inversion and migration techniques using OBH/OBS/MCS data => Rp, Rs)
- Calibration of the seismic parameters using in situ measurements
  (Rp, Rs, downhole logging: Vp, density => Vs, ODP sediment core measurements)
- Quantification of gas and gas hydrate
  (Vp,Vs, density, porosity, occupancy of pore volume; Biot-Gassmann theory)
- 3D-viscoelastic seismic forward modelling to test fluid models

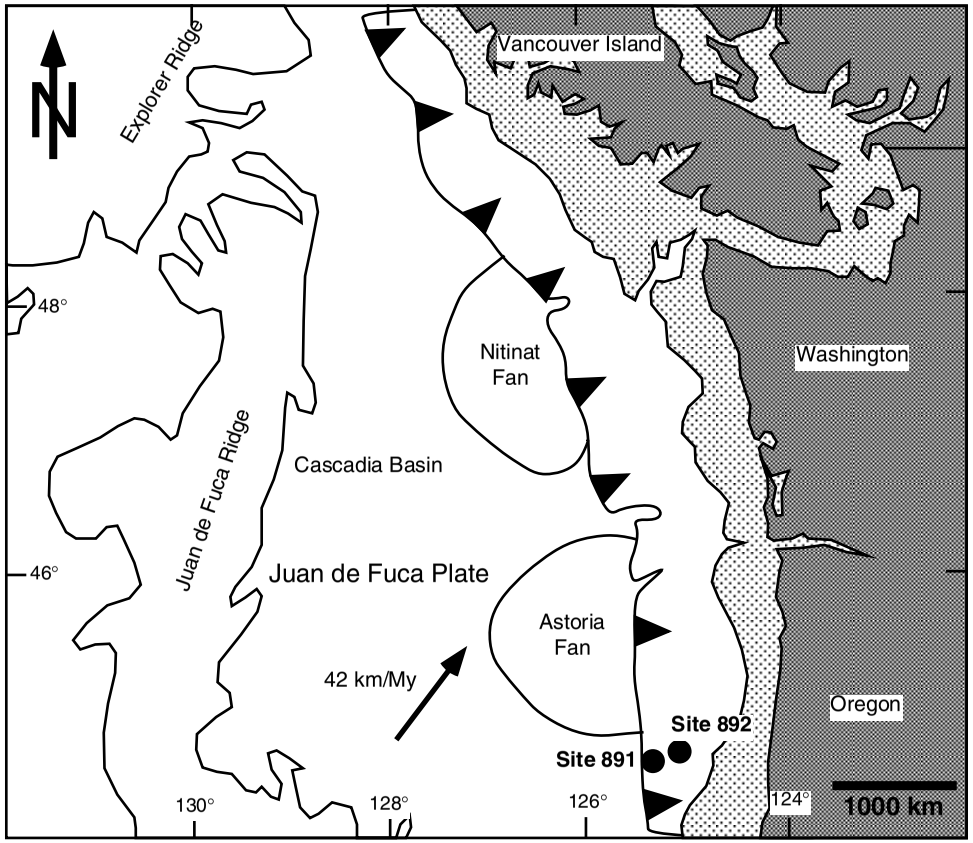

Figure 2.1.1: Map of easten Pacific and the North America continental margin, including plate kinematic vectors.

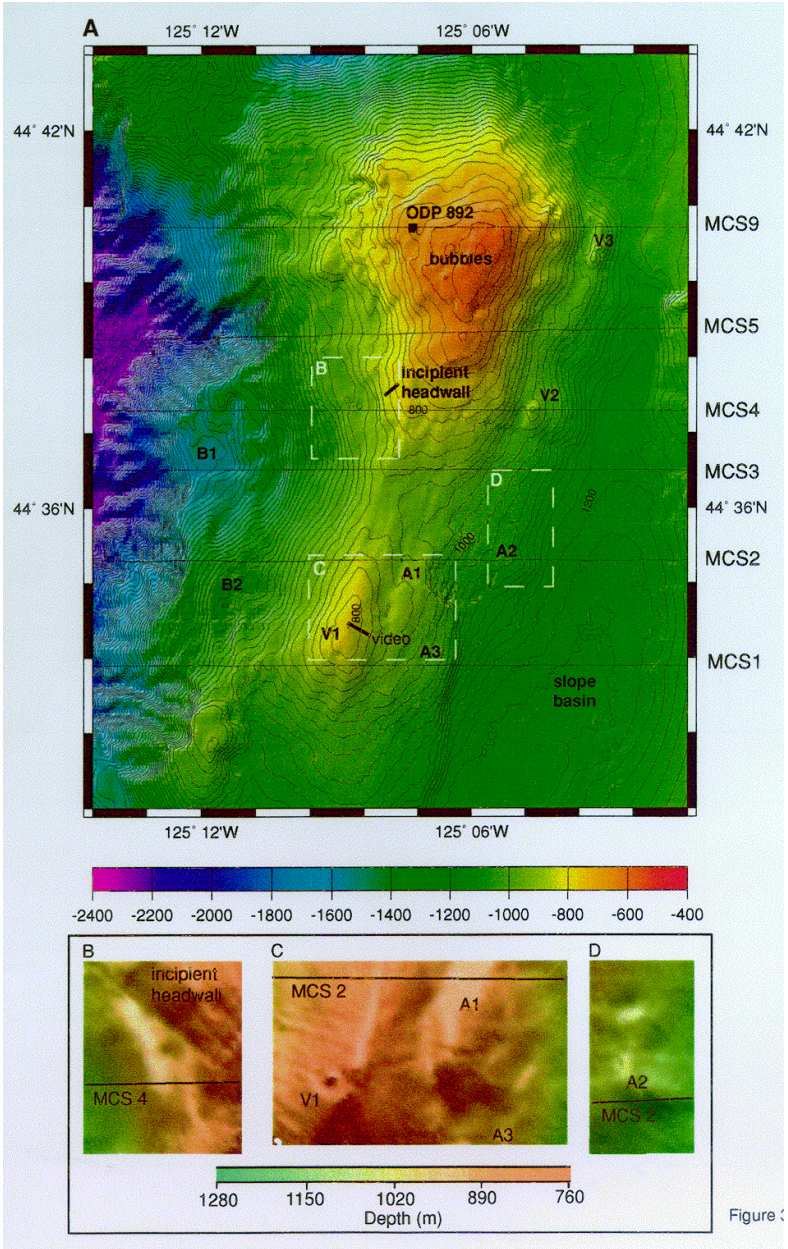

Figure 2.1.2 (right): Blow up of the study area at the Hydrate Ridge, presented as rainbow bathymetric chart (from Trehu et al., 1999)

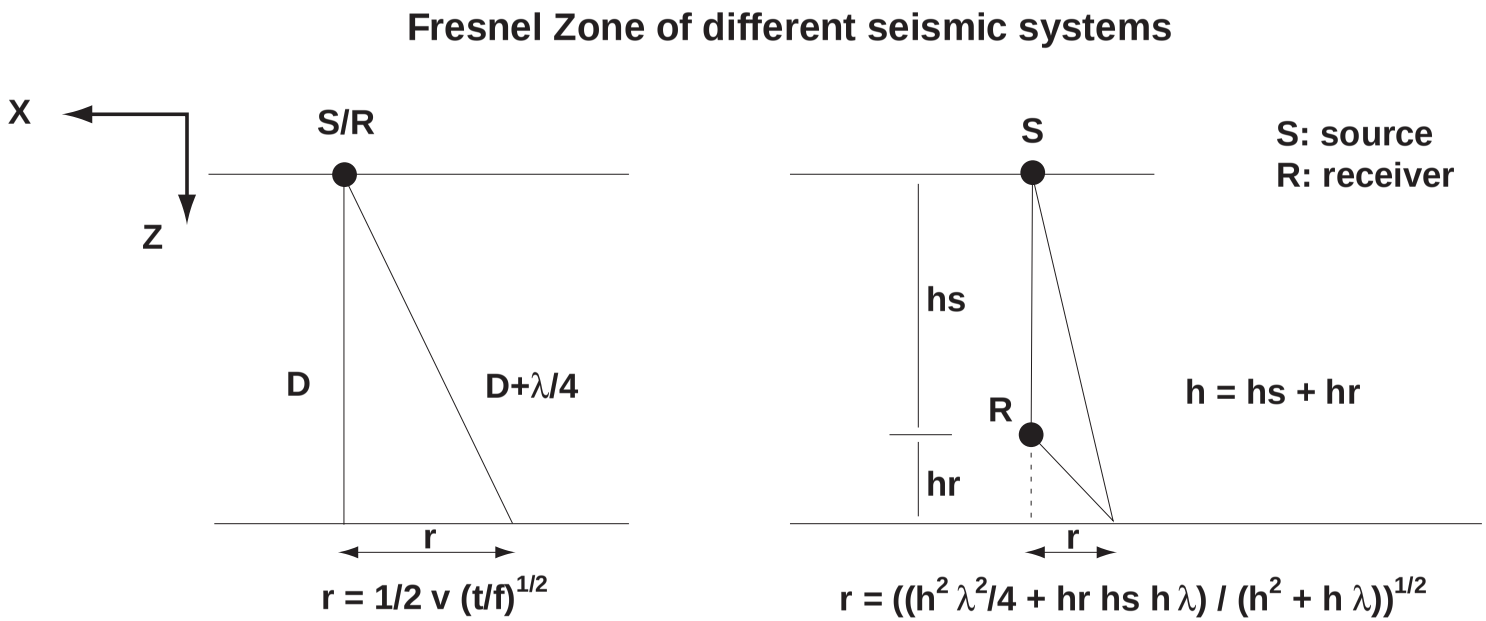

target-depth [m]	source-depth [m]	receiver-depth [m]	frequency [Hz]	Fresnel zone [m]
700	0	0	100	73
700	0	600	100	37
700	600	600	100	27
700	0	698 OBH	100	9
5000	0	0	100	194
5000	0	4500	100	83
5000	4500	4500	100	61
5000	0	4998 OBH	100	9

Figure 2.1.3: Improved resolution from employment of deep towed systems and OBH.

2.2 RESULTS OF PREVIOUS INVESTIGATIONS AND REGIONAL GEOLOGIC SETTING
(D. Klaeschen, A. Kopf)

Structural evolution of the Hydrate Ridge

At present, the Juan de Fuca Plate is subducted beneath the Oregon-Washington continental margin of North America at a rate of approximately 4 cm/a (Riddihough, 1984; Duncan and Kulm, 1989). Strong segmentation of the Cascadia margin is partly a consequence of former accretion of terranes (i.e., the geometry of the coast line), but mostly reflects modern tectonics and sedimentary dynamics. In the northern part (Washington), dominantly landward vergent thrust faults facilitate accumulation of a large accretionary prism, while seaward verging faulting is observed further south (see Fig. 2.2.1). The change in deformation can largely be attributed to abnormally low friction in the incoming sediments (Seely, 1977). This change in physical properties is associated with the high sedimentation rates (370-960 m/Ma, Shipboard Scientific Party, 1994; Goldfinger, 1994; Goldfinger et al., 1996) in the Astoria and Nitinat deep sea fans, which hinder fluid expulsion due to compaction and cause fluid overpressures.

The surface manifestation of accretion at the Cascadia margin is a series of submarine thrust ridges, and their landward continuation into the Olympic and Coastal Range mountains (Orange, 1990; Brandon et al., 1998). Onshore imbricated slices date back to early Miocene accretion, and the elevated nature of these units may act as a present day abutment to the modern prism. The nature of the Cascadia prism off Oregon has been subject to numerous seismic investigations (Westbrook et al., 1994; MacKay et al., 1995; Wallon-Pizarro, 1997; Trehu et al., 1999). At almost regular intervals, a sediment slice is detached from the incoming succession on the oceanic plate, and thrust beneath the existing wedge (Fig. 2.2.2). Between the different generations of accreted ridges, small sedimentary basins have developed, which are apparently sheltered from deformation other than slumping (see below).
Several main morphological features can be identified:

- the proto-deformation front, with the basal detachment (décollement) migrating westward into the Juan de Fuca sediments seaward of the accretionary wedge;
- the first accretionary wedge, immediately landward of the trench, where faulting and migration of deep fluids has been documented (Westbrook et al., 1994);
- the second, more landward accreted ridge, termed "Hydrate Ridge", which is composed of older sediments, characterized by landward dipping seismic reflectors, and
- the margin of the Siletz terrane (Gerdom et al., 2000), possibly acting as the backstop.

The crustal architecture of the area was subject to earlier cruises (e.g., SO108, ORWELL; see Flueh and Fisher, 1996), and an amphibic approach combining land- and sea-based stations to record seismic refraction profiles. The location of the main acquisition corresponds to seismic reflection line OR89-8 (MacKay et al. ,1992; Wallon Pizarro, 1997). Seismicity in this part of the Cascadia margin is generally high, but the events occur heterogeneously over the upper and lower plates (Fig. 2.2.3). One reason for the heterogeneity may be the Siletz terrane, a microcontinent of basaltic oceanic crust having been attached to the margin during the Paleocene/Eocene. Between the terrane and the downgoing slab of the Juan de Fuca Plate, the accretionary body comprises several zones of low velocity. This may hint to fluid overpressures (known to be near lithostatic in other accretionary scenarios; e.g., Moore et al., 1995) or free gas from gas hydrate processes in the shallow subseafloor. The latter has been of major research interest off Cascadia over more than a decade, and is addressed in the following chapter.

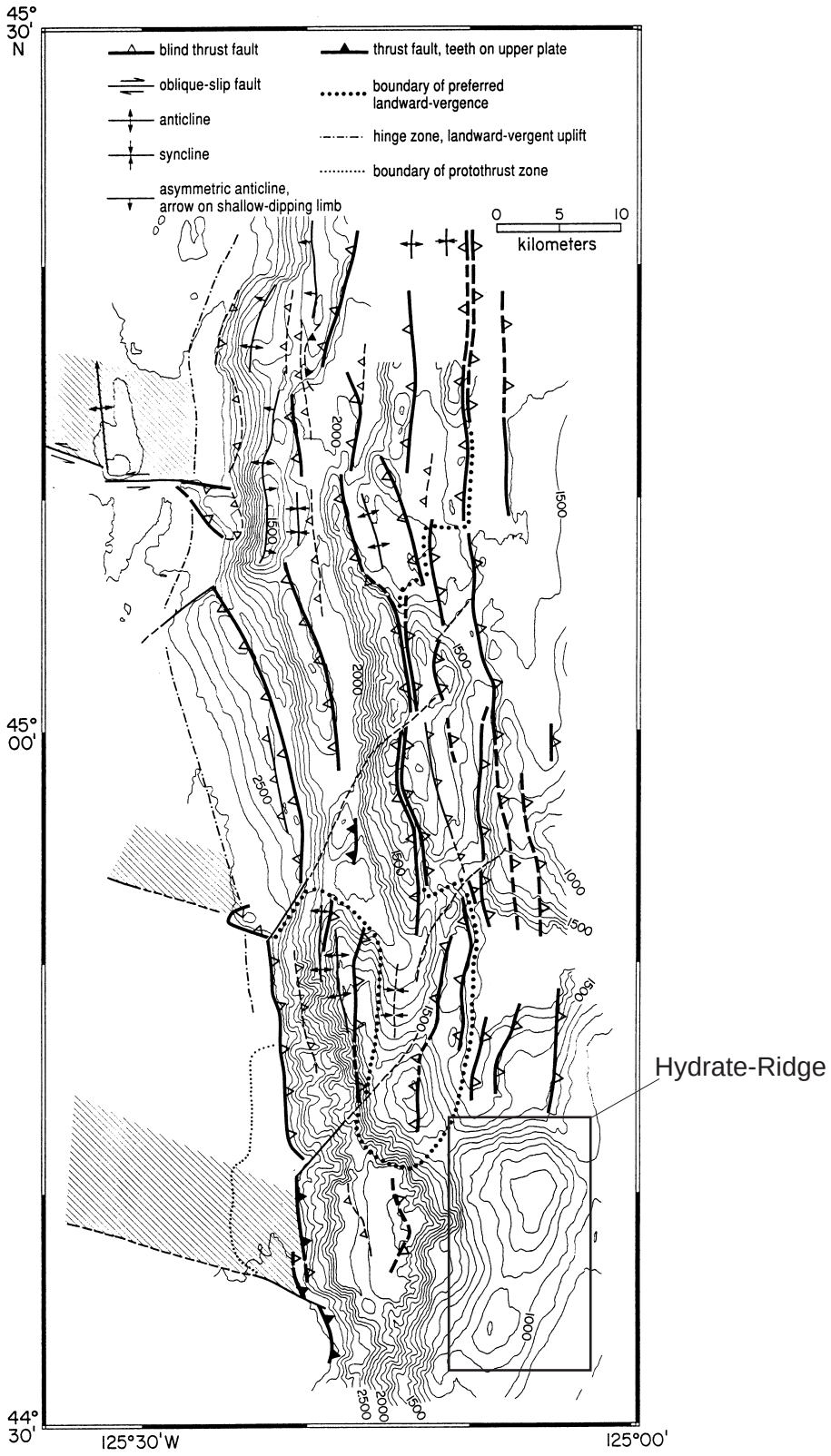

Figure 2.2.1: Tectonic map of the Cascadia accretionary prism off Oregon and Washington, showing the structural grain and sense of displacement of thrust faults. Note the seaward vergence of faulting in the Hydrate Ridge area in the south (after MacKay et al., 92).

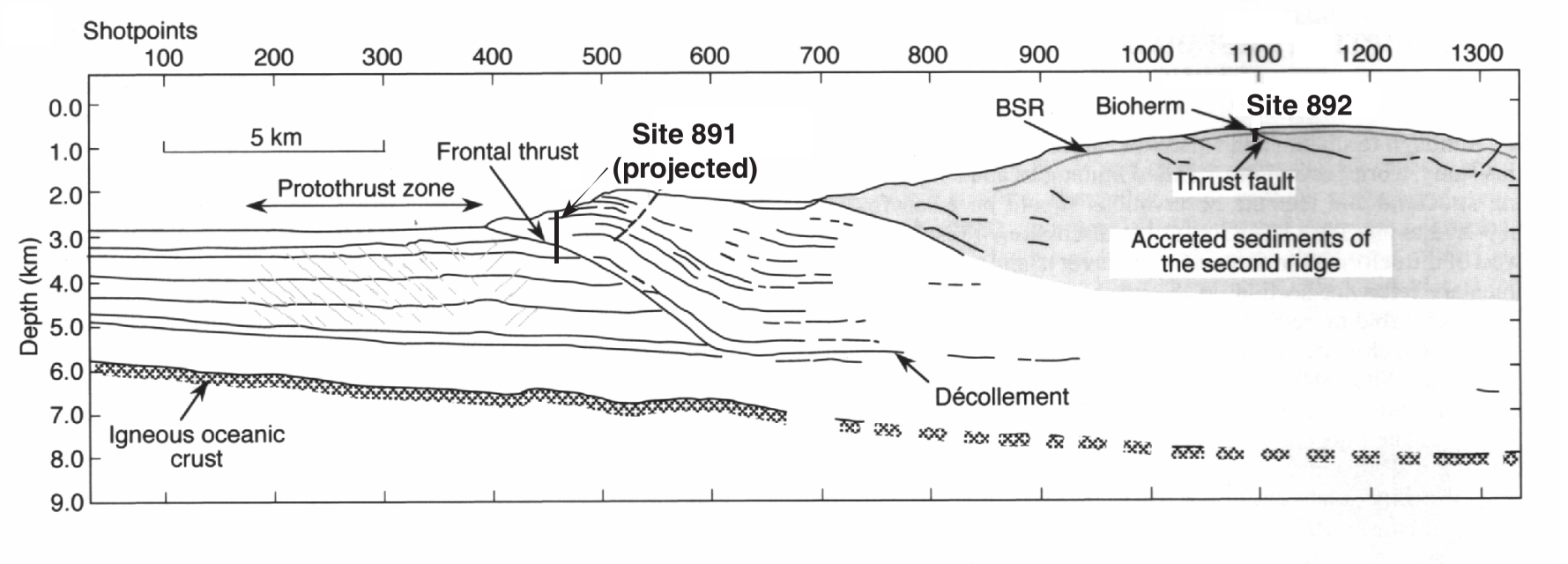

Figure 2.2.2: Cross section along line OR89-8 showing the structural evolution of the outermost (youngest) slices imbricated to the accretionary wedge. ODP drillholes (projected) relate to the results mentioned earlier (Chapter 2.1).

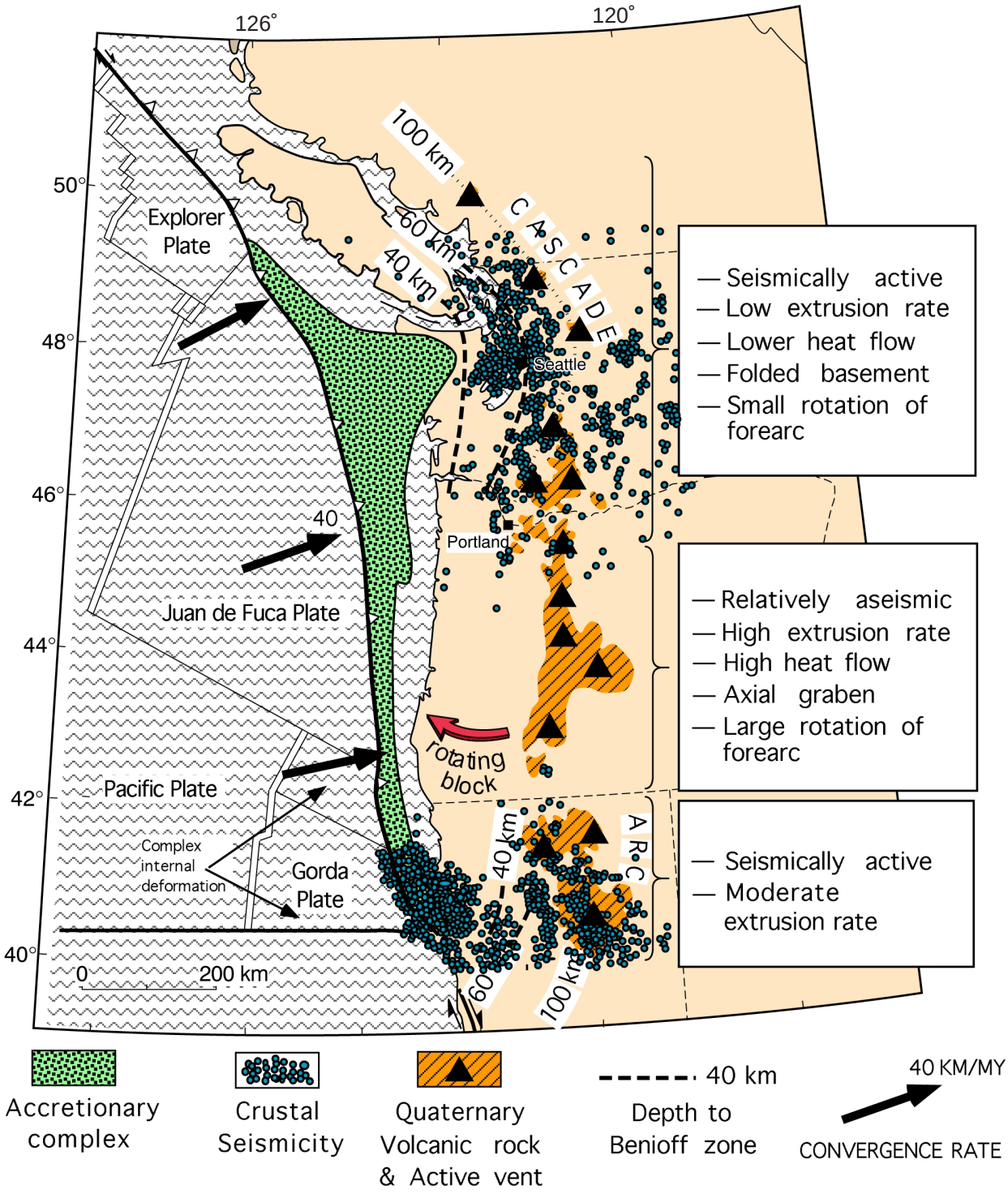

Figure 2.2.3: Map of seismicity of the Cascadia and Washington margin.

2.3 GASHYDRATE RESEARCH OFF NORTH AMERICA

(D. Klaeschen, A. Kopf)

BSR (Bottom Simulating Reflector): free gas and gas hydrates

It is assumed at present that more than two thirds of the amount of carbon available as an energy resource is bound as gas hydrate (Kvenvolden, 1988; 1993). A critical feature to assess such quantities of gas hydate as well as free gas is the occurrence of a BSR (Bottom Simulating Reflector) on seismic profiles. The prominent reflector is characterized by a polarity reversal (negative reflection coefficient) when acoustic waves enter an area of free gas at a depth where massive hydrate dissociates (Fig. 2.3.1).

In theory, the amount of free gas beneath the BSR can be quantified using wave inversion and AVA analyses (e.g. Ecker et al., 2000). However, often the controlling parameters for calibration of the seimic attributes are lacking. In previous studies, the BSR has been used mainly to identify free gas (Shipley et al., 1979; Dillon and Paull, 1983). The BSR generally follows the seafloor topography independent of the sedimentary structure at the subsurface. It generally occurs between 200 and 600 m depth beneath the seafloor (Claypool and Kaplan, 1974), until geothermal gradients force dissociation (Fig. 2.3.1; Hyndman et al., 1992; Tréhu et al., 1995). In principal, massive gas hydrate are to be expected above the BSR, although gas hydrate may well be found in areas where a BSR has not been developed (e.g., Holbrook et al., 1996). There is an ongoing debate whether the BSR results from an increase in velocity above the BSR, or if it is caused by a velocity decrease below it (e.g., MacKay et al., 1994; Pecher et al., 1996). In order to answer this question, physical acquisition and processing techniques must focus on the distinction between the gas and gas hydrate properties. Massive gas hydrate has p-wave (Vp) velocities of 3.3-3.8 km/s. In contrast, rather small amounts of free gas may lower Vp drastically (Murphy, 1984). At the moment, the biggest uncertainty is still a reliable estimate of the seismic velocities in the gas hydrate bearing sediments, if no gas hydrate was present. No models predict velocity changes owing to gas hydrate cementation (Lee et al., 1996), and only a few studies examine changes in the physical properties of sediment as a function of gas hydrate (Stoll and Brian, 1979; Zhang et al., 1999). Recently, BSRs were penetrated during Ocean Drilling Programs (ODP) expeditions Leg 146 (Cascadia Margin, MacKay et al., 1994) and 164 (Blake Outer Ridge, Holbrook et al., 1996). These studies indicate that free gas beneath the BSR is a prerequisite for a prominent appearance on seismic profiles. During ODP Leg 164, three holes were drilled into corresponding sedimentary succession with different BSR signature. The results show that gas hydrates were met even if no BSR was present (Holbrook et al., 1996), and that free gas can reach to considerable depths possibly trapped by impermeable hydrate seal (Dickens et al., 1997).

Results from ODP Leg 146

A prerequisite for successful proposals for ODP drilling is an extensive seismic survey in the area of investigation. A selected number of the regional MCS profiles collected during a cruise off Oregon in 1989 (e.g. MacKay et al., 1992) were available prior to HYDGAS cruise. Prestack-time migrations and AVA inversions for lines OR89-01 to OR89-12 (for location, see Fig. 2.3.2) served during SO150 to select the locations for the experiments. The lines cover the area from the trench to the depression landward of the second accreted ridge (forearc basin-type structure), all being WE-oriented. Two NS-trending profiles (OR89-43 and OR89-44), tieing the other profiles together, were also available. Several examples of these lines are given in Trehu et al. (1999), and have been revisited with different source-streamer configurations during SO150 cruise.

The most important profiles in the context of the HYDGAS expedition are, from north to south:
(i) Line OR89-09, where ODP drill hole 892 is located on the northern summit of Hydrate Ridge, and where two OBH/OBS deplyoments were carried out during SO150 (see Fig. 6.3.1.1);
(ii) Line OR89-05, where ODP Site 891 was drilled into the first accreted ridge (Fig. 2.3.3); and

(iii) Line OR89-02, where two future ODP Leg 204 drillsites (HR1 and HR3) are located, which coincide with the deployments of OBH/OBSs during SO150 cruise (see Fig. 6.3.1.2).

Regarding profiles OR89-09 and OR89-02, raw-sections without processing shot with various sources during cruise SO150 are presented in chapters 6.4-6.6 (see below). Some of the other lines were also revisited during SO150, and a selection is presented in the section on regional reflection data and individual small study areas (chapter 6.3).

As mentioned earlier, two sites were drilled into the Oregon forearc to investigate gas hydrates during ODP Leg 146 (Westbrook et al., 1994). The first hole, Site 891, penetrated the toe of the prism at the westernmost part of the first accretionary ridge (Fig. 2.3.3). An almost 500 m-thick succession of undercompacted Pleistocene sediments was recovered. Although no BSR can be seen in the seismic reflection data, evidence for gas hydrates was provided by freshened pore waters over a 20-30 m thick interval (e.g., Westbrook et al., 1994; Deyhle et al., in press). Site 892 was drilled further east on the crest of the northern summit of Hydrate Ridge (Figs. 2.3.2 and 2.3.3). It penetrated a well-developed BSR and a thrust fault zone carrying fluids from depth (Brown, 1995). Again, fluid composition indicated dilution from gas hydrate cage water in the interval above the BSR. Mainly the upper part of the sediment (down to 70 mbsf) shows average porosities of 60-70%, indicating a considerable undercompaction (Westbrook et al., 1994). Such large pore volumes may result from gas hydrate processes: The ice-like clathrate first displaces the surrounding sediment and forms layers (see Bohrmann et al., 1998; Greinert et al., 2000), and after dissociation (here due to core recovery) leaves highly disturbed, porous claystones.

Data crucial to the HYDGAS studies were collected during ODP Leg 146. First, numerous physical properties of the recovered core were determined on the undisturbed section by the MST (multi-sensor track), including Vp, porosity, resistivity, and density. Second, discrete samples were taken from the core to measure porosity, wet bulk and dry densities, and Vp (e.g., Fig. 2.3.4a; and Westbrook et al., 1994). Third, downhole logging measurements were performed in the partly cased hole, yielding Vp, porosity and density as in situ properties (Fig. 2.3.4b). Finally, a zero-offset VSP test was carried out at Site 892, whose velocity information is available (Westbrook et al., 1994; MacKay et al., 1994).

In summary, a wealth of seismic lines and ODP data exist as electronic material to calibrate the HYDGAS results and incorporate them into their regional context.

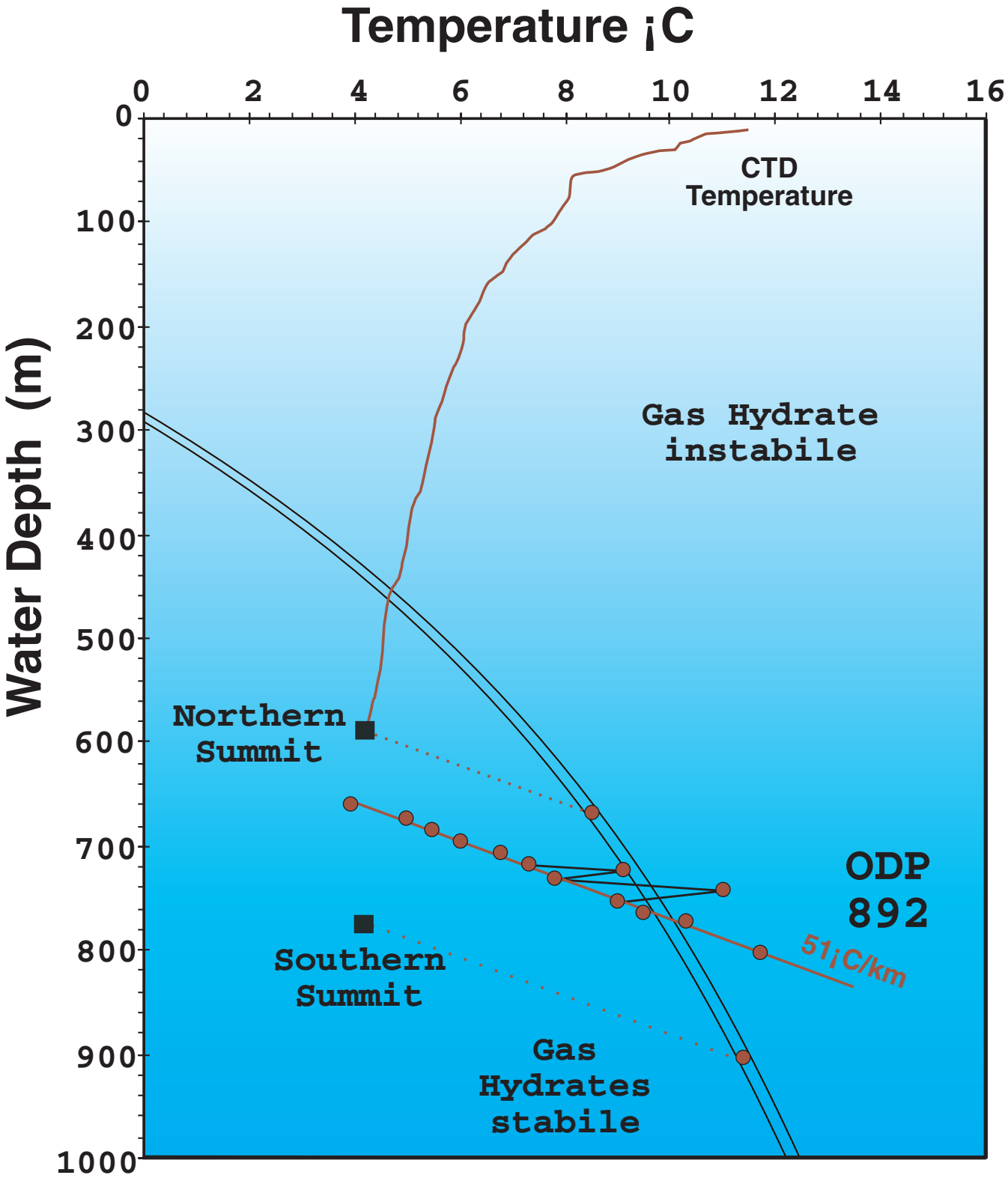

Figure 2.3.1: Gas hydrate phase diagram (Bohrmann et al., 1998)

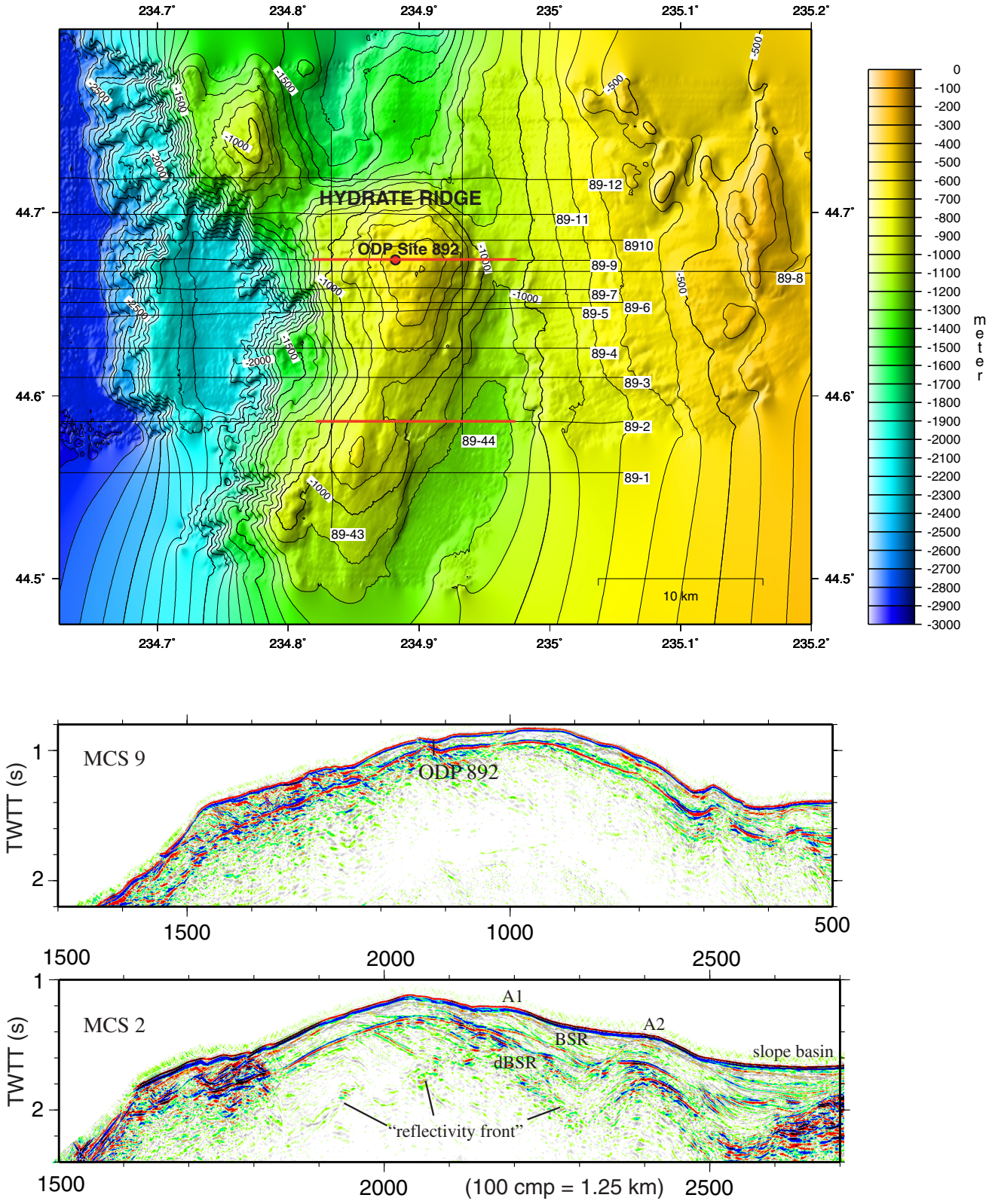

Figure 2.3.2 (top): Map view of OR89 profiles 1-12, OR89-43 and OR89-44 across the Hydrate Ridge area.

Figure 2.3.3 (bottom): Neartrace section of OR89-9 showing location of the ODP drilling during Leg 146, Site 892 on the northern ridge and seismic section of OR89-2 on the southern Hydrate Ridge from Trehu et al. (1999).

Figure 47. Depth profiles of Na/Cl, Ca/Cl, Mg/Cl, and Mg/Ca molar ratios of pore fluids, Hole 892A.

a)

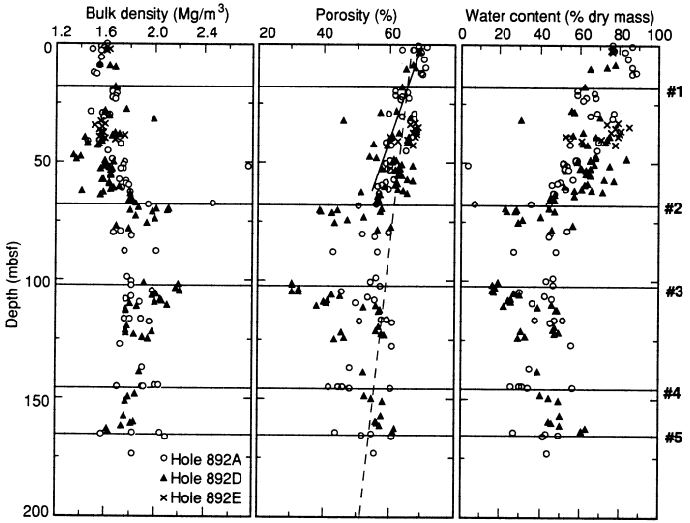

Figure 48. Index properties (bulk density, porosity, and water content) vs. depth with interpreted discontinuities shown as horizontal lines (open circles = Hole 892A, triangles = Hole 892D, and crosses = Hole 892E). Discontinuity #1 is the boundary between sediment that contains observed hydrate and sediment where there was no observed hydrate; Discontinuity #2 is at the boundary between lithostratigraphic Subunits IA and IB. Brückmann's (1989) normally consolidated porosity-depth function (dashed line) and an exponential regression curve (porosity = $70.6^{(-0.0018 \times \text{depth})}$; $R = 0.5$) for Subunit IA (solid line) are also plotted in the porosity profile.

Figure 2.3.4: Index properties (bulk density, porosity, and water content (a), gamma-ray and porosity-sensitive logs (b) and velocity logs (c) for Site 892 (Westbrook et al., 1994).

b)

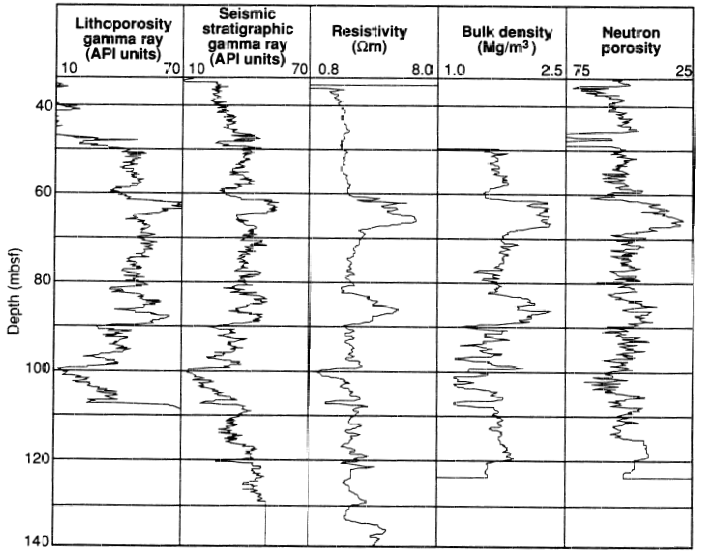

Figure 75. Gamma-ray and porosity-sensitive logs for Site 892. Total gamma-ray logs are shown for the lithoporosity and seismic stratigraphic logging runs. Porosity-sensitive logs are resistivity, bulk density, and neutron porosity. Note the character match between the gamma-ray and porosity-sensitive logs, which implies that porosity variations are caused mainly by changes in clay-mineral abundance.

c)

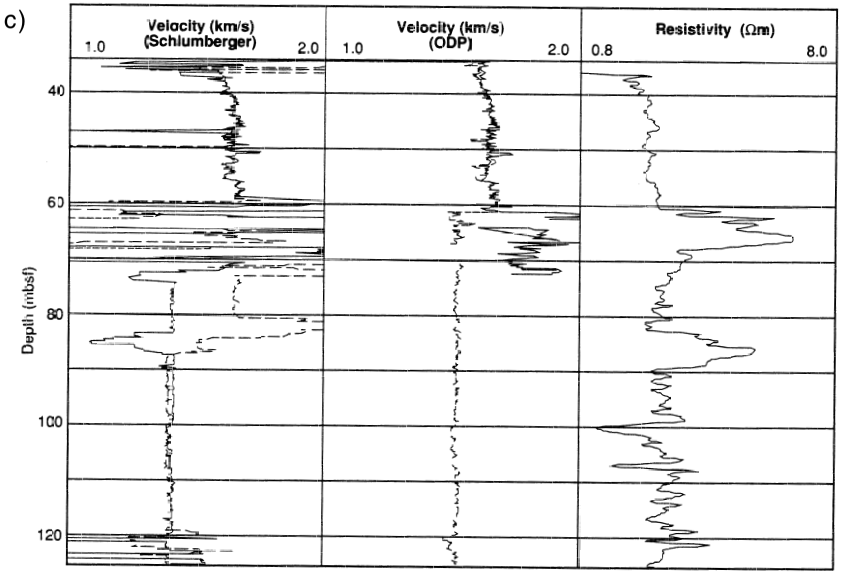

Figure 76. Velocity (Schlumberger processed and ODP reprocessed) and resistivity logs for Site 892.

3. PARTICIPANTS

3.1 SCIENTISTS

3.1.1 SCIENTISTS - Leg SO150

1. Kläschen, Dr. Dirk	Chief scientist	GEOMAR
2. Bialas, Dr. Jörg	Seismics	GEOMAR
3. Petersen, Jörg	Seismics, Processing	GEOMAR
4. Könitz, Dorit	Seismics, Processing	GEOMAR
5. Neumann, Karsten	Airguns	GEOMAR
6. Spinner, Miriam	Hydrosweep	GEOMAR
7. Bode, Ingolf	Magnetometer	GEOMAR
8. Landerer, Felix	Parasound	GEOMAR
9. Horn, Dr. Dietrich	Interpretation	GEOMAR
10. Kopf, Dr. Achim	Interpretation	GEOMAR
11. Steffen, Klaus	Airgun and OBH/S technician	KUM
12. Bohlen, Dr. Thomas	Seismics	IFG
13. Klein, Gerald	Seismics, Processing	IFG
14. Liersch, Petra	Seismics, Processing	GEOMAR
15. Müller, Alexander-Nils	Seismics, Navigation	GEOMAR
16. Versteeg, Willem	Deep-tow	Gent
17. Guidard, Stephanie	Deep-tow	Gent
18. Cresens, Wim	Deep-tow technician	Gent
19. Arsenault, Matthew	Seismics, Processing	COAS

3.1.2 SCIENTISTS - Leg SO150/2

1. Könitz, Dorit	Hydrosweep	GEOMAR
2. Bode, Ingolf	Magnetics	GEOMAR
3. Liersch, Petra	Logistics	GEOMAR
4. Bannert, Bernhard	Lander technician	KUM

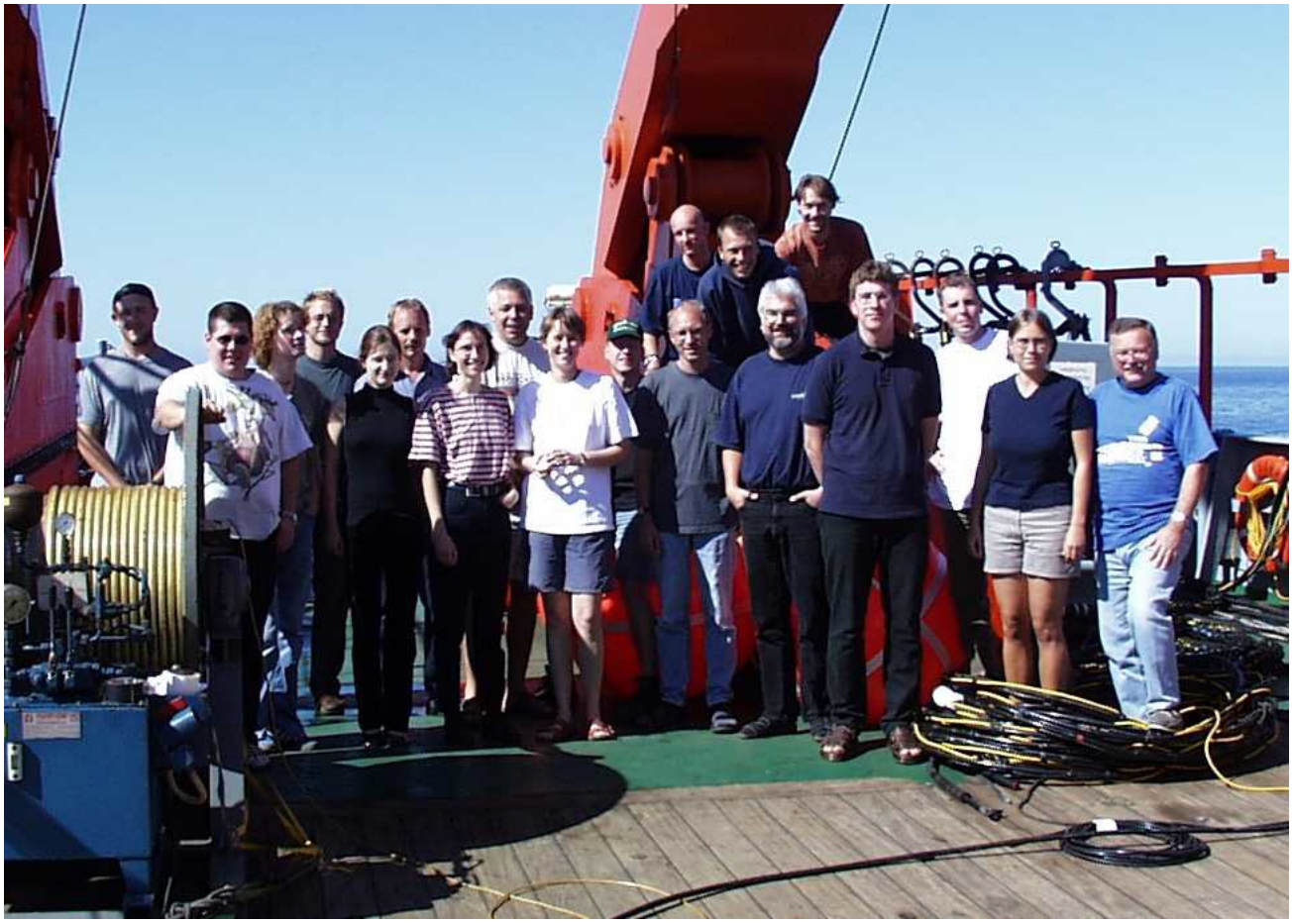

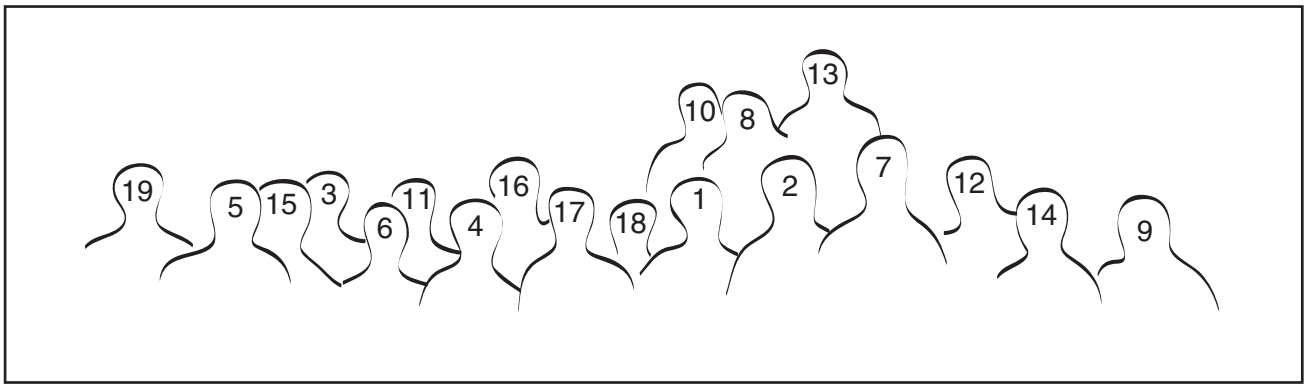

Figure 3.1.1.1: Group photograph (top) and legend (below). Numbers refer to those provided in this paragraph.

3. 2 CREW

3.2.1 CREW - Leg SO150/2

Henning Papenhagen	Master
Walter Baschek	Chief Mate
Jörn Löffler	1st Mate
Rainer Hellmann	Radio Officer
Anke Walther	Surgeon
Peter Neumann	Chief Engineer
Helmut Grund	2nd Engineer
Uwe Schade	2nd Engineer
Werner Huxol	Electrician
Rainer Duthel	Chief Electronic Engineer
Helmut Vöhrs	Electronic Engineer
Jens Grigel	System Operator
Kurt Stammer	System Operator
Joachim Stenzler	Fitter
Heinrich Riedler	Motorman
Frank Isbrecht	Motorman
Klaus Teichert	Motorman
Johannes v. Arronet	Motorman
Frank Tiemann	Chief Cook
Willy Braatz	2nd Cook
Johann Bronn	Chief Steward
Leonore Lössnitz	2nd Steward
Peter Eller	2nd Steward
Winfried Jahns	Boatswain
Manfred Gudera	A. B.
Hans-Peter Mucke	A. B.
Wolfgang Reichmacher	A. B.
Andreas Schrapel	A. B.
Günter Ventz	A. B.
Götz vom Berg	A. B.

3.2.2 CREW - Leg SO150/2

Henning Papenhagen	Master
Walter Baschek	Chief Mate
Roland Priebe	1st Mate
Rainer Hellmann	Radio Officer
Anke Walther	Surgeon
Uwe Thaysen	Chief Engineer
nn	2nd Engineer
Uwe Schade	2nd Engineer
Werner Huxol	Electrician
Rainer Duthel	Chief Electronic Engineer
Helmut Vˆhrs	Electronic Engineer
Jens Grigel	System Operator
Kurt Stammer	System Operator
Joachim Stenzler	Fitter
Heinrich Riedler	Motorman

H. Meyer	Motorman
Klaus Teichert	Motorman
Johannes v. Arronet	Motorman
Frank Tiemann	Chief Cook
Pytlik	2nd Cook
Johann Bronn	Chief Steward
Leonore Lössnitz	2nd Steward
Peter Eller	2nd Steward
Winfried Jahns	Boatswain
S. Becker	A. B.
Hans-Peter Mucke	A. B.
Wolfgang reichmacher	A. B.
Andreas Schrapel	A. B.
Günther Stängl	A. B.
Götz vom Berg	A. B.

3.3 ADRESSES OF PARTICIPATING INSTITUTIONS

Participating institutions

GEOMAR Research Center for Marine Geosciences
Marine Geodynamics
Wischhofstr. 1-3
D - 24148 Kiel
Germany
Tel. (+49) 431 / 600-2290, or -2271
Fax. (+49) 431/600-2922
mail to: dklaeschen@geomar.de or eflueh@geomar.de

College of Oceanic and Atmospheric Sciences
Oregon State University
104 Ocean Administration Building
Corvallis, OR 97331
USA
Tel. +001 541 737 2655 or -3504
FAX. +001 541 737 2064
mail to: trehu@oce.orst.edu

Renard Center of Marine Geology
Krijgslaan 281 - S8
B - 9000 Gent
Belgium
Tel. (+32) 9/2644596
FAX. (+32) 9/2644967
mail to: jeanpierre.henriet@rug.ac.be or willem.versteeg@rug.ac.be

Christian-Albrechts Universität zu Kiel
Institut für Geowissenschaften/Geophysik
Otto-Hahn-Platz 1

24118 Kiel
Germany
Tel. (+49) 431 880 3914
Tel. (+49) 431 880 4432
mail to: Khelbig@geophysik.uni-kiel.de or Tbohlen@geophysik.uni-kiel.de

Link with other U.S. Initiatives

A. Trehu, M. Torres, S. Giovannoni, C.Goldfinger, E. Suess, K. Brown, M. Kastner, N. Bangs and D. Hammond have successfully proposed drilling on Hydrate Ridge. This cruise Leg 204 with R/V Joides Resolution has now been scheduled for autumn 2002, and will drill the localities HR1 and HR3. Another pre-site survey for this leg (A. Trehu, N. Bangs), acquiring 4 x 9 km^2 3D-high resolution reflection seimic profiles (81 profiles spaced 50 m apart), was just completed successfully in 2000.

4.0 AGENDA

4.1 SONNE CRUISE SO150, 17.09. to 15.10., VICTORIA-LOS ANGELES

(J. Bialas, D. Klaeschen, A. Kopf)

Scientific cruise SO150 HYDGAS (Quantification of gas hydrates and gas in the sediment of the Cascadia accretionary wedge using seismic methods) of R/V SONNE started on the 17th of September, 2000 in the port of Victoria, B.C., Canada. Under the leadership of GEOMAR, Kiel, 19 scientists from four institutions (GEOMAR Kiel, Germany; Dept. of Geophysics, University of Kiel, Germany; Renard Center for Marine Geosciences (RCMG), Gent, Belgium; College for Oceanic and Atmospheric Sciences, Oregon State University, U.S.A.) embarked to study the nature of the so called Hydrate Ridge off the coast of Oregon, U.S.A. Owing to possible autumn storms and the short transit time into the working area, it was decided to stay in port until early morning of the 19-SEP to carefully prepare all instrumentation for the planned experiments. Three 20ft. containers with research equipment were unpacked in the process of setting up the gear. Five different seismic sources, three different streamer systems, a total of 14 ocean bottom hydrophones (OBH) and seismometers (OBS) were installed as well as a small computer network.

On the 19-SEP, 08:00 hrs. R/V SONNE left Victoria and headed towards the Hydrate Ridge area. During the transit, scientific work started on the 20-SEP, 06:00 hrs with a first releaser test and a CTD for calibration purposes of the Hydrosweep system. One Differential Pressure Gauge (DPG) an OBH and an OBS were deployed at 20:00 hrs for a first function and data quality test of the various sources and receivers. Seismic shooting of the watergun, GI-gun, 32 l Bolt gun and a small airgun array continued on selected profiles until 21-SEP, 19:00 hrs. Recordings were done with a mini streamer, a single channel streamer and a DeepTow streamer at the ODP Leg 146 Site 892.

A set of regional seismic lines to be shot with the GI-gun and the three streamers were scheduled for the night of the 21-SEP to 22-SEP, but heavy winds and rough seas forced an alternate program of Hydrosweep mapping to be installed. Swath mapping started south of Hydrate Ridge at 44°27N and was continued southwards along EW-oriented lines. The program has extended a mapping survey carried out previously (Flueh and Fisher, 1996; Suess and Bohrmann, 1997; Bohmann et al., 1999), and was interrupted by a further releaser test and DeepTow test midday the 22-SEP.

On 23-SEP, 01:00 hrs, the first regular deployment of 14 OBH/S systems took place in the area of proposed ODP drilling leg 204 (anticipated in autumn 2002) on regional seismic reflection line OR89-2. It was followed by a 40 hrs long shooting program until 25-SEP, 13:00 hrs., when the seafloor stations were recovered. A set of 11 profiles were shot along a grid of crossing lines using the different sources available. The main E-W-trending line (OR89-2) was repeatedly shot with each source to allow a comparative study of the seismic signal as a function of the source.

Due to the magnificent weather and very calm seas, the Sparker source was used successfully to acquire two grids of 18 lines in fluid venting areas near the first deployment. These small surveys in the so called Pinnacle and Southern Pockmark areas were completed between 25-SEP, 13:00 hrs, and 26-SEP, 07:00 hrs. Further profiling accross the ODP Site 892, the main target of the cruise and desired location for the second deployment, could not be completed due to a fishing vessel having been stuck on our course. Apparently, the drag net was caught on the long term observatory (CORK system) installed on top of the ODP drill hole. An instantaneous alternative set of profiles could also not be completed, because the fisherman's manouvers to free his net resulted in blocking a profile (which was later completed). Consequently, the program as well as the deployment at Site 892 was abandoned. A NS-profile, connecting the two main areas of

investigation at the northern summit (Site 892) and southern summit (proposed sites HR1 and HR3) of Hydrate Ridge, was terminated on 27-SEP, 04:00 hrs.

Deployment of 14 OBH/S instruments on the 27-SEP, 04:30 hrs. started the second main deployment. With the deployment at HR3 several days prior, we put the equipment down at the second proposed Leg 204-drillsite, HR1. Again, a set of crossing lines (EW and NS-oriented) were shot over the OBH/S assembly, using all 5 seismic sources and the 3 streamers available. After completion of the 12 profiles, recovery of all instrumentation ended this experiment 29-SEP, 10:00 hrs.

The time needed for data retrieval of the OBH/S flash memory and a first data quality control was used for further acquisition of regional lines. 7 seismic lines were shot with Sparker and GI-gun across the SE knoll, a prominent topographic high south of Hydrate Ridge. As the feature occurs in the area where the Hydrosweep survey was extended, additional mapping was conducted until 30-SEP, 13:00 hrs.

After ensuring the data quality of the experiments across the southern summit, the third experiment again focused ODP Leg 146 Site 892. Without disturbance by other vessels took, a total of 22 narrowly spaced profiles were shot across our OBH/S assembly. The schedule between 30-SEP, 14:00 hrs., and 03-OCT, 03:00 hrs., also included investigation of a pockmark field slightly east of site 892.

During data retrieval from the ocean bottom equipment, the net of regional seismic reflection lines was further complemented using the GI-gun and the three streamers. 7 lines were shot (dominantly along existing profiles from the OR89 survey) until the 04-OCT, when the OBH/S equipment was ready to be deployed a second time at the northern summit.

On 04-OCT, 12:00 hrs., an unusual experiment with a drop weight source was undertaken using a little assembly of three OBH/S instruments. A 3-ton iron weight attached to a wire line was dropped at 1.5 m/s several times onto the seafloor in an effort to test whether the drop shots could generate low frequency dispersive waves. This technique, which has been previously applied successfully on land, was tested to be applicable in unconsolidated marine sediments.

Three EW-oriented seismic profiles, acquired with the deep tow streamer across the northern summit, were completed on 05-OCT, 05.00 hrs. Afterwards, all 14 OBH/S instruments were deployed for the fourth experiment around Site 892. A set of 10 seismic lines were shot with the various sources and streamer configurations on the northern summit of Hydrate Ridge. OBH/S recovery was scheduled for late evening of 06-OCT, but was delayed until daylight owing to heavy fog and limited visibility. The night was used to shoot an additional Sparker survey in the area of ODP Site 892, to fill the missing profiles which were blocked by the struggling fisherman. All OBH/S systems were safely recovered until 07-OCT, 10:00 hrs., when visual identification of the floating systems was ensured by morning light.

Four GI-gun profiles, tying together the acquisitions at the northern and southern summit, were acquired until 08-OCT, 04:00 hrs., during which time the data from experiment four were retrieved from the OBH/Ss. In the morning hours of the same day, 11 OBH/Ss were deployed in an effort to fill the gaps in the data on the southern summit (HR3 and HR1 drillsites). With the fifth deployment complete acquisition along 11 lines started at 10:00 hrs. After a series of WE- and NS-lines, OBHs and OBSs were successfully recovered on 10-OCT, 5:00 hrs.

Afterwards, a test profile south of Hydrate Ridge was acquired several times with the deep tow streamer at various depths. The programme had to be abandoned at 11:00 hrs due to increasing wind, and in favour of an early recovery of a seafloor lander, which had been lowered during the

GEOMAR TECFLUX cruise SO 148-2 earlier in 2000 a few kilometres south of ODP Leg 146, Site 892 on the Hydrate Ridge. After a short transit, Hydrosweep mapping in the area south of SE knoll (southermost HYDGAS study area) was carried out since 10-OCT, 13:30 hrs. After a set of 16 profiles, Hydrosweep recordings were stopped at 12-OCT, 03:30 hrs., and R/V Sonne went on transit towards Los Angeles.

Off Los Angeles, the pilot was met on 15-OCT, 9:00 hrs, and R/V Sonne docked at pier LA240X at 10:00 hrs in Long Beach harbour. 16 scientists left early in the morning on 16-OCT the vessel. Three scientists stayed on board to do Hydrosweep and magnetic messurements offshore Nicagragua, Costa Rica, and Panama during the transit cruise SO-150/2 to Bridgetown/Barbados. One technician embarked to prepare the seafloor lander on the transit for transport back to Germany.

4.2 SONNE CRUISE SO150/2, 16.10. to 01.11., LOS ANGELES-BRIDGETOWN

On the 16-OCT, 13:00 hrs. R/V SONNE left Los Angeles and headed in southward direction towards Panama. Offshore Nicaragua on the 23-OCT, 12:00 hrs the scientific work started again with CTD for calibration purposes of the Hydrosweep system. At 15:00 hrs Profile 1 with Hydrosweep and magnetic recordings started. Offshore Panama a set of 11 profiles on the transit were recorded, Hydrosweep and magnatic recordings were stopped at 25-OCT, 17:00 hrs., and R/V Sonne went towards the Panama Canal. The ending of the charter of SO-150 was on the 27-OCT, 24:00 hrs on sea.

5. SCIENTIFIC EQUIPMENT

5.1 COMPUTER FACILITIES

(J. Bialas, T. Bohlen, G. Klein)

The experiments and shipboard work during cruise SO150 required special computer facilities in addition to the existing shipboard systems. For programming of ocean bottom stations, processing of seismic data, and analysis of hydrosweep recordings, several workstations were installed from the participating groups.

The scientists from Geophysics Dept., University of Kiel, installed two Linux based PC computers. These units were mainly used for high resolution processing and interpretation of OBH/S data. To enable data exchange with GEOMAR on a short term basis, both PCs were integrated into the GEOMAR workstation cluster.

Due to the large amount of data transfer, GEOMAR installed a workstation cluster onboard comprised of the following systems:

farallon SUN Ultra, 2CPU, 256MB memory, 78GB disks, 2 DAT, CD, Sun Solaris2.5
devonia SUN Ultra60, 2CPU, 1GB memory, 112GB disks, 2xDAT, 2xExabyte, Sun Solaris2.6
jurassic SUN SparcIPX, 1CPU, 64MB memory, 8GB disks, DAT, Sun OS 4.1.4
galicia SUN Sparc10, 1CPU, 96MB memory, 12GB disks, DAT, SunOS 4.1.4
OBH Pentium II 125 Mhz, 1CPU, 128MB memory, 9 GB disks, 3x PCMCIA, Windows95

For FD-modelling and data processing of the interface waves two PCs were installed:

EIS Pentium II 333 Mhz, 1CPU, 64MB memory, 20 GB disks, CD, Debian Linux, Windows NT
MOBILE Pentium II, 1CPU, 64MB memory, 4 GB disks, external DAT, Debian Linux, Windows NT

For seismic modelling and publishing, two desktop Macintosh computers were installed:

PowerMacintosh G3/300 MHz
PowerMacintosh 7100/66 MHz

In addition to these computers, two X-Windows-Terminals and several laptops/powerbooks were used. The new network service provided at the third deck cabins of the scientists was utilized, including Windows or Linux based Laptops into the network. For plotting and printing, two HP Postscript Laserprinters (papersize A3 and A4), as well as the shipboard color plotters were available.

The workstation cluster was placed in the Magnetiklabor where it was set up according to a "client-server" model, with "farallon" being the server. The Macintosh computers were located in the Reinlabor and the Chemie-Nasslabor, and were also part of the GEOMAR network. During the cruise, auxiliary wiring of the ship's computer network was provided by the system operator on R/V Sonne, and hubs were installed in the Reinlabor and Chemie-Nasslabor. Hence, the Macintoshes could be directly connected to the GEOMAR-LAN. All important file systems from the main server at GEOMAR were duplicated onto the "farallon" disks. NFS-, NIS-, and automounter services were used to ensure the computing environment was identical to that at GEOMAR. Thus, every user was able to find his/her familiar user interface. Nevertheless, a set of 5 user-accounts was established to permit full access to all data files at the various workstations. For process related file handling, each console was dedicated to one of the user-accounts. The convenience of

network mounted file systems comes with a heavy network load, particularly during playback of OBH data from tape to disk (see SO123 cruise report, Flueh et al., 1997). Overcoming this required a high-performance network, which was accomplished by a switched twisted-pair ethernet. A 12-port ethernet switching-hub (3COM-SuperstackII 1000) with an uplink connection of 100 Mbps to the server 'farallon' and dedicated 10 Mbps ports for the client workstations maintained the necessary network performance. To keep the shipboard network undisturbed by the workstation cluster, but to allow communication between them, the server 'farallon' was equiped with two network interfaces and served as a router. This provided the additional benefit of a simplified network configuration. Considerable setup work was dedicated to 'farallon', while the other workstations used the same IP-addresses and network configuration as at GEOMAR.

The network setup proved to be reliable and stable, and no disruptions in service were observed. The Macintosh computers could not access the ship's printers but, with the new network connection between ship's hub and the GEOMAR hub, switch access was possible to the GEOMAR network printers.

5.2 SEISMIC RECEIVERS

5.2.1 GEOMAR OCEAN BOTTOM HYDROPHONE/SEISMOMETER (OBH/S)

(J. Bialas)

The Ocean Bottom Hydrophone

The first GEOMAR Ocean Bottom Hydrophone was built in 1991 and tested at sea in January 1992. A total of 11 OBH and 4 OBS instruments were available for SO150. This type of instrument has proven to be highly reliable. In fact, during the HYDGAS cruise the 1500th successful deployment was achieved. Altogether, 70 sites were occupied during the SO150 cruise.

The principle design of the instrument is shown in Figure 5.2.1.1, and a photograph showing the instrument upon deployment can be seen in Figure 5.2.1.2. The design is described in further detail by Flueh and Bialas (1996). Construction of the OBH is centred around a steel pipe, to which the system components are mounted. At the top of the pipe is a flotation buoy made of syntactic foam that is rated, as are all other components of the system, for a water depth of 6000 m. Attached to the buoy are a radio beacon, a strobe light, a flag and a floating line to aid in retrieval. The hydrophone for the acoustic release is also mounted here, and connected to a model RT661CE release transponder (MORS Technology). Communication with the instrument is possible through the ship's transducer system, allowing sucessful release and range commands even at 5 kn speeds and distances of 7 to 9 km. Attached opposite the release transponder is an E-2PD hydrophone sensor from OAS Inc., and in its own pressure tube an MBS recorder from SEND GmbH with D-siwe or rechargeable batteries (see Figures 4.3.1 and 4.3.2). Finally, suspended approximately 1 m below the steel pipe is an anchor, constructed from pieces of railway tracks weighing about 40 kg each.

The Ocean Bottom Seismometer

Construction of the Ocean Bottom Seismometer (OBS) (Bialas and Flueh, 1999) is based on the GEOMAR OBH, with a few minor changes (Fig. 5.2.1.3). In contrast to the OBH, the OBS has three legs around a center post to which the anchor weight is attached (Fig. 5.2.1.4). When deployed, the OBS is positioned directly on the sea bottom to avoid collisions between the seismometer cable and the anchor. A larger floatation buoy is used to compensate for the heavier payload of instruments and the seismometer release lever. During descent to the ocean bottom, the baseplate of the seismometer release lever extends about 1 meter below the base of the anchor, hitting the seafloor first. Upon contact, upward force of the baseplate extends the

seismometer hook away from the main body of the OBS. When the hook is at about 45° to the vertical, the seismometer is released and falls to the sea floor from approximately a 1 m height, ensuring coupling between the seismometer and the sea floor approximately 1 m from the main OBS body. At this time the only connection from the seismometer to the instrument is a cable and an attached wire which retracts the seismometer during ascent to the sea surface. All three channels are preamplified within the seismometer housing and recorded by the standard Methusalem recorder as used in the OBH units. Parallel to these three channels the standard hydrophone is recorded on the fourth channel, preventing an oscillation or electrical current from being transmitted mechanically to the seismometer. For system compatibility the acoustic release, pressure tubes, and the hydrophone are identical to those used for the OBH.

Marine Broadband Seismic Recorder (MBS)

The so-called Marine Broadband Seismic recorder (MBS; Bialas and Flueh, 1999), manufactured by SEND GmbH, was developed based upon experience with the DAT based recording unit Methusalem (Flueh and Bialas, 1996) over the last few years. PCMCIA technology enables static flash memory cards to be used as unpowered storage media, avoiding a mechanically driven recording media and read/write errors due to failure in tape handling operations. In addition, a data compression algorithm is implemented to increase data capacity. Redesign of the electronic layout enables a decreased power consumption (1.5 W) of about 25% compared to the Methusalem system. Data output can be in 16 to 18 bit signed data, depending on the sampling rate. Based on digital decimation filtering, the system was developed to serve a variety of seismic recording requirements. Therefore, the bandwidth reaches from 0.1 Hz for seismological observations to the 50 Hz range for refraction seismic experiments and up to 10 kHz for high resolution seismic surveys. The basic system is adapted to the required frequency range by setting up the appropriate analog front module. Alternatively, 1, 2, 3 or 4 analogue input channels may be processed. Operational handling of the recording unit is similar to the Methusalem system or by loading a file via command or automatically after power-on. The time base is kept on a temperature-compensated DTCXO with a 0.05 ppm accuracy. Setting and synchronizing the time as well as monitoring the drift is carried out automatically by synchronization signals (DCF77 format) from a GPS-based coded time signal generator. Clock synchronization and drift are checked after recovery and compared with the original GPS units. After software preamplification, the signals are low-pass filtered using a 5-pole Bessel filter with a -3 dB corner frequency of 10 kHz. Then each channel is digitized using a sigma-delta A/D converter at a resolution of 22 bits producing 32-bit signed digital data. After delta modulation and Huffman coding the samples are saved on PCMCIA storage cards together with timing information. Up to 4 storage cards may be used, with up to 440 MB per card available. Data compression allows more than 2 GB data capacity. Recently, technical specifications of flashdisks (disk drives of PCMCIA technology) have been modified to operate below 10°C, making 1 GB drives available for data storage. The flashcards need to be copied to a PC workstation after recording. During this transcription the data are decompressed and data files from a maximum of 4 flash memory cards are combined into one data set and formatted according to the PASSCAL data scheme used by the Methusalem system. This enables full compatibility with the established processing system. While the Methusalem system did provide 16 bit integer data, the 18 bit data resolution of the MBS can be fully utilized using a 32 bit data format.

The Marine Longtime Seismograph

Although power consumption can be reduced with the MBS data logger, long term deployments (up to one year), usefull for seismological observations, could not be achieved. For this purpose the prototype of a new data logger, the Marine Longtime Seismograph (MLS) was developped by SEND GmbH under the direction of GEOMAR.

The MLS is also a four channel data logger whose input channels have been optimized for 3-component seismometers and one hydrophone channel. The modular design of the analog front end allows use of different seismometers and hydrophones or pressure sensors. Currently, front

ends for the Spahr Webb seismometer and differential pressure gauge (DPG), the Guralp seismometer, and the OAS hydrophone have been developped. With these sensors we are able to record events between 50 Hz and 120 s. The greatly reduced power consumption of 250 mW during recording combined with a high precision internal clock (0.05 ppm drift) allows data acquisition for one year. Data storage is done on up to 12 PCMCIA type II flashcards. The instrument can be parameterized and programmed via a RS232 interface. After low pass filtering the signals of the input channels are digitized using Sigma-Delta A/D converters. A final sharp digital low-pass filter is incorporated into the software by a Digital Signal Processor. The effective signal resolution depends on the sample rate and varies between 18.5 bit at 20 ms and 22 bits at 1 s. Playback of the data is done under the same scheme as previously described for the MBS. After playback and decompression the data is provided in PASSCAL format, at which point it may easily be transformed into standard seismological data formats. During cruise SO150, three DPGs were available and recorded on most of the profiles using a sample rate of 200 Hz.

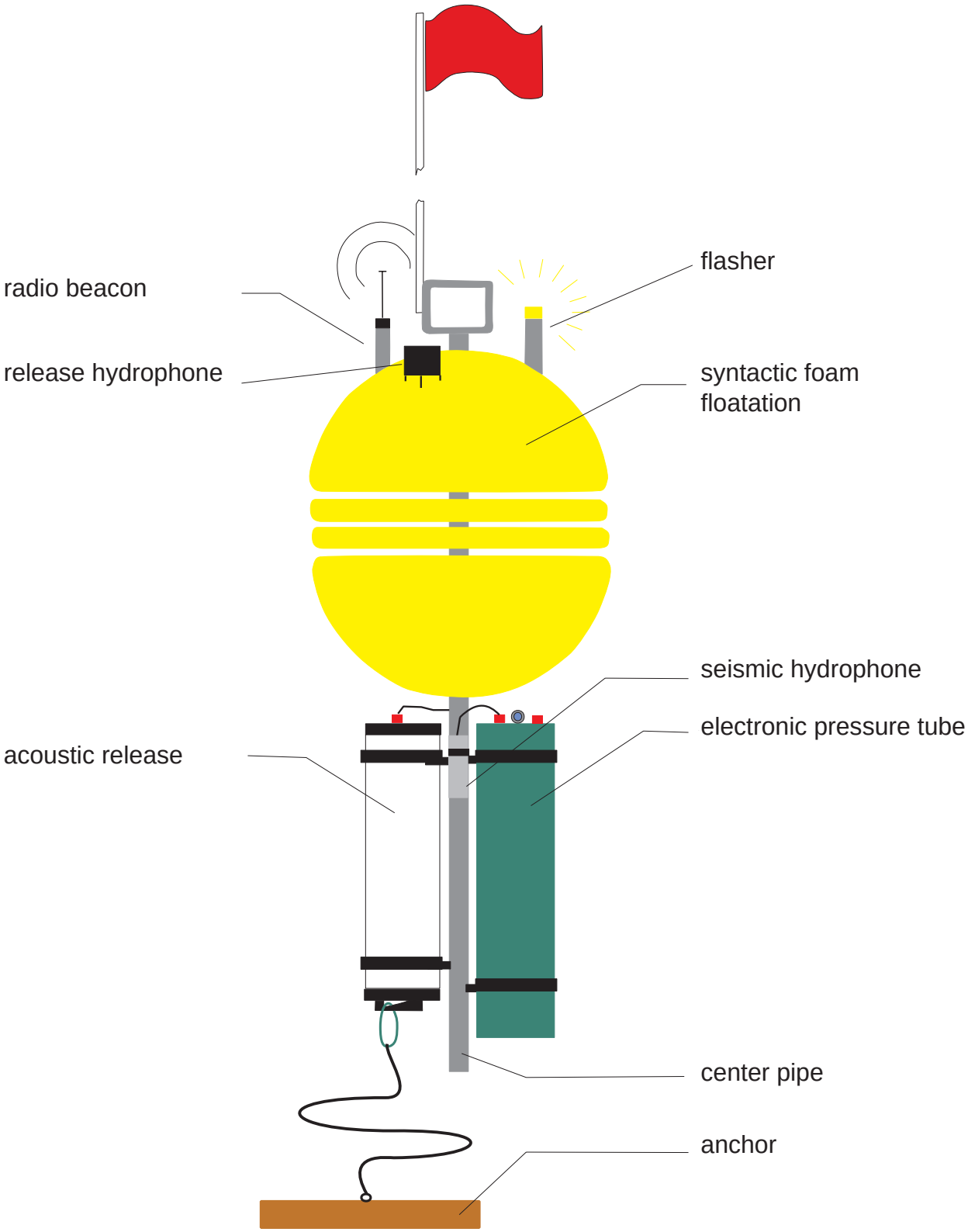

Figure 5.2.1.1: Principle design of the GEOMAR OBH (after Flueh and Bialas, 1996).

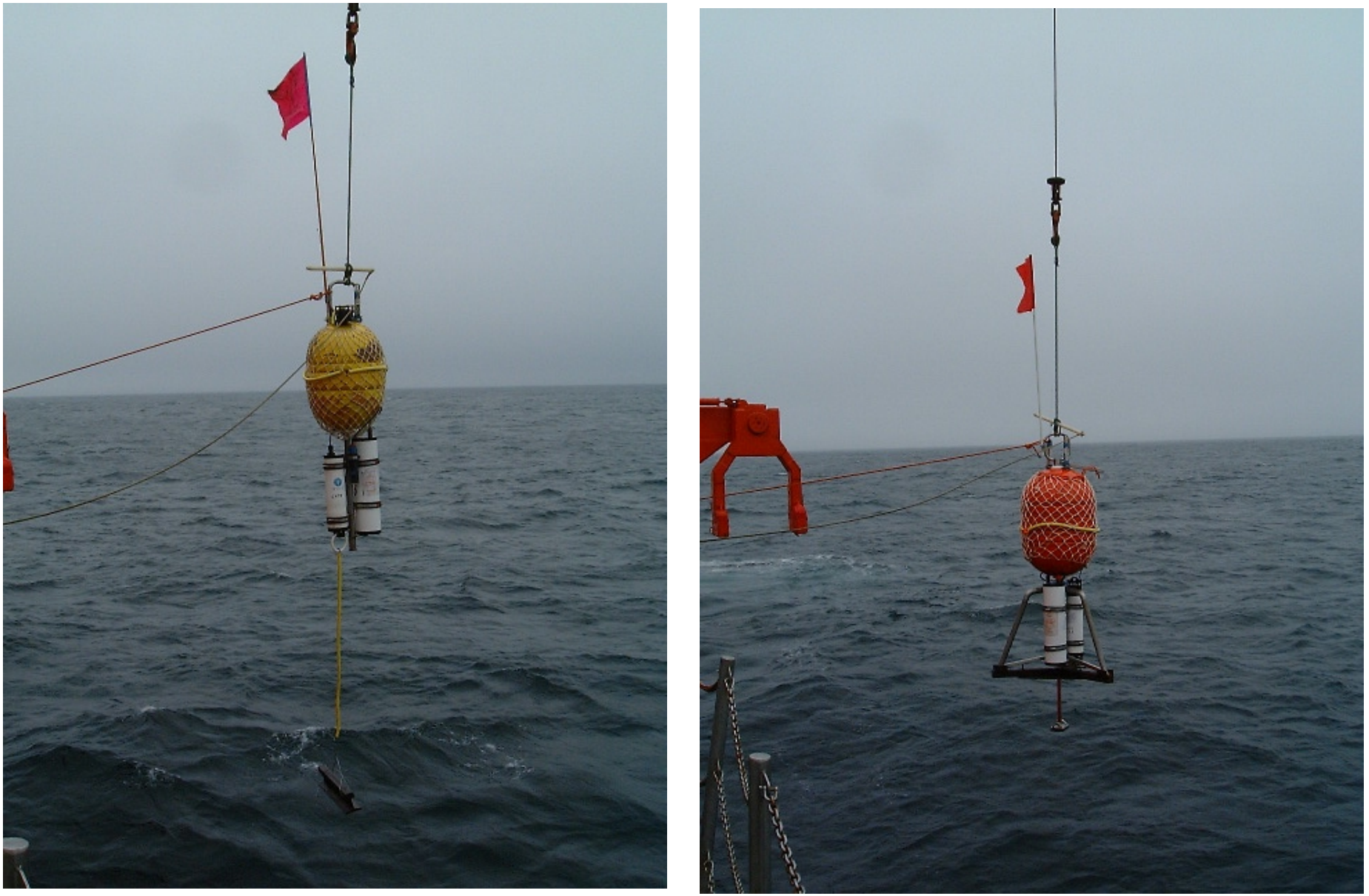

Figure 5.2.1.2: Deployment of an OBH (left) and OBS (right), respectively.

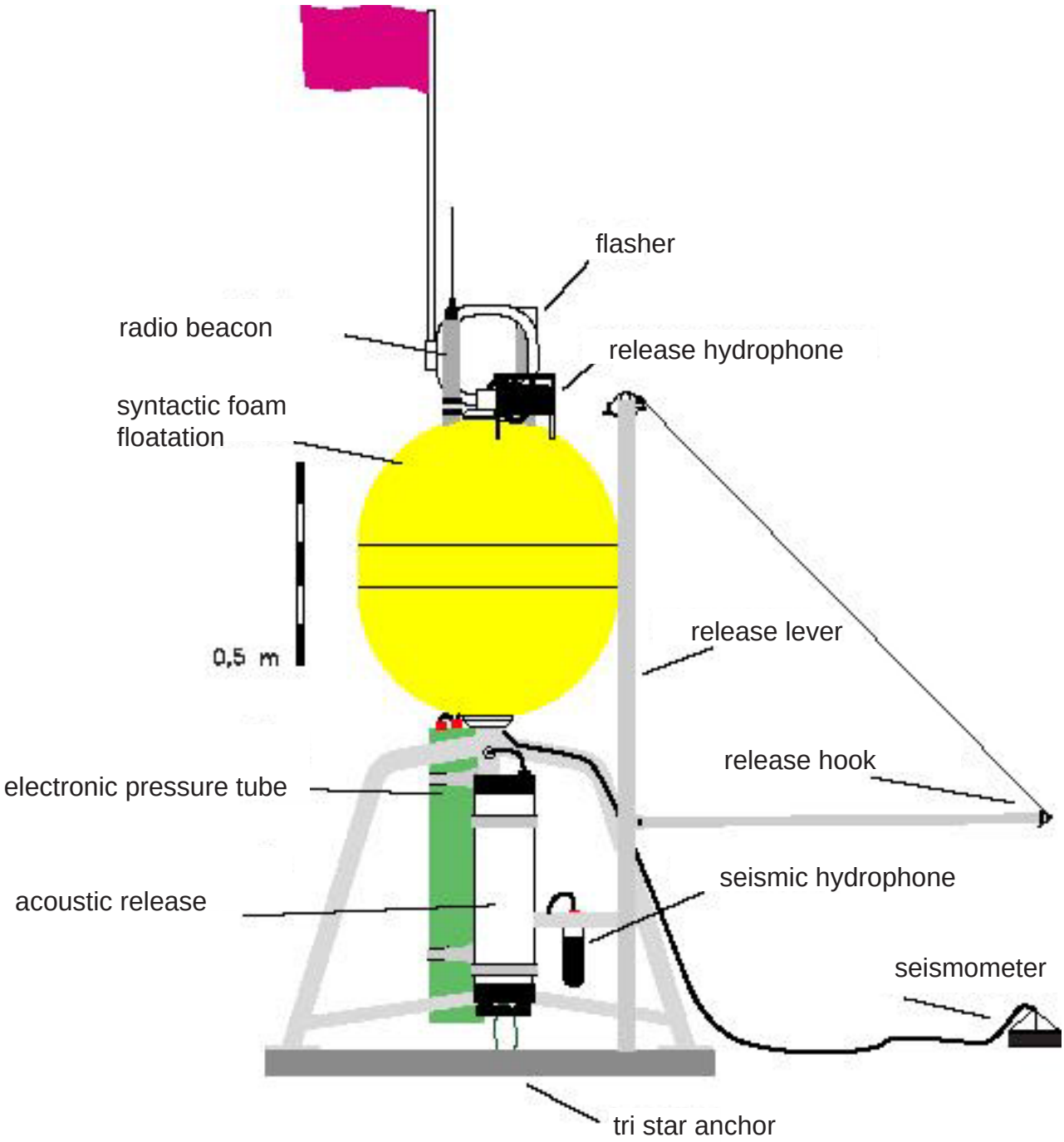

Figure 5.2.1.3: Principle of the GEOMAR OBS (after Bialas and Flueh, 1999).

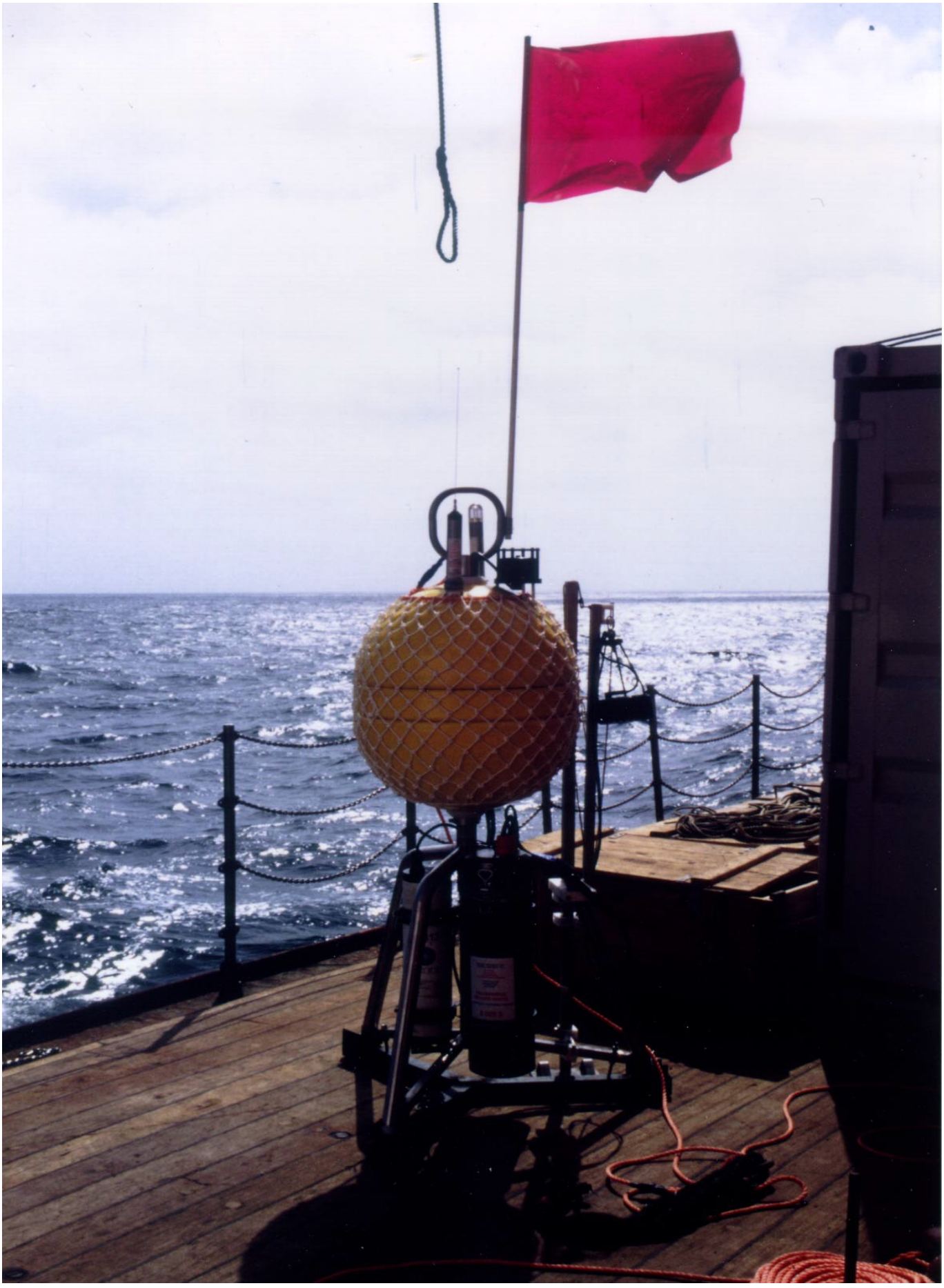

Figure 5.2.1.4: The GEOMAR OBS ready for deployment.

5.2.2 GEOMAR MINI-STREAMER
(J. Bialas)

In addition to the DeepTow and the single channel surface streamer (see Chapters 5.2.3 and 5.2.4), a mini-streamer was onboard to record reflection seismic events. The three channel unit was originally built by Prakla-Seismos, Hannover, Germany for the Deutsches Hydrographisches Institut in 1979.

The system is composed of three parts: A 50 m long active length; a 50 m long stretch length; and a 150 m towing cable. The active length is separated into three groups of 16 HHOC type hydrophones. Construction of the first and third group are identical, while the cantral group has a smaller hydrophone separation. Within group one and three the hydrophones are 1.2 m apart building a 18 m long unit. This results in an antenna directivity which is sensitive to high frequency wavefronts impinging from the near vertical. For this unit, the -3 dB point is found to be at 48 Hz for wavefronts traveling at 90° (measured from the vertical), 66 Hz / 30°, 190 Hz / 11.5° and 380 Hz / 5.7°. The central group is only 6 m long, and consists of 16 hydrophones, each 0.4 m apart. The -3 dB point is found at 110 Hz / 90°, 220 Hz / 30°, 550 Hz / 11.5° and 1.1 kHz / 5.7°. Combined, the three groups have a total directivity of (-3 dB) 18 Hz / 90°, 36 Hz / 30°, 90 Hz / 11.5°, 180 Hz / 5.7°. At the tail a depth sensor is installed which indicates the actual depth modulated as frequency changes. The base frequency at the surface is 990Hz, and increases by 100 Hz/bar (100 Hz per 10 m). Typical towing depth for the streamer is 15 m. The whole unit is stored and operated from a hydraulic winch at the stern of R/V SONNE.

One of the 4-channel-Marine Broadband Seismic recorders (MBS; see 5.2.1) were available for data recording. This unit was chosen to record the streamer signals with a 2.5 kHz sampling interval, resulting in a Nyquist frequncy of 1 kHz. This is well above the theoreticaly achieved sensitivity of the cable, but was chosen as a compromise to the expected higher frequency events from the Sparker, GI-gun, and watergun. In order to suppress the wave state induced low frequency noise (up to 5 Hz) the input impedance of the channel separator was set to 15 Hz. Together with the use of the standard OBH pre-amplifiers, a suitable signal recording was achieved. Unfortunately, disturbances of 50 Hz induced noise could not be excluded during the stay onboard. During inspection of the deck transmission cable, several parts with defective insulation were found. Hence, it is assumed that the major parts of the shield had been destroyed. As a consequence of the limited supply of spare parts, shipboard equipment did not allow complete replacement.

5.2.3 RCM SURFACE-STREAMER
(W. Versteeg, S. Guidard, W. Crescens)

The single channel surface streamer constructed by SIG Technology Instruments (Fig. 5.2.3.1) contains 10 hydrophones, spaced 50 cm apart, which have a wide band (10 to 1000 Hz) and a high output impedance. They are housed in a buyoant tube filled with an inert, highly dielectric, and oxidization resistant oil. To ensure an efficient pressure transmission between the seawater and the hydrophones, a pre-amplifier is installed in the streamer head. It has a multiplication of 39, and is powered by a battery of 600 mA, providing 300 hours of power when charged fully. The signals recorded by the streamer are AC-coupled by a condensator.

The streamer is designed with a slightly negative density, and the desired operating depth is controlled by an air valve system located on the tow cable. To assure a minimum noise level, the maximum tow speed of the streamer must not exceed 6 knots. During acquisition, the streamer was towed at port at about a 20 m distance behind the vessel.

Figure 5.2.3.1: Photograph of the Single Channel Surface Streamer.

5.2.4 RCMG DEEP TOW STREAMER

(W. Versteeg, S. Guidard, W. Crescens)

The deeptow seismic system, developed at the RCMG in Gent and adapted for the SO150 HYDGAS expedition, is primarily composed of a deeptow streamer and a high-pressure ACQ-cylinder connected to the 8000m-long cable of the R/V Sonne by a GISMA-connector containing two analog wires. To avoid the noise originating from the turbulence around this cylinder, it is located 20 m from the streamer head (Fig. 5.2.4.1). The maximum operating depth of the system is about 1500 m below sea level.

An acoustic pulse generated by a surface source, is detected by the deeptow streamer, and recorded with a Methusalem acquisition system situated in the ACQ-cylinder. This system is fed by a 12V battery which is also located in the cylinder. The deeptow streamer is also equiped with depth sensors, and analog depth-signals are transmitted to a depth monitor in the laboratory via the GISMA-connector.

Numerous tests and modifications were performed to optimize the deeptow to its new configuration. Unfortunately, the Methusalem unit showed a lot of DC-biasing impossible to be omitted, resulting in the transmission of the reflected analog streamer signals via the depth sensor cables to RCMG's acquisition system. This configuration has two primary disadvantages. First, there is no "online" control of the submersion depth of the deeptow streamer, and second, only one channel of the multi-channel streamer could be connected at the time. Owing to the wealth of previous tests, it was possible to estimate the deeptow streamer depth as a function of cable length. For instance, a length of 1100 m corresponds to a submersion depth of the deep tow streamer of about 500m bsl (below sea level). As a rule of thumb, the angle between the streamer and the seasurface is about 30°, assuming the vessel's speed is 3.0 kts.

The ACQ-cylinder

A special high-pressure cylinder has been manufactured by McArtney to facilitate the connection between the 8000m cable of R/V Sonne and the deeptow system. This stainless steel cylinder houses the battery-powered Methusalem acquisition and recording system.

The deeptow streamers

The single and multi-channel streamers (SIG Technology Instruments) are constructed of polyurethane 1185A tubing with densities of 1.12 g/cm^3 and 1.15 g/cm^3, respectively. Different hydrophones (8 for a single-channel streamer and 8x4 for the 8-channel streamer) are located inside the tubes. Although optimum immersion depth is 1700 mbsl, they are designed to withstand pressures up to 24 MPa (approximately 2.5 km water depth).

Single-channel streamer

The 11m single-channel streamer (SIG.B.8.1.11) has a diameter of 45 mm and contains 8 hydrophones spaced 1 m apart (Fig. 5.2.4.2). The depth transducer is placed in the compartment at the head of the section (Figure 5.2.4.2). This streamer was used until some oil was found in the pre-amplifier compartment, at which point it was replaced by the multi-channel streamer.

Multi-channel streamer

This 100 m long streamer (SIG.B.8X4.100) contains 8 channels each with 4 hydrophones spaced 0.25 m apart. The depth transducers are located in the compartment at the head and at the tail of the section (Figure 5.2.4.3), but only one depth sensor (at the head) could be connected.

Unfortunately, only one channel could be connected succesfully. Given the experience from previous expeditions, it was decided to connect the channel nearest to the streamer head.

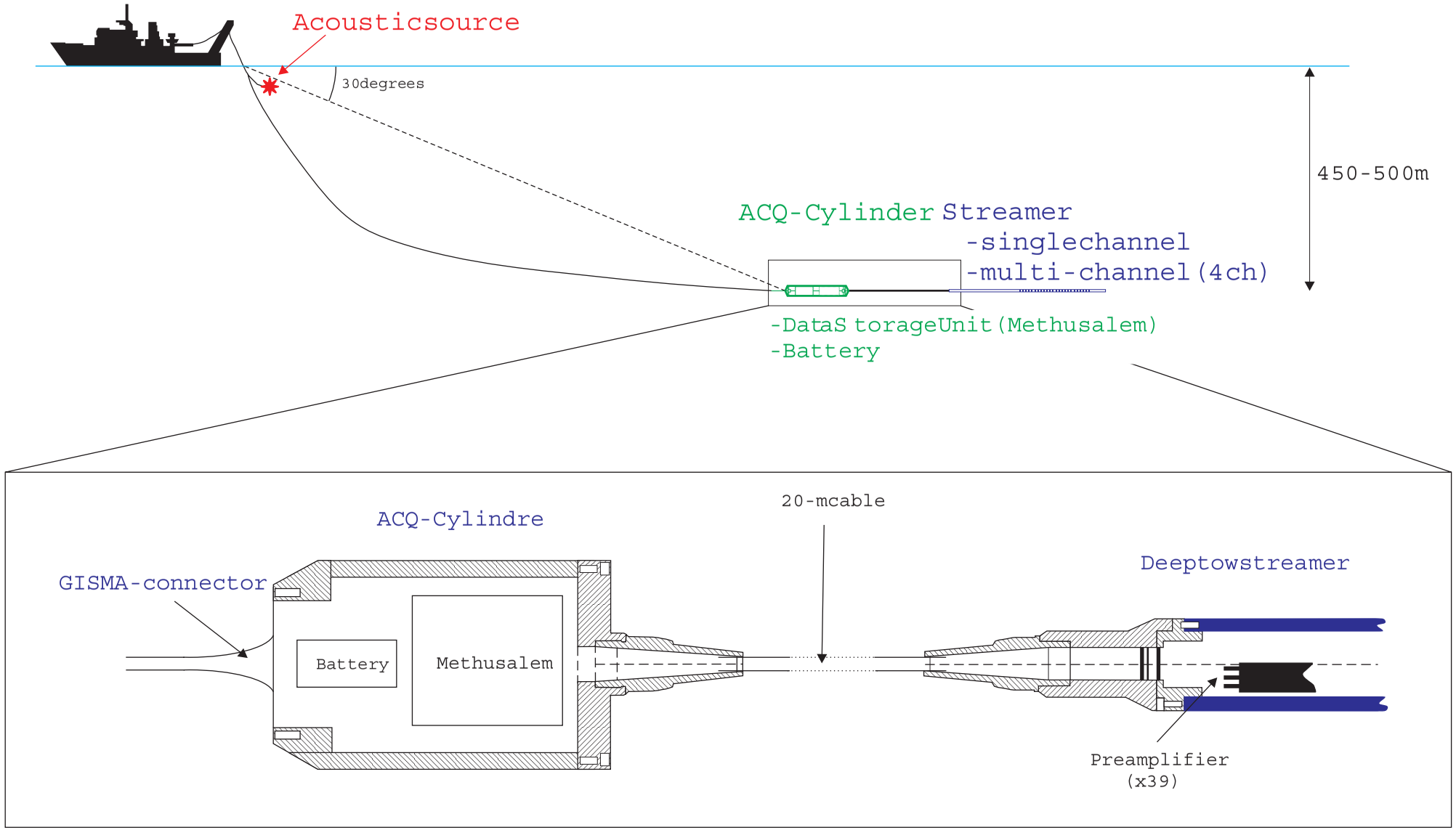

Figure 5.2.4.1: Sketch of the deeptow system.

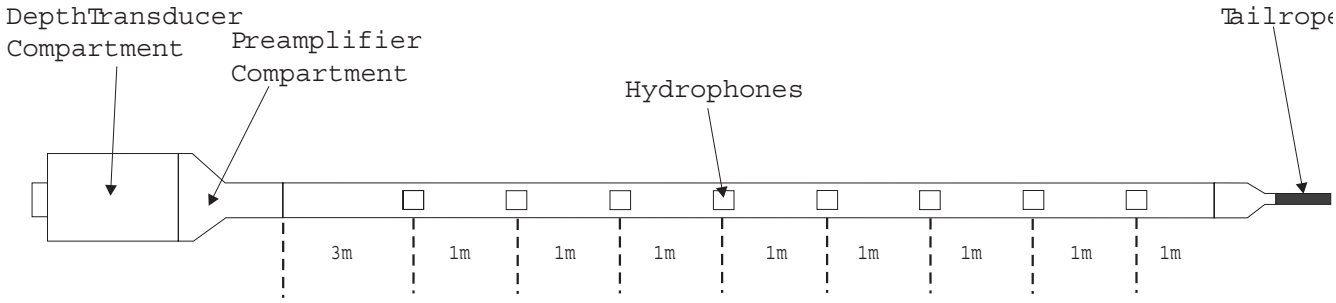

Figure 5.2.4.2: The single-channel deeptow streamer.

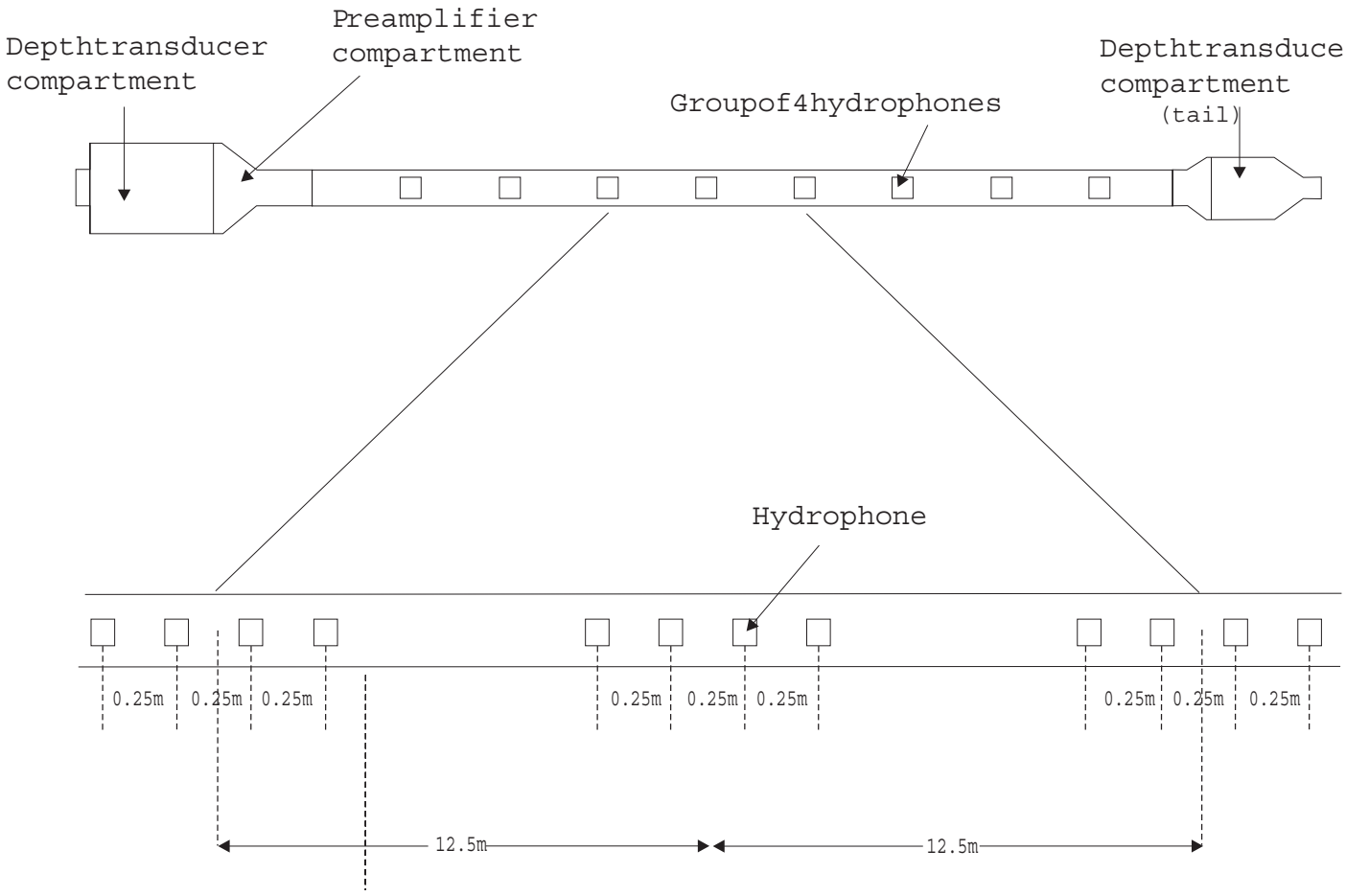

Figure 5.2.4.3: The multi-channel deeptow streamer.

Acquisition System
Streamer signals were recorded on a 24-channel recording and monitoring system (Delph24-system; Triton-Elics) and plotted on a 10 in. thermal Alden 9315CTP plotter. Before the signal is digitized by this system, an analog high-pass filter and built-in adjustable amplifier (Rockland) is used. In two-channel recording mode of the Delph24-system (i.e., recording of both the deeptow and surface streamers) a high-pass filter without amplifier (Teltron) is used for the surface streamer. The maximum gain of the amplifier is 70 dB, which makes it possible to digitize at full scale a 1 mV input signal over 16 bits. The maximum input level (minimal gain) is 3.6 V. All digitized data are stored on the hard disk in a compressed Elics format. This format can be converted to a SEG-Y format by means of a special conversion program.

Navigation information is read from the serial COM2-port provided by the vessel's D-GPS, and placed in the shot-headers of the seismic data. The navigation information can be extracted by the earlier mentioned conversion program and written in a navigation file, where the shot-number is linked to its navigation information.

For quality-control purposes, it is possible to do elementary, real-time processing of the data, such as applying various AGC-modes and bandpass-filtering. In profile mode, these data can be displayed on screen as scrolling seismic information. In addition, a graph of the electrical energy in mV (control mode for one shot) and a FFT-spectrum for one shot can be monitored.

5.3 SEISMIC SOURCES
(J. Bialas)

One of the focuses of this cruise was the examination of gas hydrate reflection events in various frequency bands. For this, up to five different seismic signal sources were used, including 32l Bolt airgun, Prakla 7 gun array with individual volumes ranging from 0.6 l to 2.0 l, a 1.5 l GI-gun, a 0.25 l watergun, and a 5 kJ multi-electrode Sparker (see below).

External Trigger
The trigger signal was supplied from the ship's Ashtech GG24 GPS/Glonass receiver, which can provide a 1 ms long 5 V-TTL pulse at intervals between 0.2 and 999 s. The impulse should be stable to within the accuracy of the GPS Time, which is 70 ns. Shotbreaks, necessary for subsequent data processing and intstrument location, were stored on a MBS recorder and displayed in real time for quality control. For this process, the same procedure as for the OBHs was used (see Chapter 5.2.1) and the trigger signal was converted into a 5 V TTL pulse of 300 ms length by a circuit provided from the ship's technical support staff (WTD). The impulse was delivered to the BOLT Par Airgun Firing Circuit FC300, the Real Time Systems LongShot Seismic Source Controller, the Bolt watergun trigger, the Sparker trigger unit as well as to the Delph-24 and the MBS recording units. All units triggered on the first rising flank of the TTL impulse while the LongShot triggered on the falling flank. Exact position calculation for the shot time was done by post-processing using shot time and UTC time values stored with D-GPS coordinates in the ship's database. From earlier cruises it was known that the coordinates stored within the database were provided by the Atlas ANP 2000 system, which does not copy the exact GPS time values, but adds time stamps of its internal uncontrolled clock to the high precision coordinates of the D-GPS system. Accuracy of the time values mainly depends on the operator's ability to manually set the ANP clock to GPS time. This is clearly a somewhat biased method compared to the efforts of precise positioning. To enable the most accurate GPS related time stamps within the ANP system prior to each seismic survey the system operators were informed to reset the ANP.

Besides the alternatively used sources up to three streamers were towed behind R/V SONNE at one time. The towing configuration of all equipment is shown in Figure 5.3.1.

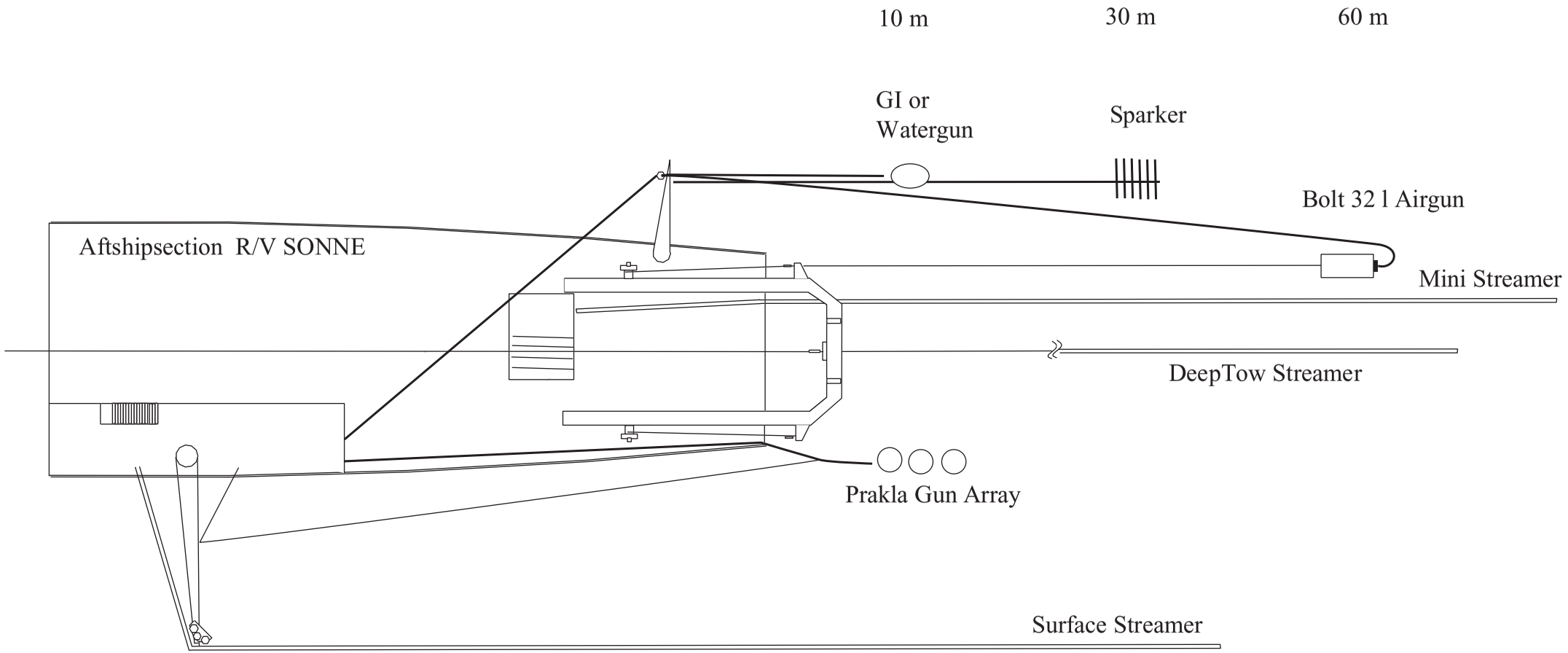

Figure 5.3.1: Sketch of tow configuration at the stern of R/V SONNE
Mini Streamer, DeepTow and Surface Streamer towed together if possible;
Sparker, GI, Watergun, Prakla Array and 32 l gun towed one at a time.

All units triggered on the first rising flank of the TTL impulse, while the LongShot triggered on the faling flank. The resulting shot times are listed in Table 5.3.2.

Source	trigger delay	aim point	total delay
Bolt gun	0	60	60
Prakla array	300	50	350
GI-gun	300	60	360
Watergun	0	17	17
Sparker	0	17	17

Table 5.3.2: Table showing the final delay times summed from trigger and aim point delays.

5.3.1 SPARKER

(W. Versteeg, S. Guidard, W. Crescens)

A Sparker utilizes the discharge of a large capacitor to create an electrical current (i.e., "sparks") between charged electrodes and the surrounding water, vaporizing the water and effectively causing numerous small explosions. Bubble oscillations are minimized by the use of more than one electrode.

During SO150 HYDGAS survey, a SIG multi-tip electrode sparker was used (Fig. 5.3.1.1). This electrode comb consists of 120 electrodes which were fired with a total energy of 500 Joules. This energy was delivered by an EG&G 231 power supply unit and an EG&G 232 trigger unit. The Sparker was triggered by the ships seismic trigger at an interval of 3 s.

The moderate weight of the cable and the electrode comb allows easy handling of the device. The sparker was towed on starboard approximately 25 m behind the ship away from the propeller wash (see Fig. 5.3.1)

5.3.2 WATERGUN

(W. Versteeg, S. Guidard, W. Crescens)

Although the energy for the watergun is derived from compressed air, it does not inject air directly into the water, much like an airgun. Release of a shuttle forces the internal water into the surrounding water at a high velocity, creating a near-vacuum behind it. The implosion, as the displaced water rushes into the void, provides the main seismic source. The absence of gas ensures minimal bubble oscillations. However, one disadvantage is that the signal consists of a low-frequency precursor signal caused by the discharge/exhaust of the water.

During this survey, a S15 watergun (Sodera), with a volume of 0.25 l (15 in^3) at a pressure of 150 bar, was used in a special high-resolution mode (Fig. 5.3.2.1). More specifically, it was towed below a fender at a stable depth of 0.2 m (see diagram) with a specially adapted pressure outlet. Interaction between the watergun signal and its ghost minimizes the precursor signal and maximizes, by positive interference, the high frequencies (frequency band). The gun was triggered at an interval of 5 s via a Bolt-airgun controller by an external trigger provided on R/V Sonne. The gun was towed starboard at a distance of approximately 25 m behind the ship (see Fig. 5.3.1).

Figure 5.3.1.1: Photograph of the Sparker with Power Unit.

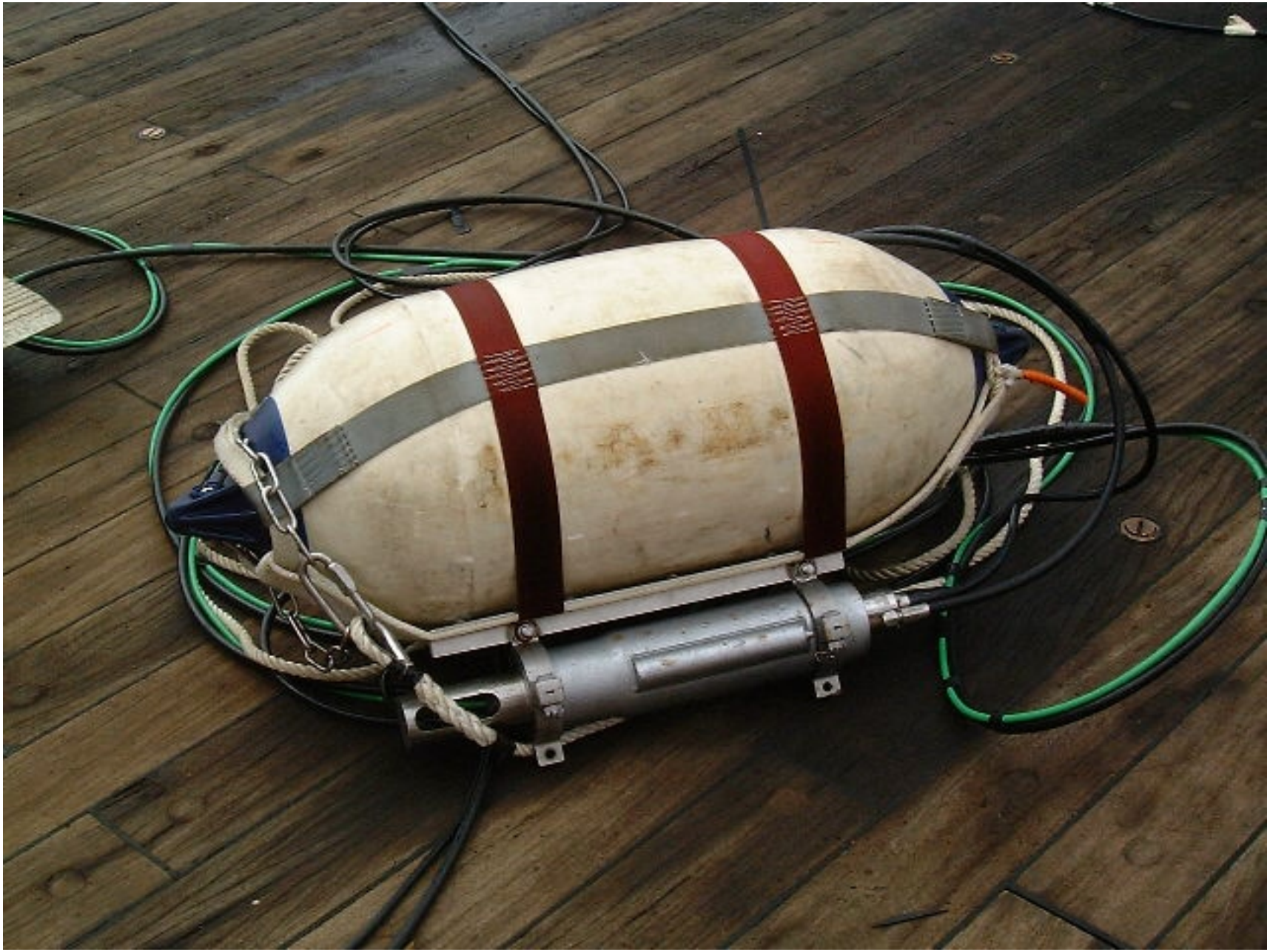

Figure 5.3.2.1: Photograph of the Watergun.

5.3.3 GI-GUN

(J. Bialas)

For SO150 HYDGAS cruise, the Geophysics Group from the University of Bremen provided a GI-Gun (Generator-Injector gun; manufactured by Sodera) for high-resolution surveys shpwn in Fig. 5.3.3.1. Basically a GI-Gun consists of two airguns in one. The first gun, the generator, produces the primary pulse. Depending on the used chamber volume, which can be adjusted by volume reducers, the bubble can be significantly suppressed by triggering the second part of the gun, the injector, after a delay if the bubble collapses. Operation of this gun is very simple, especially as it is unnecessary to pressure it up prior to deployment.

The following GI-Gun configuration has been used:

Mode	Generator Volume (in^3)	Injector Volume (in^3)	Delay (ms)	Discharge Port
True GI	105	105	27	large

The GI-gun was operated through the LongShot seismic source controller where ports 7 and 8 were reconfigured for GI-gun mode. A special software layout, provided by RealTime through GEOMAR accounts, enabled the use of the Prakla gun array (see Chapter 5.3.4) and the GI-gun without major reconfiguration of the control unit. The attached shot break hydrophone was used for automatic shot point adjustment. With the LongShot sensor display, the near field source wavelet was controlled and remained constant over the entire survey. A single gun hanger towed the GI-Gun approximately 10 m behind the ship's stern in a water depth of 2.5 m. Towing depth remained stable due to a fender on top of the gun hanger. Following the recommendation of the Sodera handbook, the gun was operated at a pressure of 140 bar and an shot interval of 7 s, and worked without problems.

5.3.4 AIRGUN-ARRAY

(J. Bialas, K. P. Steffen, K. Neumann)

In addition to the high and low frequency guns, a small airgun array was set up using the airgun slide at port aft of R/V Sonne. The array comprised of 7 Prakla VLA and VLF type guns, with volumes of 2.0 l, 1.2 l, 2 x 0.65 l, and 3 x 0.33l (Fig. 5.3.4.1). Parts of the array were provided on loan from the Institut für Geowissenschaften, Sektion Geophysik, Universität Kiel. Compared to trials undertaken during earlier cruises with R/V Sonne, some modifications in terms of single chamber volume, gun spacing and towing depth were done. As a consequence the frequency content of the array signal could be enhanced and the bubble period could be further suppressed. Single gun volumes and separations are shown on Fig. 5.3.4.1. Towing depth of the array was 2.5 m when three fenders were used as floatation buoys to carry the array. Shooting of the array was synchronized using a LongShot source controller with two FourShot power supplies. Two ports of the power supplies were reconfigured to operate the GI-gun, while the remaining 6 ports were used for the Prakla array. As a consequence, one of the 7 guns was always deployed as a spare. The source controler read the sensor signals submitted from each gun at shot release to synchronize the individual shot delays to the same aiming point with an accuracy of 1 ms. The array was operated at a pressure of 140 bar and a shot interval of 10 s. Despite problems with irregular sensor signals, all guns operated without major failures.

Figure 5.3.3.1: Photograph of the Sodera GI-Gun

Easily visible are floatation and gun hanger
The source hydrophone is mounted to the side of the gun.

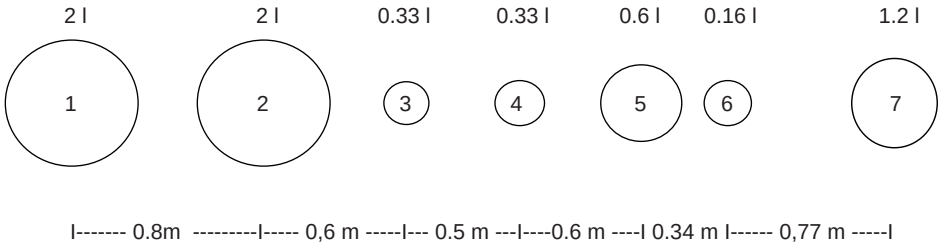

Figure 5.3.4.1: Configuration for Prakla Type Airgun Array
Guns were towed at 2.5 m depth.

Figure 5.3.4.2: Photograph of the Prakla Type Airgun Array.

5.3.5 32L BOLT-GUN

(J. Bialas, K. P. Steffen, K. Neumann)

The seismic signals of the lower frequency band were generated by one of three Model 800 CT BOLT airguns (one on loan from UTIG); a photo of one of the guns is shown in Figure 5.3.5.1. Each gun has a volume of 32 l (2000 in^3), and generates a signal with a main frequency centered around 6 to 8 Hz, including higher harmonics. The pier winch towed one gun at a time attached to a block on the A-frame. The other two guns were available in case of gun failure. Trigger cables and airhoses were deployed manually. Each gun was suspended on two fenders with an additional float attached to the supply lines to prevent contact between the gun and the towing wire. With several streamers operating at one time, the gun in operation needed to be towed further to starboard in order to give way for the GEOMAR mini streamer deployed through the A-frame centre. Since the DeepTow was operated on the LWL cable through the pulley in the centre of the A-frame, all other equipment was shifted to the sides to prevent a collision with the deep sea cable. As requested on previous cruises, an elongation of the small starboard aft crane would have helped significantly to improve the towing capabilities. A sketch of the towing configuration is shown in Figure 5.3.1. The gun was towed 60 m behind the vessel and operated at 140 bar in a 7 to 8 m depth. While onboard the guns were stored inside the A-frame, allowing them to be launched without using an additional winch. Handling of the guns was smooth at all times, mostly owing to the newly molded bold eyes on the guns that facilitated secure handling by the crew. The recent modifications on deck (closing the slip) provided an easier launch and recovery operation compared to earlier cruises (e.g., SO103 cruise; Flueh et al., 1995). Water currents required the ship to be turned out of the sailing direction which reduced the available space for towing equipment at the aft. On several lines the GEOMAR mini-streamer could not be deployed as there was no space left between the gun and the deep sea cable. Again an elongated boom could have helped to span the towing cable and provide a larger distance between the starboard gun and the midship-operated deep sea cable. However, the small boom used to lower the core carrier on starbord and the magnetic boom on port were used to hold pressure hoses and streamer cables farther to the side, preventing them from being damaged. This configuration is probably not appropriate during weather conditions with a high sea state. Booms at the aft are necessary to further spread the towed equipment away from each other. Other than during regular wide angle surveys the gun was shot at a 17 s interval. This was well within the capability of the ship's compressor system, which worked smoothly and caused no delays or interruptions despite only one of the Leobener compressors was available.

5.3.6 DROP WEIGHT

(J. Bialas, K. Steffen, K. Neumann)

One focus of SO150 cruise was to generate low frequency dispersive waves in an effort to see if those events could be induced by other means than a 32 l airgun. It would be most advantageous if energy could be released directly at the seafloor with the additional chance of direct release of shear energy. For test purposes a retired gravity core weight of 3 tons was provided by GEOMAR as a drop weight source (Fig. 5.3.6.1). The weight was connected to the ship's Geo-winch and lowered into the water 60 m above the seafloor. From this height the weight was lowered at 1.5 m/s, the maximum operational speed of the winch, until the weight hit the ground. Touchdown of the weight was controlled by the cable tension display and by use of a bottom pinger connected to the cable 50 m above the weight. Shipboard SSBL transponder navigation enabled the position control of the weight. Spending an additional 10 m of cable after each dropping event ensured that only a single signal was released, while subsequent smooth touches due to heave of the vessel were suppressed. After lifting the weight, this procedure was repeated

Figure 5.3.5.1: 32 l Bolt PAR 800 CT airgun.

Figure 5.3.6.1: 3 to. weight of a core sampler used as drop weight source.

three times until the vessel moved further along the profile. As this was a first trial to check if there is sufficent energy released to be recorded on nearby OBHs and OBSs no attempts were undertaken to construct a trigger mechanism. Seismic signals will be detected based on the timing of the tension release which was noted by hand and also stored digitally in the ship's navigation data base.

5.4 THE MAGNETOMETER
(I. Bode, J. Bialas)

A Geometrics G801/3 Proton Precession Magnetometer was used during Cruise SO150 on transit from Long Beach, U.S.A., to Bridgetown, Barbados. The magnetometer uses a gasoline-filled sensor with a 300 m marine cable and a control unit. During the measurement procedure, an electrical current is generated during the first of two cycles. A body made of three interconnected coils transfers the current to the marine cable. Each coil is oriented at angles of 120° to its neighbours. The magnetic field of the coilbody forces the protons in the gasoline to align in the same orientation. When the current is turned off before the second measurement cycle, the magnetic field of the coilbody ceases, leaving the protons to realign to the Earth's magnetic field (for the transit area off Costa Rica, this is in the range of 39.000 to 42.000 nT). At this time, the precession of the proton's spin reaches a frequency that is directly proportional to the intensity of the Earth's magnetic field. This frequency can be measured as a very small, AC electrical current created by magnetic induction in the coil. The current is measured, amplified, counted, transformed to magnetic field intensity values and recorded with a precision of 1 nT. To reach this precision, it is necessary to minimize the influence of any artificial magnetic field, especially the effect of the ship's metal hull. Thus, the sensor was towed 300 m behind the ship (i.e., approximately 3 ship lengths distance) by a winch having been installed port on the aft deck of R/V Sonne. Measurement's results together with UTC time have been stored every 3 s via a digital multiport with customized software.

After data backup, the files were resampled to 10 s intervals and coordinated with the ship's navigation GPS-coordinates (for aditional information, see Section 5.5.3 on navigation of this cruise report). After median filtering, data were displayed using GMT plot routines.

5.5 SHIPBOARD EQUIPMENT

5.5.1 HYDROSWEEP
(M. Spinner, N.A. Müller)

For continuous bathymetric profiling, the HYDROSWEEP multibeam system from STN ATLAS-ELEKTRONIK was available onboard R/V Sonne. Using a frequency of 15.5 kHz and 59 beams in a swath of 90°, it can map the seafloor with a scanline width of up to twice the water depth. Range of the central beam is up to 10000m with an error of 1% and for the outer beams up to 7000 m with a precision of about 1% if the roll is less than 10° and the pitch is less than 5°. Corrections for roll, pitch, and heave are automatically applied. Due to the fixed angle between beams, coverage is a function of the water depth, and varies from about 170-200m in depths of 5000-6000m.

To calculate depths from echo time delays, the velocity of sound in the different water layers is required. HYDROSWEEP uses a second set of transducers and a calibration scheme with soundings along track to determine an average water sound velocity profile (Schreiber and Schencke, 1990). However, in certain areas this algorithm fails (von Huene and Flueh, 1994), so direct measurement of sound velocity at different depths using a CTD is required to improve the results.

Postprocessing of HYDROSWEEP data includes merging of navigational data, calculation of depth and positions of the footprints of the beams, removal of artifacts and erroneous datapoints, and generation of a digital terrain model (DTM). The ATLAS HYDROMAP software, based on the CARIS software package, is available onboard for that purpose. However, for several reasons outlined in von Huene and Flueh (1994) and Weinrebe (1997), the academic software MB-System (Caress and Chayes, 1996) from Lamont-Doherty Earth Observatory is used for HYDROSWEEP data processing.

5.5.2 PARASOUND

(F. Landerer)

The PARASOUND sub-bottom profiler is a seismic system which measures the internal geological structures of the sedimentary cover along the ship's track. It utilizes the so called parametric effect, which produces additional frequencies through non-linear acoustic interaction of finite amplitude waves. If two sound waves of similar frequencies (e.g., 18 kHz and 22 kHz) are emitted simultaneously, a signal of the difference frequency (e.g., 4 kHz) is generated for sufficiently high primary amplitudes. The new parametric component is emitted within a cone of a 4° opening angle. Therefore, a seafloor area of approximately 7% of the actual water depth is covered. Although this helps to achieve a high vertical and lateral resolution, no signals from the seafloor or sedimentary layers dipping more than 2° are returned to the receiver due to the narrow cone of 4°: This restricts the successful application of PARASOUND to relatively flat areas.

The PARASOUND system is permanently installed on R/V Sonne, and operated on a 24-hour watch schedule. The hull-mounted transducer array has 128 elements within an area of 1 m^2, requiring up to 70 kW of electric power due to the low degree of efficiency of the parametric effect. In two electronic cabinets, beam formation, signal generation and the separation of the primary (18 and 22 kHz) and secondary frequencies (4 kHz) are carried out.

Since the two-way travel time in the deep sea is relatively long compared to the length of the reception window (up to 266 ms), the PARASOUND System sends out a burst of pulses at 400 ms intervals, until the first echo returns. The coverage in this discontinuous mode is dependent on the water depth and produces non-equidistant shot distances between bursts.

The main tasks of the operators are system and quality control as well as adjustment of the reception window. Because of the limited penetration of the echosounding signal into the sediment, only a short time window close to the seafloor is recorded.

The PARASOUND System is equiped with the digital data acquisition system ParaDigMA, developed at the University of Bremen. The data are routinely stored on removable hard disks using the standard, industry-compatible SEGY-format. Of the emitted series of pulses, usually only every other pulse can be digitized and stored, resulting in recording intervals of 800 ms for a given pulse sequence. Back-up storage of the data were made on DAT-tapes using Unix software.

5.5.3 NAVIGATION

(J. Bialas, G. Klein)

An integral part of marine surveys is the collection of precise position information (latitude, longitude, altitude above/below a reference level). Since 1993 the global positioning system (GPS) is commercially available and widely used for marine surveys. 24 satellites operate in

synchronous orbits, with at least 3 satellites visible anywhere at any moment (Seeber, 1996). The full precision of this originally military service yields positioning accuracies of a few meters, yet is restricted to military forces and usually unaccesible to commercial users (Blondel and Murton, 1997). For civilian purposes the precision is in the order of 100 m.

More accurate positioning can be obtained by utilizing the Differential GPS (D-GPS) service (Blondel and Murton, 1997; Knickmeyer, 1996). D-GPS uses several reference stations to determine the ship's position in real time and enhances accuracy from 1-5 m. Since cruise SO-109 (Herzig et al., 1997), D-GPS service has been available onboard the R/V SONNE. The ship's ASHTEC system provides a validated accuracy better than 5 m in the area of the HYDGAS investigations.

D-GPS values were available from the ship's navigation database and were extracted using a PC based end user interface program. This program allows the user to select the desired variables from the ship's sensor values and specify the output formats. The volume of data can be controled by adjusting the interval of extracted values which can be as short as 1 s. Stored on the 'wiss-data' directory, the extracted ASCII file is accessable from every workstation connected to the shipboard network via ftp or volume access. Surprizingly, the output data format seperates decimal values by a colon instead of the standard American dot notation. According to the ship's system operator, this is due to the chosen set up of the desktop program on the PC. Therefore, a reformating program must be written prior to further computaional use of the values.

From earlier cruises it is known that the coordinates stored within the database were provided by the Atlas ANP 2000 system. This system does not copy the exact GPS time values but, adds time stamps based on its internal clock to the high precision coordinates of the D-GPS system. Accuracy of the time values is mainly dependent on the operator's skills of manually setting the ANP clock to GPS time. This is a somewhat crude method compared to precise positioning. Prior to each seismic survey the system operators were informed to reset the ANP to insure accurate GPS related time stamps within the ANP system.

In the continuing effort to maintain accurate and quality service, the system operator onboard the R/V SONNE provided a new method for coordinate extraction from the ship's database. An email service was established which provided the requested time interval via ftp on the 'wiss-data' directory. The 'wiss-data' file system is available throughout the entire shipboard network and therefore the coordinate files could easily be copied via ftp into the GEOMAR Sun computers. This service required remarkably less time than the manual extraction via the WERUM database front end. To retrieve the coordinates from the system the user need only send an email with the necessary commands:

to: dvsadm@sonne.rf-gmbh.de
subj: nav
message:
start 23.09.2000 22:10
end 24.09.2000 23:00
line line-name
ftp

The user will find the requested data as ASCII file within the 'wissdata' directory under:

"\wissdata\navdata\line-name.nav",

which from where it can be transferred via anonymous FTP(login ftp) from the wissdata server NTIX (192.1.2.242).

The knowledge of the actual position of the vessel, related to way points and stations of deployment, is important for most scientific experiments. This information was made available for all scientific crew as a set of images accessable by web browsers from any computer linked to the shipboard or GEOMAR networks. The system manager provided the raw NMEA D-GPS strings (GPGGA/GPVTG) in the Reinlabor, where a Linux-PC was logging and evaluating the information for the current position of the vessel, ship speed, and distance to the next way point. This was accomplished by a shell script program using the Generic Mapping Tools (GMT). The ship's track of the previous hour is displayed in two different scales, one being fixed to cover most of the study region, and the other adjusted to the current operation requirements. The scale for the adjustable range plot as well as the list of way points and currently deployed stations was maintained on the Linux-PC in the hydroacoustics laboratory and incorporated into the online track charts. A feature to start and end the seismic profile navigation log from the hydroacoustics PC was also implemented into the package.

5.5.4 NETWORK-CONNECTIONS

(J. Grigel, J. Bialas)

Onboard R/V SONNE, a Switched 10/100 MBit Twisted Pair network is operative (Fig. 5.5.4.1). The heart of the network is the Zeichenraum, the office of the system operator, where all the server computers are housed. From here, all network connections are distributed over the vessel. A 3COM 3300 Swith (24 ports) serves as a connecting device for the single laboratories. At this level, each individual laboratory is connected by its own Twisted Pair cable. The unused wires of these cables are used for a second connection. NT server, Linux data base server, Linux gateway and Linux printserver are connected through private ports at the switch. Within the laboratories, 10 Mbit-hubs are available for local PC connections, while 100 Mbit-hub or DualSpeed-hub are optionally available. The second connection established with the spare cables is used to directly interconnect laboratories.

Cabins on third deck level are also connected to the ship's network using a 100Mbit-hub, which is located in the ship's office. A Linux mailserver, located in the radio operator's room, is also incorporated via this hub. Hubs in the geology and seismic laboratories have a follow up link from other labs (magnetics, chemistry). The connections to other individual cabins are anticipated to be installed during the next yard servicing period.

There are still BNC connections in use, which are serving for four Vax computers and several DEC terminal servers. A second BNC connection is available for the three Hydrosweep HP workstations, while another two connections are available for auxiliary tasks. A serial 25-wire cable is used to distribute GPS outputs into the laboratories.

Across this cable, a Windows-NT-Server-network with approximately 30 NT workstation clients is operated. In addition, ten Linux PC, four MicroVax (navigation), three HP workstations and about a dozen DOS/Win9x and other operating systems are served. One of the Linux computers serves as Gateway, and is routinely updated with the IPs of the scientist's computers without any reconfiguration. The same unit is operated as a DNS server, and incorporates the names of the GEOMAR computers into the shipboard network successfully.

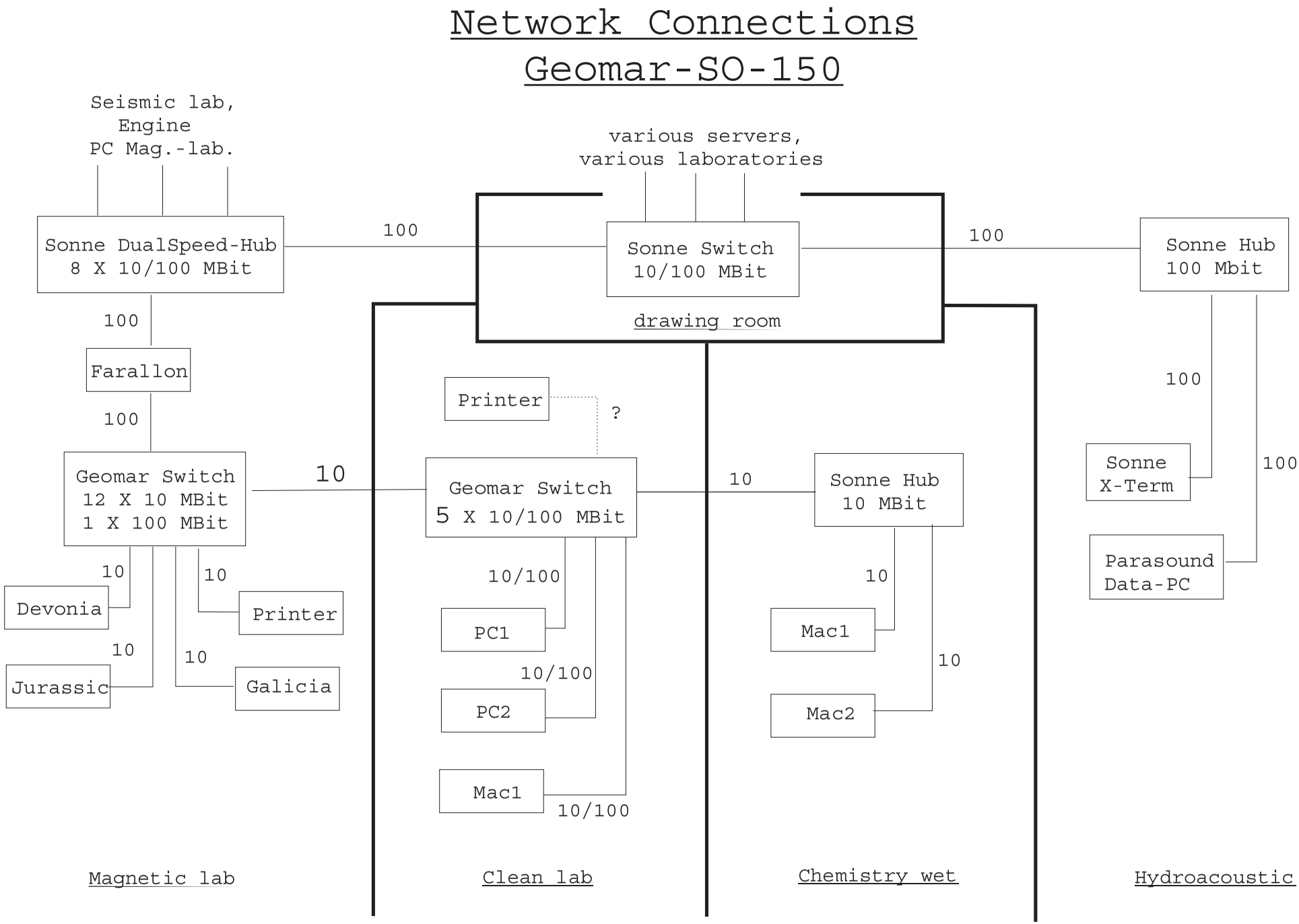

Figure 5.5.4.1: Network Connections Onboard R/V SONNE.

Parameters of the Class-C-subnet are:
Network address: 192.1.2.0
DNS-Domainname: .dfcg
Default Gateway: 192.1.2.2 (FQDN: gatenix.dfcg)
= DNS-Server
= NTP-Server
(= Router)
NT-Server: 192.1.2.242 (FQDN: ntix.dfcg)
= Primary Domain Controller der NT-Domain DFCG
= WINS-Server
= DHCP-Server
Mailserver: 192.168.2.100 (FQDN: sonne.rf-gmbh.de)
= SMTP-Server
= POP3-Server
= HTTP-Server (Webmail-Frontend)

Geomar route (Domain geodynamik.geomar.de) was set to IP 192.1.2.205, which is established as static route into network 193.174.124.0 on the Gateway.

A Linux-PC (caesar.dfcg, 192.1.2.223) operates as lpd print server, which enables 7 HP network printers (3x LJ4, 1x LJ5000, 1xDJ2500, 1x DnJ650C, 1x DnJ750C) to be accessable from the Linux domain by special filter queues. In addition, this server provides access to the printers and disks of the NFS server for Macintosh computers by Appletalk/IP. This server is also responsible for providing the home account of user wiss on the DualBoot NT/Linux PCs.

5.5.5 SSBL-TRANSPONDER

(J. Bialas)

The knowledge of the precise position of equipment towed behind the vessel is one of the crucial tasks in marine seismic surveys, and hence requires particular technical solutions. While one is not short of solutions for surface equipment, subsurface towing makes positioning a challenging endeavour. In the absence of GPS and RADAR support, acoustic solutions have to overcome the unknown parameters, e.g. depth of a deep tow streamer. For short range operations, R/V Sonne is equiped with a Simrad Super-Short-BaseLine (SSBL) system. Depending on the capabilities of the deployed system, a responder could be installed or, when space is limited, a transponder can be mounted onto the deep sea cable. The responder has the advantage that the requested ping is transmitted directly through the deep sea cable, so that the distance between the towed system and the vessel is passed only once. In contrast, the transponder is activated by a primary ping sent through the water column and then responds. Given the responder system requires half the travel distance of the transponder, the precision of the former is superior. A hull mounted receiver detects the pings from the underwater unit and calculates distance, azimuth and depth from this information. These values are related to the ship's GPS position, and get stored later as calculated geographical coordinates in the ship's navigation data base (together with a sensor and position status digit). Due to their geometric design, the hull-mounted receivers can only operate within a certain receiver cone. Due to the vertically mounted transducer onboard R/V Sonne, the opening of this cone has a symmetrical downward orientation. As a consequence, the transponder is best operated when located underneath the vessel. The farther the offset (when operating the transponder behind the ship), the sooner it will be located at the outer limits of the receiving cone. Then, relocation lacks precision, or may even fail.

The SSBL system was used with the deep tow streamer to ensure accurate location of its position. As there is no larger system carrier or depressor attached to the system, the more precise

responder system with its fibre optic link could not be installed, and we had to refer to the transponder. The unit was attached 50 m above the streamer connection. Transponder readings were recorded with 500 m and 1000 m of cable length.

Figure 5.5.5.1 displays the transponder readings from this run. For this purpose the database was checked for transponder values with good sensor and position status values. Sensor status values were either 3, 'no data available' or 4, 'some data available'. The position data status was either 1, 'no data were available', or 0, 'some data were available'. It turned out that those were only available from the 500 m cable measurement, meaning the transponder was out of range when 1000 m of cable were used. The remaining values do show severe data gaps (Fig. 5.5.5.1) within which the status values are not trustworthy. In general, the good values are consistent over time. However, there are still incorrect values enclosed which result in a distance larger than the allowed cable length. Systematic re-evaluation of the results is needed, so that the depth information only serves in addition to other information (e.g., travel times, compasses, depth sensors, etc.). Heavy depressors will help to locate the deeply towed unit closer to the vessel, and therefore will enhance the depth range in which the SSBL can successfully be used.

During cruise SO150, the deeptow streamer was mainly operated at a 1000 m cable length. Given this exceeds the operating range of the SSBL system, we did not go further from the tests described above.

Displayed are only transponder measures with good system status. Origin of the arrows are the calculated transponder position. Length of the arrow is the calculated horizontal distance between transponder and vessel. Azimuth of the arrows represent the calculated direction from the transponder to the vessel. Azimuth of the arrows have been rotated 90° clockwise for better display purposes

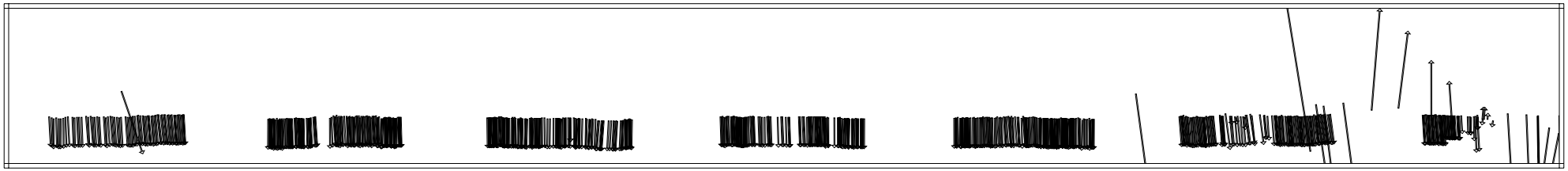

Figure 5.5.5.1: Positioning of the DeepTow streamer using the Simrad SSBL Transponder

Displayed are only transponder measures with good system status
Origin of the arrows are the calculated transponder position
Lenght of the arrow is the calculated horizontal distance between transponder and vessel
Azimuth of the arrows represent the calculated direction from the transponder to the vessel
Azimuth of the arrows have been rotated 90ß degrees clockwise for better display purposes.

6. THE EXPERIMENTS UNDERTAKEN

6.1 MULTIBEAM SWATH MAPPING

(M. Spinner, N.A. Müller)

Multibeam bathymetry was continuously recorded during the entire cruise, including the transit to Bridgetown, Barbados.

Given that a detailed bathymetric chart of the area already exists, the hydrosweep acquisition was not a main goal of the cruise. Nevertheless, it was an alternative to the delicate seismic measurements in poor conditions. As a result of bad weather, a closer mapping of the area south of the Hydrate Ridge between 44°26.4'N/125°21.0'W and 44°18.0'N/124°45.0'W was undertaken. In a first step, data were acquisitioned in a quite coarse grid (1.2" distance between the profiles). In order to achieve a close overlapping of the profiles at all depth ranges, acquisition was completed by further measurements with a finer grid (1/3 of the earlier spacing) at the end of the HYDGAS cruise.

The hydrosweep data were processed onboard using the MB software developed at Lamont-Doherty Earth Observatory (Caress and Chayes, 1996). Postprocessing of hydrosweep data included a merging of navigation data, a calculation of water depths and positions of the beam's footprints, removal of artifacts and erroneous datapoints and the generation of a Digital Terrain Model (DTM).

The raw data were converted to depth by complete ray tracing through the different water layers. The sound velocity profile measured by the CTD probe on 20-SEP at 44° 27.3'N/125°21.0'W acted as a reference (Fig. 6.1.2). MB-Clean, a MultiBeam-System module, was used for a first filtering of the data, the remaining erratic points were elliminated by manual editing afterwards. Edited sweeps were assembled, gridded and contoured with the GMT software (Wessel and Smith, 1995). To visualize the fine tectonic grain no further filtering was applied, making it possible to estimate the quality of the data. Figure 6.1.1 shows a contour plot of the area south of Hydrate Ridge surveyed during SO150.

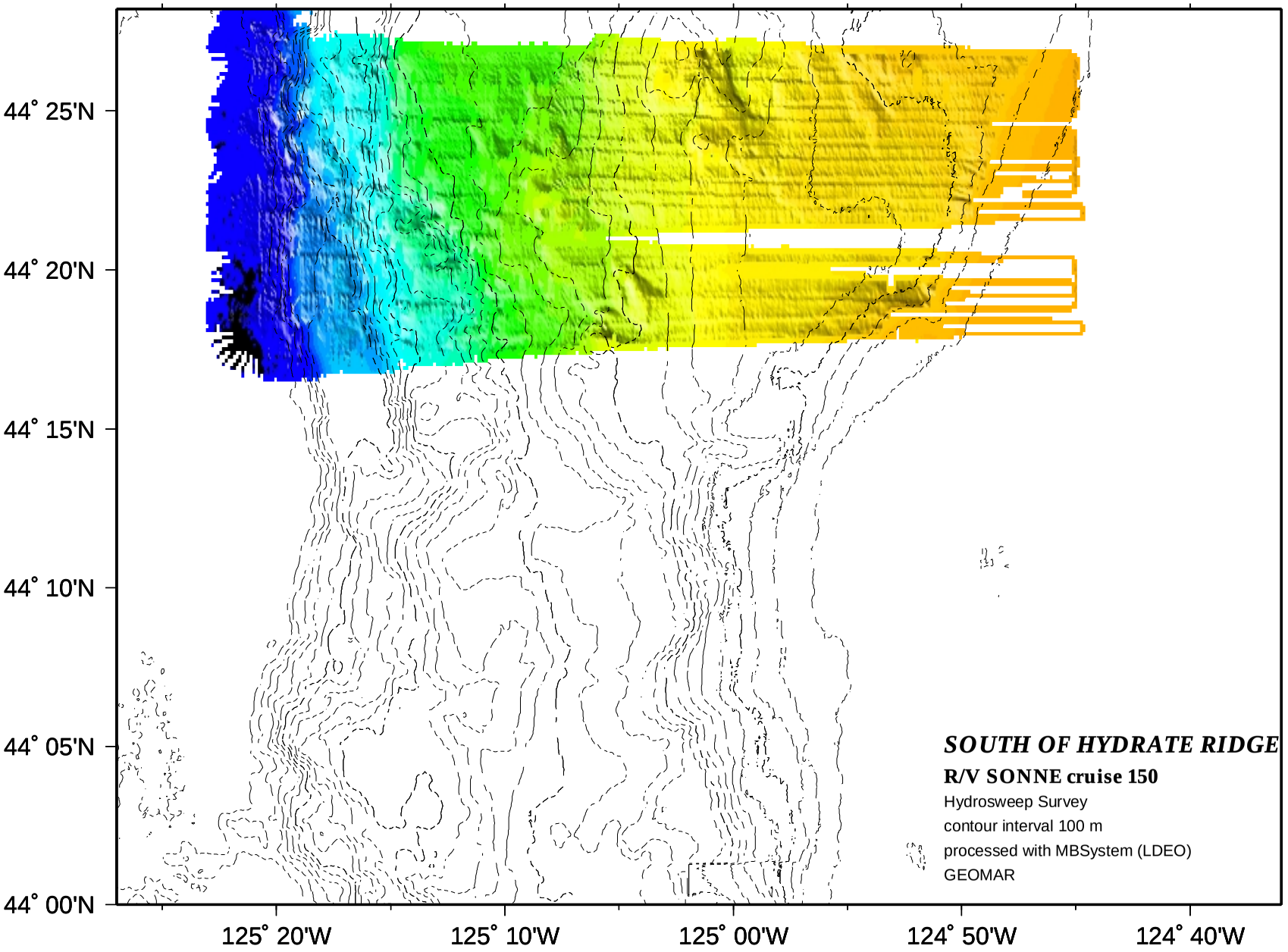

Figure 6.1.1: Bathymetrical contour plot of the area south of Hydrate Ridge surveyed during SO150.

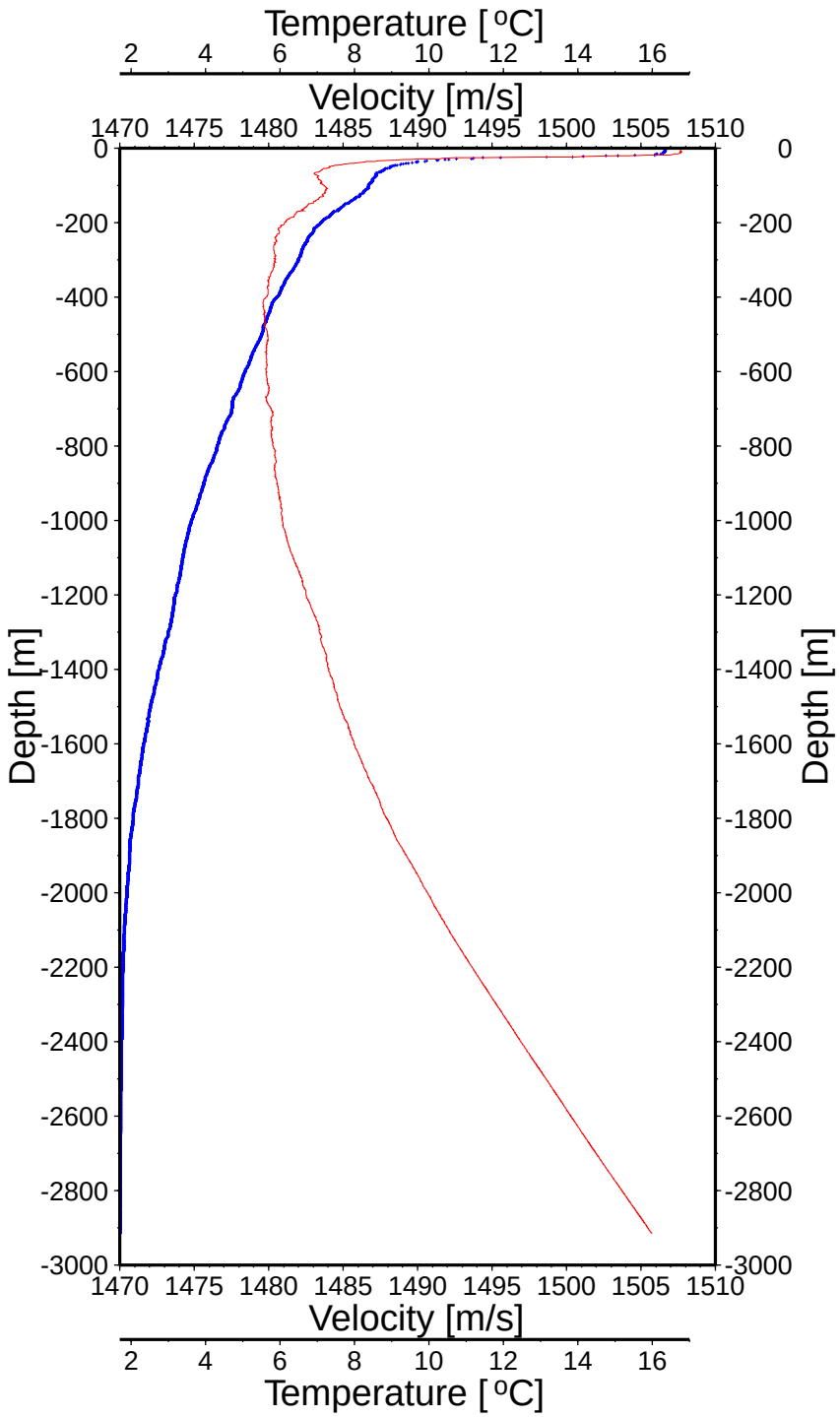

Figure 6.1.2: Water velocity and temperature profile from CTD
Values are read during rising of the CTD.

6.2 PARASOUND

(F. Landerer)

In order to achieve high resolution images of the uppermost sedimentary layers of the seafloor, PARASOUND surveys were conducted along all seismic lines. The data were recorded digitally using the PARADIGMA system and printed online on a colour printer. Where the seafloor slope angles were sufficiently small (usually <2°), data quality was satisfactory throughout the survey. The images show a maximum penetration of 60-70 meters below the seafloor, especially in poorly consolidated sedimentary sequences. However, accreted, partly consolidated or cemented areas had both poor resolution and penetration. All depth values have been computed from travel times assuming a constant velocity of 1500 m/s. The recorded raw data could not be processes onboard, because the necessary software is unavailable. However, the data will be processed post-cruise to improve resolution.

The Parasound images presented in this section have been selected to give an overview of the quality and scientific meaning of the data. Other examples are found in the various chapters of the report, e.g. Fig. 6.3.4.4 (Pinnacle structure) or Figs. 6.3.6.2 and 6.3.6.3 (southern pockmark field).

The first example (Fig. 6.2.1) shows a section of seismic line P124, comparing the images collected by PARASOUND and the GI-gun recorded with the deep tow streamer. Two blank zones are clearly visible in the Parasound echo, underneath small topographic elevations on the gently dipping slope, whereas the deep tow image shows diffraction hyperbolas at these locations. Hence, it remains unclear whether the blurred white patches indicate the presence of free gas, or whether they are artifacts owing to the topography with which the Parasound system cannot cope. Seafloor and upper sedimentary structures are resolved in much more detail with the Parasound system, limited, however, to a penetration depth of about 30 m. The BSR has not been imaged with the PARASOUND system. Blank zones were encountered on numerous other profiles (e.g. Fig. 6.2.2), with the seafloor-parallel layering of the sediment disturbed, or unresolved. Reprocessing of the digital data onshore may allow refinement of the images for further interpretation.

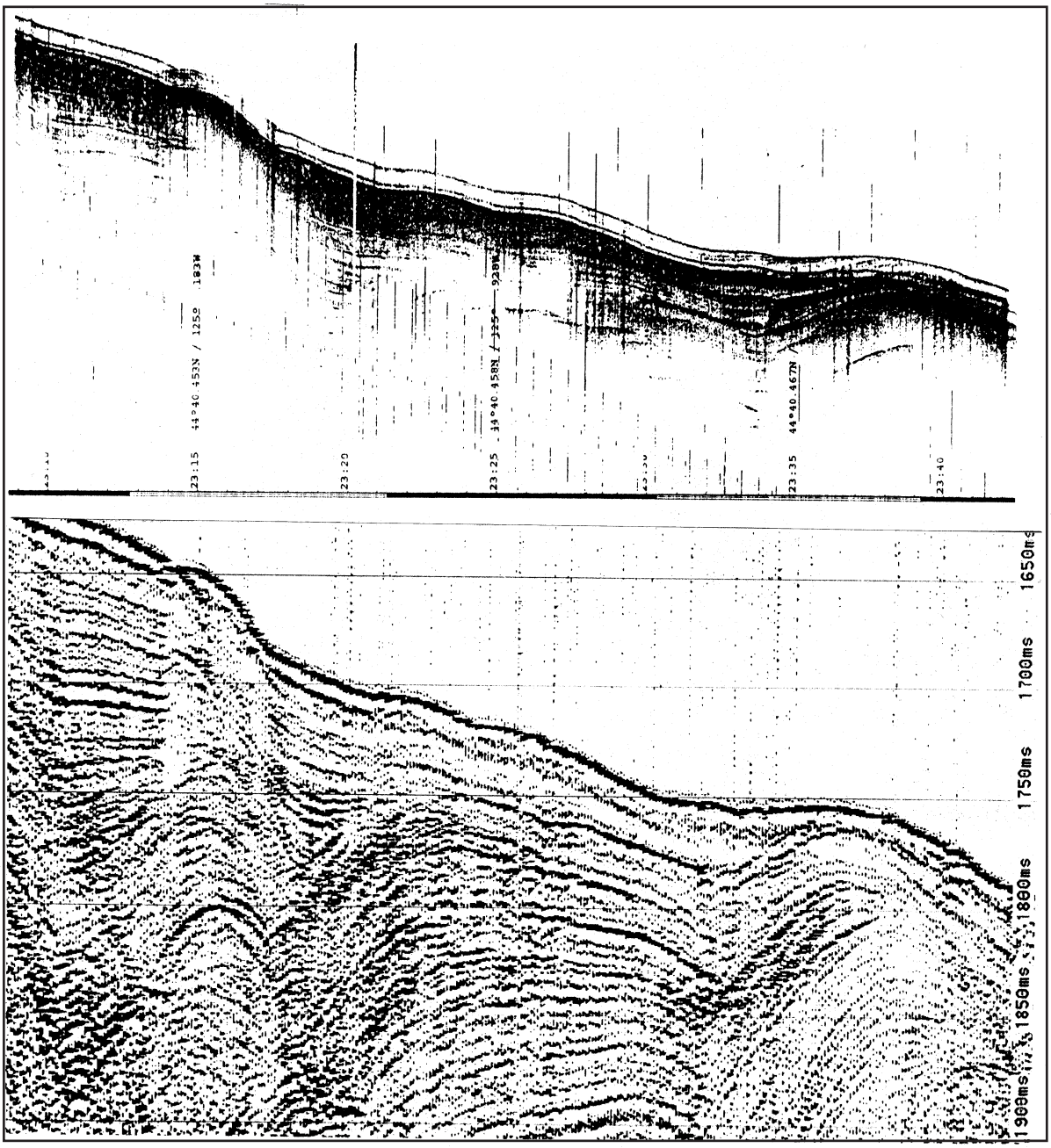

Figure 6.2.1: Parasound and Deeptow Seismic Section along Profile 124.
The images illustrate the differences in lateral and vertical resolution as well as penetration depth.

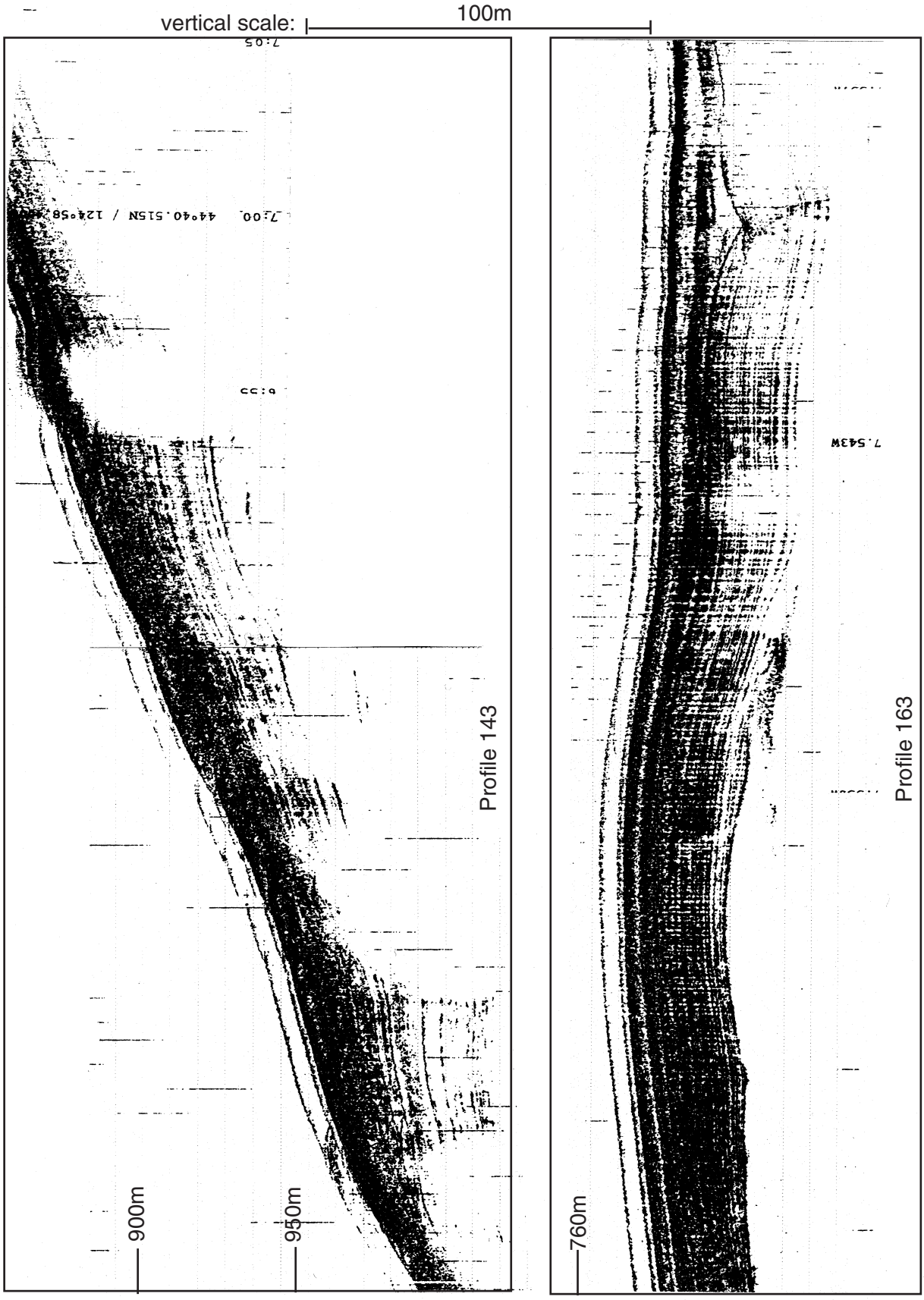

Figure 6.2.2: Parasound images of the upper sedimentary layers with blank, lense-shaped zones, posssibly indicating methan gas.

6.3 SEISMIC WORK

6.3.1 INTRODUCTION

(D. Klaeschen)

The main scientific experiments carried out using the OBH/OBS and multiple streamer seismic acquisition focussed on the following objectives:

Multiple acquisition geometry

As a first general requirement to increase the subsurface resolution, a broad frequency range is necessary. Owing to the limited frequency range of each individual source, the main E-W-oriented profile in each location was shot with 5 different sources across the seafloor receiver assembly. As a second requirement for an increase in resolution, the receivers have to be positioned close to the BSR target area. On this cruise, both requirements were achieved by the use of OBH/OBS stations and a deep-tow system. In addition to a three channel mini-streamer, a single channel surface streamer floating on the water surface revealed high quality data due to missing ghost effects of towed systems in the upper water column. Data quality benefitted from the very calm sea during the periods of acquisition.

The combination of towed reflection systems (with their limited aperture, but high lateral resolution) and OBH/OBS (without aperture limitation) spaced approximately 200m apart offers a wide range of analysis techniques to characterize the subsurface, and especially the BSR signature. At least one additional OBH per main experiment locality was towed several hundred meters above the seafloor to record the far field signature of the different sources used. This source signature, which could only be recorded when the deep-tow systems was not operative, is needed for certain postcruise data analyses and applications of waveform inversion methods.

To characterize the BSR signature not only on the main E-W-profiles, a series of additional N-S-profiles were shot with the GI-Gun and recorded by the OBH/OBS and the surface and mini streamers. This strategy allows us to tie the data with adjacent E-W-profiles of the multichannel OR89-survey. Given the narrow spacing, the data represent a first-order attempt to characterize the subsurface in 3D. Moreover, the orthogonal profiles are needed to relocate the exact OBH/OBS positions. Relocation of the data have previously shown that some OBH/OBS stations were affected by lateral shifts of more than 100m (e.g., due to the water currents).

Identification of portions of free gas and massive gas hydrates in the sediment

A wealth of seismic imaging and inversion methods have been applied to exploration of gashydrates (e.g. MacKay et al., 1994; Yuan et al., 1996; Pecher et al., 1998, Hobro et al., 1998; Ecker et al, 2000). In this study, we focus on the subsurface velocities (P and S-waves) and the AVO behaviour (amplitude variations at different angles or offsets) of the BSR, and reflection strength using different source frequencies to map the BSR.

If, for instance, a signal is reflected from a sharp boundary between a solid (gas hydrate) and a gaseous phase, the amplitude of the reflection does not vary with the frequency. If, however, the reflection originates from a transition zone, its amplitude varies with frequency. As long as the transition is small relative to the wavelength, the reflection amplitude is frequency independent and appears as a sharp interface. However, if the transition thickness is similar to the seismic wavelength, the amplitude of the reflection decreases. Given further that the attenuation of gas-bearing sediments is strongly frequency dependent, this multispectra survey offers a wide range of analysis techniques to characterize the massive gas hydrate and free gas layers.

Pure gas hydrate has physical properties comparable to those of ice (Sloan, 1990a; b). As a result, the presence of massive hydrate in the uppermost tens of meters beneath the seafloor leads to an increase in P-wave velocity, depending on the pore volume occupied by hydrate. In contrast, only minor amounts of free gas (< 1%) in the pore space reduces the P-wave velocity considerably. By contrast, the S-wave velocity is not significantly affected by free gas. The effect that hydrate saturation has on the P- and S-wave velocity depends largely on the hydrate distribution in the pore space of coarse-grained sediments. In natural samples, the spectrum ranges from dispersed nodules over cementration of the whole rock framework to massive layers of pure hydrate (Bohrmann et al., 1998; Ecker, 1998; Bohrmann et al., 1999).

S-wave velocity provides important information not only on the hydrate content of the sediment, but also on its shear strength. Since no shear-wave source for the bottom is available so far, efforts have to concentrate either on the analysis of P- to S-wave converted arrivals as well as on interface waves (Scholte waves) on the 3 component OBS stations.

The AVA/AVO characteristics provide major constraints on both the change in physical properties across a reflector, whereas the normal incidence reflection coefficient is controlled by the contrast in Vp and density. The variation in amplitude with angle of incidence provides constraints on Vp, density and Vs, as the amplitude variation is controlled by the differing amounts of energy transmitted through the interface and converted at the interface into S-waves. As AVA is dependent not only on P-wave velocity structure, but also on S-wave velocity structure, the AVA behaviour of the reflection will constrain the change in physical properties at the base of the hydrate occurrence. Consequently, it enables quantification of the hydrate distribution. To analyse the AVO/AVA behaviour in dipping subsurface strata, an uncollapsed true amplitude (TA) migration must be applied to the OBH/OBS data. The successful inversion of the AVO/AVA requires a wide range of angles of incidence (unlimited aperture), and provides a first-order estimate of the vertical reflection coefficients, Rp and Rs, which can be used to identify free gas as well as gas hydrate zones.

Calibration of seismic parameters based on in situ measurements
Additional high resolution P-wave and density information is needed in order to calibrate the extracted reflection coefficients from the AVO analyses into with the velocities and density. This can be achived by traveltime inversion methods and empirical velocity-density relations. However, on the main experiment on the northern summit of Hydrate Ridge, independent drilling information (Vp and density logs) exists from Site 892 (see ODP Leg 146 results; Westbrook et al., 1994). Based on the knowledge of the source signature, synthetic seismograms can be calculated so that the data from logging and coring match the HYDGAS data. The aim is to match the AVO charaterisic of the synthetics calculated from borehole data with the HYDGAS data by a systematic variation of the poisson ratio. By this procedure the reflection coefficients can be calibrated with the elastic parameters of the subsurface. As soon the calibration was successful, further extrapolations can be made at greater distance from the calibration site drilled during Leg 146.

Quantification of the amount of gas hydrate and free gas
The majority of the approaches to quantify the amount of gas hydrate and free gas are based on the P-wave velocity information alone (e.g. Pearson et al., 1983; Lee et al., 1993; Lee et al., 1996). If additional shear velocity can be extracted, a more complete modelling can be applied under consideration of the elastic modulus (Erickson and Jarrard, 1998). A more recent modelling technique proposes a three phase theory (Carcione and Tinivella, 2000), which is equally valid for consolidated and unconsolidated sediment (e.g. massive hydrate above a free gas layer). Depending on the saturation of gas hydrate and free gas, the calculations made by Carcione and Tinivella show a complex AVO pattern. As soon as the modelled AVO curves of the gas hydrate concentrations and free gas saturations coincide with the AVO curves of the HYDGAS data

calculated at the calibration Site 892, the lateral amplitude variations further away from the site can be interpreted as changes in concentrations and saturations of the hydrate and gas layer under the assumption that the physical properties in the sediment column do not change significantly.

3D-viscoelastic seismic forward modelling for verification of models
Using the high resolution bathymetry collected during previous cruises of R/V Sonne together with the wealth of new and already existing seismic information, a 3D subsurface model can be extrapolated with reasonably good accuracy. To test the quality of the predicted model, 3D viscoelastic modelling can be used to simulate the recorded wavefields. Here, not only the P-wave arrivals, but also the converted shear waves and the frequency dependency are of interest. The latter include the attenuation term and can be used to cross-check the final results.

Scientific work during the cruise
The seismic work on SO150 was a challenge for both the ship crew and the scientists, because six different recording systems together with six possible source configurations had to be handled alternately: Concerning the recorders, three remotely operated systems on the seafloor were used: DPG, OBH, OBS. In addition, 3 ship-based recording systems were operative (sometimes at a time): mini-streamer, surface-streamer, and deep-tow streamer (see chapter 5.2). The six possible source configurations of a Sparker, Watergun, GI-Gun, Airgun-Array, 32-Bolt Guns and a drop weight (see chapter 5.3) in combination with all the recording systems required a completely new strategy for the seismic processing, archiving and data flow management (see chapter 6.3.2). The main experiments were time-consuming, and initial results are presented in chapter 6.4 (ODP Leg 146, Site 892) and chapters 6.5 and 6.6 (anticipated ODP leg 204 locations, Sites HR3 and HR1). In order to make use of the extra time required for data retrieval and data quality control of these main experiments, additional high resolution reflection lines were acquired.
A set of regional high resolution reflection lines, which coincide with the traces of profiles of the OR89-survey, are described in chapter 6.3.3. The pinnacle area, an actively venting chemoherm structure, has been investigated acquiring a set of 8 lines with source of Sparker and Parasound (chapter 6.3.4). Two pockmark areas (on the northern and southern summit of Hydrate Ridge; see chapters 6.3.5 and 6.3.6), which were previously related to regional faulting, local seafloor elevations and discontinuous strata in the subsurface (Bohrmann et al., 1999), have been mapped with different sources. An additional profile south of Hydrate Ridge has been shot using the Sparker and GI-Gun and recorded using the surface and deep-tow streamer. This SE-Knoll structure, where active venting has been observed (Trehu et al., 2000), is found to be a similar feature as Hydrate Ridge. A special experiment used a drop weight of 3t to generate seismic waves, especially Scholte Waves, which were recorded with three different recording systems (OBH, OBS, and DPG) at the ODP Leg 146, Site 892 (see chapter 6.7).

Prior to the HYDGAS cruise the regional MCS profiles OR89-01 to OR89-12 and OR89-43 to OR89-44 collected during the cruise off Oregon in 1989 (e.g. MacKay et al., 1992) were reprocessed at GEOMAR. Special attention was payed to preserve the amplitude information during processing. A prestack time migration followed by an AVO inversion gave two additional subsurface images, the Rp-reflection strength and the AVA-gradient strength. As the prestack seismic amplitudes of a common image point (CIP) gather behave approximately linear with the sine squared of the angle of incidence, the two linear coefficients, intercept and gradient, are related to the elastic properties of the subsurface. The intercept corresponds to the P-reflection coefficient, while the gradient is a complex function of P- and S wave-velocities, P- and S reflection coefficient and density contrast. The AVO gradient describe the amplitude behavior with the angle of incidence. The most importent profiles in the context of the HYDGAS expedition are displayed in Fig. 6.3.1.1 and 6.3.1.2 with the locations of OBH/OBS positions on the northern and southern summit of the Hydrate-Ridge, respectively.

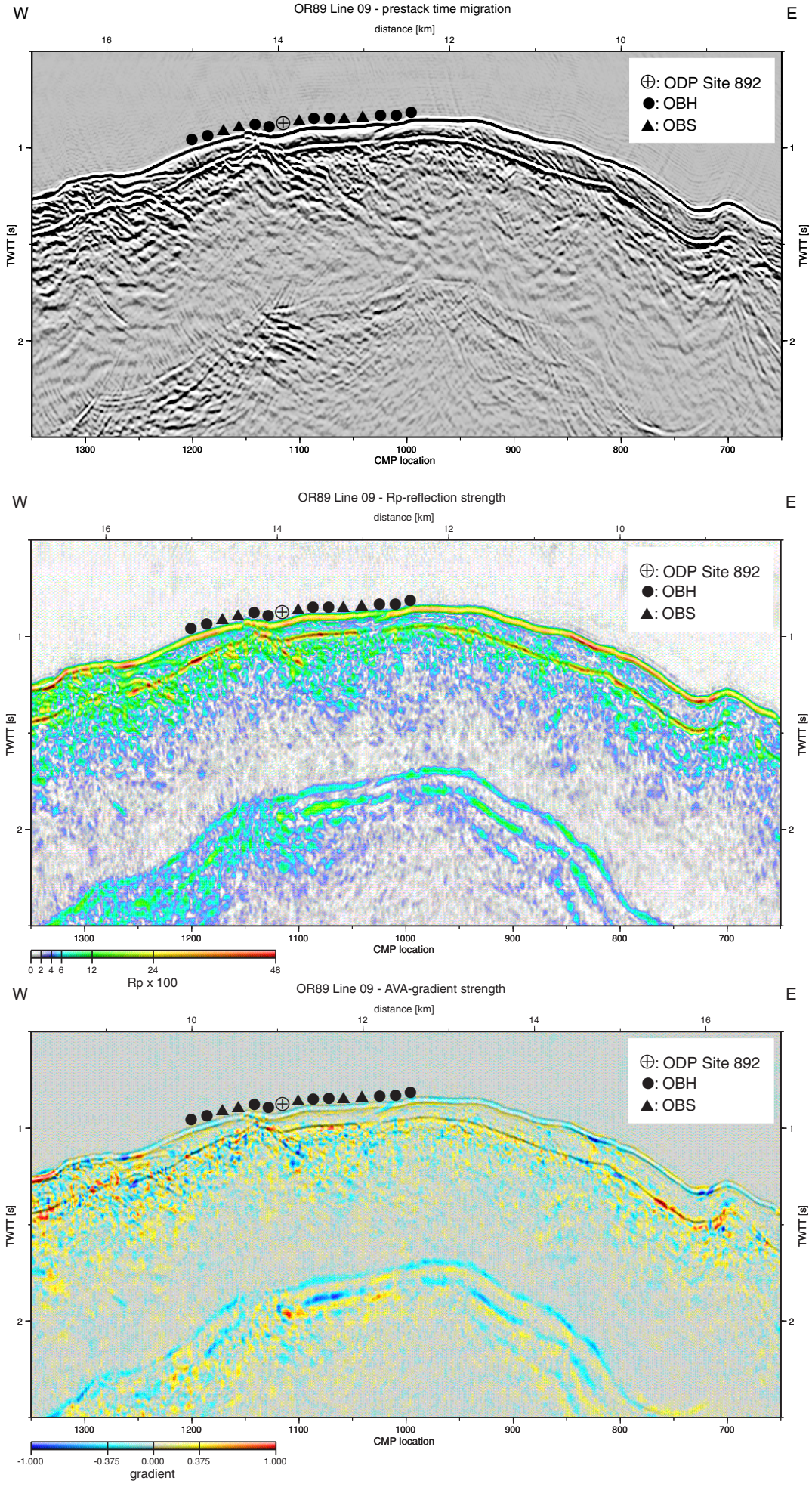

Figure 6.3.1.1: Prestack time migration of OR89-09 and the results from an AVA inversion (Rp-reflection strength and AVA-gradient strength).

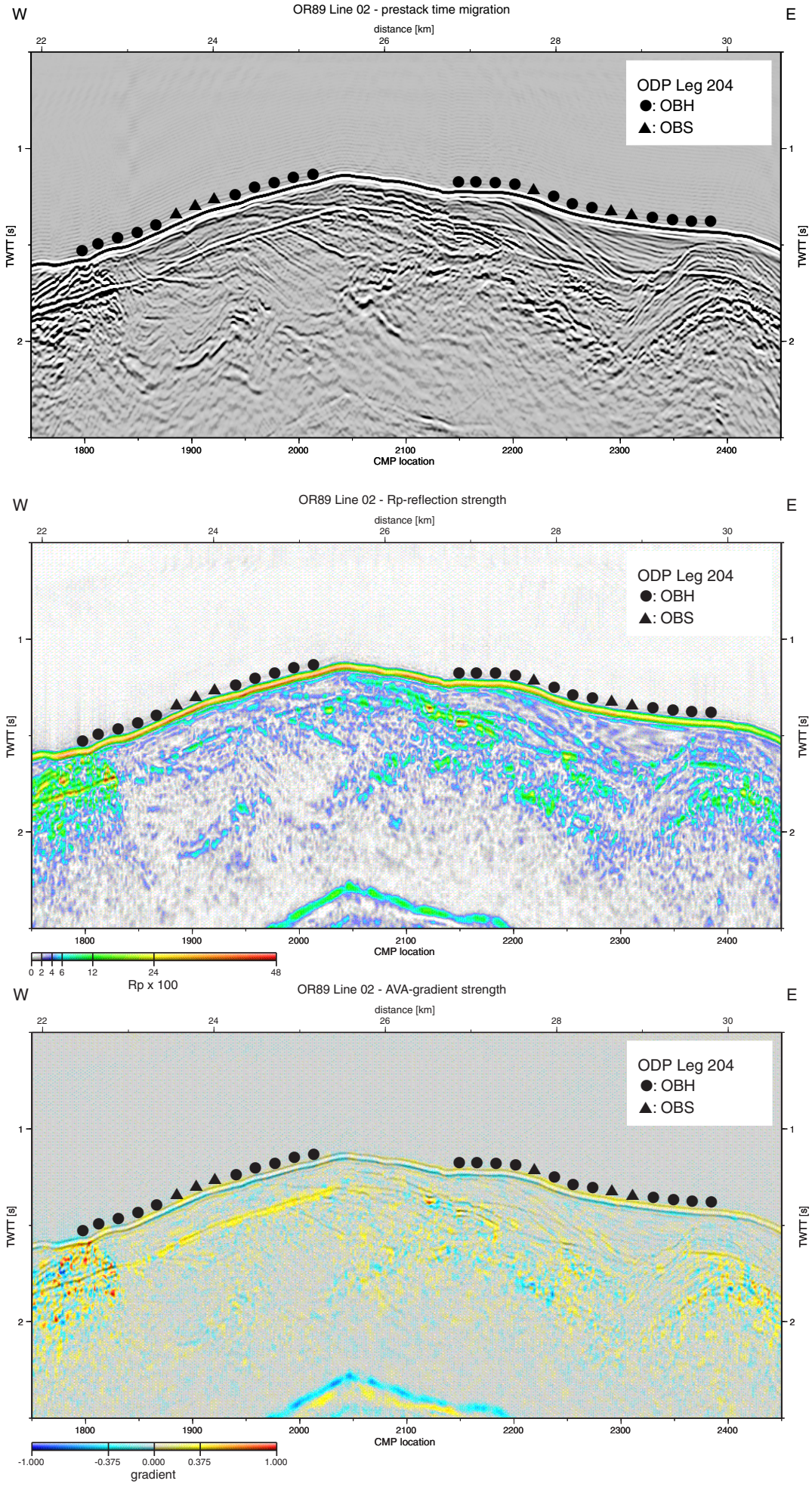

Figure 6.3.1.2: Prestack time migration of OR89-02 and the results from an AVA inversion (Rp-reflection strength and AVA-gradient strength).

The newly acquired streamer data presented in this report are not corrected for the final delay times summed from trigger and aimpoint delayes, as listed in Table 5.3.2.

Detailed lists of the OBH/OBS deployments and of the sources used for shooting are provided in Appendix 9.1 and 9.2. A map overview of the profiles shot with the different sources is displayed in the Appendix 9.3, Figures 9.3.1-9.3.5.

6.3.2 SEISMIC PROCESSING AND DATA ARCHIVING

(G. Klein, J. Petersen, D. Könitz, D. Klaeschen)

Data Processing

The OBH/S data recorded on the MBS units have to be converted into standard SEG-Y format for further processing. The program structure was modified from the existing REFTEK routines to meet the OBH/S requirements and GEOMAR's hardware platforms. Because the GEOMAR OBH/S operates in a continuous mode, most of the modifications to the existing program package had to be done to the parts of the program which handle continuous data streams.
A flow chart shown in Figure 6.3.2.1 illustrates the processing scheme applied to the raw data. A detailed description of the main programs follows below:

send2pass

For the PC-cards used with the MBS recorder, data expansion and format conversion into PASSCAL data format is performed using DOS based PC. The program send2pass reads data from the flashcards used during recording. Decompressed data are written onto the PC's hard disk using PASSCAL data format. Either 16 or 32 bit storage is available. This enables compatibility with the DAT recordings (s.b.). After ftp transmission to a Sun workstation, ref2segy and all other software can be used to handle and process the data files and store them as SEG-Y traces.

ref2segy

Downloading the raw data from DAT tape to a hard disk of a Sun workstation is done by the program ref2segy. In addition, MBS data stored in the "reftek" format could be read optionally. It produces a pseudo SEG-Y trace consisting of one header and a continuous data trace containing all samples. For each channel (different amplifications) one file is created with the name derived from the start time, the serial number of the Methusalem system, and the channel number. In addition, a log and an error file will track the download process. In a second mode PASSCAL disk files written by send2pass, in either 16 or 32 bit format, can be read in and included with the standard processing scheme. The file size of the data is directly related to the recording time. For instance, a recording time of one hour sampled at 200 Hz will produce a file size of 1.44 MB per channel. A record with two channels and a recording time of two days will produce a total data volume of 70 MB.

merge

If a read error occurs during the download process, the ref2segy program has to be restarted. This may lead to several data files with different start times. Merging these files into a single file is performed by the merge program. Gaps between the last sample and the first sample of the consecutive data traces are filled with zeros. Overlapping parts are cut out.

segy2trig

The trigger signal, provided by the airgun control system, is recorded simultaneously on an additional Methusalem unit during the shooting period. These data are treated as a regular data recordings and processed via the ref2segy program. Then the segy2trig program detects the shot times in the data stream by identifying the trigger signal through a given slope steepness, duration and threshold of the trigger pulse. The output is an ASCII table consisting of the shot number and

the shot time. Accuracy of the shot time is one of the most crucial matters in seismic wide-angle work and must be reproduced with a precision of one sample. Due to this demand the shot times have to be corrected with the shift of the internal recorder clock. Additionally, the trigger file contains the profile number, the start/end time of the profile and the trigger recording. The shot times are part of the ukooa file, which links them with the coordinates of the source and the hydrophones.

ukooa
The ukooa program is used to establish the geometric database by calculating the positions of sources at any given shot time and offset from the ship. The source is placed on the ship track using simple degree/meter conversions and then written to a file in UKOOA-P84/1 format. This file will be used when creating a SEG-Y section via the dat2segy program. The program requires the trigger file to contain the shot times, the ship's navigation (see Chapter 5.5.3) and a parameter file containing information for the UKOOA file header as basic input information.

dat2segy
The dat2segy program produces standard SEG-Y records, either in a 16 or 32 bit integer format, by cutting the single SEG-Y trace (from the merged ref2segy file) into traces with a defined time length. It reads both the ukooa file with the geometry information and the downloaded raw data as produced with the ref2segy program. In addition, the user can use several parameters for controlling the output. These parameters are information about the profile and the receiver station, number of shots to be used, trace length, time offset of the trace and reduction velocity (to determine the time of the first sample within a record). Also the clock drift of the recorder is taken into account and corrected. The final SEG-Y format consists of the file header followed by the traces. Each trace is built up by a trace header followed by the data samples. The output of the dat2segy program can be used as input for further processing with GEOSYS, SEISMOS or Seismic Unix (SU).

Besides these main programs for the regular processing, additional features are sometimes needed for special handling of the raw data:

divide
The program divide cuts the raw data stream into traces of a given length without offset and time information, storing the output in SEG-Y format. The routine is useful for a quick scan of the raw data or if a timing error has occurred.

segyhdr
The routine segyhdr prints all the header values of the raw data on the screen.

segyshift
Segyshift modifies the time of the first sample, allowing the whole raw data trace to be shifted by a given value. This is very useful when shifting the time base from Middle European Time to Greenwich Mean Time or any local time. Because of recording problems, the data sometimes show a constant time shift, which can be corrected as well with segyshift.

castout
The program castout allows the user to remove a specified time window from the raw data stream. When the shooting window is much smaller than the recording time, one can reduce the data volume by cutting out only the useful information. This will reduce the demand on disk space.

relobs3D
Due to drifting of the OBH/S instruments during deployment and errors in the ship's GPS navigation system, the OBH/S positions may be mislocated by up to several 100 m. Since this

error leads to asymmetry and incorrect traveltime information in the record section, it has to be corrected. This is accomplished with the program relobs3D.
For input, the assumed OBH/S location, shot locations and the picked traveltimes of the direct wave near to its apex are needed. To achieve a reliable, corrected position in 3D, it is necessary to pick at least two profiles cross-cutting each other at a certain angle. The calculation algorithm can handle up to three input profiles. By shifting the OBH/S position, relobs3D minimizes the deviation between computed and real travel times using a least mean square fitting algorithm (assuming a constant water velocity).
Due to the short shot spacing used and the high accuracy required, the most critical issue to the relocation process is the determination of shot coordinates. If a discrepancy exists between the results from relobs3D calculations of the cross-cutting profiles, this indicates that source offsets from the GPS position are determined inaccurately.
More detailed analysis using these profiles has to be done and will lead to exact shot coordinates and OBH locations respectively.

Data organization
During HYDGAS cruise SO150, a large number of profiles with varying orientations were shot across each of the deployments of ocean bottom receivers. Since working on individual profiles is no longer efficient with this survey design, the data organization was modified to include a variety of profiles in an individual survey run.
A master directory of all required programs and script files was kept and copied to each of the survey runs when needed. For an uncomplicated performance, a setup script (CREATE SURVEYRUN) has to be copied and executed in the new directory of the survey run. The names of the survey runs correspond to the range of profiles included in them. All changes could be easily maintained in the master file and quickly copied to the subsequent directories using update scripts kept in the master directory (see structural outline in Figure 6.3.2.2). Shell scripts contain most of the settings for the programs which were needed for the preprocessing of the seismic data in the given directory structure. They are described below in the chronological order of their application:

data
This directory contains raw data of OBH, OBS, streamer (STR) and trigger recordings. Applying ref2segy to the Passcal files creates the Rddd.0? directories, which contain the pseudo seg-y data. The variable ddd denotes the julian day, while the ? represents the recording window. For a single recording window, there will be only one Rddd.01 directory if no merging is necessary. During cruise SO150, MBS recorders were programmed in two time windows using different sampling rates due to limited flash disk capacities, resulting in two R-directories. To obtain the shot times, segy2trig has to be run on the trigger pseudo seg-y file. The resulting p???.trig file is copied to the ukooa directory. Additionally, there is a directory called d2slogs containing logfiles from the dat2segy program.

ukooa
Shell scripts used to create ukooa files are ukooa2skew.sh and skew2rel. Inputs to the former are the trigger file, navigation file and a specific pID.inp.skew file that contains the OBH/OBS recording times and skew values of the clock drift of the recorder as well as station coordinates. The shell script must be edited for profile numbers and the distance between the source and the vessel's GPS antenna. The output of ukooa2skew.sh are ukooa files named p???.uko.skew. Files containing the preliminary coordinates are used for raw data plots and the relobs3D process. After having performed this relocation, the improved positions are edited into the file pID.inp.skew.rel which is copied from pID.inp.skew. The ladder serves as input to skew2rel creating final ukooa files p???.uko.skew.rel. These are used for creating the final SEG-Y data.

shells
Directory shells consist of the main shell scripts used in the preprocessing phase. To obtain SEG-Y files, d2s.sh (which calls dat2segy) must be run. When running the d2s.sh for numerous stations and profiles, the required syntax can be produced using an additional script called d2s.input. Editing of profile and OBH/OBS/STR numbers as well as specification of recording windows for this survey. Entering the profile number and the reduction velocity on the command line (e.g. d2s.input 142 3000), the desired d2s.sh command lines are created, and may be redirected into a calling script. the d2s syntax to produce SEG-Y files after relocation can be obtained similarly using d2srel.input. Thus far, a specific time offset has to be chosen within the d2s.sh script, but this should be incorporated into the command line syntax shortly.
For plotting OBH data with Seismic Unix there are two source plot scripts available, su_plot.source and su_plot.trace, that are linked to the master directory and need generally not be changed. To avoid file access problems arising from simultaneous command calls, a directory su_plot_p??? is created for every profile. The profile specific settings for the su_plot scripts can be specified in a copy of the file suplot.settings which then has to reside in the new directory with the name su_plot.pxxx.source-specifier. Plot parameters for each station have to be given on the command line and the additional script suplot.input may help to obtain the correct command line syntax analog to d2s.input. Specification of profile number, source-specifier and chosen time offset are required (e.g., su_plot.input 142 gi 1).

In order to perform the relocation of the station coordinates, shell scripts pickthem3D.sh and relobs3D.sh are used. The former enables picking of the direct wave via suxwigb (Seismic Unix). Relocation calculation is then carried out by relobs3D.sh which displays picks and calculates new positions using SU and GMT software.

perm
The perm directory contains SEG-Y files and .ps files created by d2s.sh and su_plot.pxxx.src. After performing data processing with Seismos software, processed SEG-Y files are transferred to this directory.

Since the large amount of data had to be spread across several physical hard disks, it was arranged that the raw data could be kept on any of the hard disks provided they had the same directory structure. Only the directories shells, ukooa, nav and perm need to be in the same logical directory hierarchy.

OBH/OBS-data analysis and results
A primary objective of SO150 cruise was to acquire data with four different sources using a broad range of frequencies. As an example, OBS station 34 is shown for profile 101 (watergun), profile 102 (Prakla airgun array), profile 103 (gi-gun), and profile 113 (32 liter bold airgun). All profiles were shot across the ODP Site 892 in W-E and E-W direction, respectively. The figures present the hydrophone, vertical, and one horizontal component.

To examine the frequency ranges of the different sources, filter panels were performed using the Ormsby frequency filter operator. The results are illustrated in Figures 6.3.2.3-14.

In the lower section of the figure the amplitude spectra of the corresponding band pass filter panels are appended. For Ormsby frequency filter, the amplitude spectra of the used operators are characterized by linear slopes. The filter applied with minimum delay characteristics is described by four corner frequencies: Lower stop/pass band boundary and upper pass/stop band boundary. The frequencies on the filter panels correspond to the lower and upper pass frequencies.

Input for the frequency analysis was raw data in SEG-Y format with complete geometry information. The sampling rate was 0.4 ms for the watergun and 1 ms for the other three sources. All data had a velocity reduction of 3 km/s applied. Several recordings were influenced by a DC-shift. To centre the amplitudes around zero, a 0-3 Hz high-pass Kaiser frequency filter in minimum delay characteristic with 60 dB attenuation between the pass and reject zone was applied prior to data processing.
To focus the source signal a water correction was applied using a water velocity of 1490m/s. Ideally, the direct wave should be horizontally displayed. Unfortunately, there is still an asymmetry in the data, which was not compensated for by applying the relobs relocation program.

As for the preliminary results, the main energy at the BSR is clearly shown in the filter panels. On the horizontal component, there is a polarity change from positive to negative offsets.

The airgun array produced a so called "bubble" (around 450-500 ms). A deconvolution is recommended to compress the basic source wavelet which results in improved temporal resolution of the seismic data. There is still some low frequency noise in the data which could be removed by a fk-filter.

Data recorded with the MBS recorder on flash discs were transformed into the PASSCAL format via a PC or Notebooks and then transferred to a SUN workstation. On the workstation they were transformed into a so-called PSEUDO-SEG-Y format. Both, the PASSCAL and PSEUDO-SEG-Y raw data were archived on DAT on SUN workstations.

After navigation data were merged, and SEG-Y formatted traces with the appropriate header words were created, the data are processed according as described above. The SEG-Y data are archived on DAT tapes after the shipboard processing.

For the exchange of the OBH/OBS data, the SEG-Y-format on disk with a Sun tar-format was chosen. The raw segy data is in Integer2 format with trailer bytes between the record structure of SEGY. The processed data is in IBM-floating point without trailer bytes between the records. For UTM transformation into Cartesian coordinates use: WGS84 spheroid, central meridian 123°00.0 W, northern hemisphere.

Below is the definition of the segy trace header for the GEOMAR OBS wide-angle reflection data. The extension of the standard SEG-Y header from 181 to 240 byte is a layout in order to process the data on the GEOSYS/SEISMOS software system. Reading bytes directly into this header will allow access to all fields.

```
BytePos Bytes Information      Comments (note: not all headers available in processed data)
1-8     (2x4) lineSeq, reelSeq;      /* Sequence numbers within line and reel, resp.*/
                    /* here station and shot number Def: 1, 1 */
9-12    (4) profNumber;         /* Original field record number */
                    /* Here profile number */
13-16   (4) traceNumber;            /* Trace number within the original field record.*/
                    /* Here station (receiver) Number  */
17-20   (4) energySourcePt;      /* Energy source (shot) point numbe */
                    /* Def: 0 */
21-24   (4) cdpEns;             /* CDP ensemble number: shot number */
                    /* Def: 0 */
25-28   (4) traceInEnsemble;     /* Trace number within CDP ensemble */
                    /* Here azimuth in seconds of arc for unprocessed data*/
29-30   (2) traceID;            /* Trace identification code:
                  1=seismic data (Def)  4=time break   7=timing
                  2=dead            5=uphole      8=water break
                  3=dummy           6=sweep       9..., optional use */
31-34   (2x2)  vertSum, horSum; /* Def: 1, 1 */
35-36   (2) dataUse;         /* 1=production (Def), 2=test */
37-40   (4)     sourceToRecDist;  /* Distance in (m) */
41-44   (4) recElevation;        /* Elevation in (m), Def: 0  */
45-48   (4) sourceSurfaceElevation; /* Def: 0 (m)  */
49-52   (4) sourceDepth;        /* Def: 0 (m)  */
53-60   (2x4)  datumElevRec, datumElemSource;     /* Def: 0, 0 (m) */
61-68   (2x4)  sourceWaterDepth, recWaterDepth;   /* Def: 0, 0 (m) */
69-70   (2) elevationScale;     /* Scale elevations Def: 0 (10**0) */
71-72   (2) coordScale;      /* Scale coordinates
                            Def: -2, means coordinates multiplied
                            by 10**(-2) to get real value for unprocessed data.
              NOTE: for processed data -100 means to divide by 100 to get the real value */
73-80   (2x4)  sourceLongOrX, sourceLatOrY;     /* Either Cartesian or geographic */
81-88   (2x4)  recLongOrX, recLatOrY;
89-90   (2) coordUnits;      /* 1= meter or feet; 2=sec of arc */
91-92   (2) weatheringVelocity;   /* Def: 0 (m/s) */
93-94   (2) subWeatheringVelocity;  /* Reduction velocity, Def: 6000 (m/s) */
95-96   (2) sourceUpholeTime;    /* Def: 0 (ms) */
97-98   (2) recUpholeTime;        /* Def: 0 (ms) */
99-102  (2x2)  sourceStaticCor, recStaticCor;   /* Def: 0, 0  (ms ) */
103-104 (2) totalStatic;                /* Def: 0 (ms) */
105-106 (2) lagTimeA;                   /* T(shottime) - T(first sample) */
107-108 (2) lagTimeB;                   /* Def: 0 (ms) */
109-110 (2) delay;                  /* Def: 0 (ms) */
111-114 (2x2)  muteStart, muteEnd;  /* Def: 0, 0 (ms) */
115-116 (2) sampleLength;      /* Number of samples in this trace */
                    /* ( > 32767 )? = 32767
                        set long samp_rate in 185-188 byte */
117-118 (2) deltaSample;          /* Sampling interval in microseconds. */
119-120 (2) gainType;             /* 1=fixed (Def), 2=binary,
                     3=floating, 4... opt.*/
121-122 (2) gainConst;            /* Gain of recording channel  */
123-124 (2) initialGain;          /* Gain of preamplifier in db */
125-126 (2) correlated;           /* 1=no (Def), 2=yes */
127-130 (2x2)  sweepStart, sweepEnd;       /* min. and max. amplitude of trace */
131-132 (2) sweepLength;          /* Here defined as
              fraction of second of shot time  */
133-134 (29)    sweepType;              /* Source type:
              1=linear,  2=parabolic,  3=exponential,  4=others
              5=bohrhole explosive,  6=water explosive,  7=airgun (Def)
              or fraction of microsecond of shot time for high resolution data */
135-138 (2x2)  sweepTaperAtStart, sweepTaperAtEnd;  /* Start and end of trace (ms) relative to Tred(0) */
139-140 (2) taperType;            /* scaling factor for last two values Def: 1 (x10) */
141-144 (2x2)  aliasFreq, aliasSlope;       /* Def: 0, 0  */
```

```
145-148 (2x2)  notchFreq, notchSlope;        /* Def: 0, 0  */
149-152 (2x2)  lowCutFreq, hiCutFreq;    /* Def: 0, 0  */
153-156 (2x2)  lowCutSlope, hiCutSlope;    /* Def: 0, 0  */
157-166 (5x2)  year, day, hour,           /* Source (shot) time, the fraction of sec */
                                                minute, second;
                                                /* is set in millisec between 131-132 byte
                                              is set in microsec between 133-134 */
167-168 (2) timeBasisCode;          /* 1=local, 2=GMT, 3=MET (GMT + 1 hour) (Def) */
169-170 (2) traceWeightingFactor;     /*  */
171-172 (2) phoneRollPos1;         /* Component: 1=time code, 2=radial, 3=transverse
                        4=vertical, 5=hydrophone (Def)  */
173-174 (2) phoneFirstTrace;        /* Methusalem instrument number in YYNN */
175-176 (2) phoneLastTrace;        /* Channel number */
177-178 (2) gapSize;          /* Source charge in cubic inches (airgun)
                                              or kg (explosives) */
179-180 (2) taperOvertravel;          /* Def: 0=meaningless  1=up, 2=down    */
                                              /* !!! Following is extension !!! */
181-182 (2) compNo;               /* 1=time code, 2=radial, 3=transverse
                      4=vertical, 5=hydrophone (Def)  */
183-184 (2) samplingRate;             /* samples/sec */
185-188 (4) numberSamples;          /* ( <= 32767) ? sampleLength | ( > 32767) */
189-190 (2)       shotPointNo;
191-192 (2) ADCoeff;               /* Coefficient of A/D converter in mv/digit */
193-194 (2) receiverCoeff;             /* Conversion coefficient of receiver,
                      pascal/cm2 for hydrophone,
                      velocity(m/s)/volt for geophone */
195-196 (2) receiverType;             /* 1=hydrophone (Def), 2=geophone, 3...*/
197-200 (4) lengthData;           /* Def: 0 (ms), not used here */
201-204 (4) distance;             /* Source to receiver distance in (m)  */
205-208 (4)      (float) scaleFactor;          /* Scale factor same as in <segy.h>
                Here azimuth in second of arc for processed data */
209-210 (2)      azimuth;              /* Orientation of the component in min */
211-212 (2) eigenperiod;          /* Eigenperiod of geo- or hydrophone in (ms) */
213-216 (4) minAmpl;              /* Min. peak amplitude within trace     */
217-220 (4) maxAmpl;              /* Max. peak amplitude within trace */
221-222 (2) stationNo;            /* Station number */
223-224 (2) channelNo;            /* Channel number (Default: 1) */
225-228 (4) sourceCharge;             /* Charge in kg (explosive) or cc (airgun) */
229-230 (2) redVelocity;          /* reduction velocity in (m/s);
                      Def: 0 if no reduction velocity se */
231-232 (2) timeOffset;           /* Time offset in (ms) of first sample
                      relative to reduced source time:
                      positive if earlier than reduced time  */
233-236 (4) redTime;              /* Reduced time in (ms) = distance/redVel  */
237-238 (2) unused2;
239-240 (2) instNo;            /* Methusalem instrument number */
```

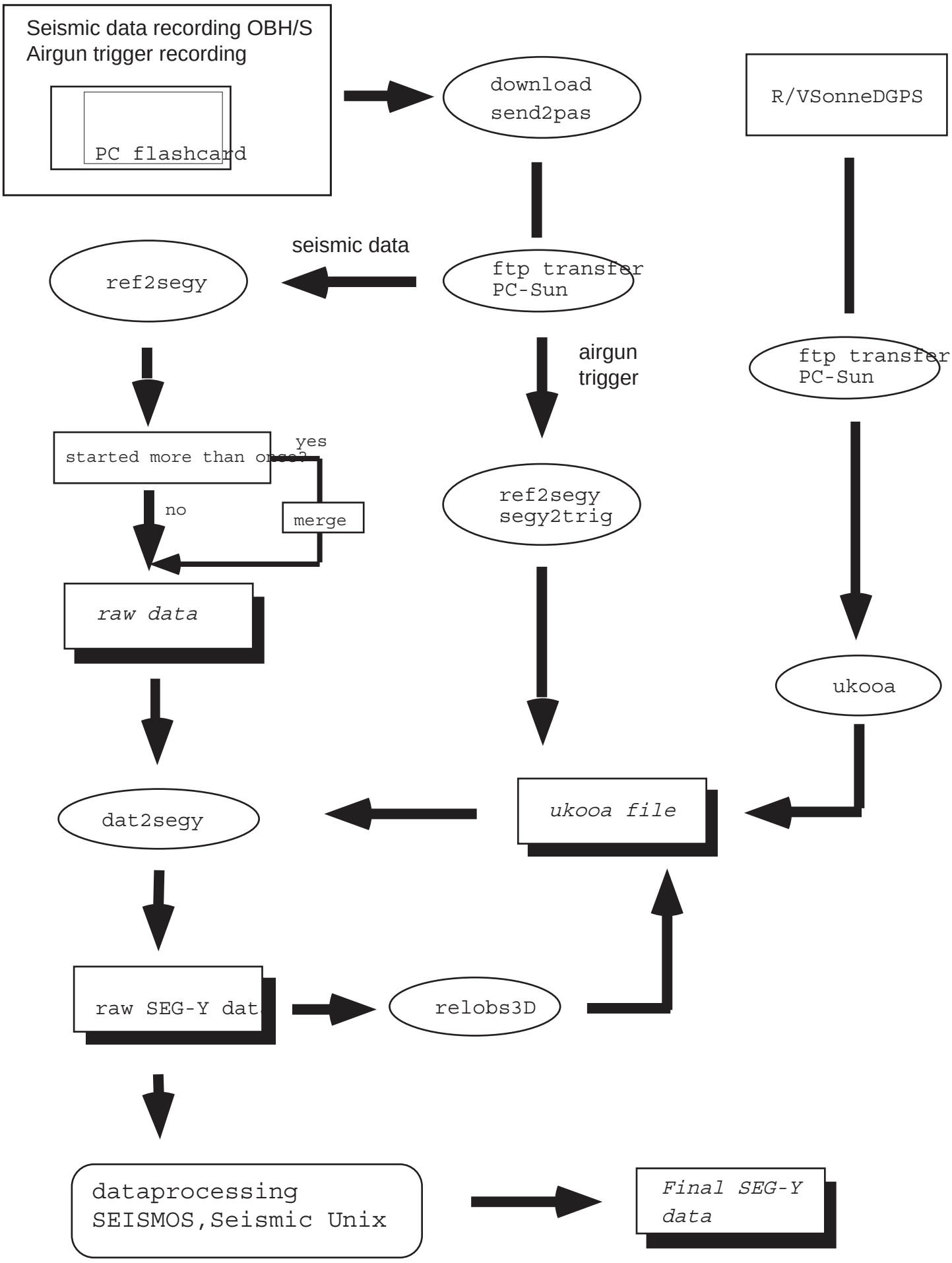

Figure 6.3.2.1: Processing flow of OBH/S data from raw data toSEG-Y records.

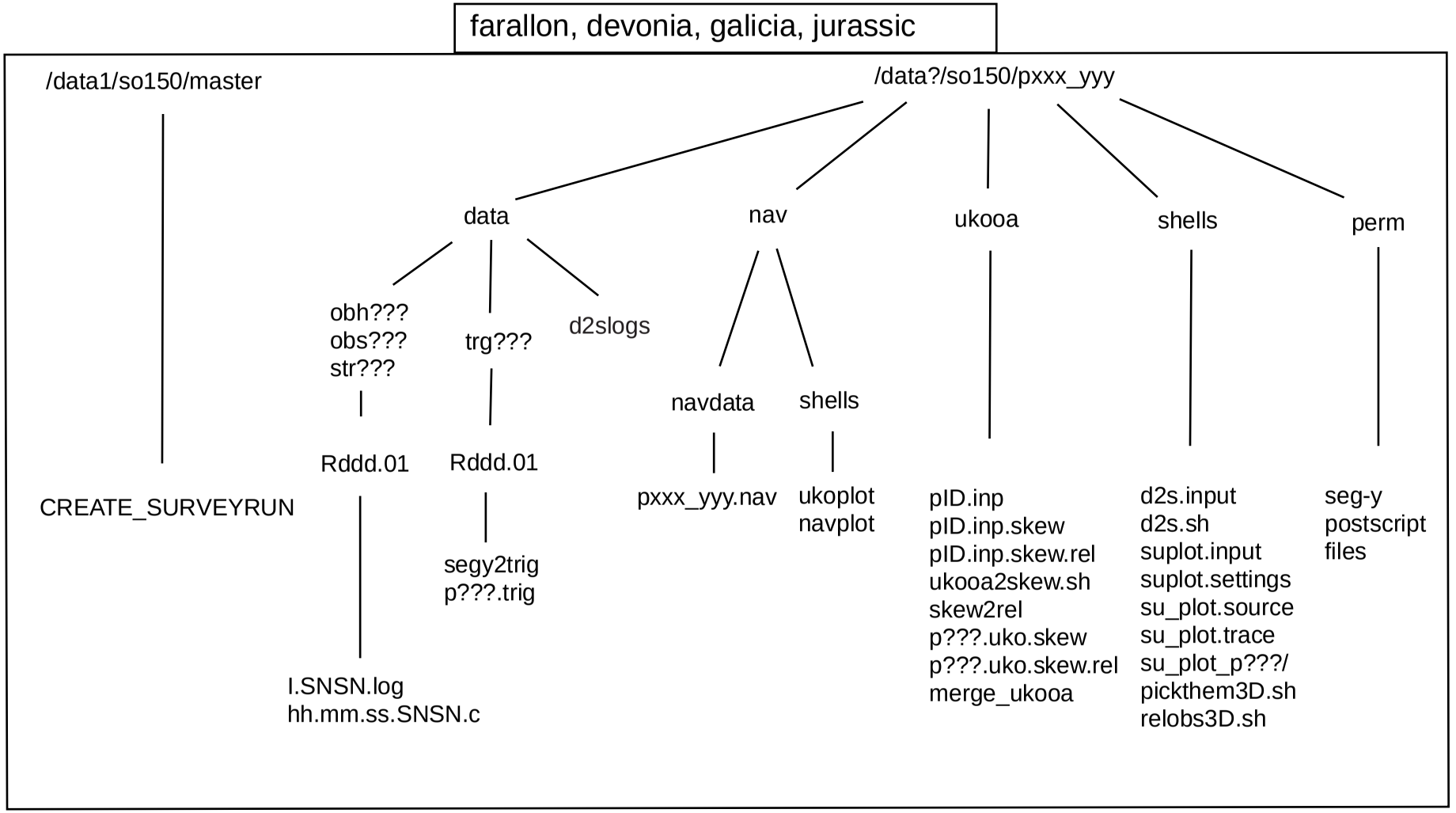

Figure 6.3.2.2: Directory and path distribution for seismic data processing.

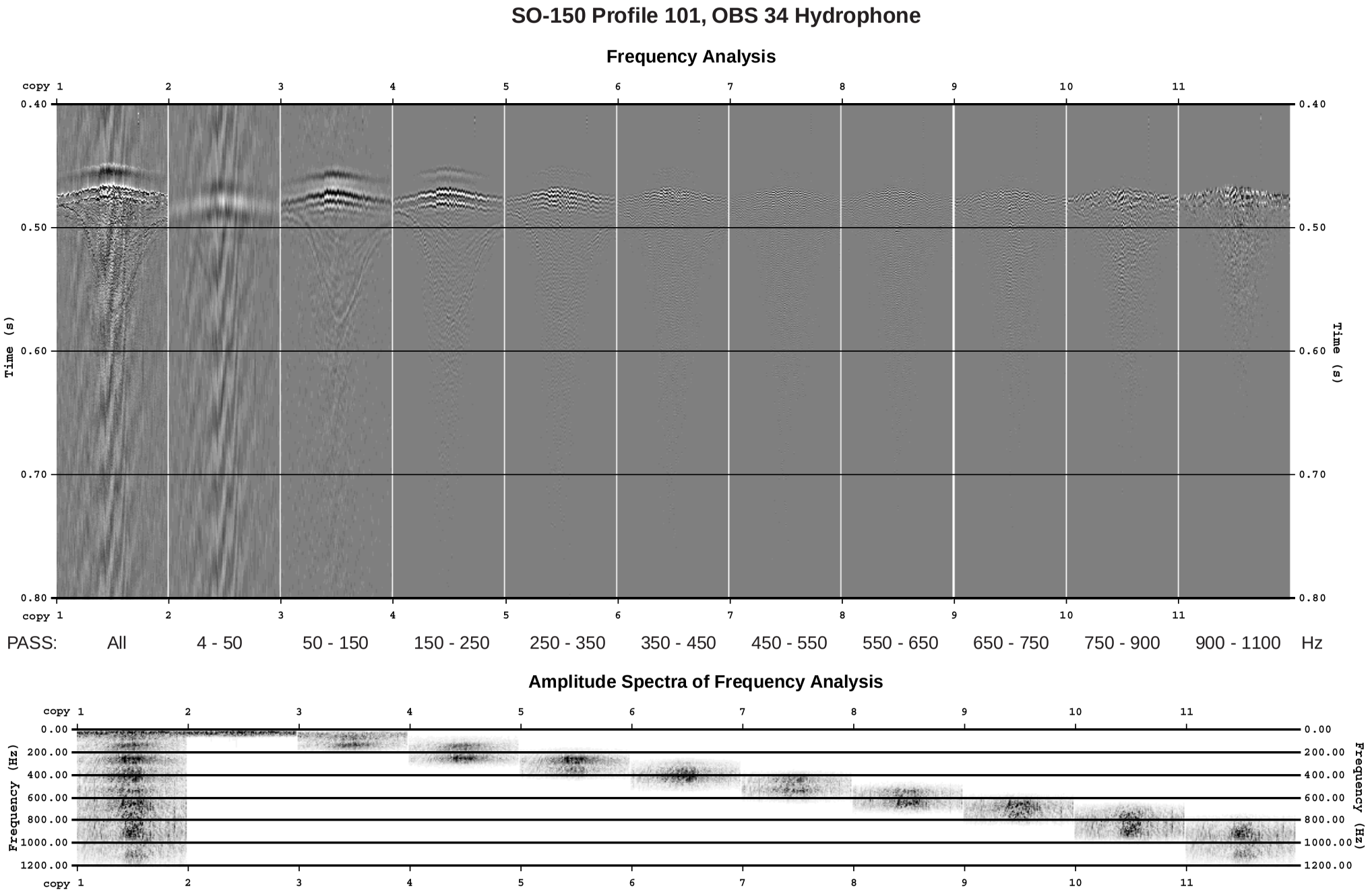

Figure 6.3.2.3: Frequency Analysis, OBS 34 Hydrophone, Profile 101

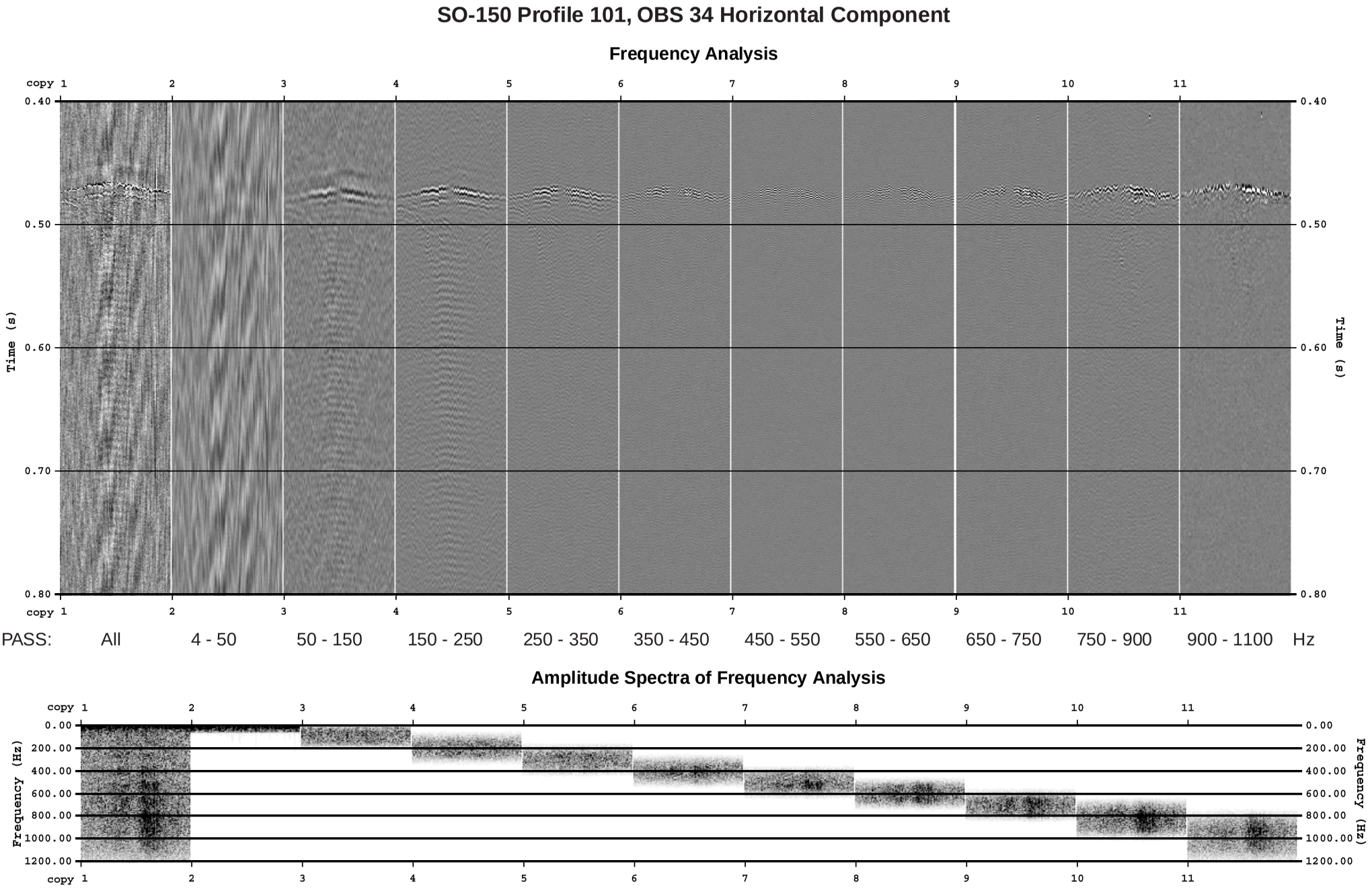

Figure 6.3.2.4: Frequency Analysis, OBS 34 Horizontal Component, Profile 101

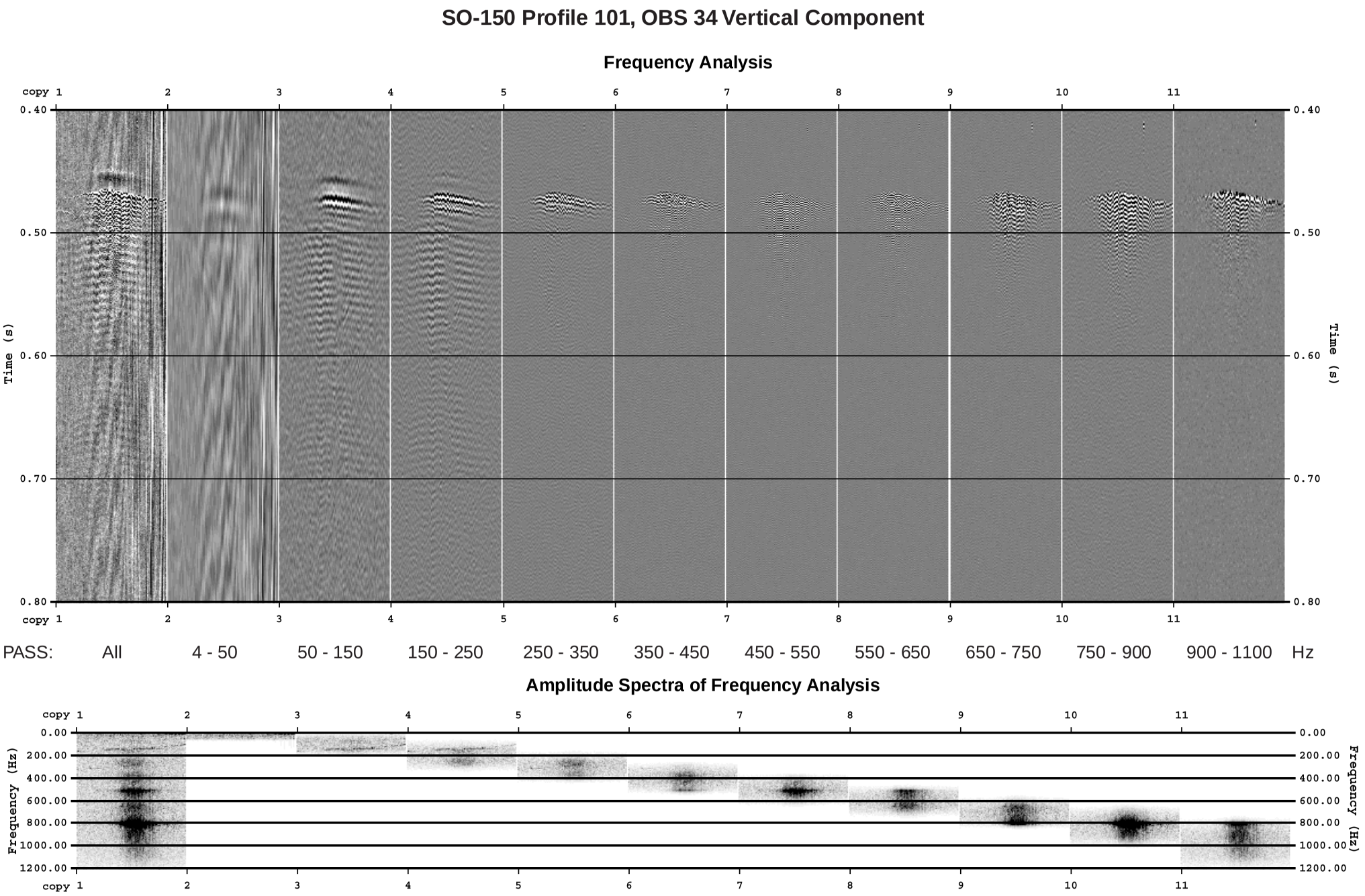

Figure 6.3.2.5: Frequency Analysis, OBS 34 Vertical Component, Profile 101

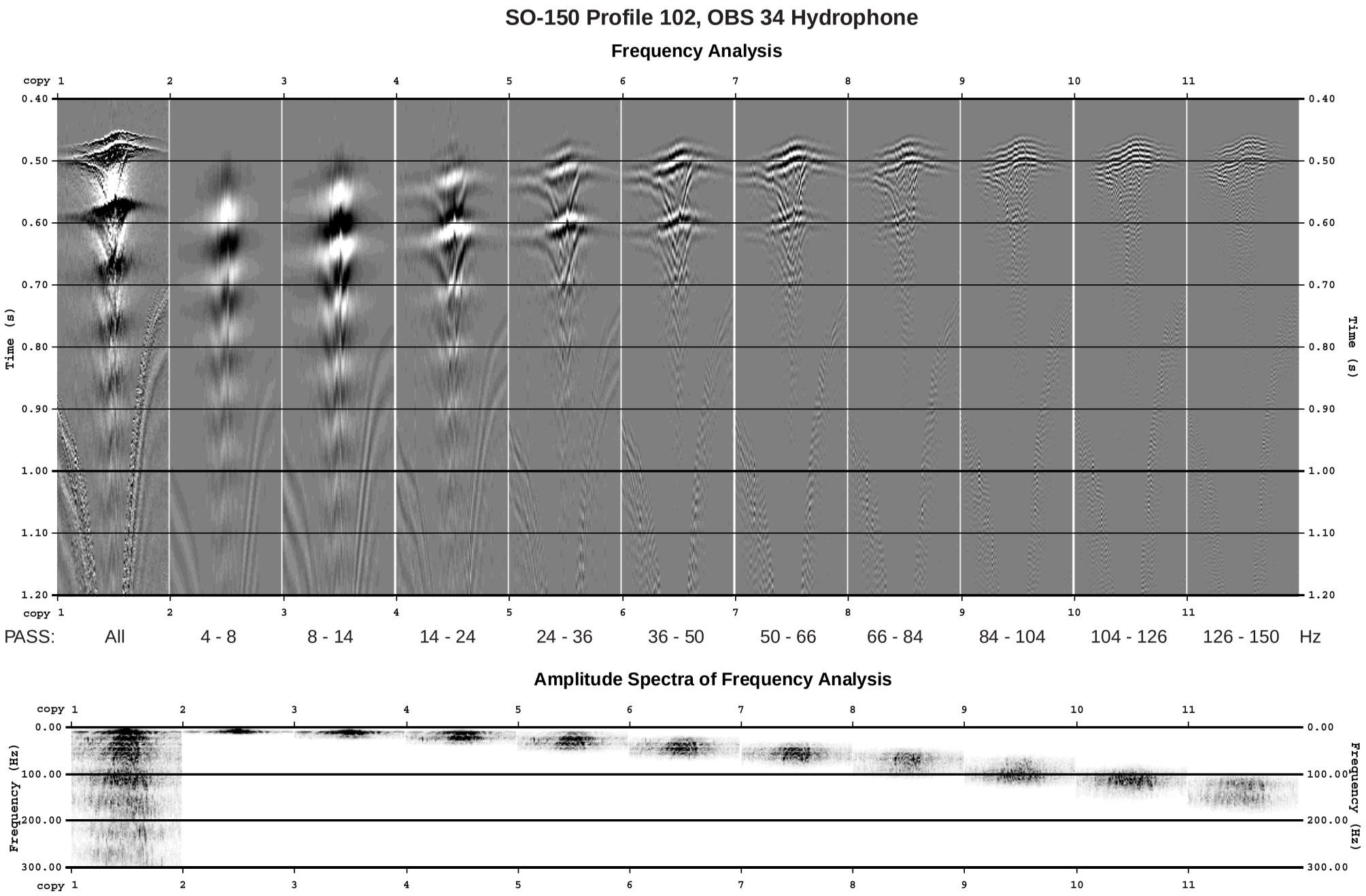

Figure 6.3.2.6: Frequency Analysis, OBS 34 Hydrophone, Profile 102

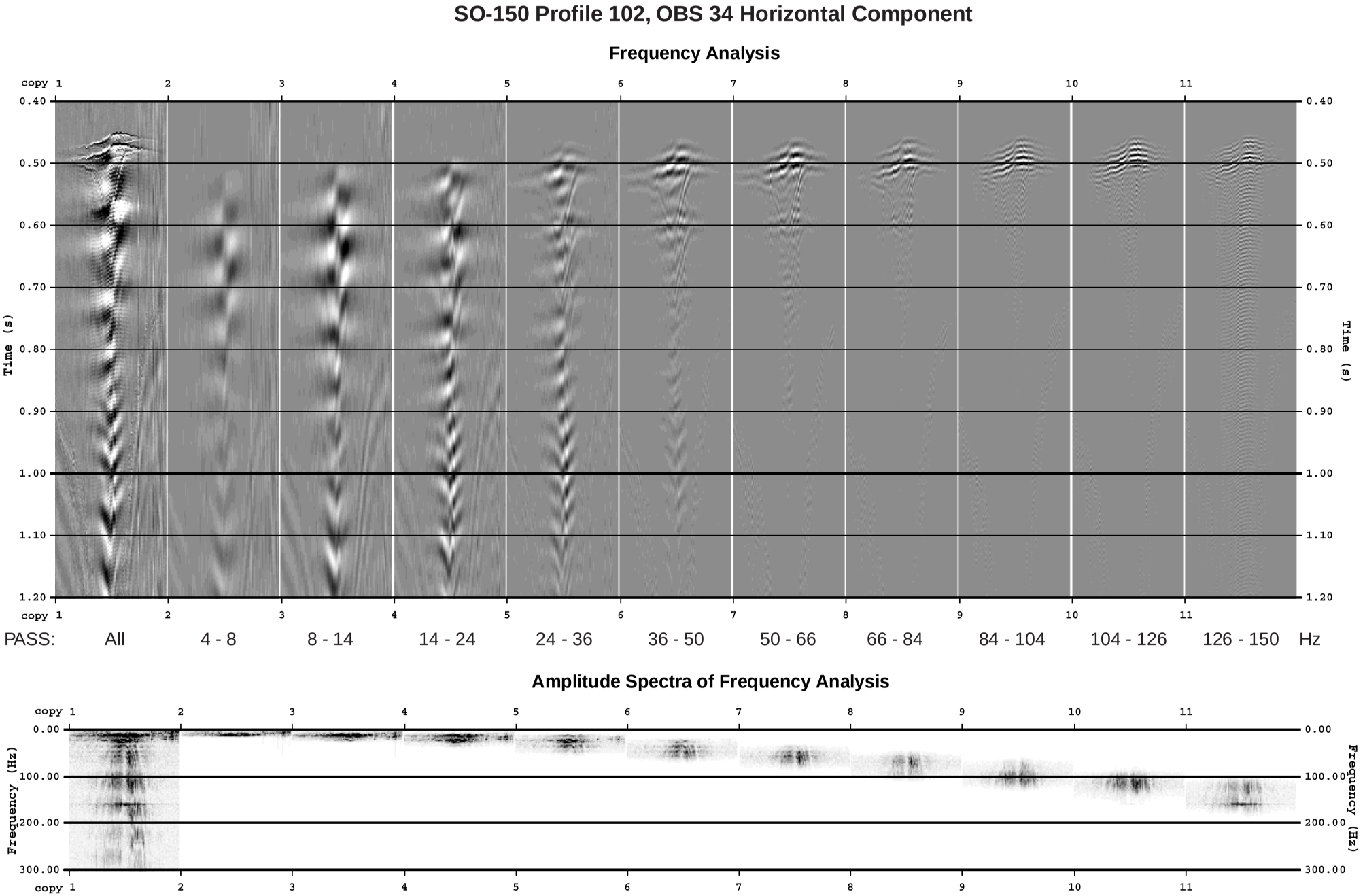

Figure 6.3.2.7: Frequency Analysis, OBS 34 Horizontal Component, Profile 102

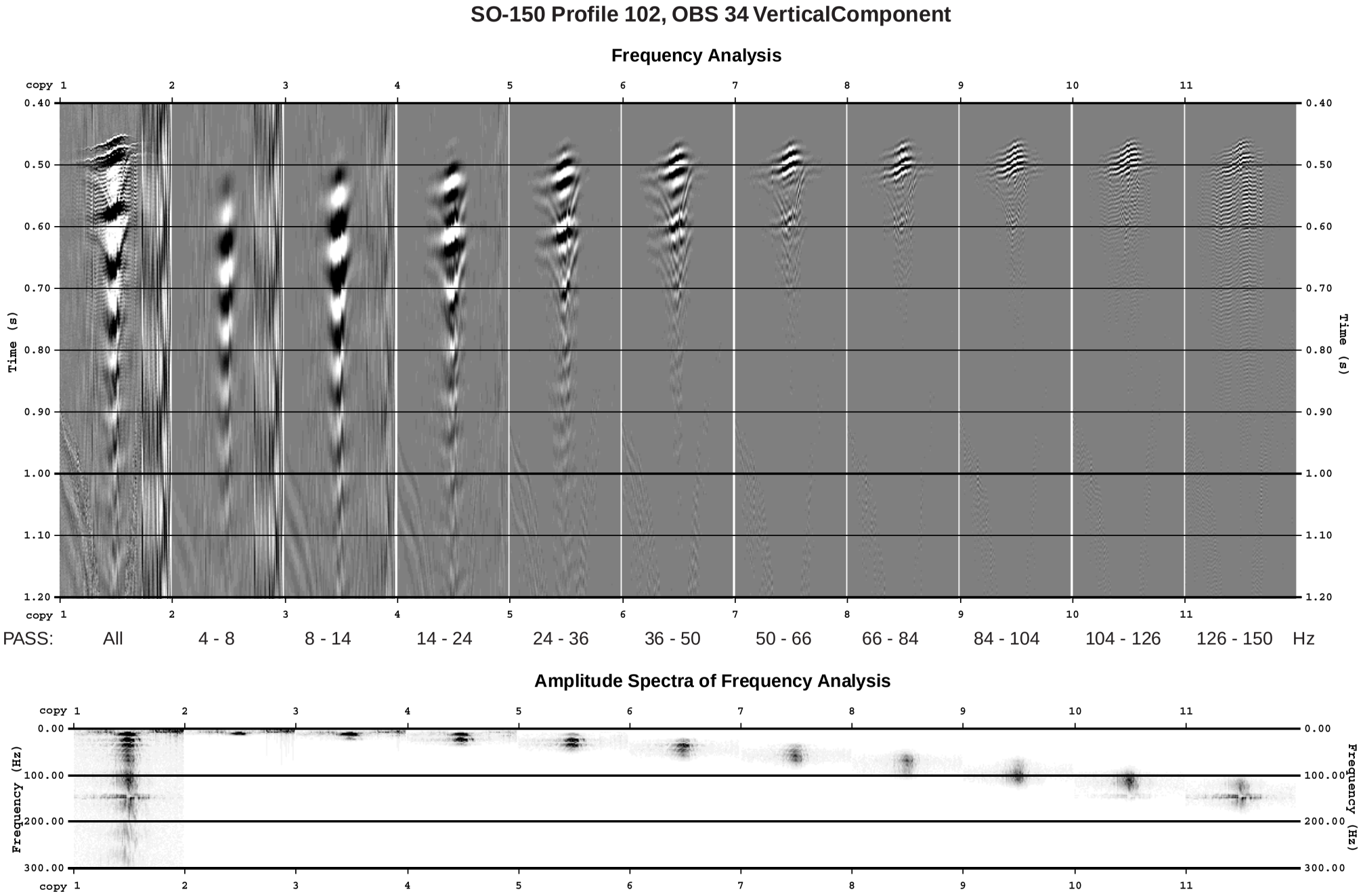

Figure 6.3.2.8: Frequency Analysis, OBS 34 Vertical Component, Profile 102

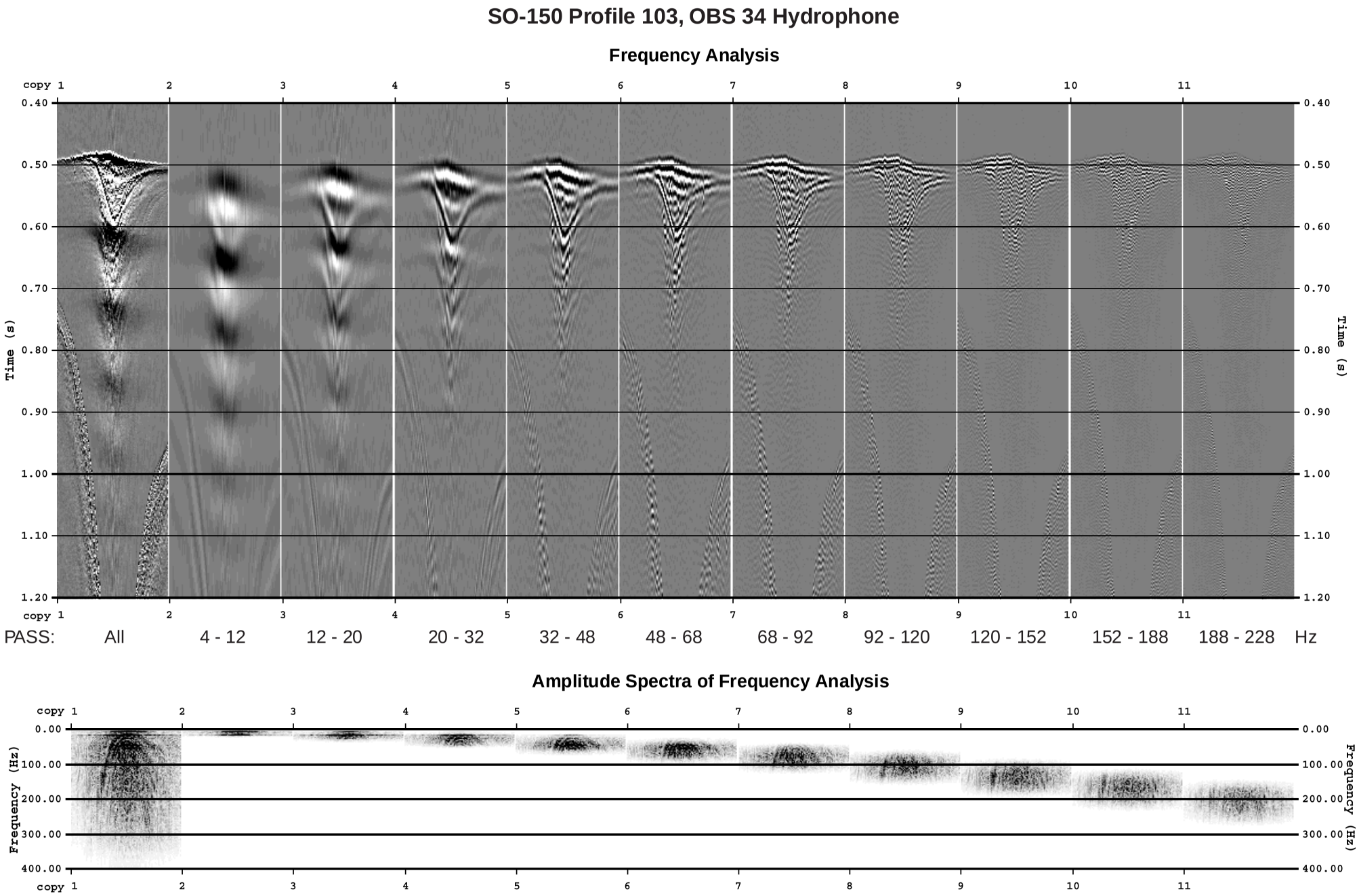

Figure 6.3.2.9: Frequency Analysis, OBS 34 Hydrophone, Profile 103

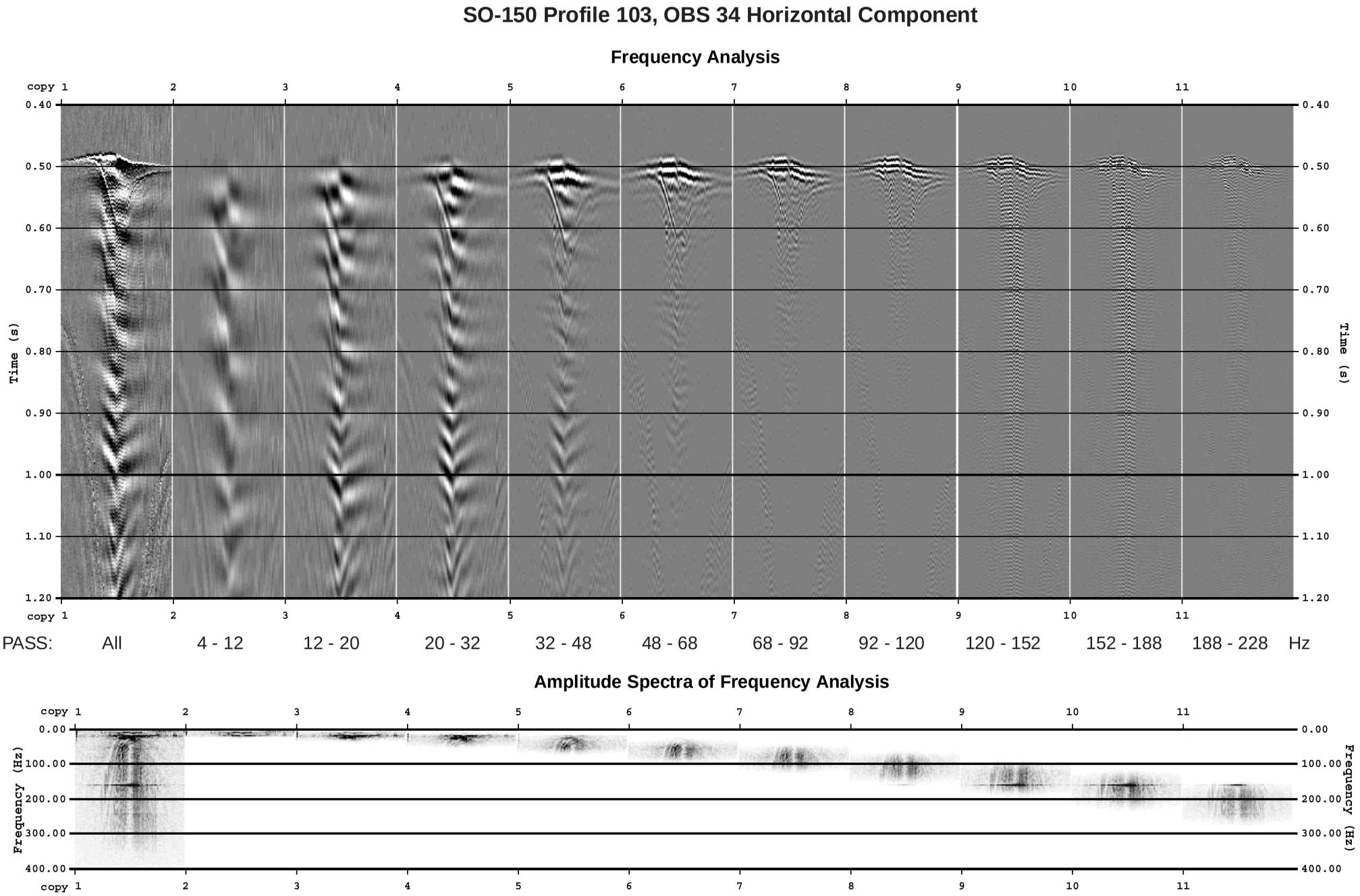

Figure 6.3.2.10: Frequency Analysis, OBS 34 Horizontal Component, Profile 103

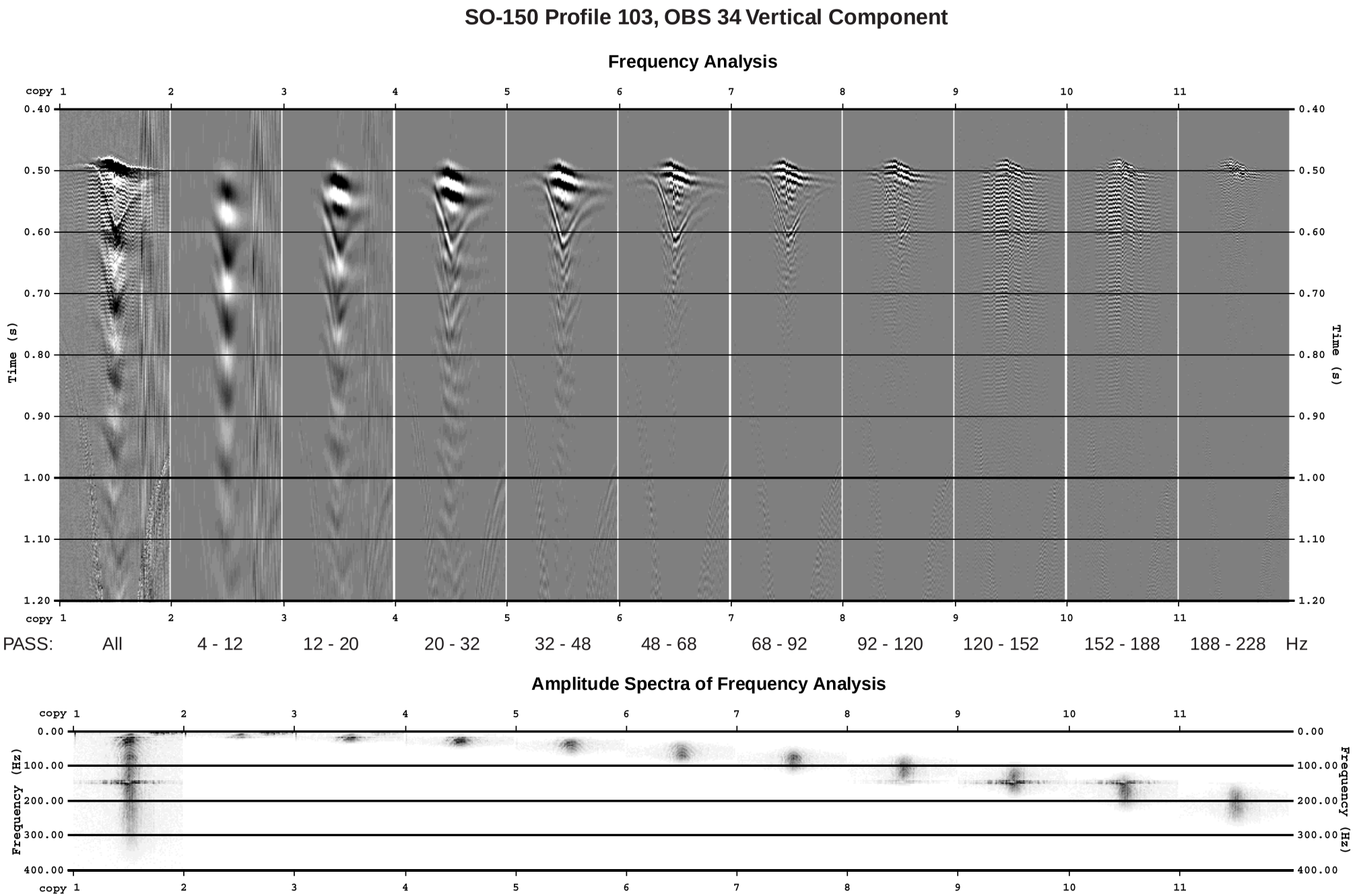

Figure 6.3.2.11: Frequency Analysis, OBS 34 Vertical Component, Profile 103

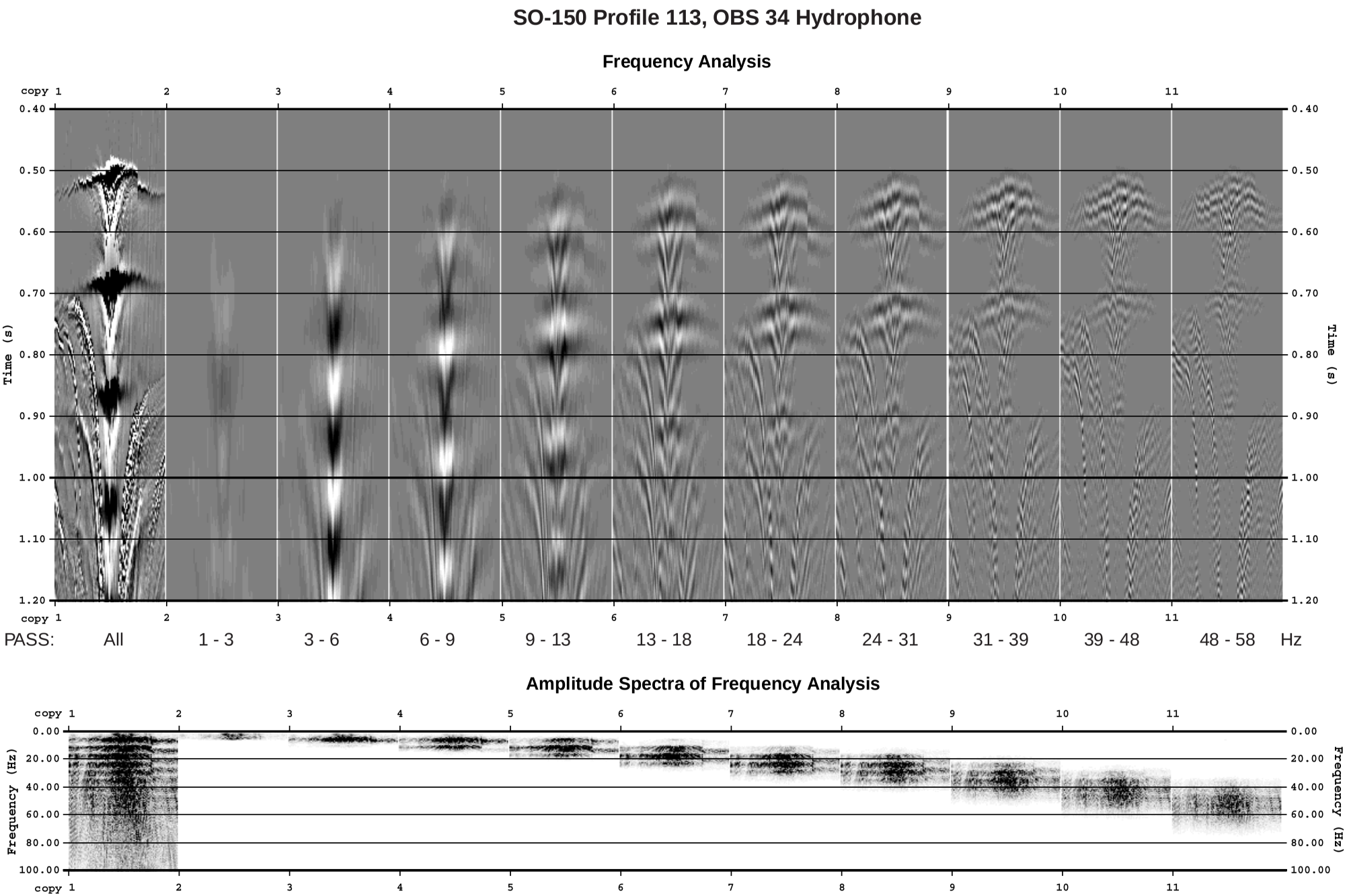

Figure 6.3.2.12: Frequency Analysis, OBS 34 Hydrophone, Profile 113

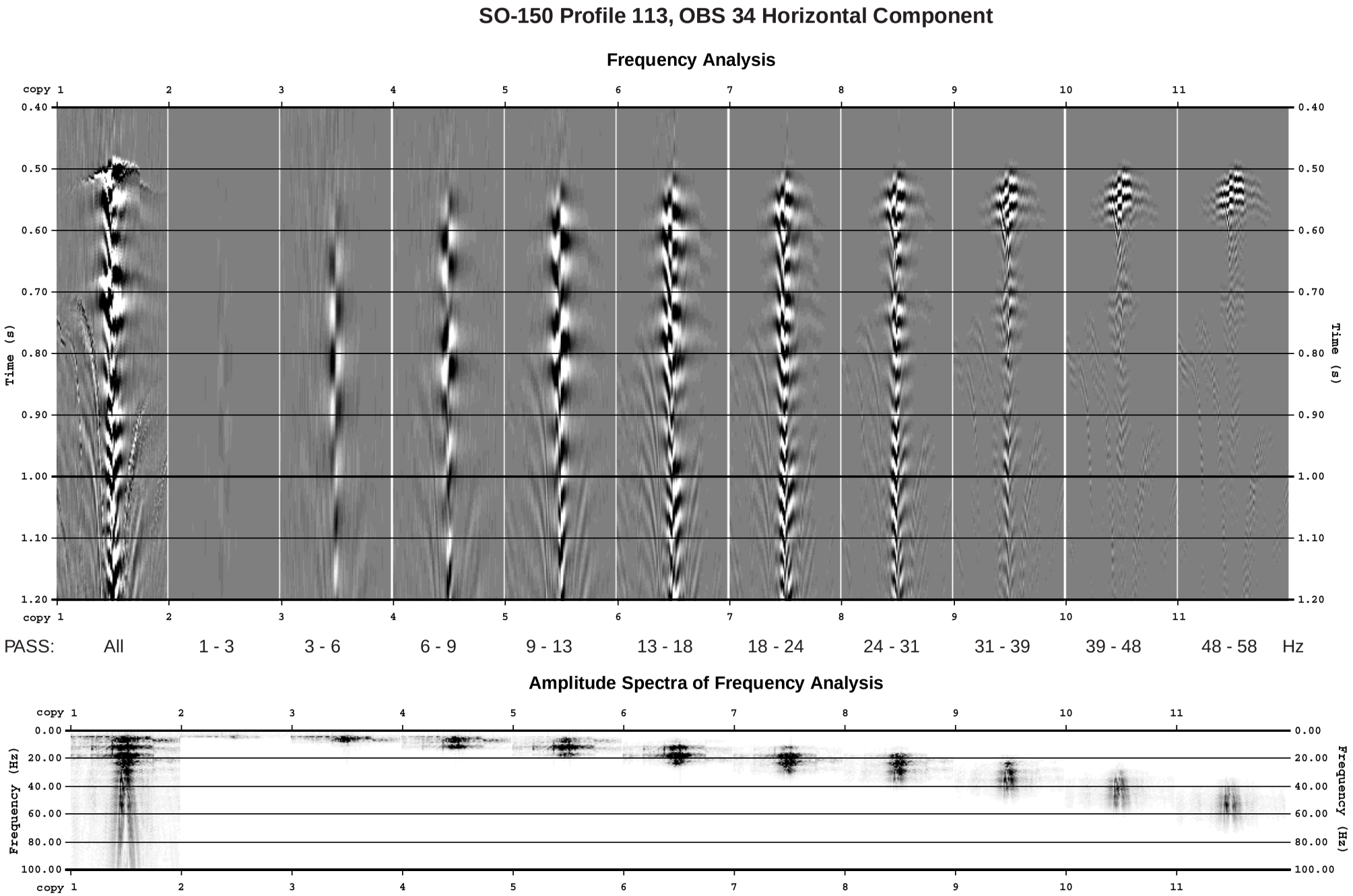

Figure 6.3.2.13: Frequency Analysis, OBS 34 Horizontal Component, Profile 113

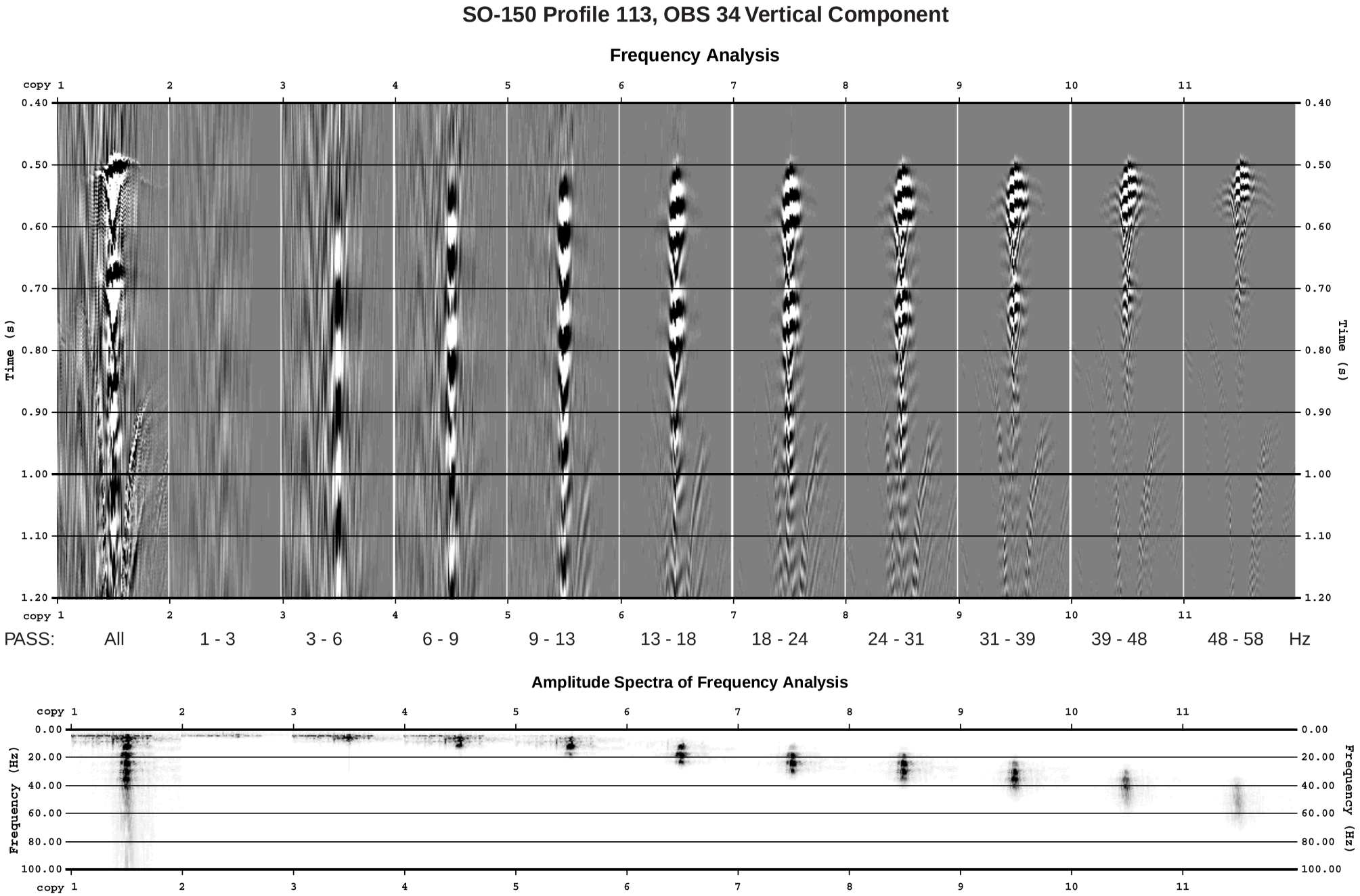

Figure 6.3.2.14: Frequency Analysis, OBS 34 Vertical Component, Profile 113

6.3.3 REGIONAL HIGH RESOLUTION REFLECTION SEISMIC

(A. Kopf, D. Horn, F. Landerer, T. Bohlen, D. Könitz)

In this section, selected seismic reflection profiles are presented in addition to the main experiments and narrow-standing grids. The lines partly resemble profiles from the earlier OR89 survey (all EW-oriented) in conjunction with ODP Leg 146, but also include new positions acquired (NS-trending) to refine the 3-dimensional understanding of the area. All lines shown in this chapter are in bold on the track chart presented in Figure 6.3.3.1.

EW-profiles

Going from north to south, a set of WE-trending seismic reflection lines are shown. The northernmost profile, P121 is shot along OR89-11 with the GI-gun and received by the deep tow streamer. In the west, the base of the second (Hydrate) ridge rises from 3.7 s TWT water depth to only 1.4 s TWT at the crest. While the bulk forming the second ridge seems to be imbricated slices with a seaward vergence, the frontal (western) part of the second ridge shows some seaward-dipping listric normal faults. As a result, the seafloor is rather rough and at depth no continuous reflections can be traced. Towards the central part of Hydrate Ridge, a prominent BSR is visible at 0.2-0.3 s TWT (Fig. 6.3.3.2). This BSR runs eastward into the stratified sediments overlying the leading edges of thrust slices of the third accreted ridge. However, the continuation of the latter is not part of the line anymore. The deeper structure is complex and difficult to interpret without further data processing. Still, occasional landward dipping reflectors may represent the thrust planes along which imbrication took place.

Profile P122, partially following line OR89-08, is a textbook example of imbricated slices towering to form the northern summit of Hydrate Ridge. Its frontal, westward flank comprises shallowly landward dipping accreted sediments (Fig. 6.3.3.3). Towards the crest, the BSR becomes more profound at a shallow depth of only about 0.1 s TWT. At the base of the eastern flank, a smaller ridge is seen. The seismic signal is blurred in this area, suggesting that the underlying strata is deformed (possibly redeposited from a formerly position near the crest). However, the BSR follows that seafloor high at equidistance, suggesting that redeposition has taken place sufficiently long ago to allow for equilibration of the hydrate system. Further east, a series of thrust ridges in the underground structure is overlain by subhorizontal sediments. The anticlinal tops of the little ridges sometimes pierce, or at least affect, the sedimentary cover and are cross-cut by the BSR (Fig. 6.3.3.3).

Further south at about 44°39 N latitude, P125 overlies the previously investigated profile OR89-06 (see Figs. 2.3.2 and 6.3.3.1). From the base of the second ridge, two steep escarpments (stepping about 0.4 s TWT) result from normal faulting and mass wasting. The internal structure remains unclear for most of the Hydrate Ridge, with very thin sedimentary cover on top of accreted material (shots 600-1350, Fig. 6.3.3.4). On the hinterland-facing flank, a cover of up to 0.1 s TWT is found, which increases to a maximum of 0.15 s TWT in the depression between the 2nd and 3rd ridge. The decrease in sediment thickness (relative to the northern lines) can be attributed to a tectonically more active part of the prism, with the most recent movements not long enough gone to have allowed significant sediment accumulation on top of it.

Profile P164 (tracing OR89-04) largely resembles P125, some 3 km to the north. Again, the frontal part of the second accreted ridge is affected by faulting and accordingly is characterized by a rough seafloor morphology (Fig. 6.3.3.5, shots 1750-2100). Hydrate Ridge itself has a strong BSR at 0.15-0.2 s TWT. With some difficulty, it can be traced some km into the sediment fill to the east. Like its two counterparts to the north, line P164 shows seaward vergent reflectors beneath the sediment fill, probably representing the boundary between thrust slices when imbrication and uplift occurred.

Along line P165 (OR89-03), some profound changes in the seismic image can be observed (Fig. 6.3.3.6). Like its predecessor, it was acquired with the GI-gun and deep tow streamer. Although revealing the same sharp escarpments at the base of the outer flank, suddenly sedimentary structures are observed (shots 100-400). The features on top of a bright, rough reflection (the base of old accreted material?), the more recent products of accretion, show only gentle folding or duplex-type accumulations. The BSR intersects them, as well as the more deformed sediments, at a depth of 0.2 s TWT (Fig. 6.3.3.6). Shallow dipping features in the hinterlandward part of the line are proposed to be faults. Some of them affect the overlying slope apron (e.g., at shot 1650), proving deformation and lateral shortening are active here.

The only WE-line shown in this section, which is not a re-shot of already existing lines, is P82 (see Fig. 6.3.3.1 for location). It is roughly midway between the former lines OR89-02 and OR89-01, and runs across the southern summit of the Hydrate Ridge. The line ties both the NS-profiles P51 and P83, and the "Pinnacle" and "southern pockmark" areas together (see below).

On the southern summit in the west, the Pinnacle can be seen as a sharp needle at shots 200-220 (Fig. 6.3.3.7). Underneath, layering parallel to the seafloor can be seen on top of deformed accreted material. The latter is characterized by being cut through by the BSR. Between Hydrate Ridge and the landward ridge (shots 1100-1450, Fig. 6.3.3.7), a wedge-shaped basin fill has accumulated. The initial stages of deposition must have been a direct consequence of Hydrate Ridge being thrust beneath the eastward ridge. In order to stabilize itself, the latter was affected by slumping and sliding (see base of the stratified sequence being rough and lumpy; shots 800-1000). After it was accomodated for the movements geometrically, turbidites filled the depression. The uppermost slope sediments were then deposited in a tectonically quiet phase, as indicated by their undisturbed nature and constant thickness over the entire basin and eastward flank of Hydrate Ridge.

Profile P84 at a latitude of about 44.27°N was acquired with the GI-gun and the deep tow streamer in EW-direction (Fig. 6.3.3.8). It illustrates a wide, plateau-like area of well-layered sediments in its western part. Going east it climbs the flank of a prominent ridge, the SE knoll, which is comprised of accreted strata. Given morphological similaities and the development of a BSR in the subsurface, SE knoll can be envisaged as the souther counterpart to Hydrate Ridge further to the north. Concerning a more detailed description and discussion of the varaiability of the BSR, the reader is referred to Chapter 6.3.7 below.

NS-profiles

The first profile to interconnect all EW-lines so far described is P43 (Fig. 6.3.3.1). It was acquired in SN-direction using the Sparker and the two surface streamers (Fig. 6.3.3.9). The southern part of the line shows 0.3-0.4 s TWT thick, more or less undisturbed sediments overlying accreted strata. The well-stratified sediment is deposited from both the east and the west into the depression, which represents the syncline between the 2nd and 3rd accreted ridge (the same which is intersected by profile P82 in the WE-direction). Sedimentation is most likely a result of oversteepening of the ridges during tectonic shortening. Gravity flows and slumps help the prism to maintain a stable taper. When going further to the north, the northern summit of Hydrate Ridge shows a thin undisturbed slope cover, immediately underlain by highly disturbed accreted sediment with a chaotic seismic facies. Faulting is observed along gently dipping planes to the SW. A well developed BSR is located some 0.15 s TWT below the seafloor of the ridge, but also continues layer-discordant into the synclinal fill (Fig. 6.3.3.9).

Profile P51 was run parallel to P43, but about 4.5 km eastward (Fig. 6.3.3.1). Again, it was acquired with the Sparker and surface streamer configuration, coming from the southern flank of the northern summit of Hydrate Ridge. To its south, a NNE-SSW-striking smaller ridge is cut at a narrow angle, before sediments thicken rapidly towards the basin fill between the 2nd and 3rd

ridge (Fig. 6.3.3.10). The line was a re-shoot of the best part of OR89-44 (Fig. 2.3.2). The most spectacular feature on this line is the subsurface structure of the small ridge. What looks at first glance as some possibly slumped material may well be the product of backthrust faulting. Such faults are clearly seen at depth further to the north, and can also be identified in the Sparker data. Penetration is very limited and what appears to be refraction from surface morphology could also be shallow-dipping faults. The sediment below the slope apron is highly deformed and does not reveal structural trends. The BSR on this line can clearly be seen beneath the little ridge, ranging in depth between 0.25 and 0.3 s TWT.

Moving further outward towards the trench and deformation front, the third NS-line to be presented is P83. It is located at 125°11.0 W longitude, running parallel to the first accreted ridge. From the seafloor topography it can be seen that shortening is rather intense, with some rough mounds between shots 150-450 (Fig. 6.3.3.11). The line was acquired with the GI-gun and the deep tow streamer, however, data quality is limited here. It is obvious from this profile (as well as from the previous two parallel lines P43 and P51) that along strike, a strong variation exists between basin-type layered deposits and ridges of deformed material. This suggests that transpressional rather than fully compressional stresses are experienced by the material in the overriding forearc. Such faulting has previously been reported, and seems to occur roughly in a SW-NE-direction (Goldfinger et al., 1996). The almost systematic increase in water depth (or continuous dip of the Hydrate ridges southern flank) to the south of the study area is also to be noted. The region of maximum deformation (rough seafloor, see above) is followed by a rather gentle morphology to the south. Here, the distinct BSR beneath the rough surface fades when entering the less deformed sediments (Fig. 6.3.3.11). Given that the intensity of the reflector is controlled by the amount of free gas beneath it (see Chapter 2.3), there seems to be a causal link between availability of gas (i.e., enhanced formation pressures) and deformation.

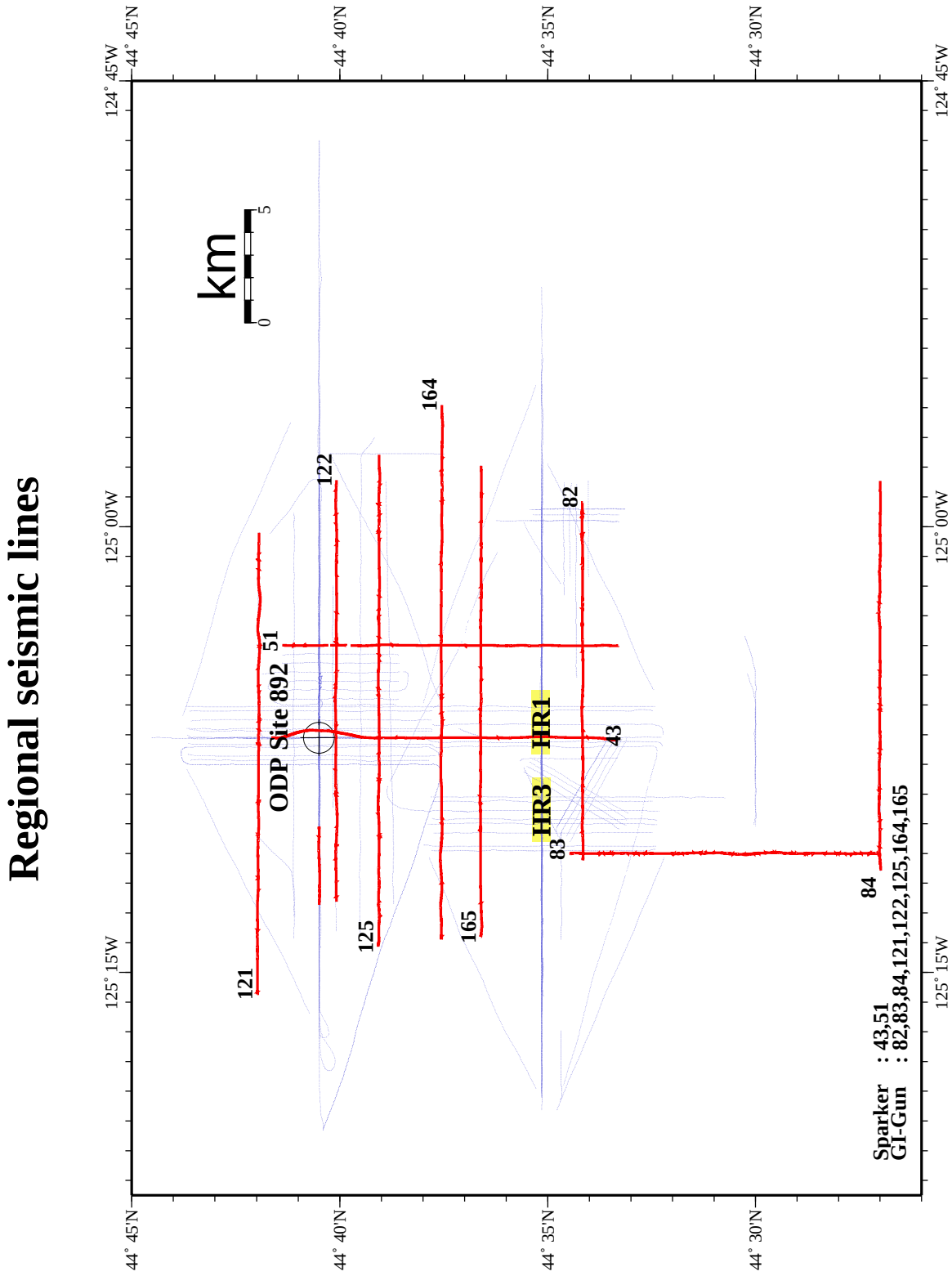

Figure 6.3.3.1: Location map of regional seismic lines.

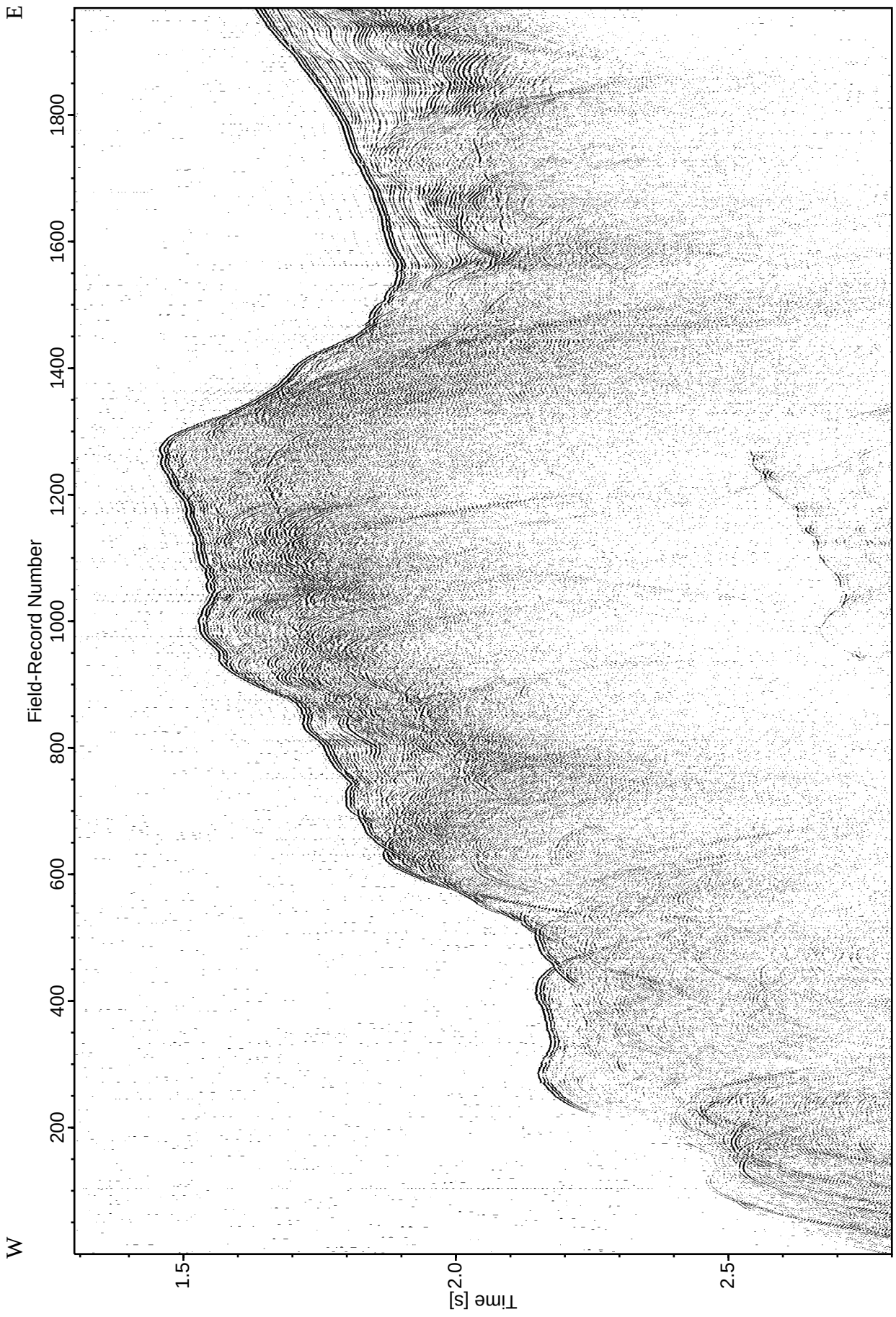

Figure 6.3.3.2: Record section with source GI-Gun, Profile 121.

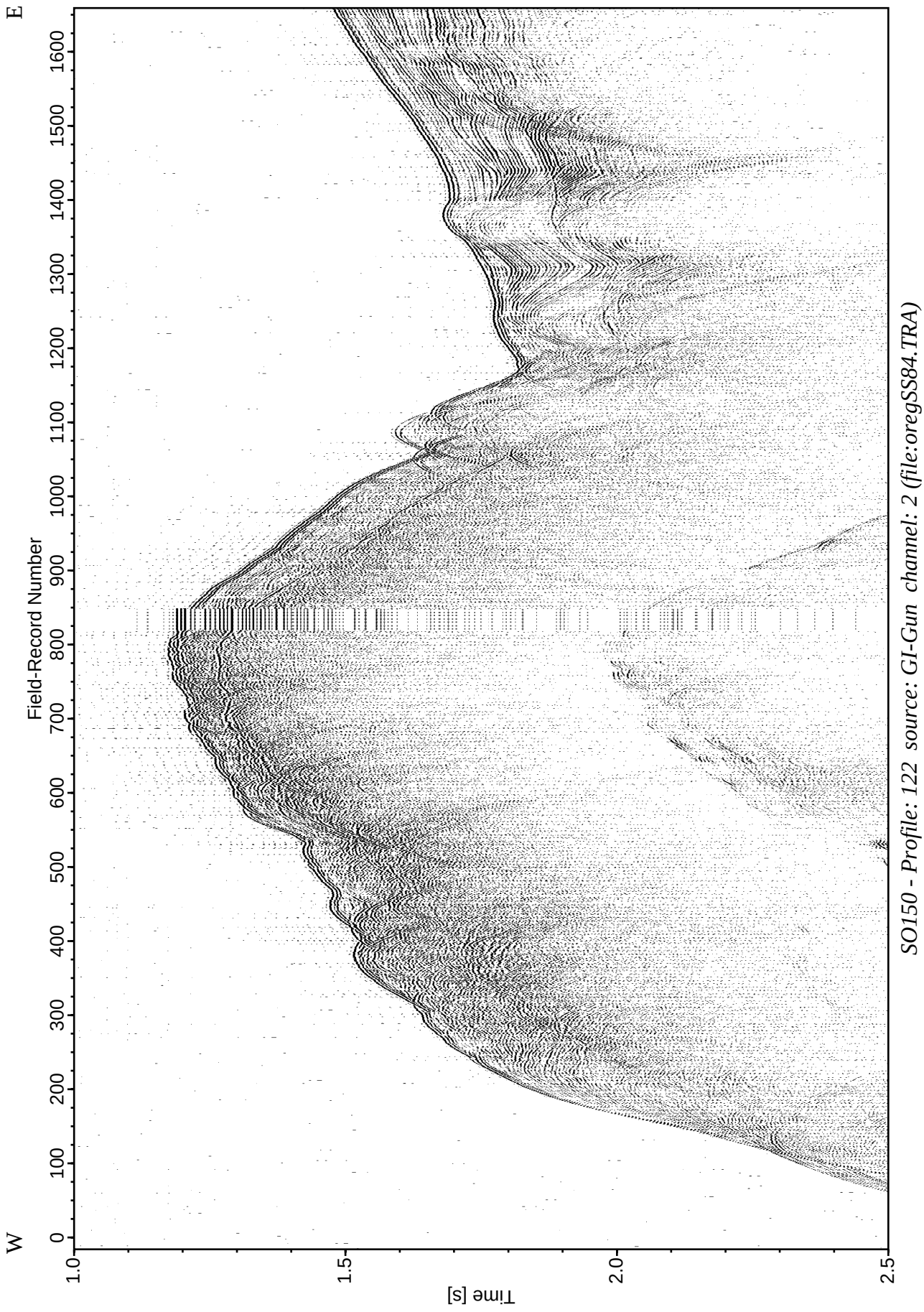

Figure 6.3.3.3: Record section with source GI-Gun, Profile 122.

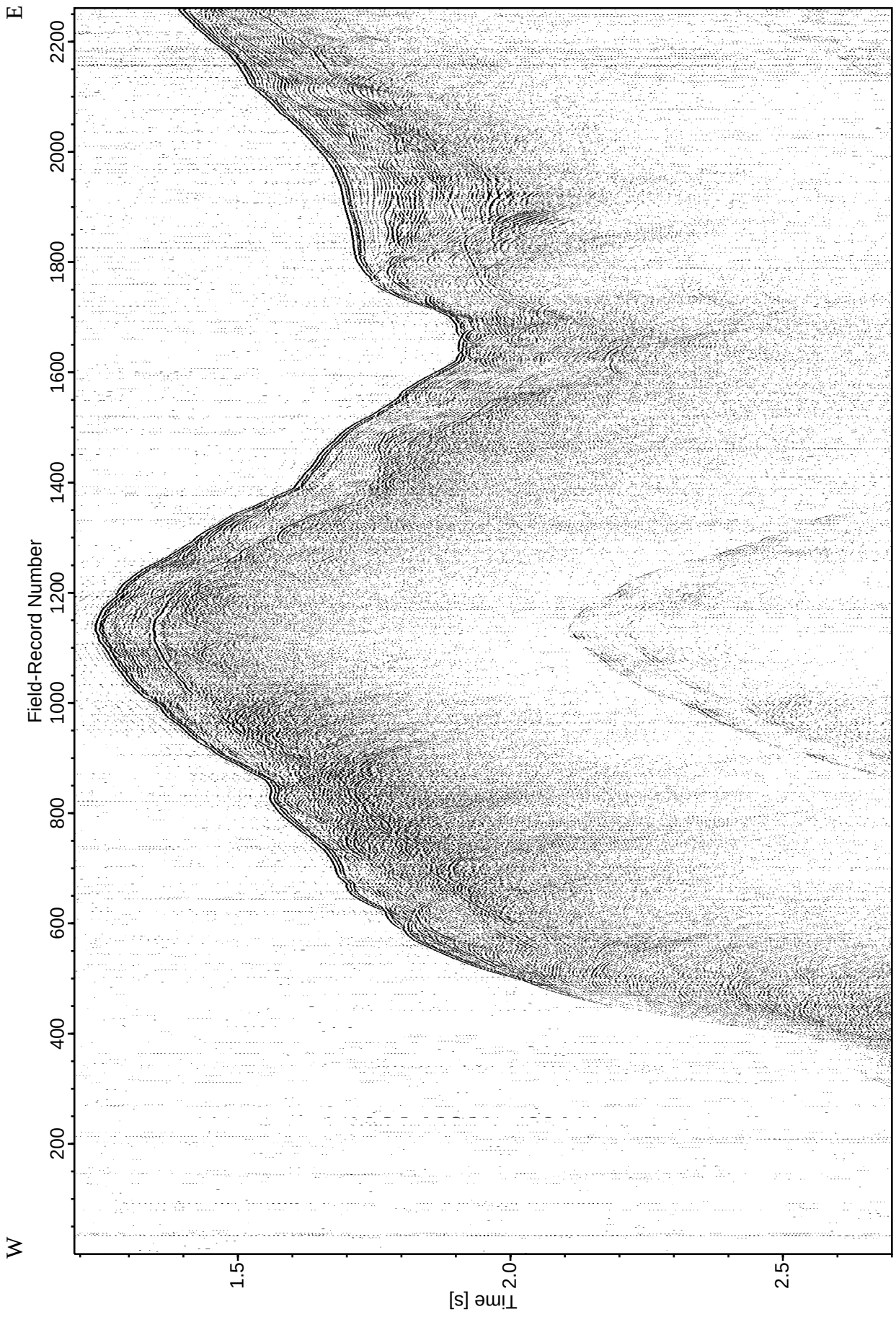

Figure 6.3.3.4: Record section with source GI-Gun, Profile 125.

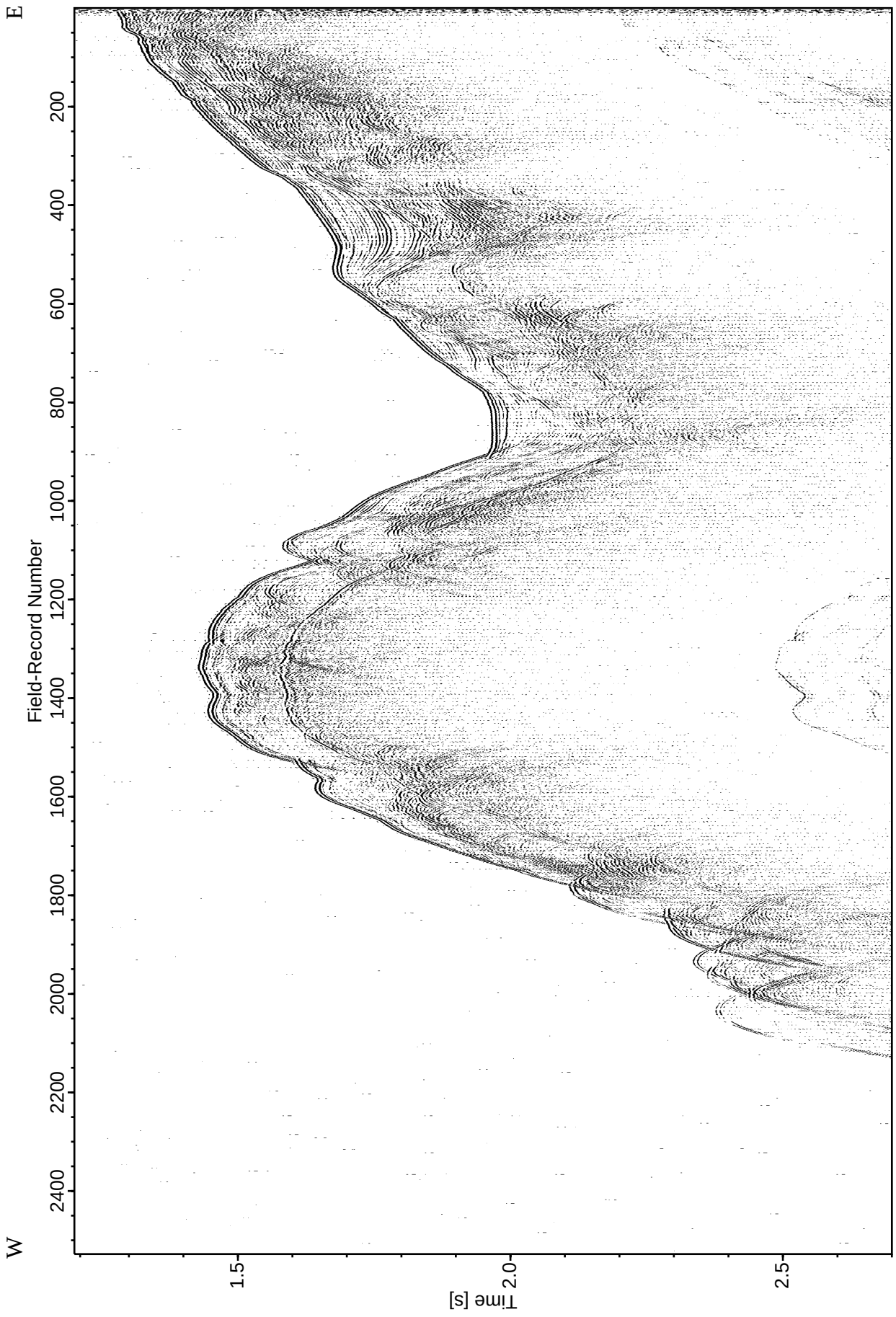

Figure 6.3.3.5: Record section with source GI-Gun, Profile 164.

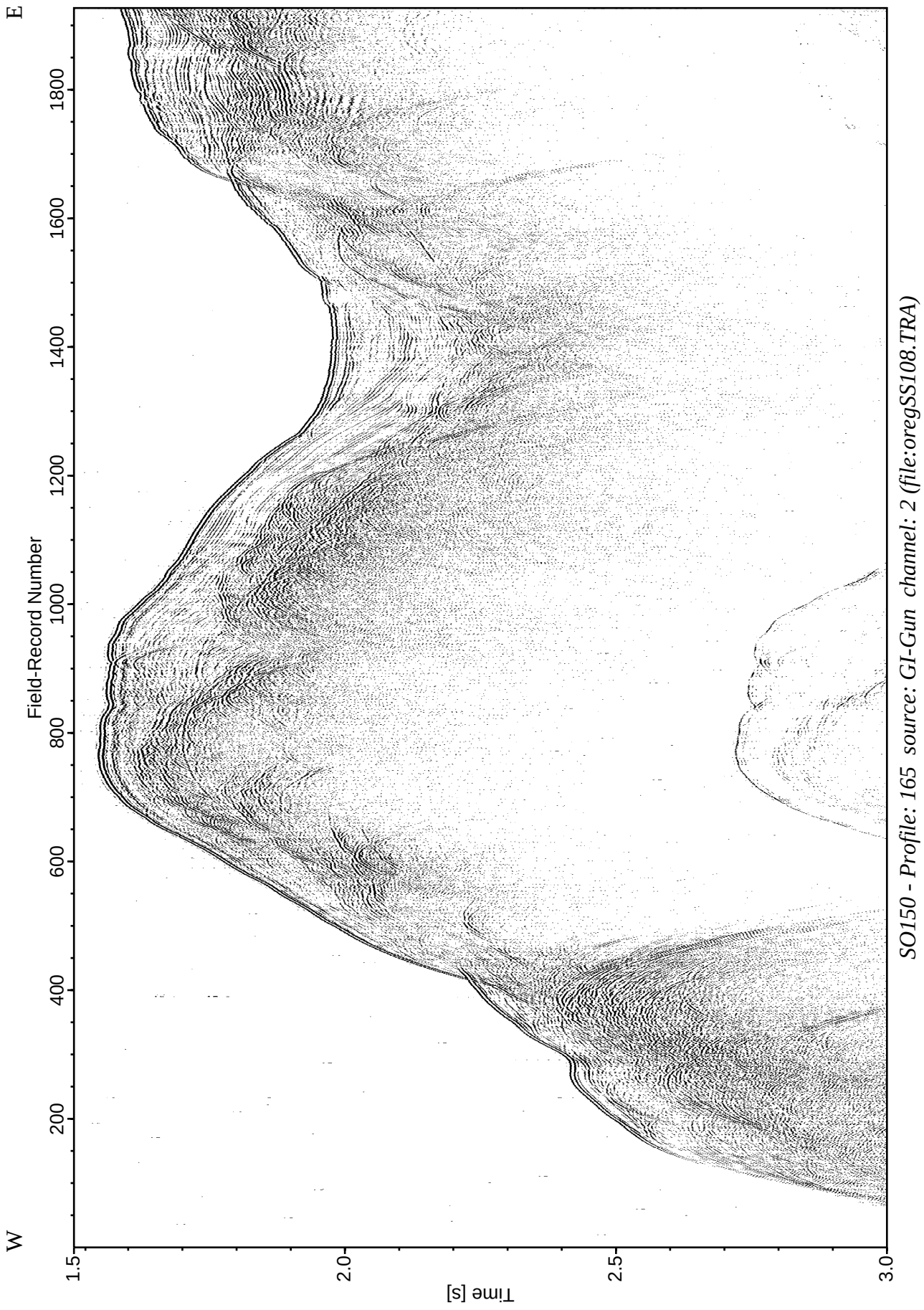

Figure 6.3.3.6: Record section with source GI-Gun, Profile 165.

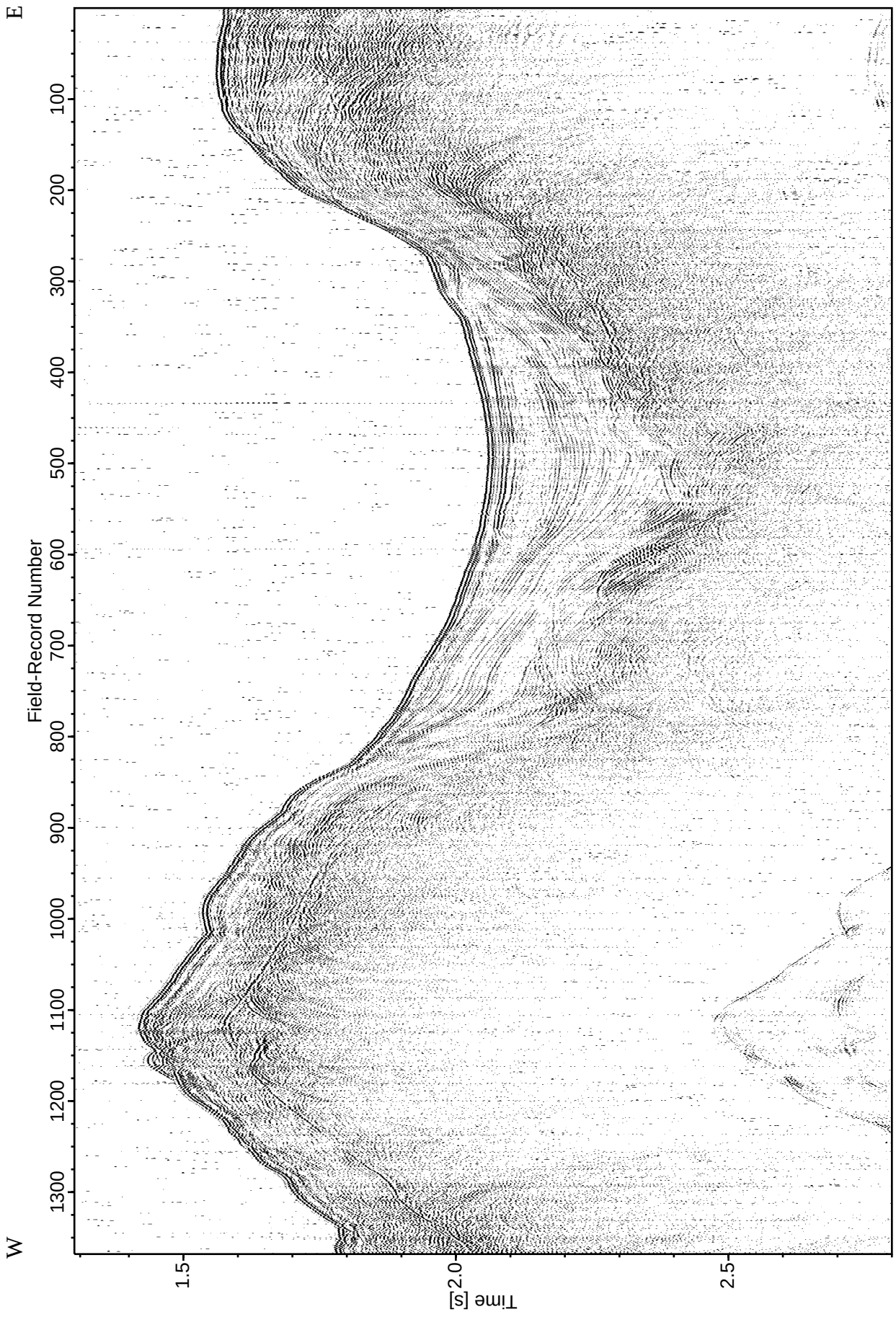

Figure 6.3.3.7: Record section with source GI-Gun, Profile 82.

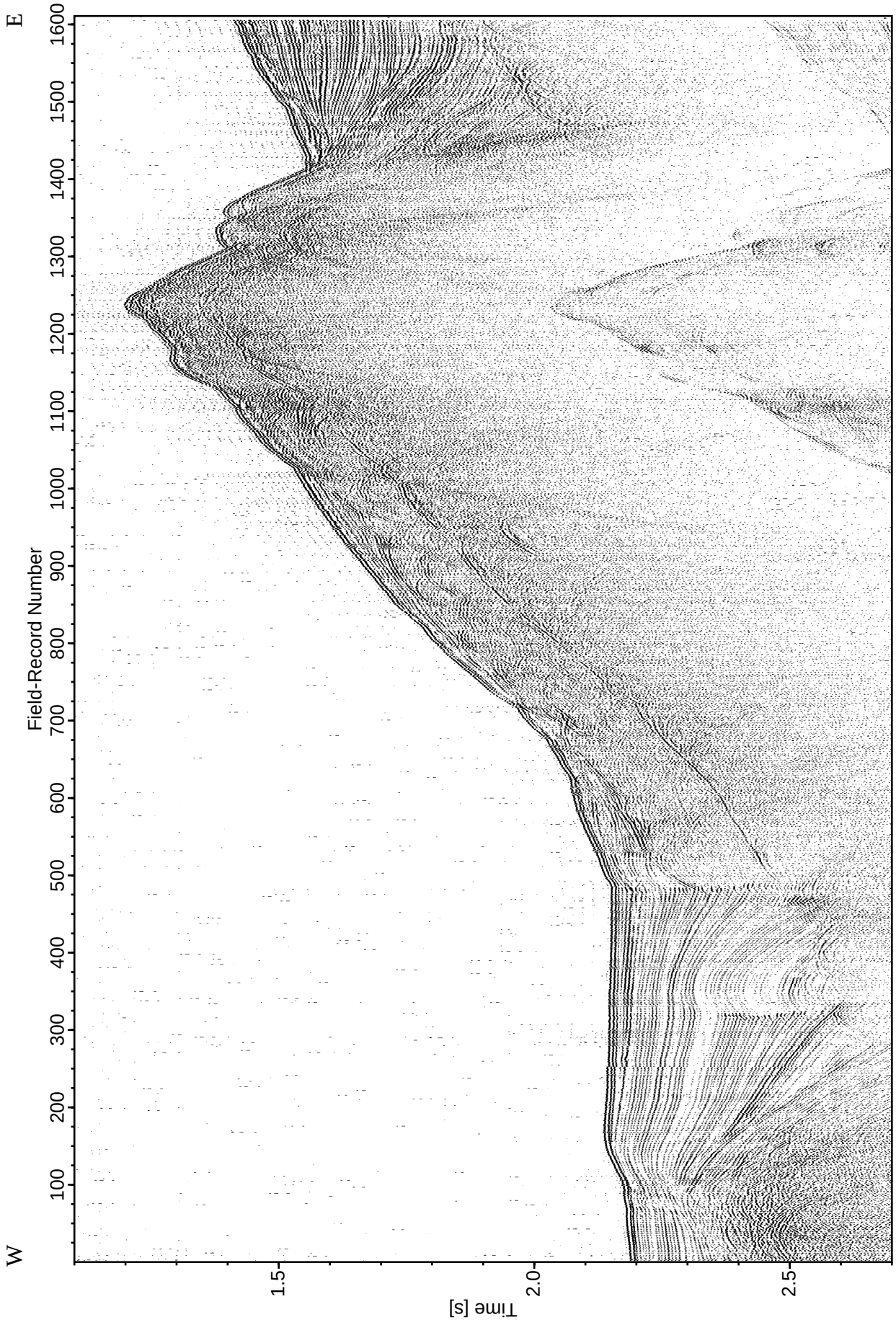

Figure 6.3.3.8: Record section with source GI-Gun, Profile 84.

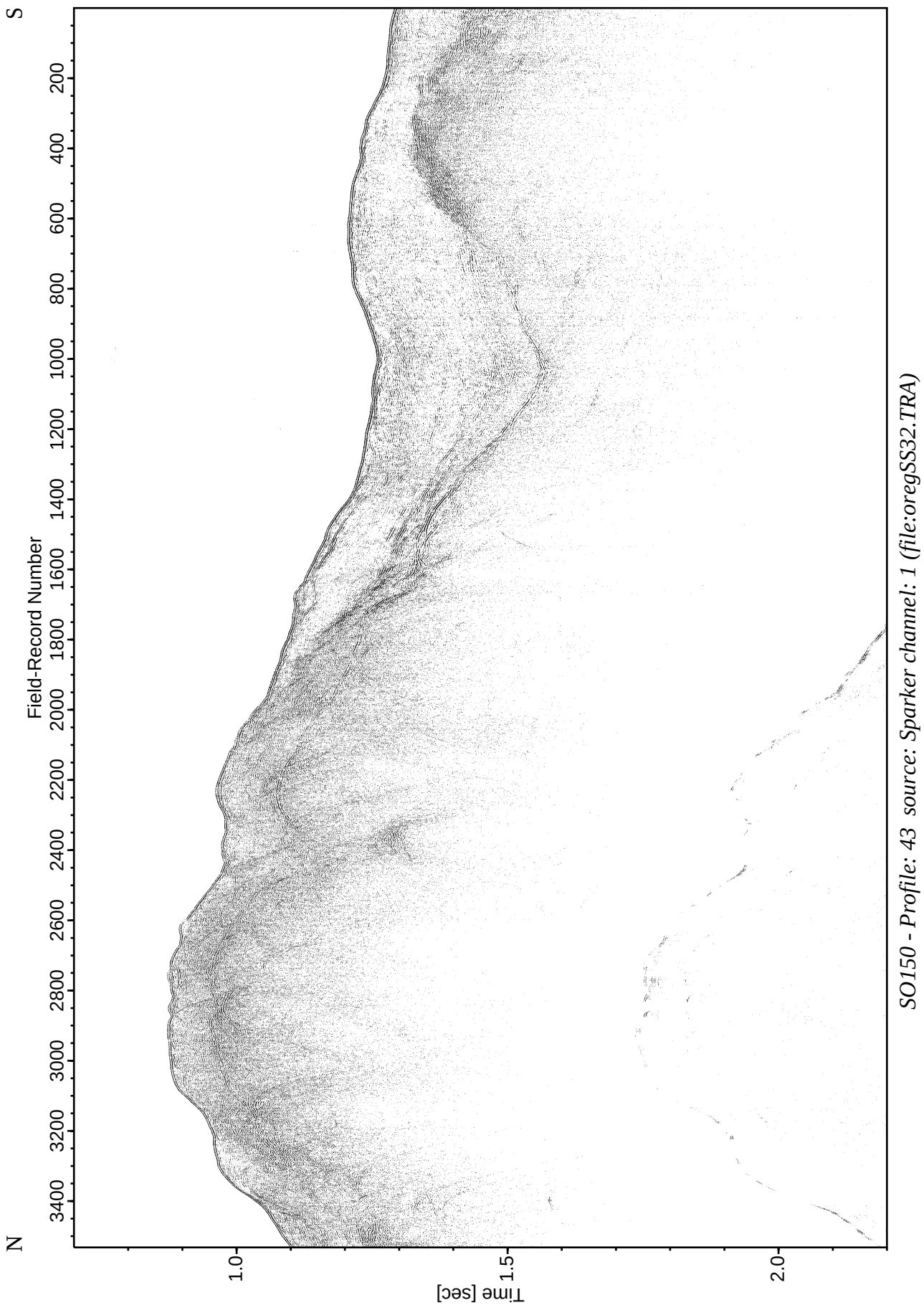

Figure 6.3.3.9: Record section with source Sparker, Profile 43.

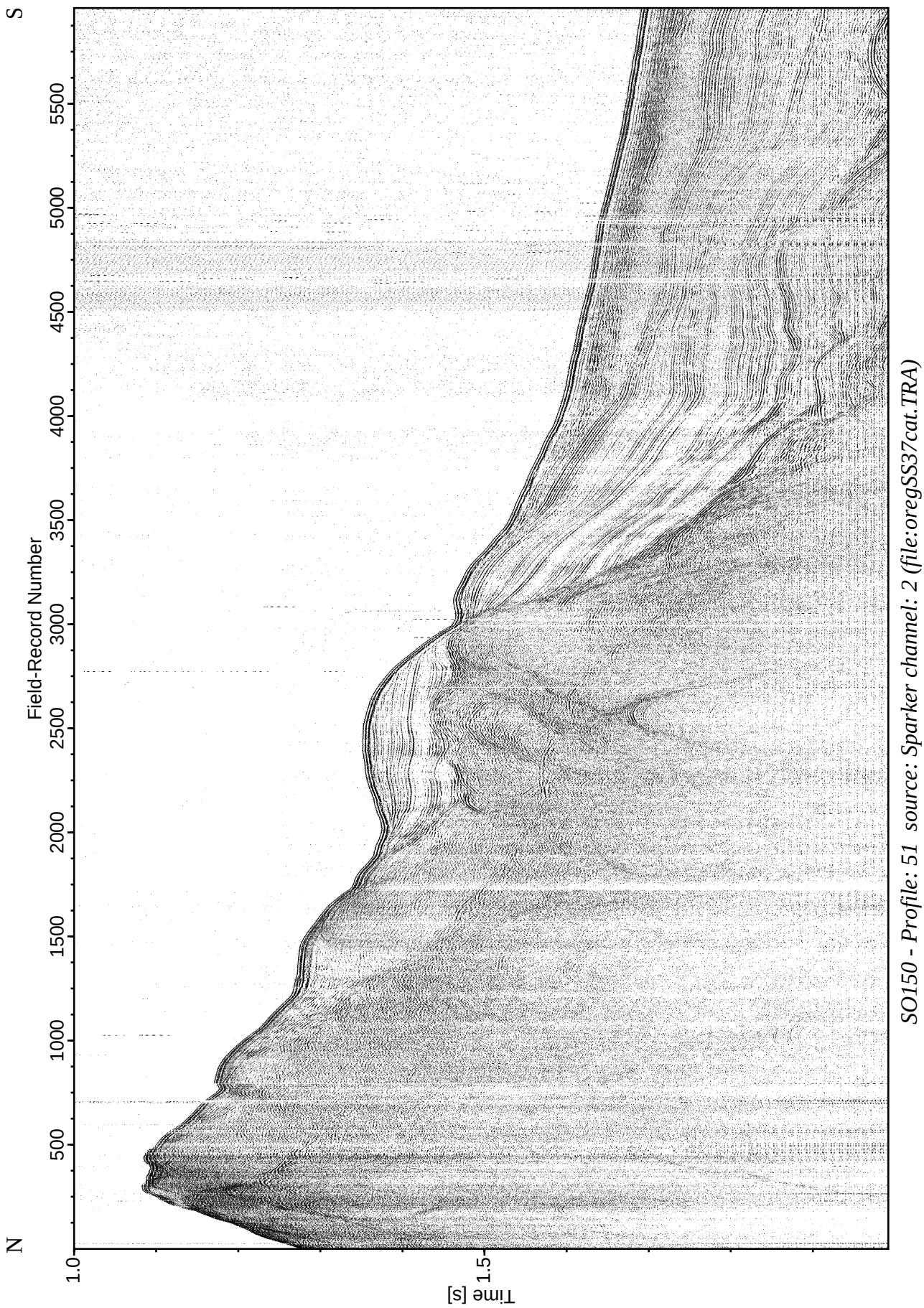

Figure 6.3.3.10: Record section with source Sparker, Profile 51.

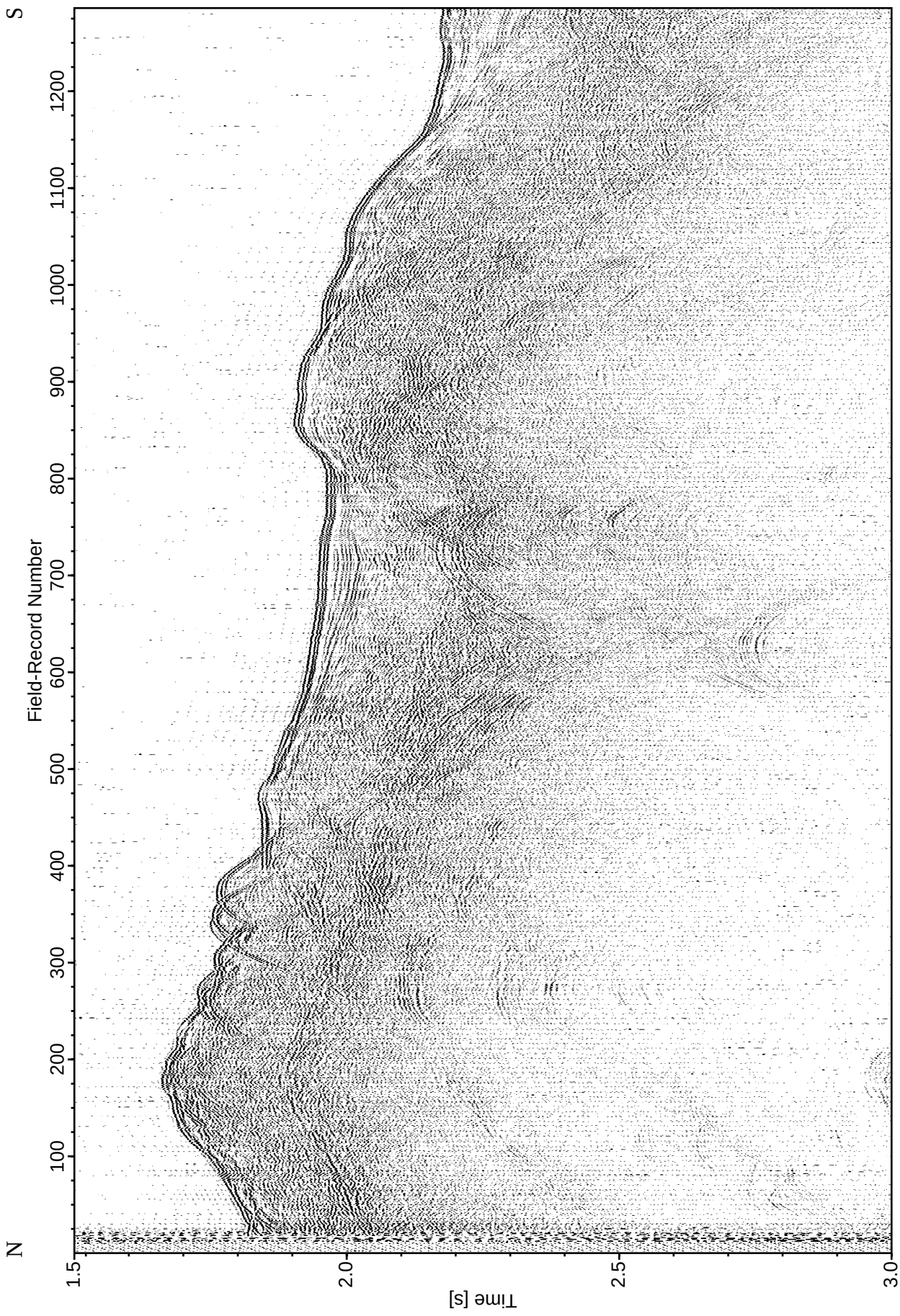

Figure 6.3.3.11: Record section with source GI-Gun, Profile 83.

6.3.4 PINNACLE AREA

(D. Horn, A. Kopf, M. Arsenault)

The pinnacle was first recognized during seafloor mapping in 1998, and was at the time interpreted as a mud volcano (Trehu et al., 1999). However, within the TECFLUX programme, dives with R/S Alvin submersible revealed that the approximately 30 m high feature represents a so called chemoherm. The chemically precipitated carbonate is juxtaposed to a fluid vent approximately 500 m southwest of the summit of the southern Hydrate Ridge. Re-visiting the area for a detailed high-resolution 3D seismic survey (Anne Trehu, cruise report TTN 112, June/July 2000, unpublished data) confirmed that a broad cliff of carbonate rock covers the flank. It can also be identified on acoustic backscatter imagery as a bright spot (Chris Goldfinger, unpublished data).

The Pinnacle Area is located on the southwestern flank of the southern summit of Hydrate Ridge. The area was surveyed by a set of 8 lines with the Sparker (lines P33-36 shot in a general SE-NW and lines P38-41 in a NE-SW direction), which were recorded by the surface streamer. In addition, seismic reflection lines P82 (E-W), P16 and P177 (both NS-oriented) intersect the Sparker array at oblique angles. The location of the area and the orientation of the seismic profiles are shown in Fig. 6.3.4.1. Parasound recordings have been collected for all profiles.

During the SO150 cruise, the chemoherm's crest was crossed along lines P41, P36, P82 and P177, while lines P16, P33 and P38 reveal some of its basal structure along strike (Figs. 6.3.4.2, 6.3.4.3).

As a first order estimate from the seismic data, the areal extent of the base of the Pinnacle extends about 250 x 450 m (Fig. 6.3.4.1). The carbonate needle stands some 30 to 40 m above the seafloor in this area, and is surrounded by a moat (line P16, Fig. 6.3.4.3) which may possibly be caused by differential subsidence. Active venting of the Pinnacle at present is indicated by a faintly reflective, blurred cloud in the overlying water column, as evidenced from Parasound profiles (Fig. 6.3.4.4) and Sparker lines P36 and P41 (Fig. 6.3.4.2). The plume extends to about 15 m above the feature.

The section beneath the Pinnacle is found to be non-reflective, which may be caused by either well cemented carbonate on the seafloor hampering penetration of the signal, or by methane-rich fluid discharged from depth. Both processes may in fact be operative, the first being a consequence of the latter (e.g., Ritger et al., 1987). A disruption of the BSR underneath the pinnacle as well as a non-reflective zone on reflection line 82 recorded with the deep tow streamer (Fig. 6.3.4.3). Fluid migration is suggested to be conductive along permeable, deep-seated faults in the area (e.g. Sample and Kopf, 1995; Brown, 1995).

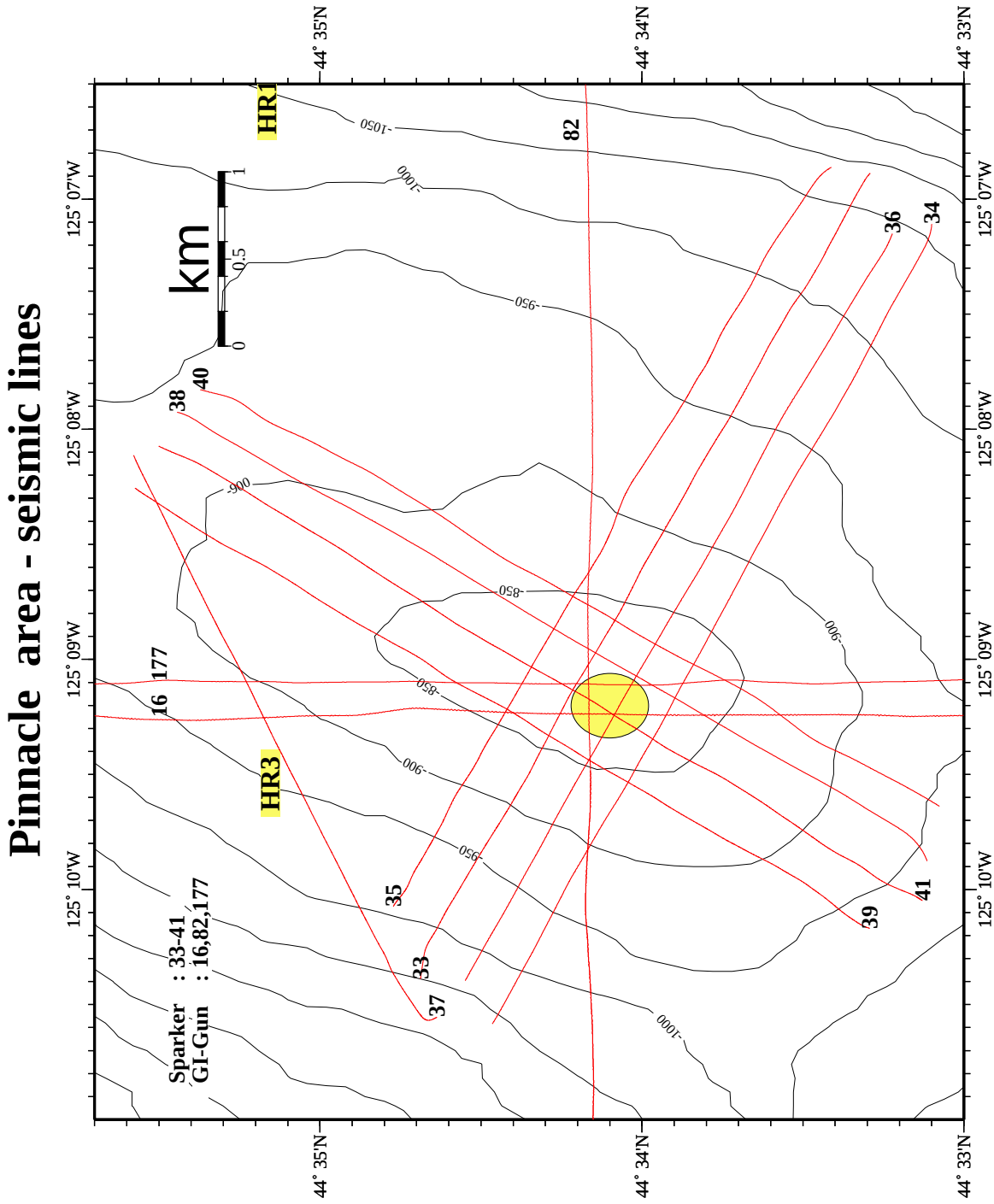

Figure 6.3.4.1: Location map of seismic lines in the Pinnacle area on the southern Gas Hydrate Ridge (water depth [m]).

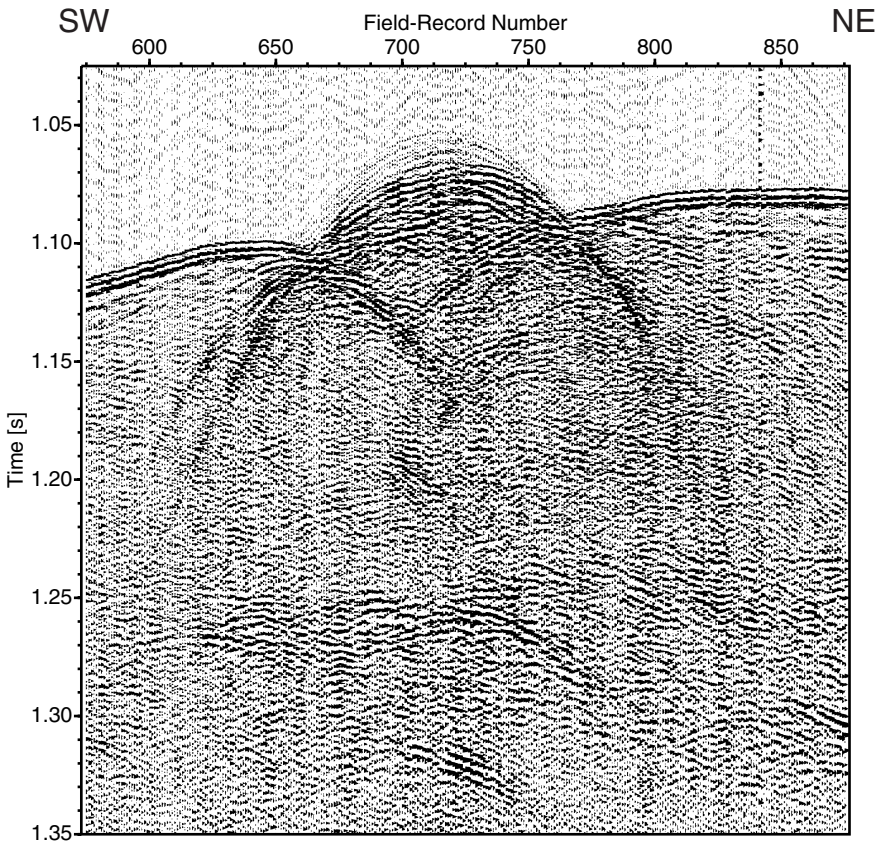

profile: 41

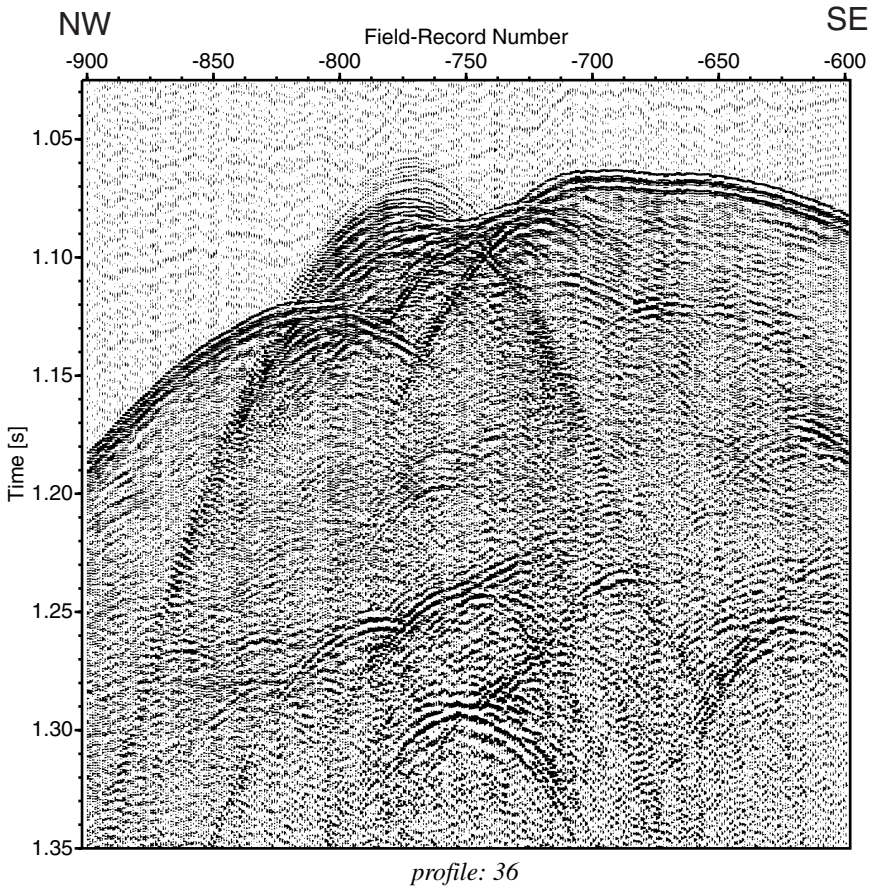

profile: 36

Figure 6.3.4.2: Sparker profiles 36 and 41 showing the elevation of the Pinnacle, the moat and the faintly reflective "cloud" in the overlying water column (active vent).

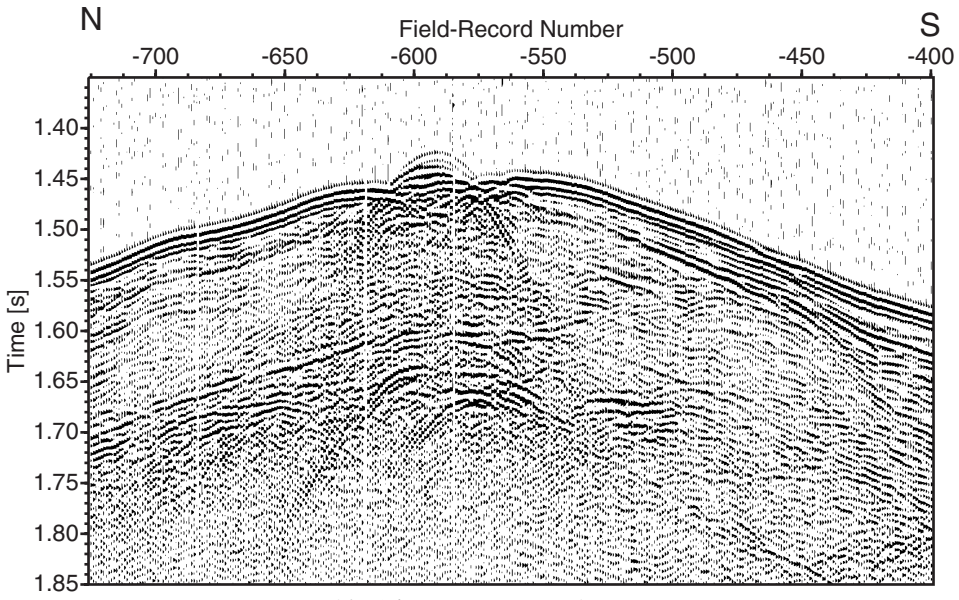

profile 16 : GI-Gun / Surface Streamer

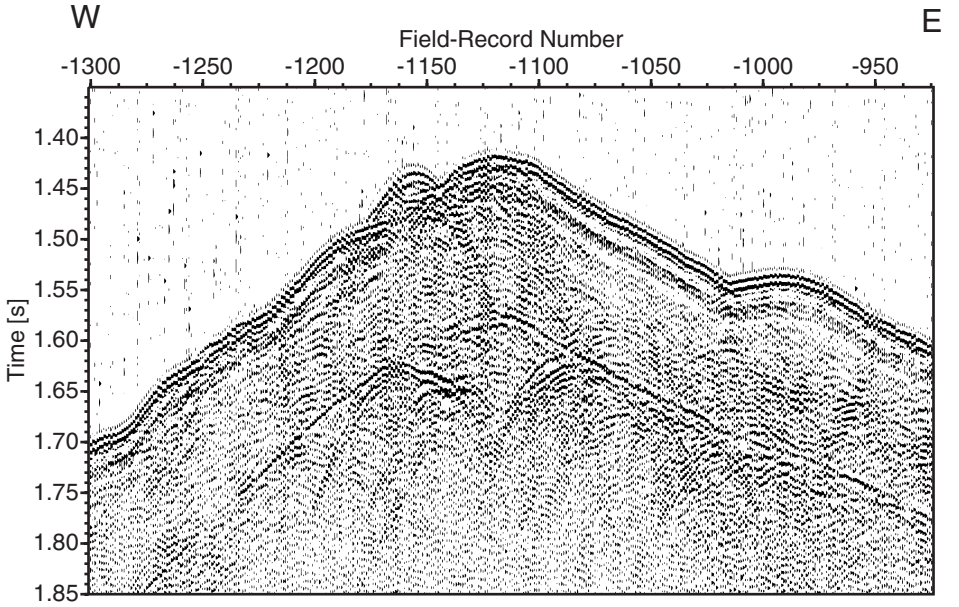

profile 82 : GI-Gun / Surface Streamer

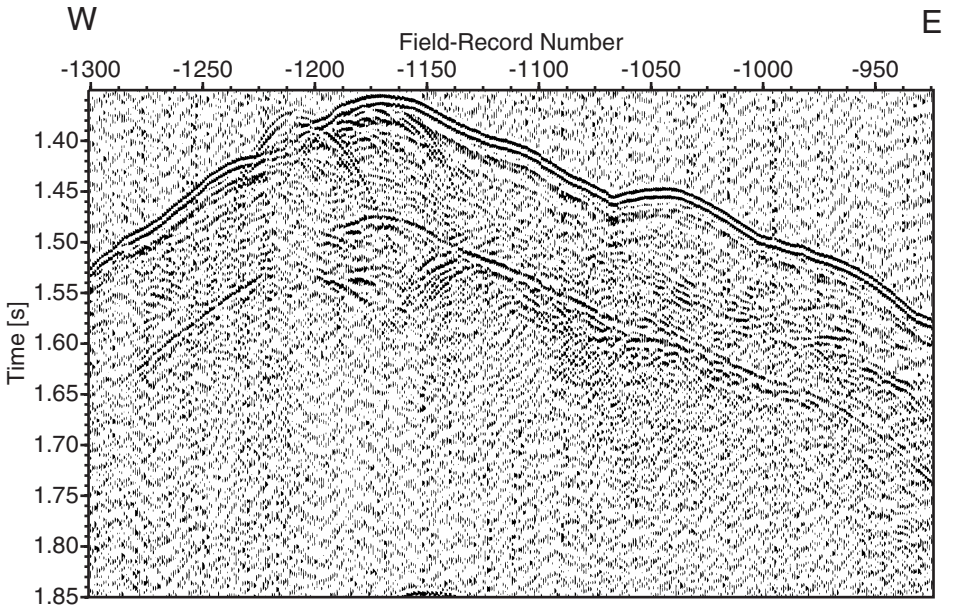

profile 82 : GI-Gun / Deep tow

Figure 6.3.4.3: GI-gun profiles 16 and 82 showing the nonreflective zone beneath the Pinnacle and a disruption of the BSR, in particular on line 82 recorded with the DeepTow streamer.

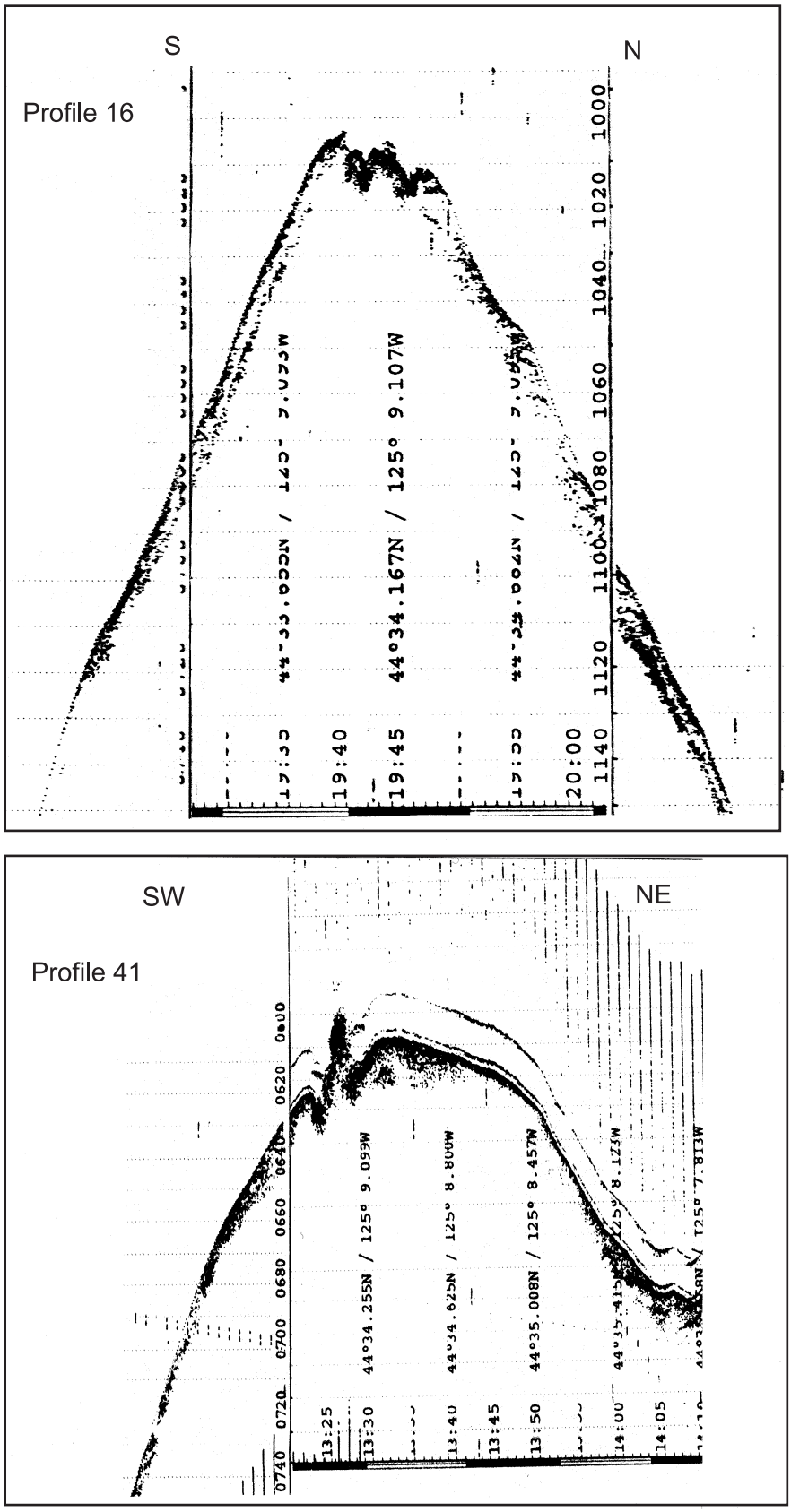

Figure 6.3.4.4: Parasound records along seismic profiles 16 (top) and 41 (bottom) showing the topography of the Pinnacle and the surrounding moat.

6.3.5 NORTHERN POCKMARK AREA

(A. Kopf, D. Horn, M. Arsenault)

Pockmarks are well known seafloor features resulting from fluid venting, and generally create circular craters or scars in the subseafloor and seafloor sediment (Hovland and Judd, 1988). They have been demonstrated to evolve from elevated gas discharge in a diatreme-like fashion (Brown, 1990). In the Hydrate Ridge region, numerous fields with pockmarks and other seepage features have been discovered during recent TV-guided surveys (see OFOS imagery during SO143, TECFLUX; Bohrmann et al., 1999). On acoustic backscatter maps, they can often be identified as subcircular patches of higher reflectivity, generally ranging from 250 to 500 m in diameter (Chris Goldfinger, unpublished data). However, in this paragraph we summarize not only negative pockmark features (i.e., seafloor depressions), but some slightly elevated mounds which are also associated with gas seepage.

The northern pockmark area surveyed included 8 lines in a N-S-direction (P87-90 and 92-94), which are tied together by W-E-profile P91, as well as numerous acquisitions along regional seismic line OR89-9 (Fig. 6.3.5.1). It is located east of Site 892. Parasound data were acquired along all profiles surveyed, however, no seepage-related structures can be identified in any satisfactory detail. This is mostly related to the limited resolution when the beam encounters steep seafloor topography. However, the seismic lines reveal several very interesting seafloor and subsurface features, which only partly resemble those in the southern pockmark area (see Chapter 6.3.6 below).

The most common observations are small topographic highs, or bumps, on the seafloor at the central part of the profiles (e.g., P88 and P91; Figs. 6.3.5.2 and 6.5.3.3). It can be also noted that the BSR beneath these features is discontinuous and sometimes appears to be displaced by some tens of ms. Such behaviour is known from other areas (Costa Rica margin), and has previously been related to migration and expulsion of warm fluids. A clear relationship between faulting and an interrupted seafloor reflector can be observed along line P87 (Fig. 6.3.5.4). The minor elevation of these features relative to the surrounding seafloor is suggestive of moderately thick carbonate crusts and concretions at shallow depth, as have been recovered frequently using the TV grab on R/V SONNE (e.g., Bohrmann et al., 1999).

The strongest disruption of the otherwise continuous BSR reflection is seen at profile P89 when entering the northern flank of the ridge (Fig. 6.3.5.5). A seismically opaque vertical zone apparently corresponds to a prominent topographic seafloor high. In addition, the southern branch of the BSR reflection is pulled upwards, and is detected about 30 ms above its assumed northward continuation. Again, fluid movements are a likely explanation.

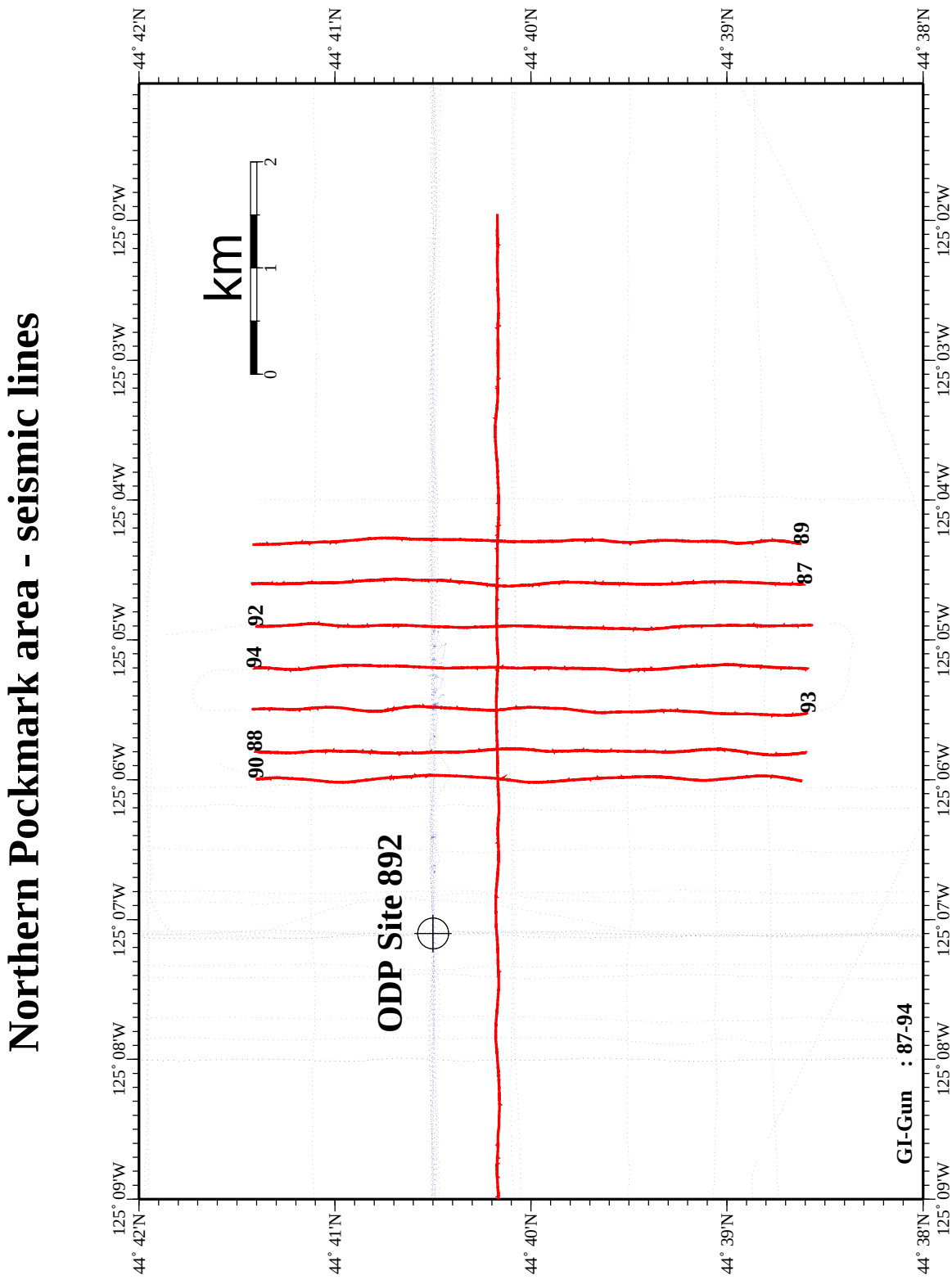

Figure 6.3.5.1: Location map of seismic lines in the Northern Pockmark area.

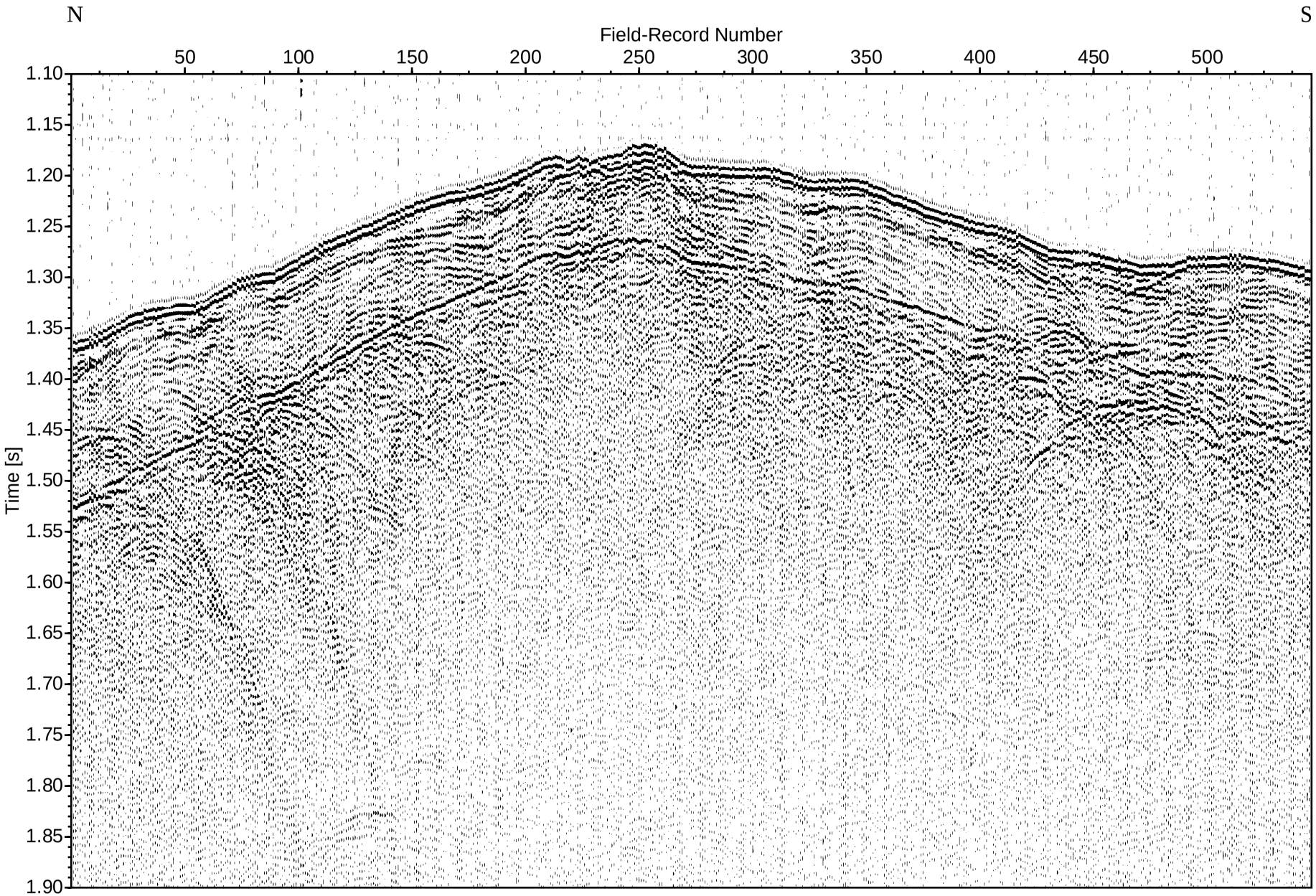

Figure 6.3.5.2: Seismic line P88.

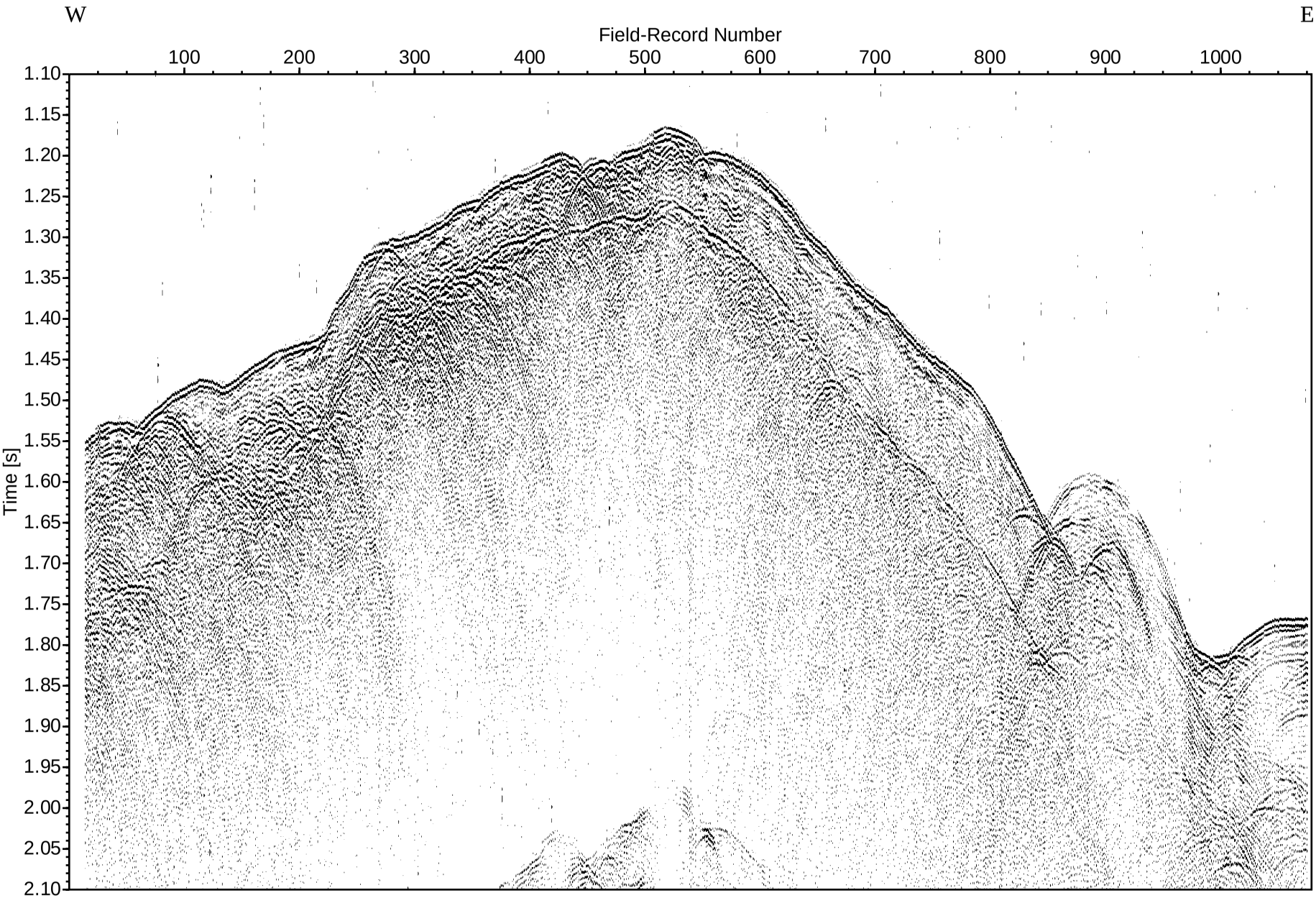

Figure 6.3.5.3 W-E-oriented seismic line P91, showing a particularly rough BSR reflector.

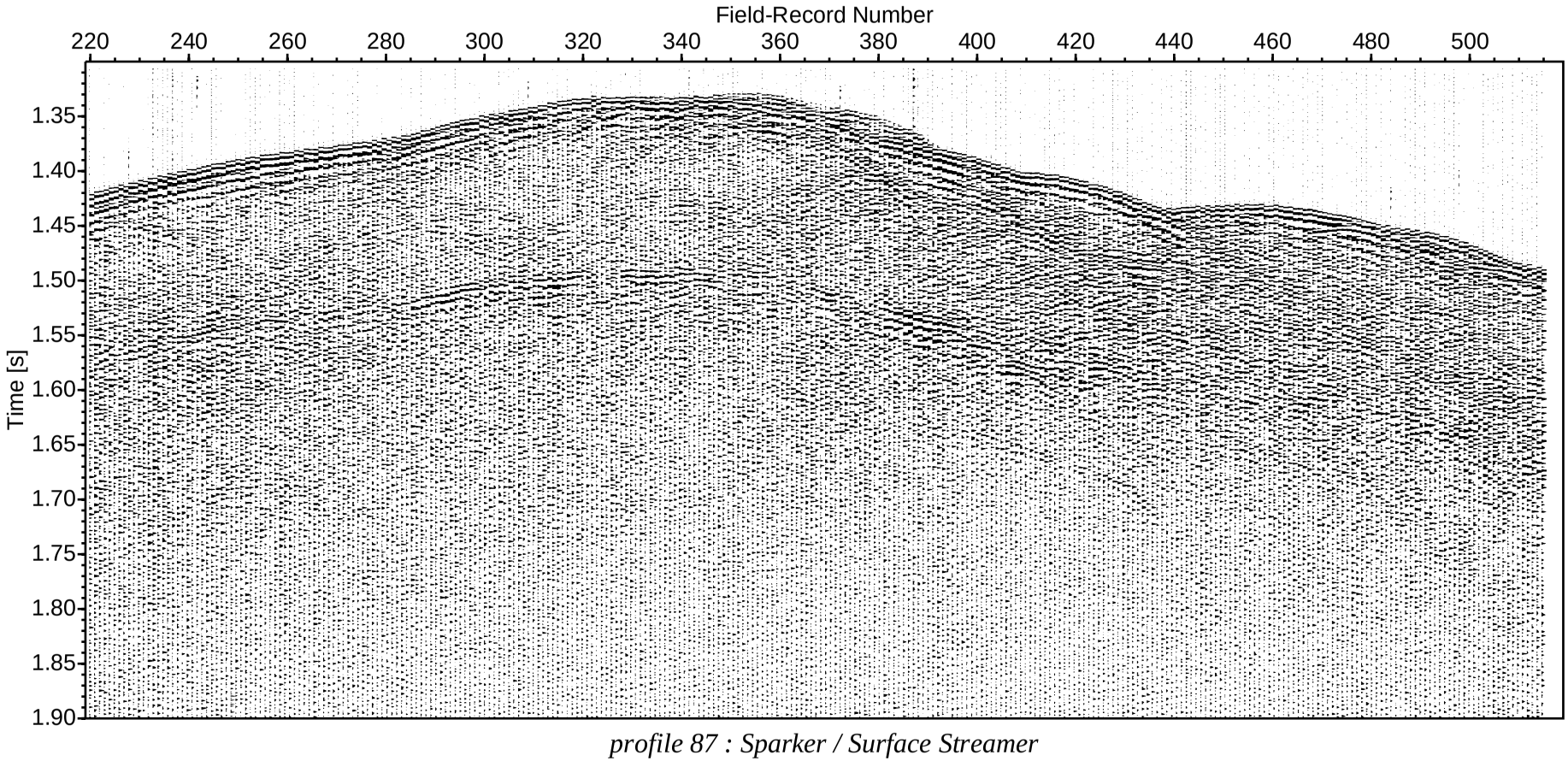

Figure 6.3.5.4: S-N-oriented seismic line P87, illustrating steep faults apparently having been venting and facilitating precipitation of authigenic phases.

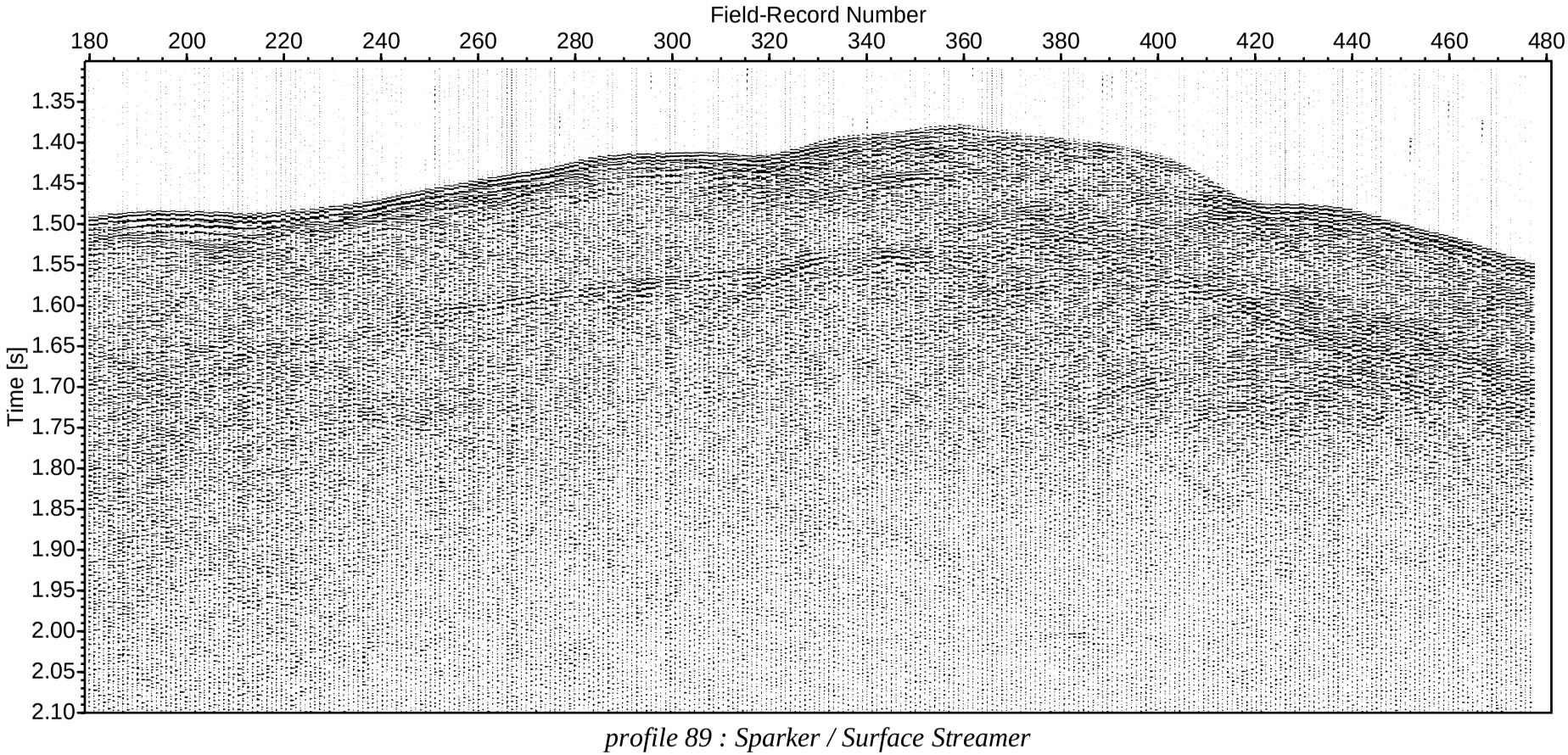

Figure 6.3.5.5: S-N-oriented seismic line P89 with a prominent BSR being intersected by a zone of possibly gas bearing material underlying a seafloor updoming feature.

6.3.6 SOUTHERN POCKMARK AREA

(D. Horn, A. Kopf, M. Arsenault)

Two pockmark fields have been investigated in more detail during HYDGAS cruise SO150. The locations are east of the ODP Site 892 near the northern summit, and east of the proposed drillsites HR1 and HR3 off the southern summit of Hydrate Ridge, respectively. The trackchart of the seismic profiles acquired during the small survey of the southern Pockmark Area is shown in Figure 6.3.6.1. A total of 7 Sparker lines (P52-54 shot in W-E direction, and P56-58 in N-S direction) were recorded by surface streamer, while three reflection lines were acquired with the GI-gun and the surface and deep tow streamers (P81-82, P174). Parasound data were recorded along all seismic lines except P57 (due to computer failure).

The seismic data have sufficient penetration and resolution in the sedimentary section, and the presence of distinct coherent reflections allow for an in-depth interpretation of the structural setting and pockmark, evolution in the southern area.

The seismic lines, as well as the Parasound data show distinct topographic uplifts of the seafloor in the survey area, in certain cases with steep escarpments (5-15 m vertical displacement) mainly at their northern and western flanks (Figs. 6.3.6.2 and 6.3.6.3). Depressions are less frequent and have only been observed in a few cases, e.g. on line P56 (Fig. 6.3.6.3), possibly indicating higher gas flux. On the Parasound records, a very distinct white shadow zone without reflectivity is present beneath the sea bottom anomalies.

The pockmarks and mounds occur in a plateau-like area at approximately 950 m water depth. The plateau is bound to the west by a steep escarpment dipping seaward (Fig. 6.3.5.4 and 6.3.5.5). They are apparently related to regional faulting, with chaotic disturbances of the sedimentary succession at depth. A distinct seafloor uplift accompanies these zones, but it cannot yet be decided whether these elevations are the result of enhanced dewatering of the sediment pile, or fluid influx from deeper levels (see Fig. 6.3.5.5). Sediment thickening to the south causes a wedge-shaped geometry, which may facilitate layer-parallel fluid migration. On seismic line P81 (Fig. 6.3.5.6), several units can be distinguished on the basis of seismic stratigraphy. The structure appears to be an anticlinal ridge having undergone moderate shortening. The base of the wedge (unit IIIB) is overlain by a section of almost constant thickness (IIIA, see Fig. 6.3.5.7), which in turn is overlain by a succession of beds with reduced thicknesses to the south (units IIC-A). In contrast, the uppermost overburden (unit I) retains a constant thickness, and may be deposited in a phase of tectonic inactivity of this part of Hydrate Ridge. However, all units described are affected by fluid discharge, as is seen by the conduit-type zone of opaque seismic signals beneath the topographic elevations (dotted areas in Fig. 6.3.5.7).

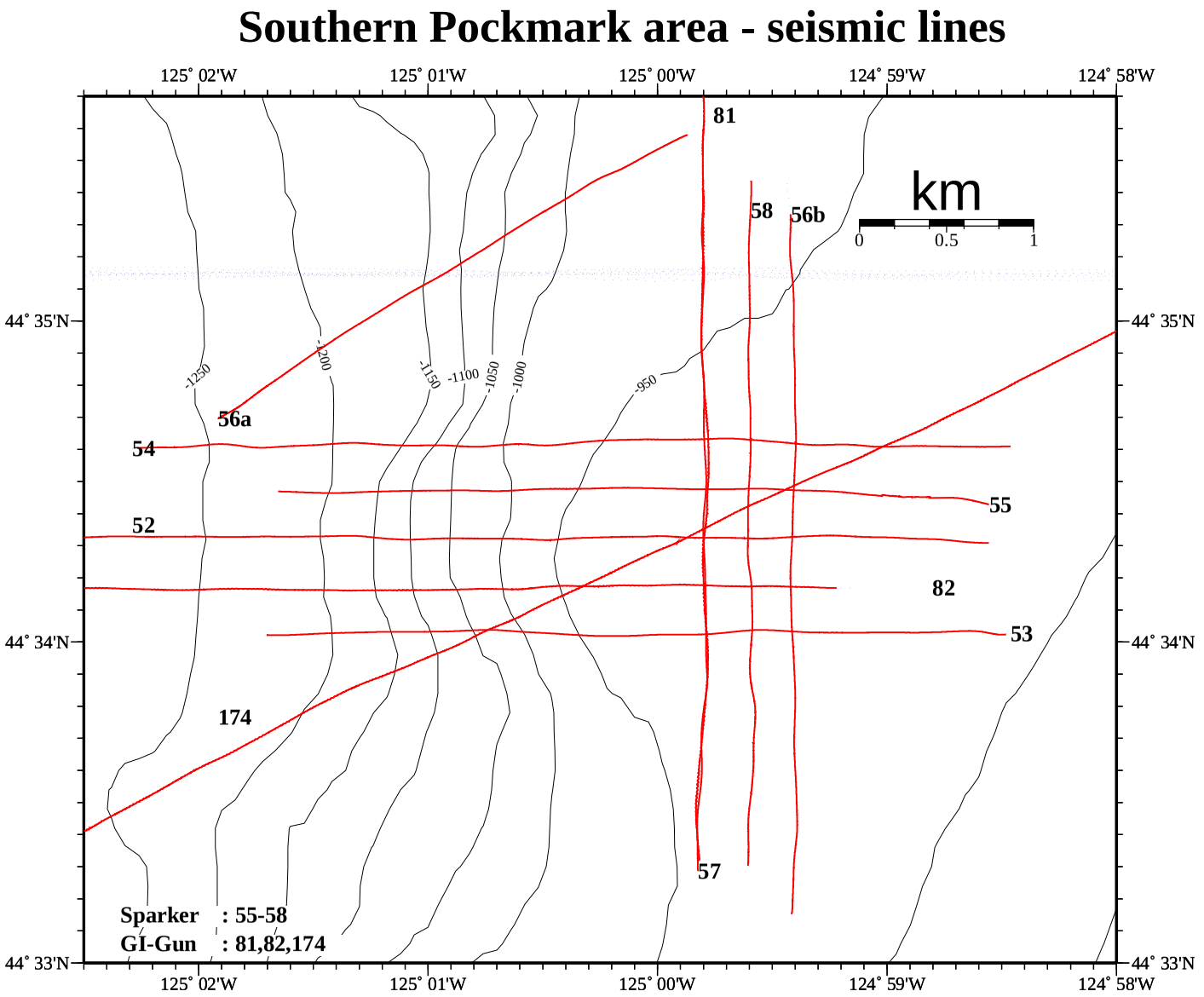

Figure 6.3.6.1: Location map of seismic lines in the Southern Pockmark area.

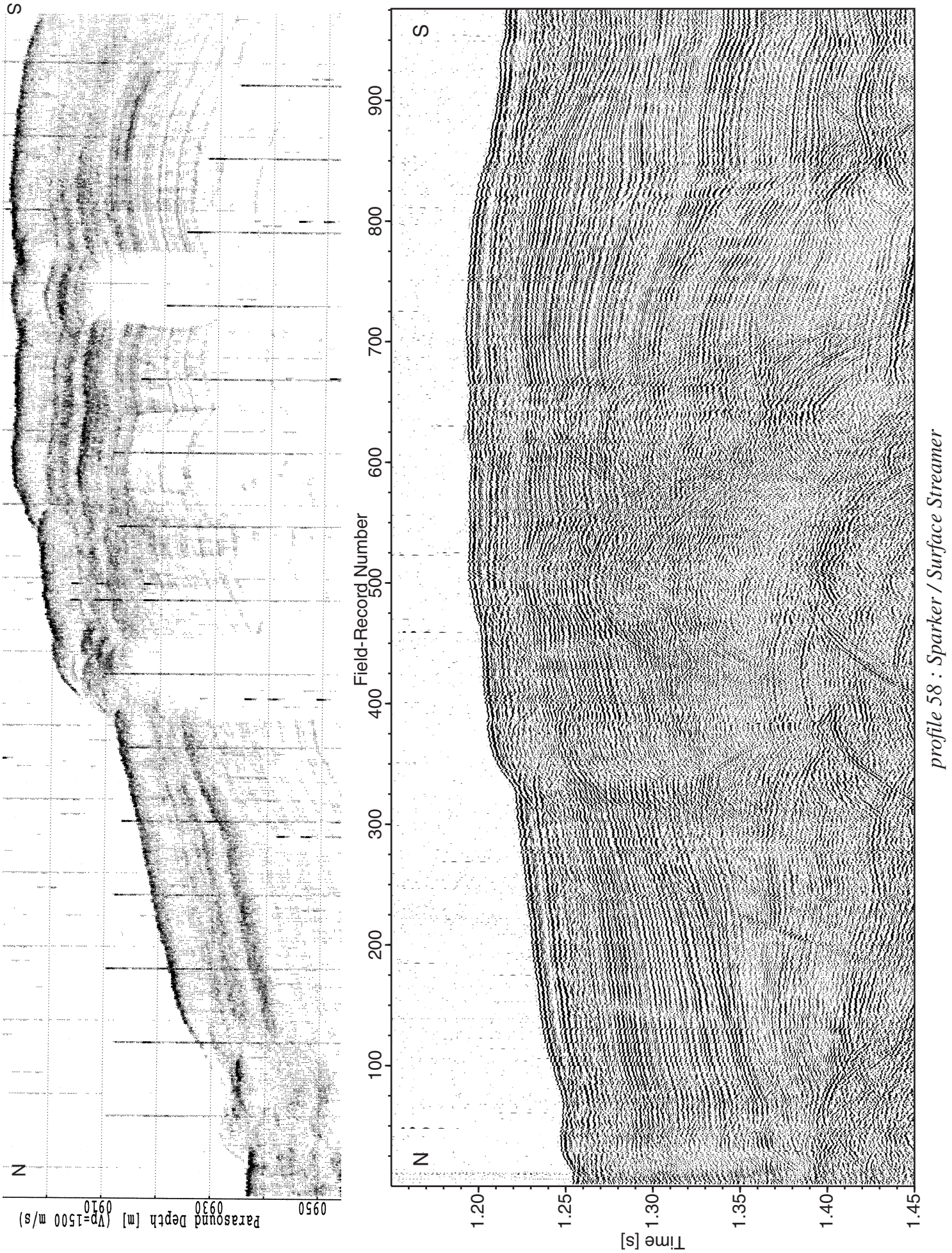

Figure 6.3.6.2: Sparker Profile 58 and Parasound data recorded along the seismic line showing several zones with shallow gas bearing conduits (white shadow zones in Parasound and highly disturbed zones on the Sparker line).

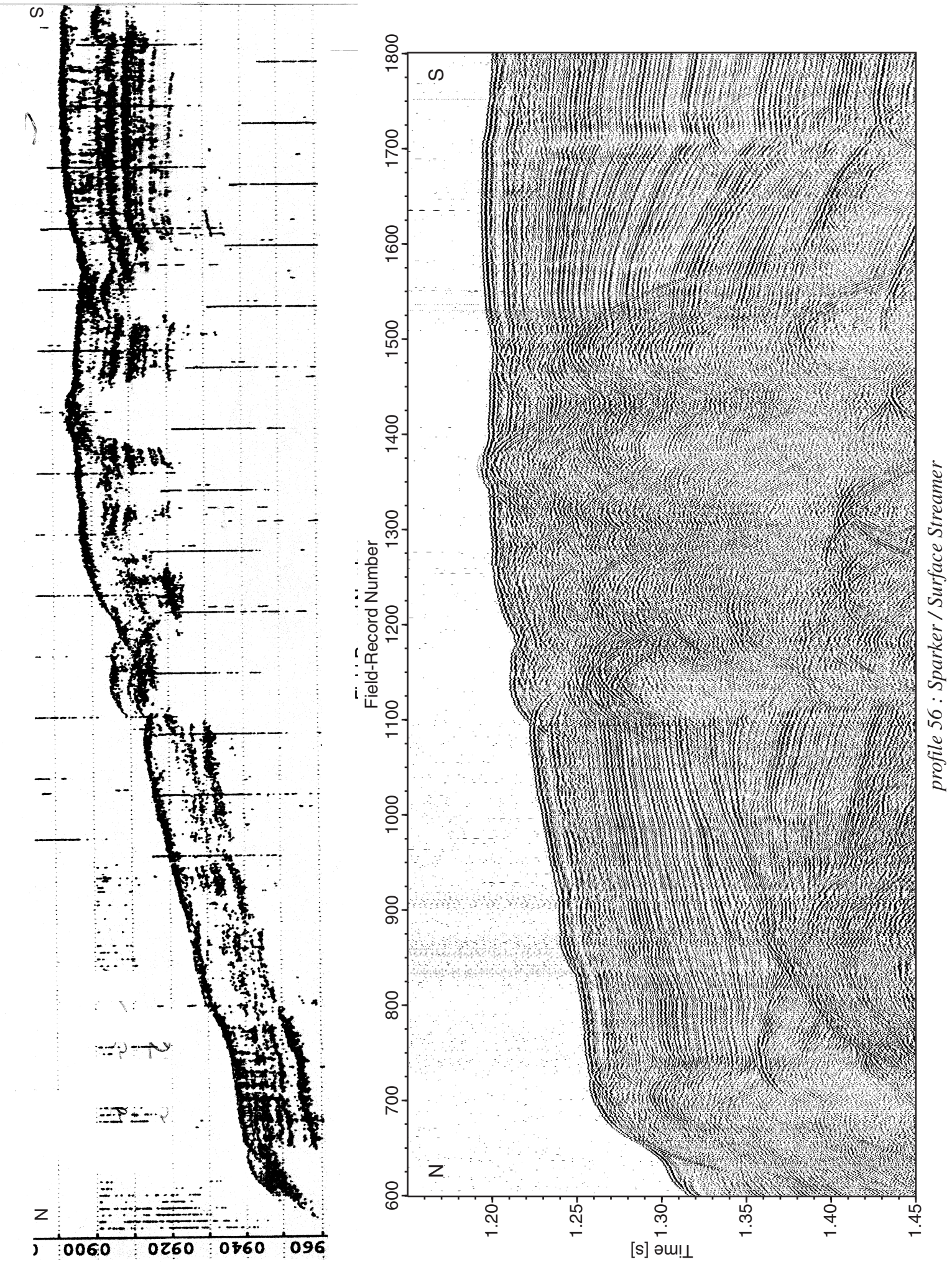

Figure 6.3.6.3: Sparker profile 56 and Parasound data recorded along the seismic line (for explanation see fig. 6.3.6.2).

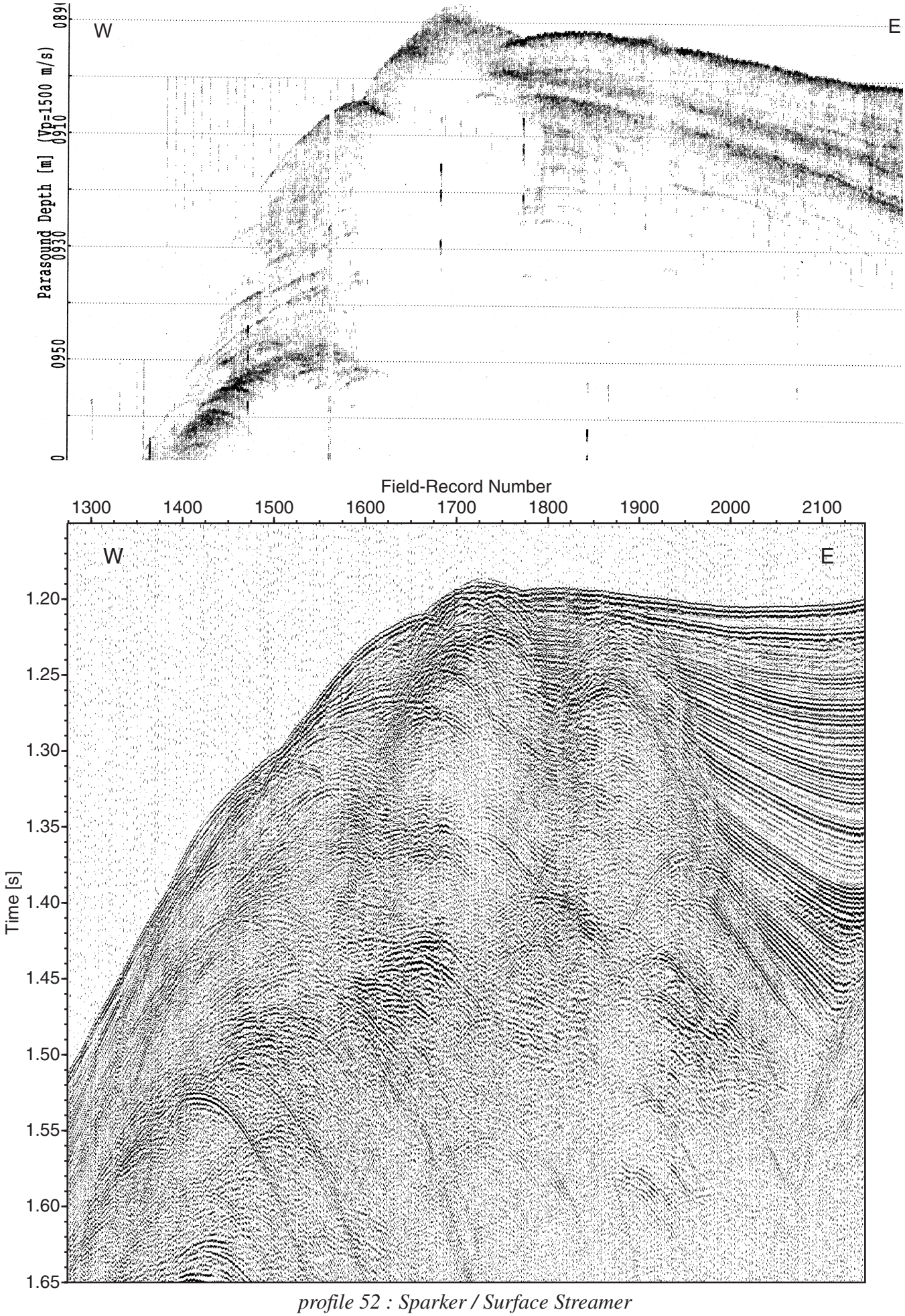

Figure 6.3.6.4: Sparker profile 52 and Parasound data showing strong disturbance within the section and pockmarks at the seafloor due to shallow gas bearing conduits at the edge of the western escarpment.

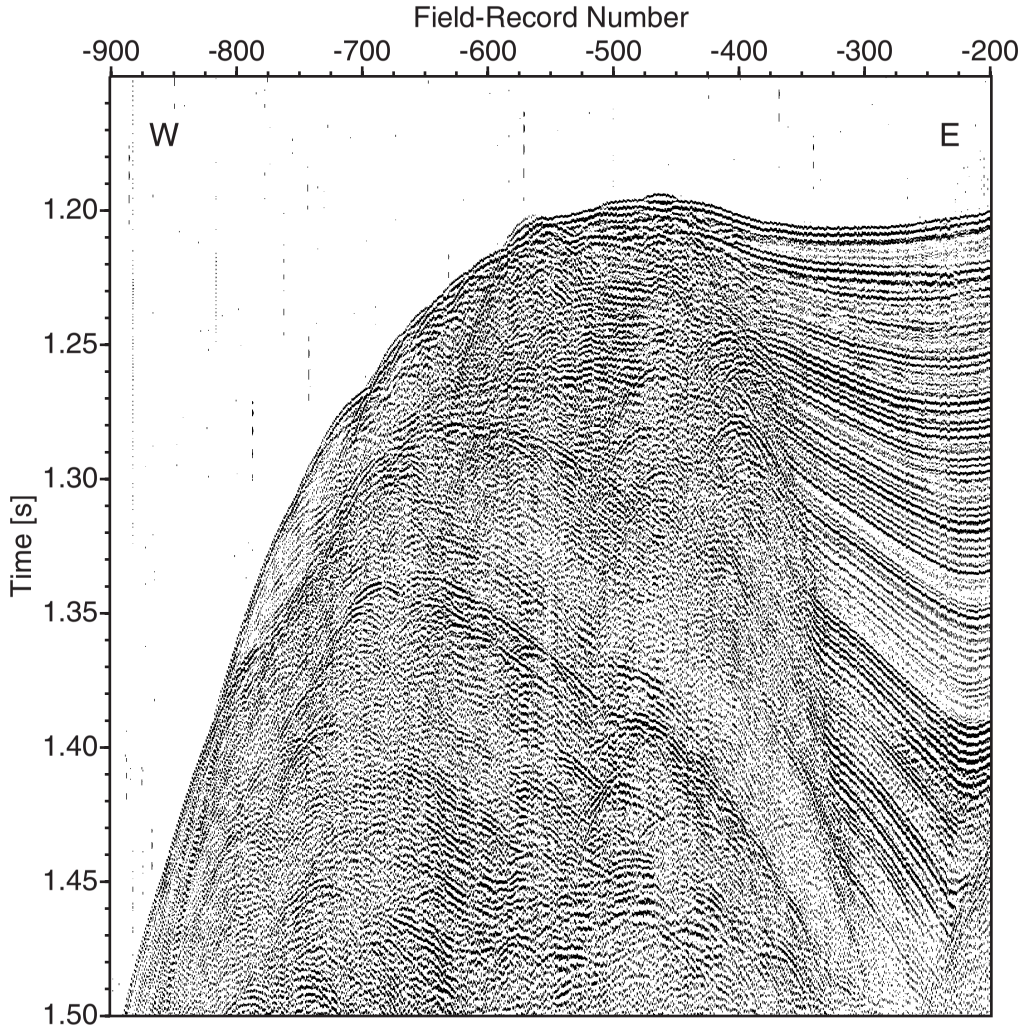

profile 55 : Sparker / Surface Streamer

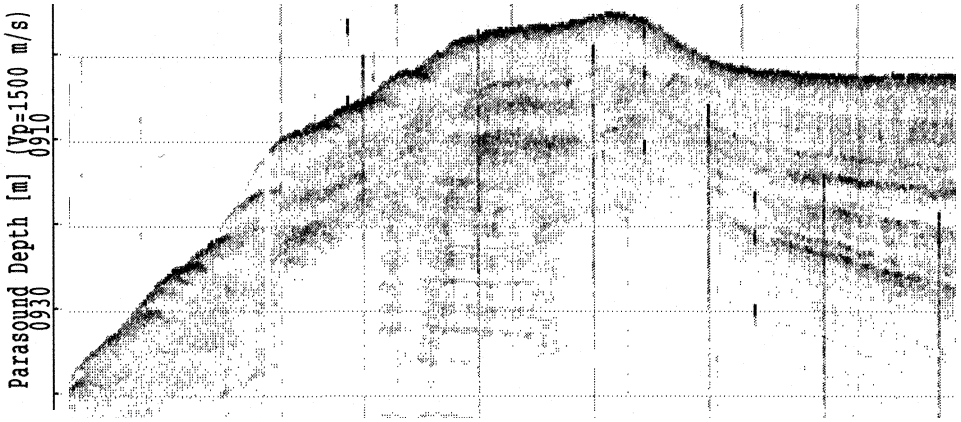

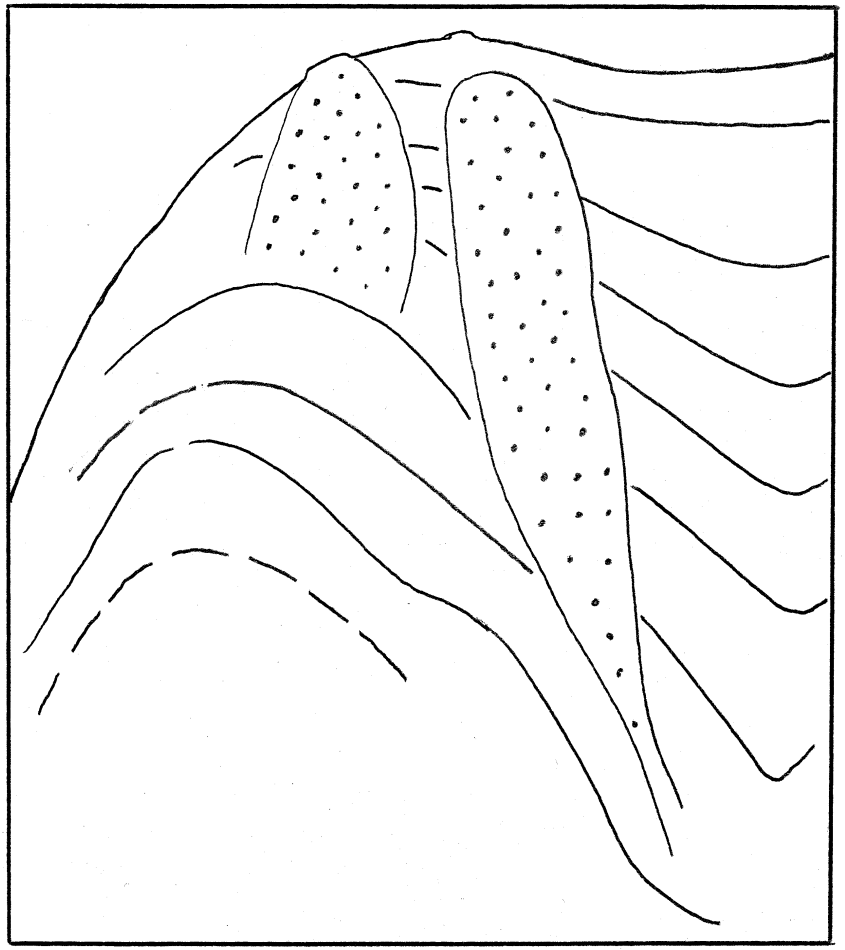

Figure 6.3.6.5: Sparker profile 55, Parasound data and structural interpretation of the anticlinal ridge at the flank of the escarpment with strong disturbances of the section due to gas bearing conduits (dotted areas).

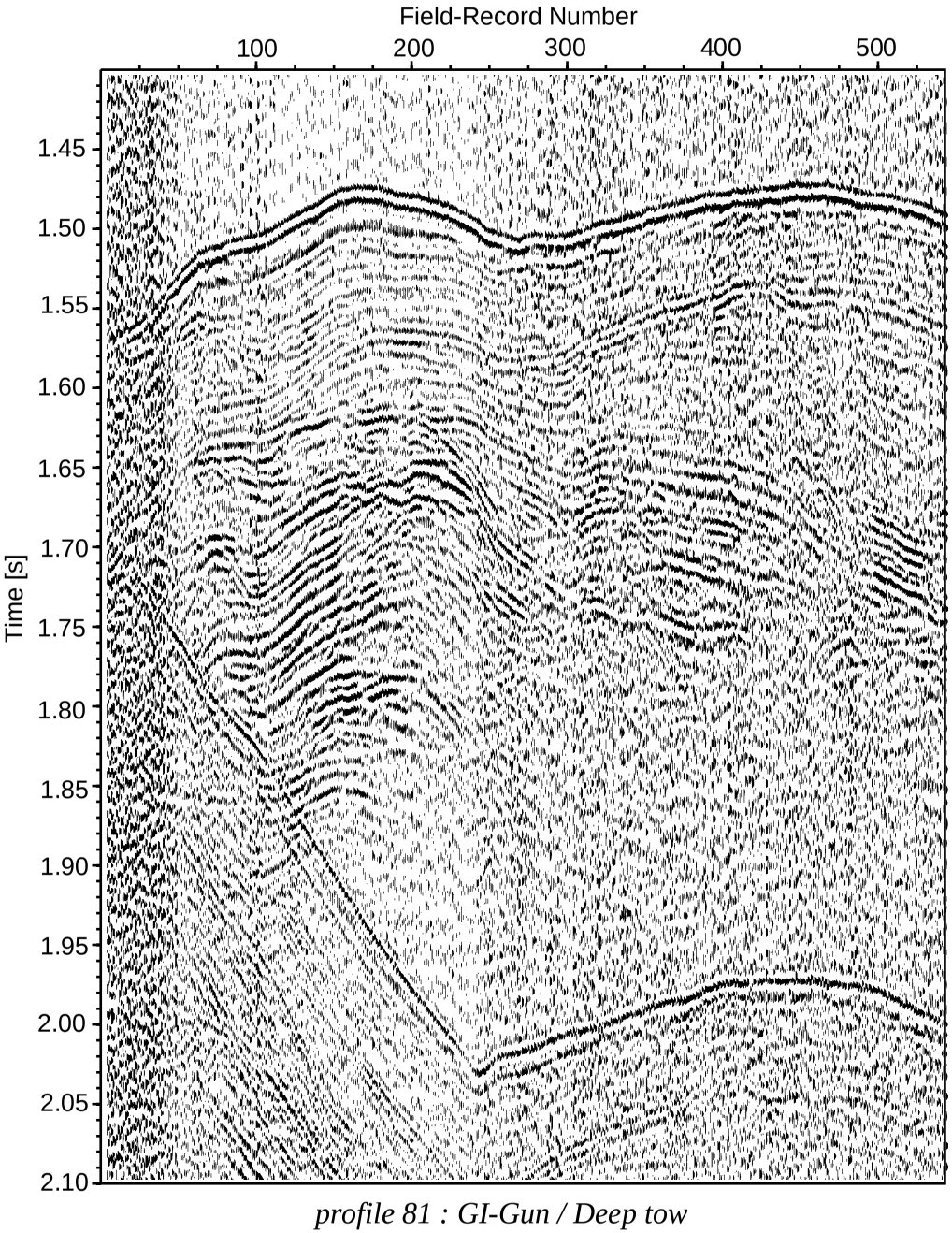

profile 81 : GI-Gun / Deep tow

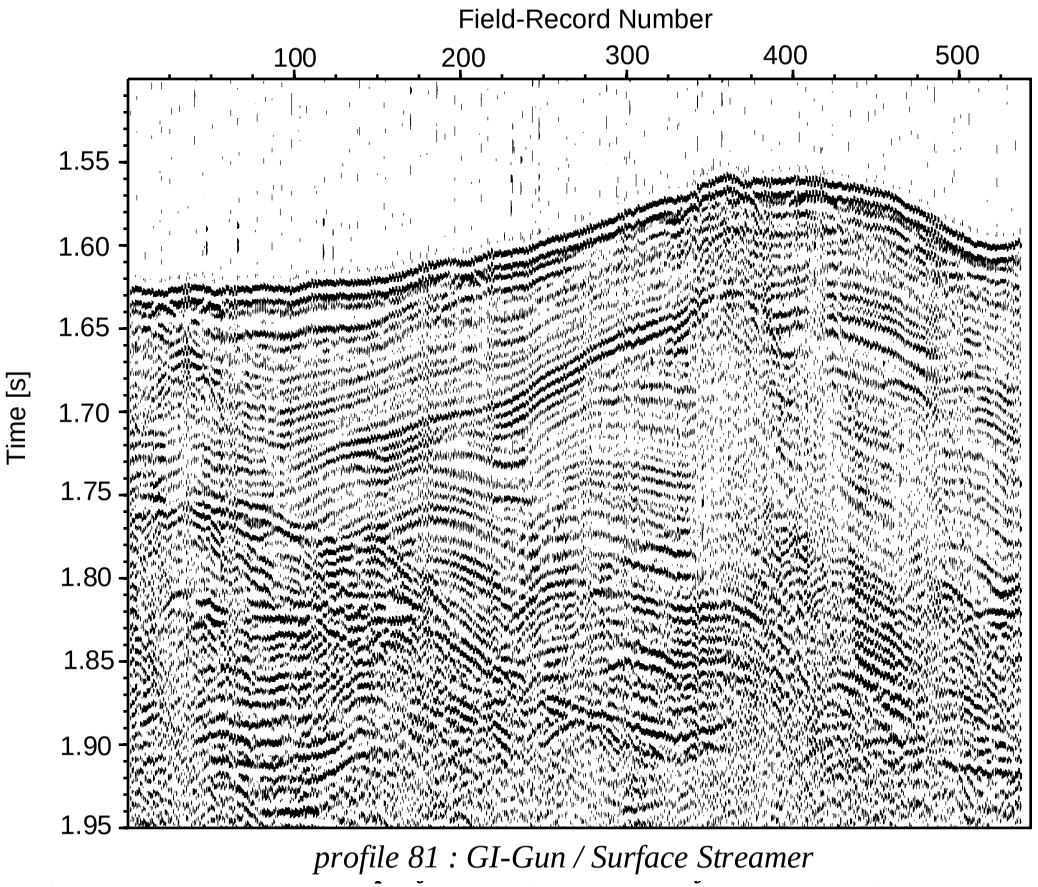

profile 81 : GI-Gun / Surface Streamer

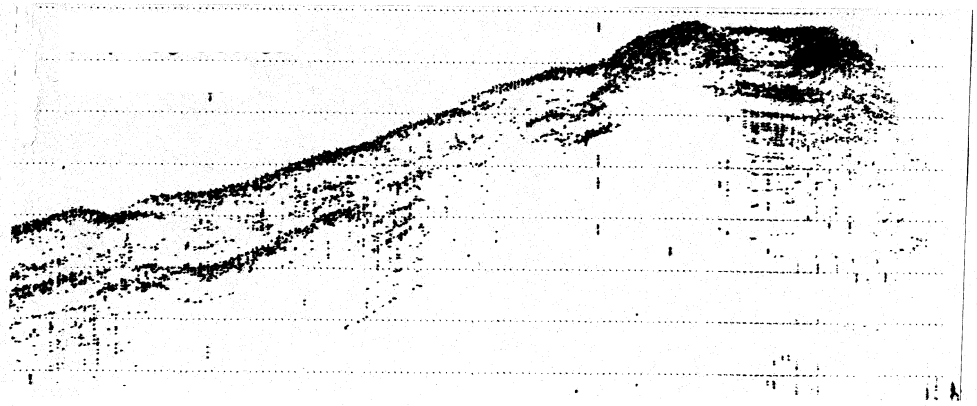

Figure 6.3.6.6: GI-gun profile 81 recorded with surface streamer (upper right) and deep tow streamer (left). Note that the nothern seafloor culmination in the deep tow display is artifical since the streamer had not reached its cruising depth. For interpretation see figure 6.3.6.7.

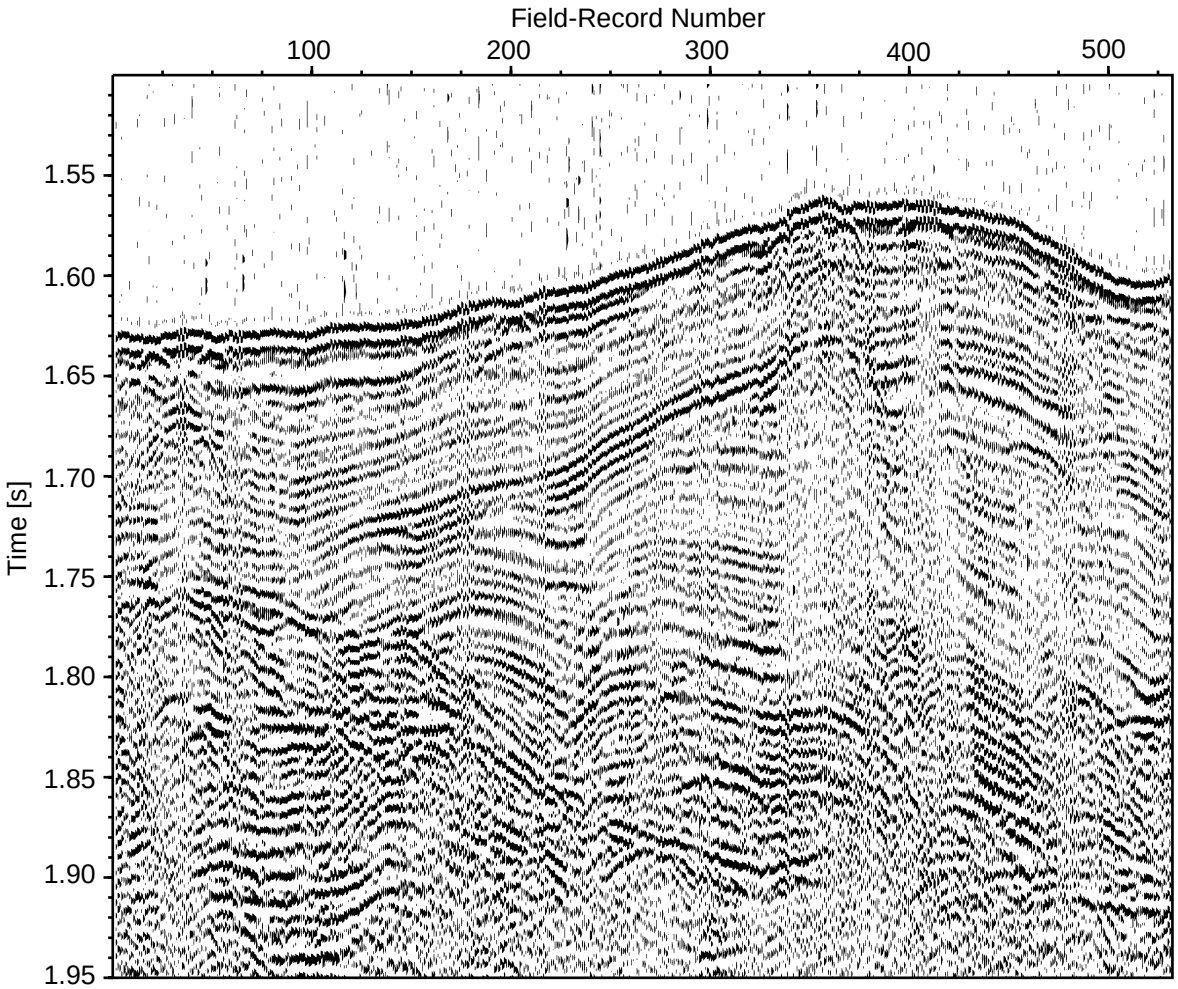

profile 81 : GI-Gun / Surface Streamer

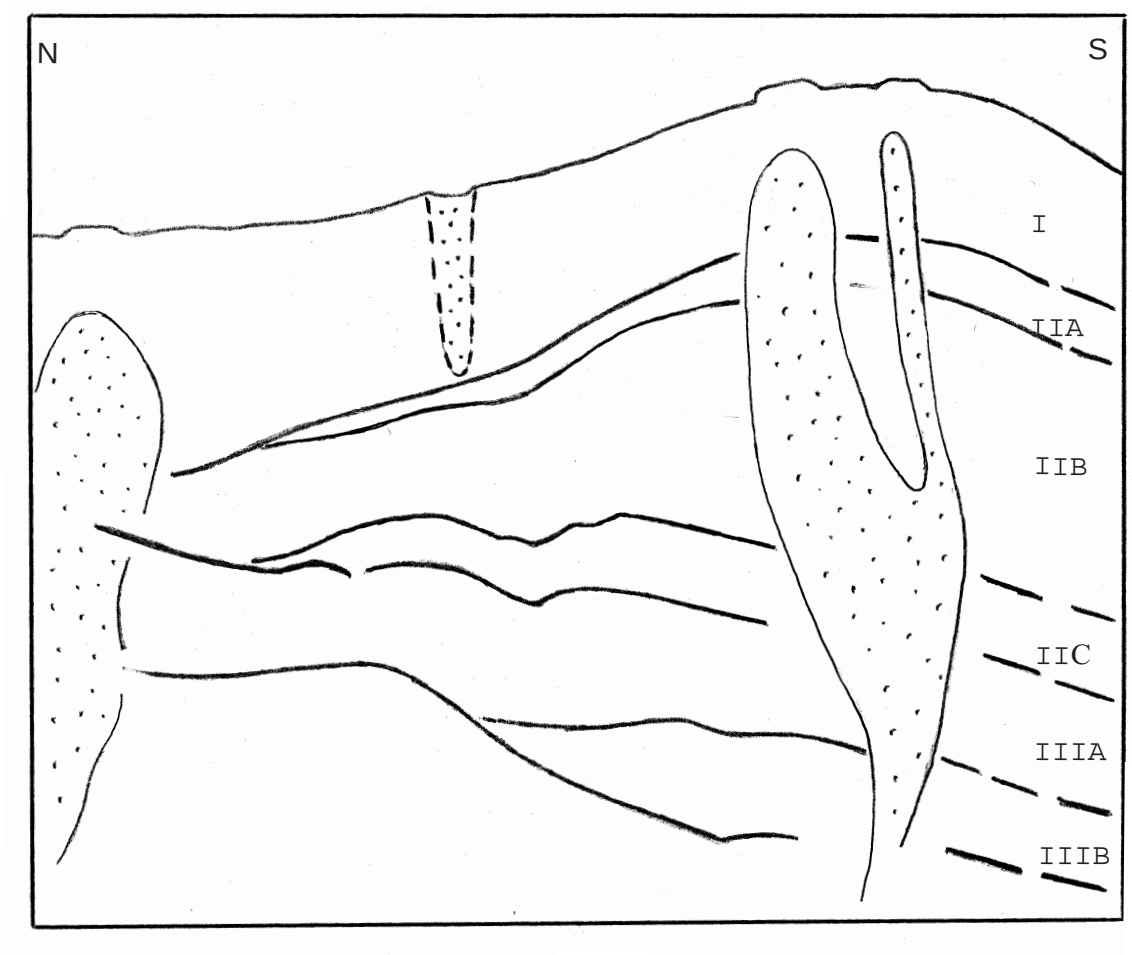

Figure 6.3.6.7: Structural interpretation (bottom) of seismic profile 81 (top) on the basis of seismic sequence stratigraphy and gas bearing conduits (dotted areas).

6.3.7 SE KNOLL

(A. Kopf)

The SE knoll, at a latitude of about 44.27°N, was investigated on two E-W-oriented profiles because of its morphological resemblance to Hydrate Ridge further to the north. The complete line P84 is already described and illustrated in the chapter on regional seismic reflection profiles (Fig. 6.3.3.8). Both on the SPARKER line and the line acquired with the GI gun (Figs. 6.3.7.1 and 6.3.5.2), a distinct BSR can be recognized over the entire width of the knoll. The BSR fades out and eventually disappears to the west into the layered sedimentary succession of a plateau. Gentle folding of the deeper sediments reflects the tectonic shortening.

The change in intensity of the BSR, being more profound at the base of the knoll, seems related to its inclination relative to the seafloor reflector. Note also the BSR increasing in apparent depth in the TWT section. This continuous inclination of the BSR seems to be associated with the overlying sedimentary sequence. Some of the wedge-shaped succession has obviously been incorporated into gentle folding. Gas and fuid venting is suggested to occur at the flank slope break at the eastern border of the plateau. Here, the BSR is slightly offset by a thrust fault, which proposed to be carries warm fluid from depth (Fig. 6.3.7.1). Consequently, first evidence is in favour of the SE knoll being a feature similar to Hydrate Ridge.

Figure 6.3.7.1: Record section with source GI-Gun, Profile 84.

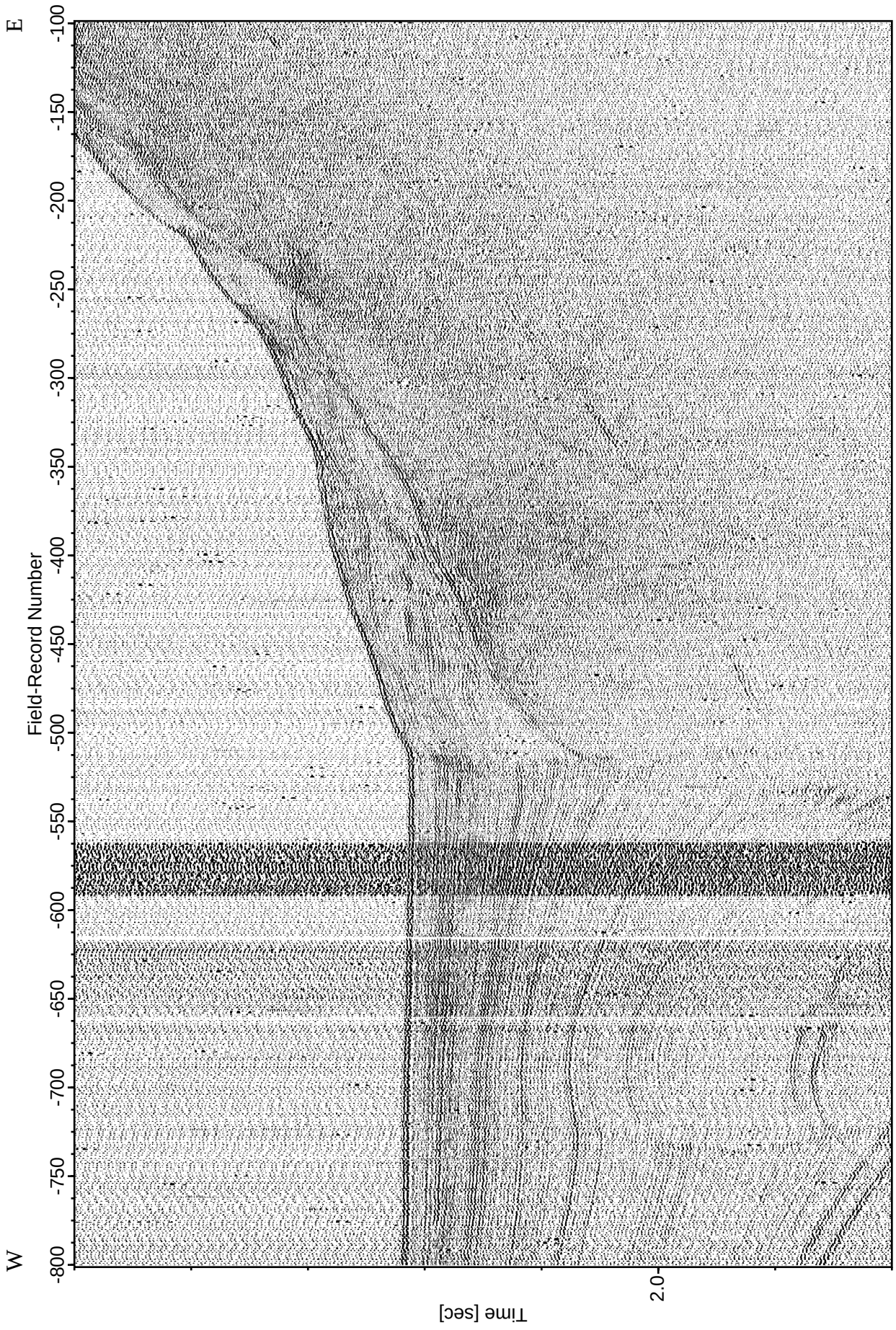

Figure 6.3.7.2 : Record section with source Sparker, Profile 85.

6.4 EXPERIMENT ODP Leg 146, SITE 892

(D. Klaeschen, D. Könitz, P. Liersch, J. Petersen, G. Klein)

The refraction and wide-angle reflection seismic experiment across the ODP drill site 892 was conducted in two seperate deployments of OBHs and OBSs on 30.09.-03.10. and 05.10.-07.10. The main WE-profile, along which the seafloor stations were placed, is the formerly acquired line OR89-09 (see MacKay et al., 1995; Trehu et al., 1999). It cross-cuts the northern summit of the Hydrate Ridge in an EW-direction at 44°40.5 N latitude (Fig. 6.4.1). During the first deployment, a total of 4 OBSs and 10 OBHs were aligned at an aimed 200 m spacing in a WE-direction across Site 892. The recorders of the stations were all synchronized and started with frequencies corresponding to the sources used when shooting the array (Fig. 6.4.1). First, a 10 km long WE-line was shot with the watergun, followed by a 20 km long line with the airgun array in the opposite direction. After the next tag, the 20 km lines were shot once more with the GI-gun before continuing with seven 10-km long NS-cross lines at a 200 m spacing across the central seafloor stations (Figs. 6.4.1. and 6.4.2). All cross lines were shot with the GI-gun and the surface streamer, while for the longer EW-profiles, the deep tow system was additionally used for acquisition. After completion of the NS-grid, the 32l Bolt gun was used as a low frequency source on a 32-km long EW-profile across Site 892, before the experiment terminated and the stations could be recovered again. It turned out that three of the stations (OBHs 36, 38, 40) had not recorded data at all due to faulty connectors. Station 35 (OBH) gained somewhat lower data quality, while the remaining receivers operated nicely.

In summary, the results from the first deployment (stations 32-45) were not entirely satisfying, such that gaps in the acquisition were attempted to be filled by the second deployment. Another 4 OBSs and 7 OBHs were positioned on the seafloor, this time trying to (i) fill the spaces where stations with faulty connectors had sat previously, (ii) reduce the spacing in crucial areas to 100m between stations, and (iii) to get 3D information by adding stations N and S of the ODP drillsite (51 and 52; Fig. 6.4.2). In addition to the EW-profiles with the watergun, GI-gun, and airgun array after recording of the stations started, another 5 NS-profiles of equal 10 km length were shot to complement the previous 7. As a result, a narrowly spaced grid is available as an useful addition to the data from the stations. The second deployment was completed with a 32 km long EW-profile across the OBH/OBS assembly with the Bolt gun. After recovery of the equipment and retrieval of the data, it was found that only one OBH (50) and one OBS (56) failed to provide good data. On the other hand, OBH 59 was suspended above the seafloor by a tether and gained excellent results.

Various data examples of OBH, OBS and streamer data for different sources are displayed in Fig. 6.4.3 to Fig. 6.4.29.

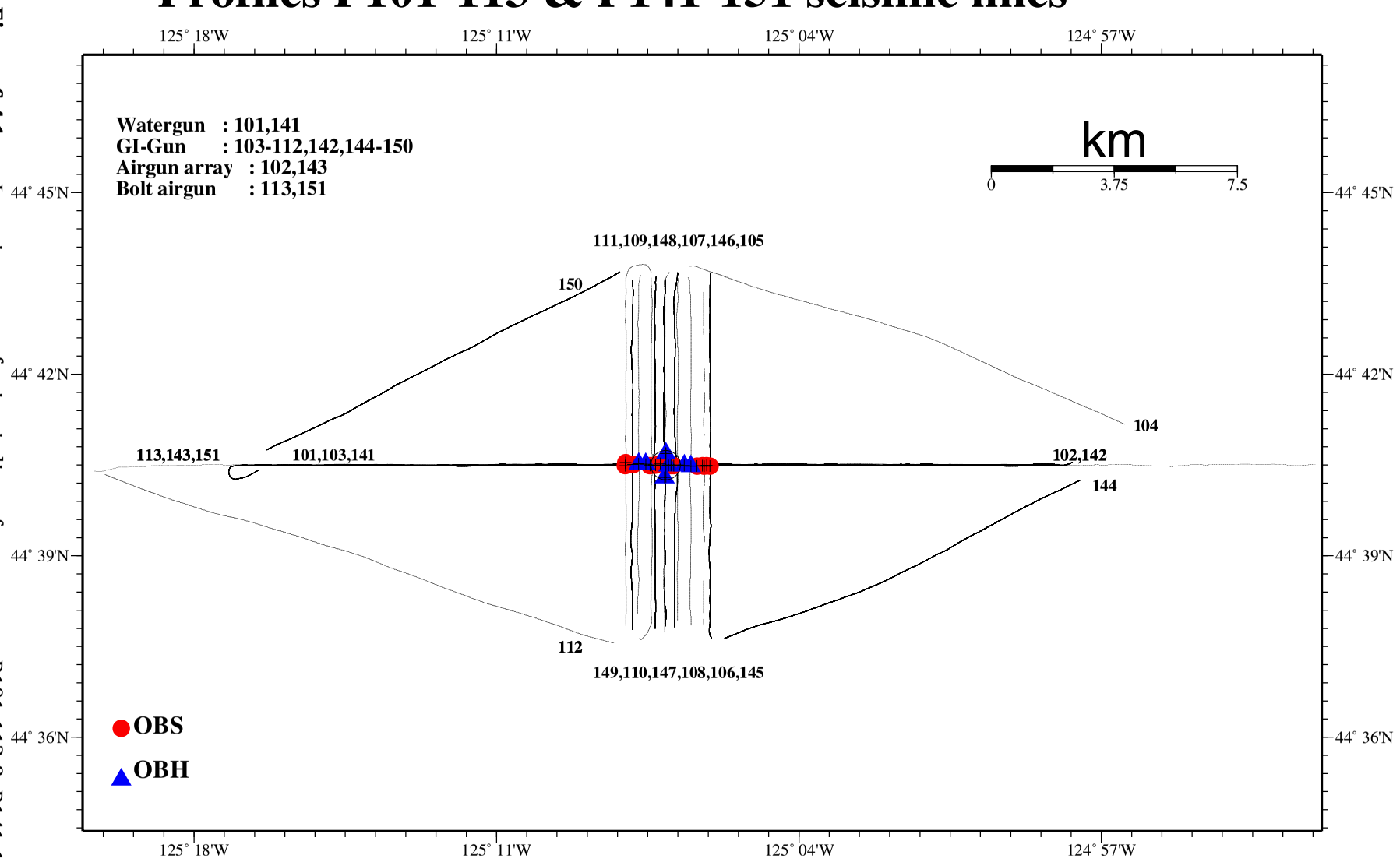

Figure 6.4.1: Location map of seismic line of survey run P101-113 & P141-151.

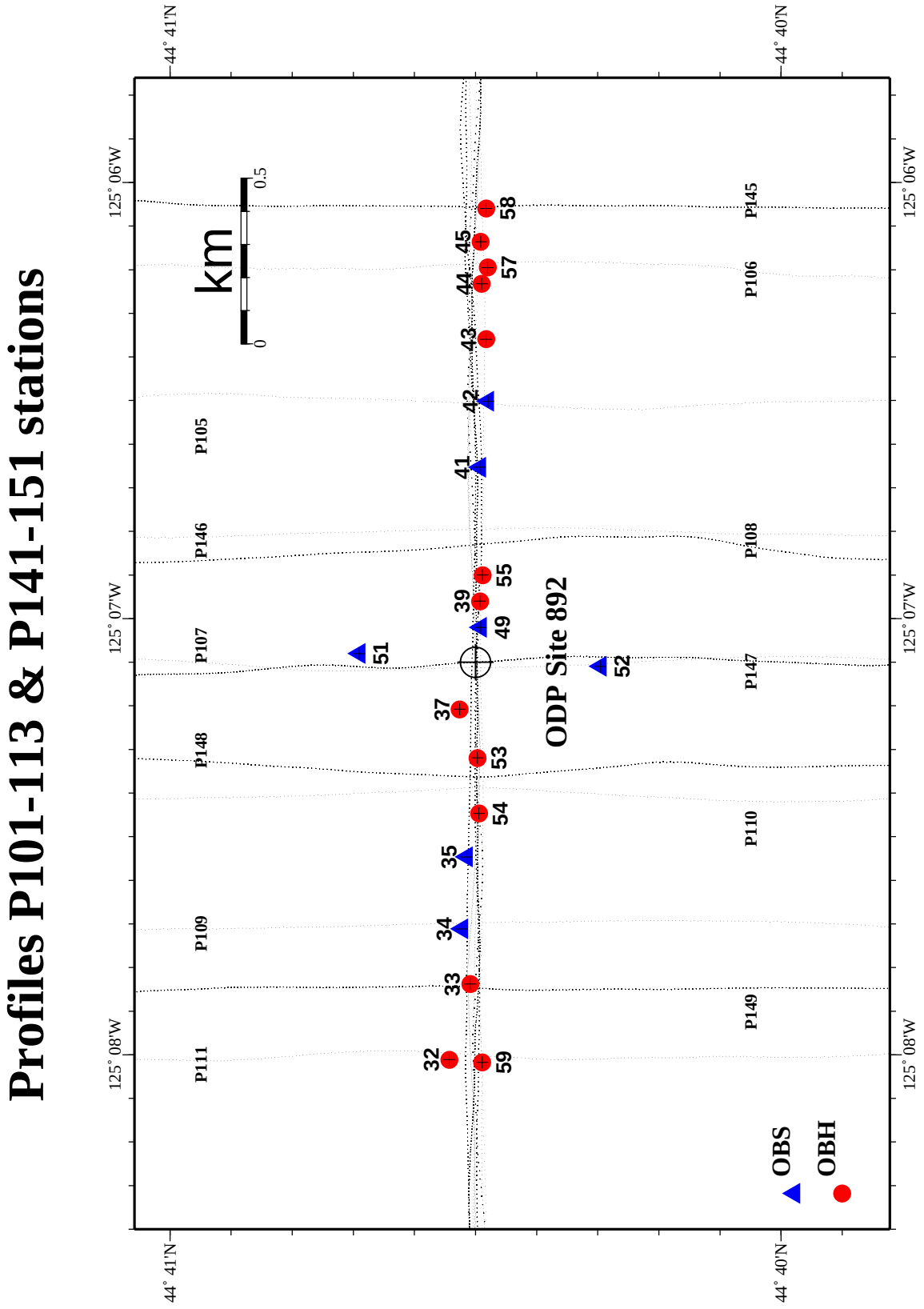

Figure 6.4.2: Location map of OBH/OBS stations for P101-113 & P141-151.

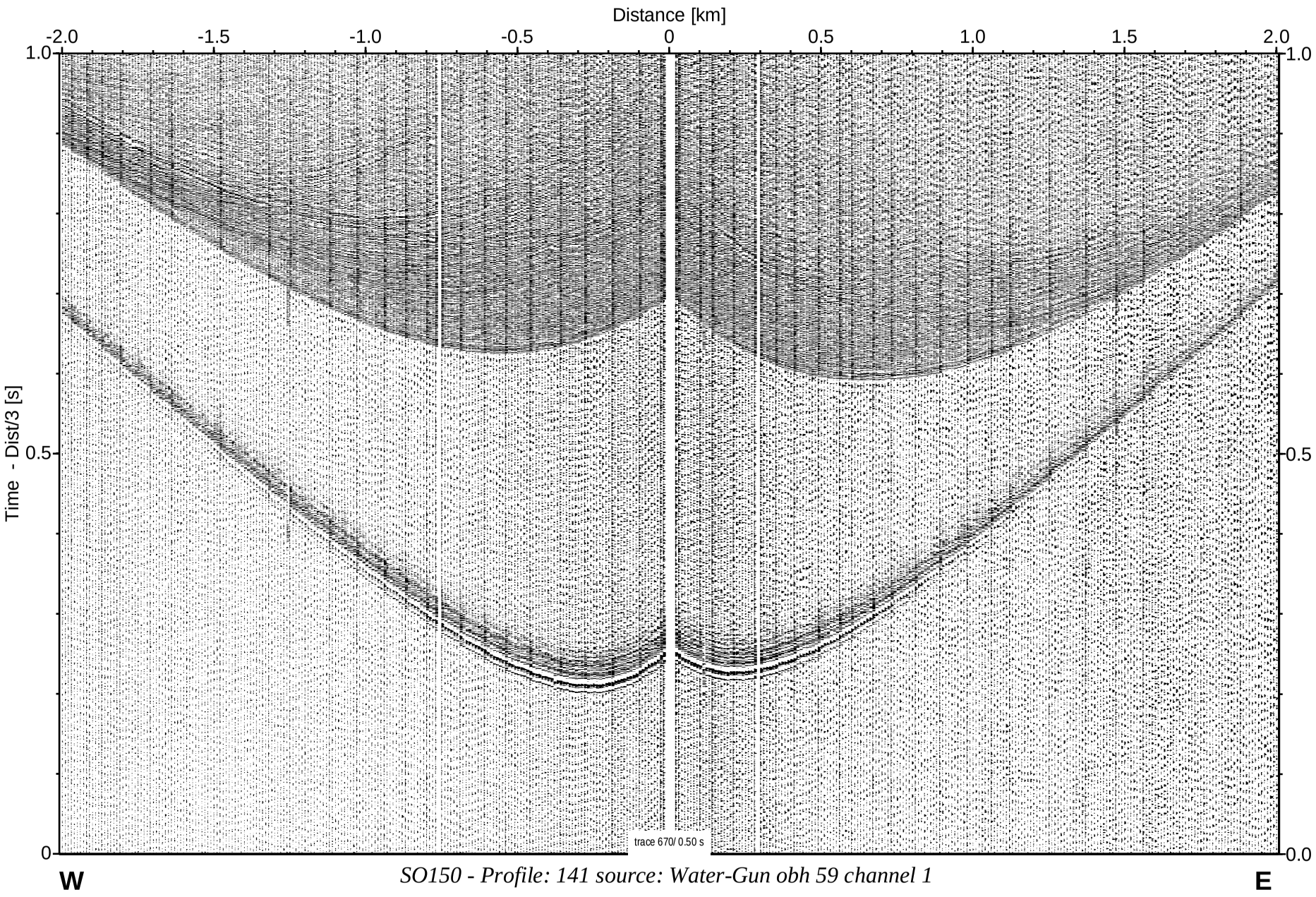

Figure 6.4.3: Record section from obh 59 , Profile 141.

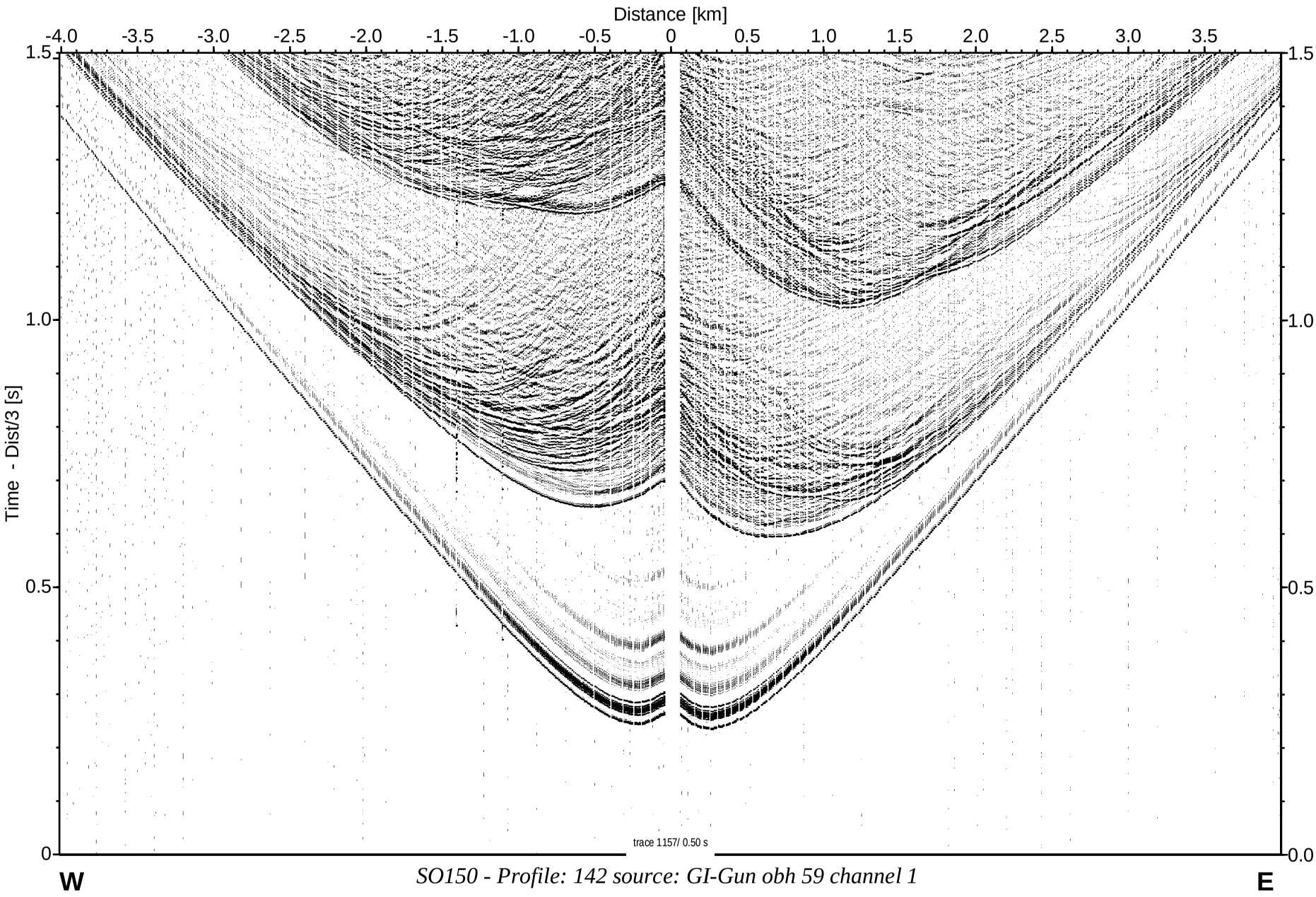

Figure 6.4.4: Record section from obh 59 , Profile 142.

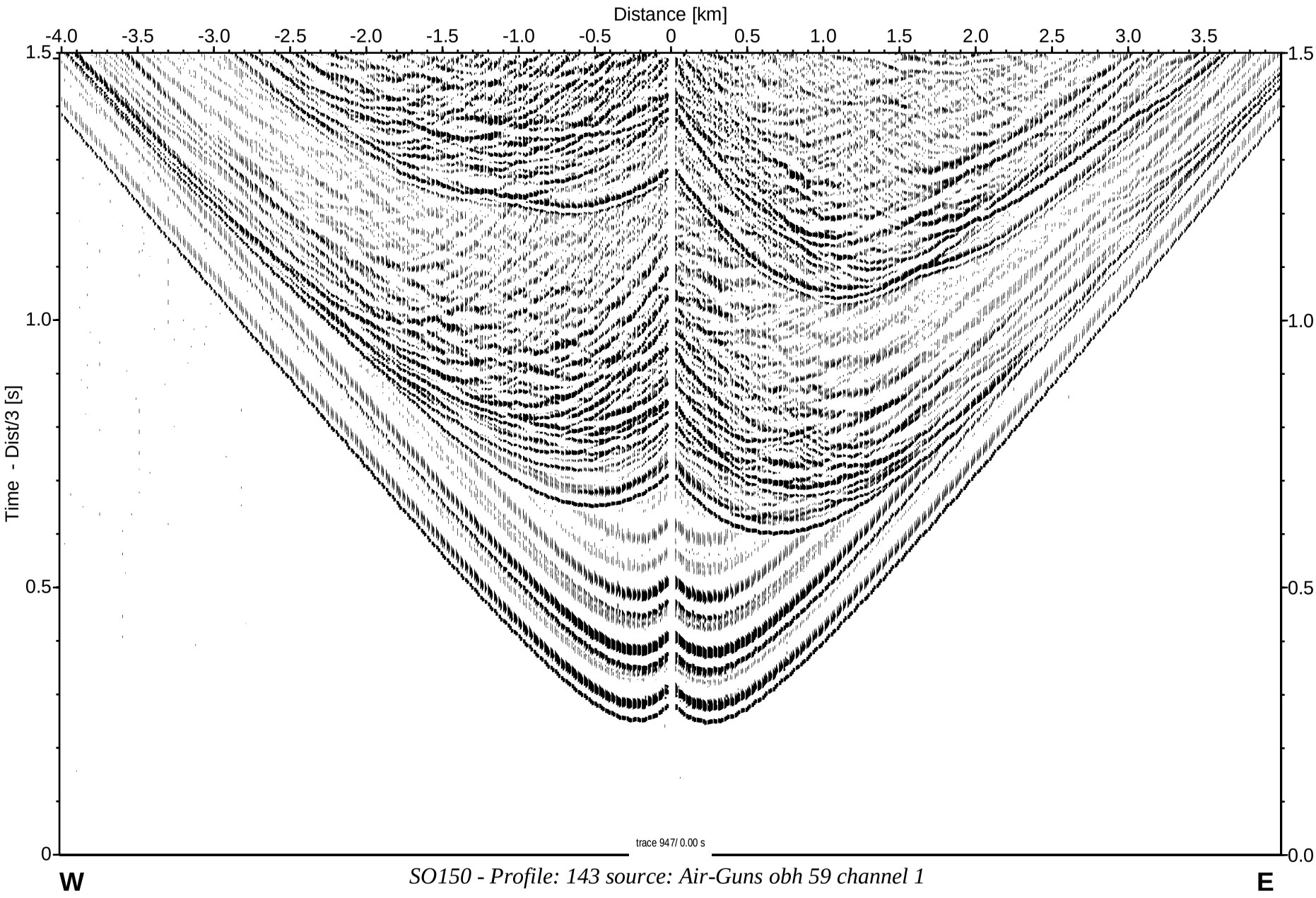

Figure 6.4.5: Record section from obh 59 , Profile 143.

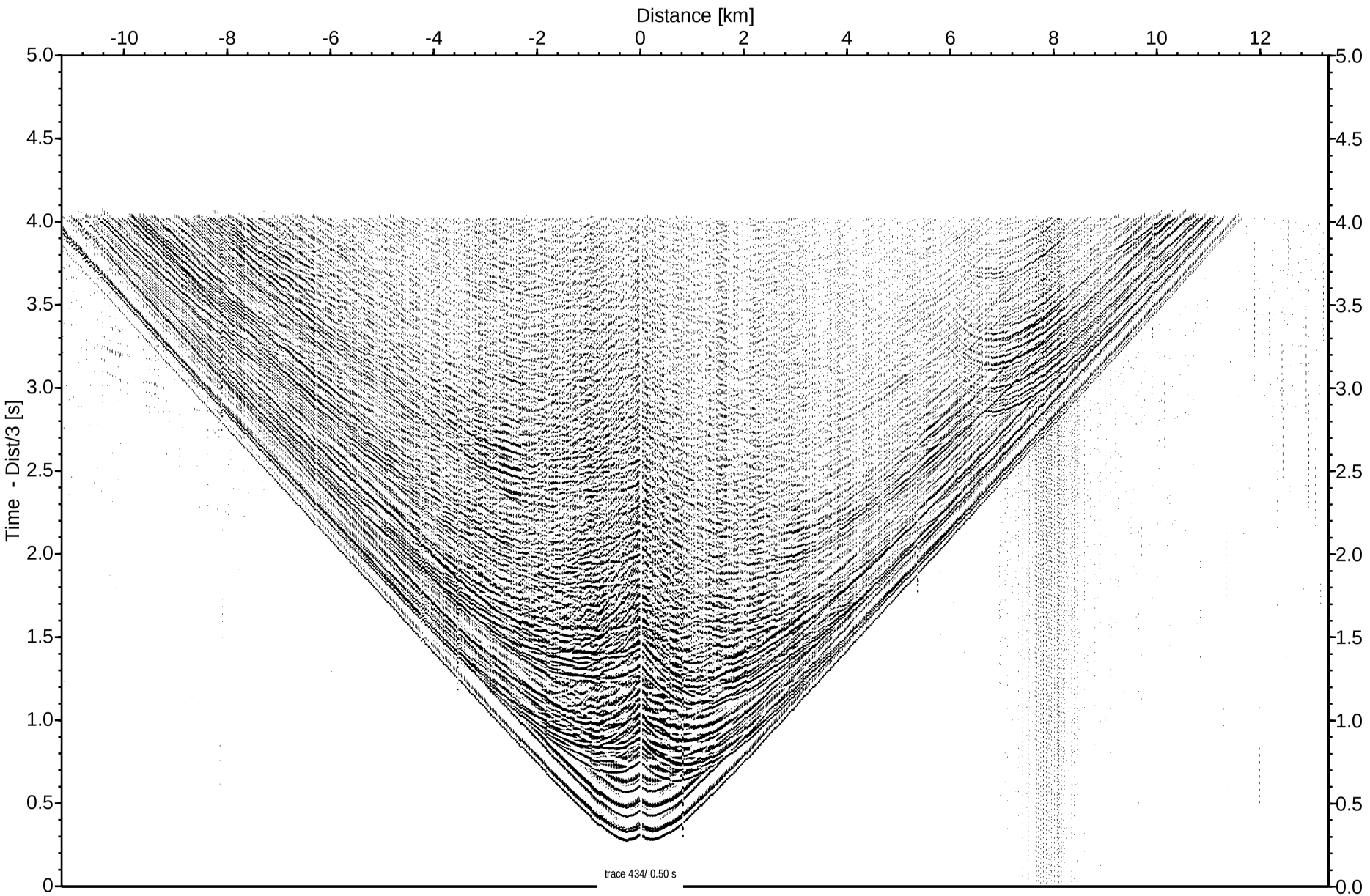

SO150 - Profile: 151 source: Bolt-Gun obh 59 channel 1

Figure 6.4.6: Record section from obh 59 , Profile 151.

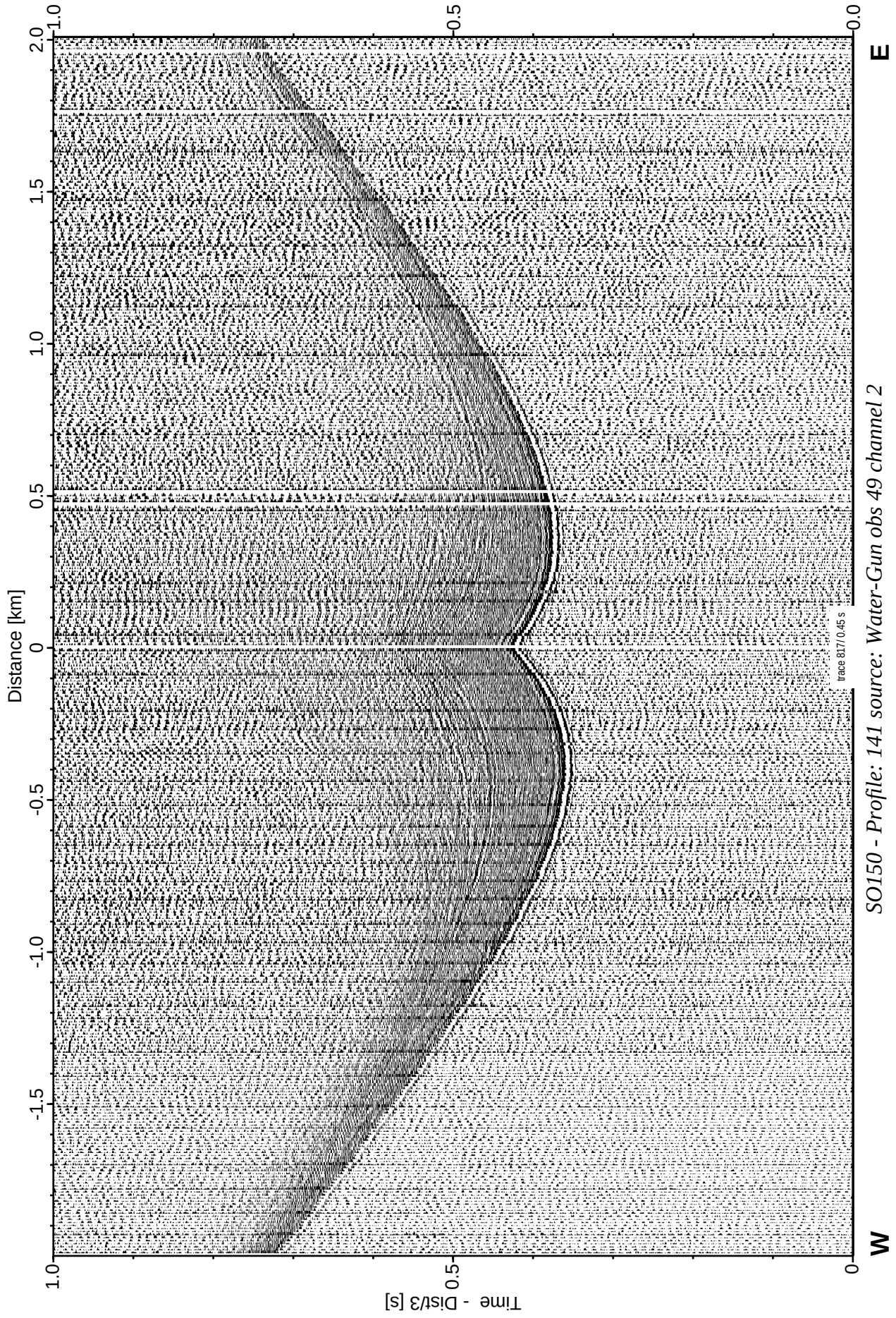

Figure 6.4.7: Record section from obs 49 horizontal component 1, Profile 141.

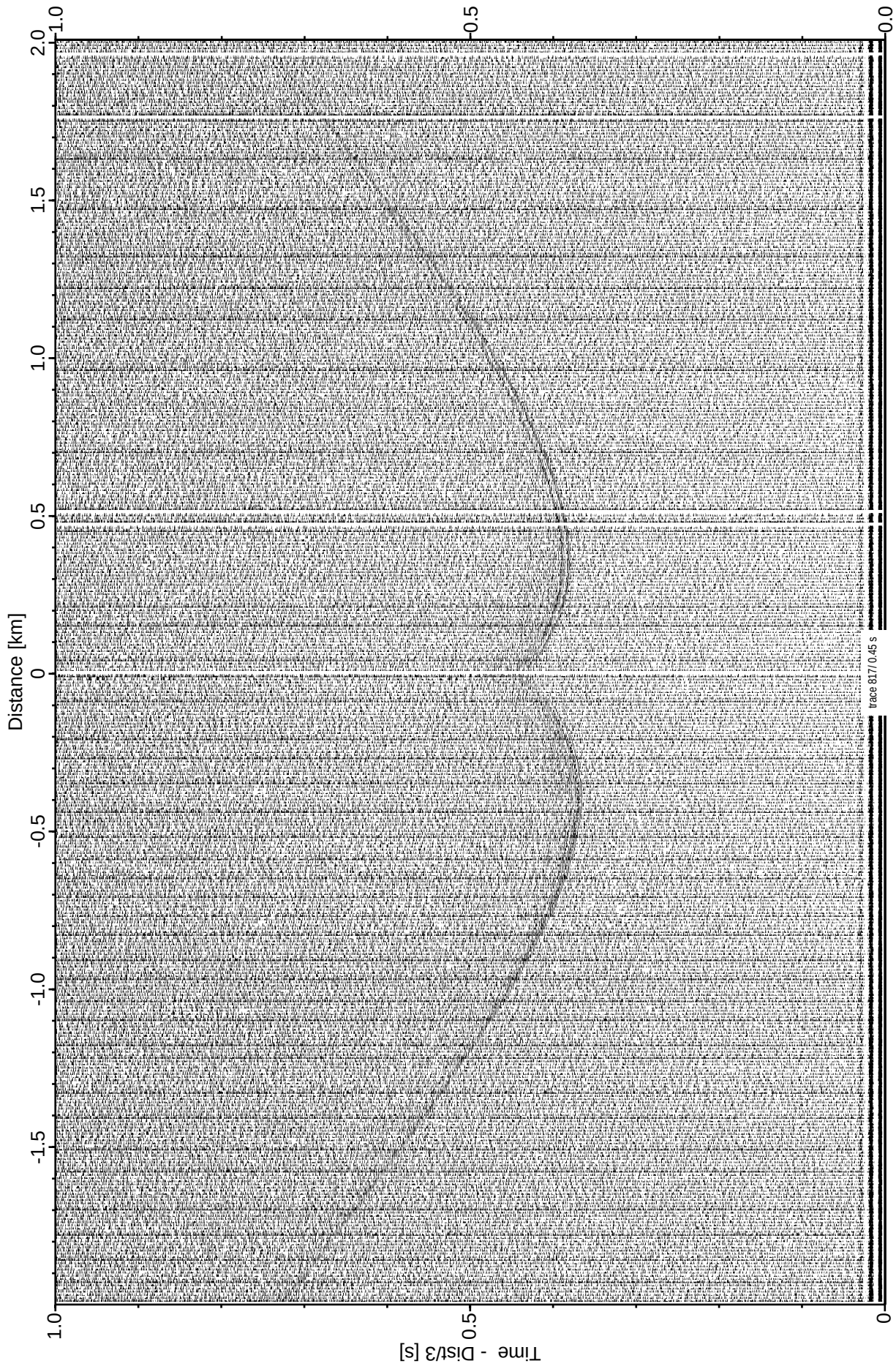

Figure 6.4.8: Record section from obs 49 horizontal component 1, Profile 141.

Figure 6.4.9: Record section from obs 49 horizontal component 2, Profile 141.

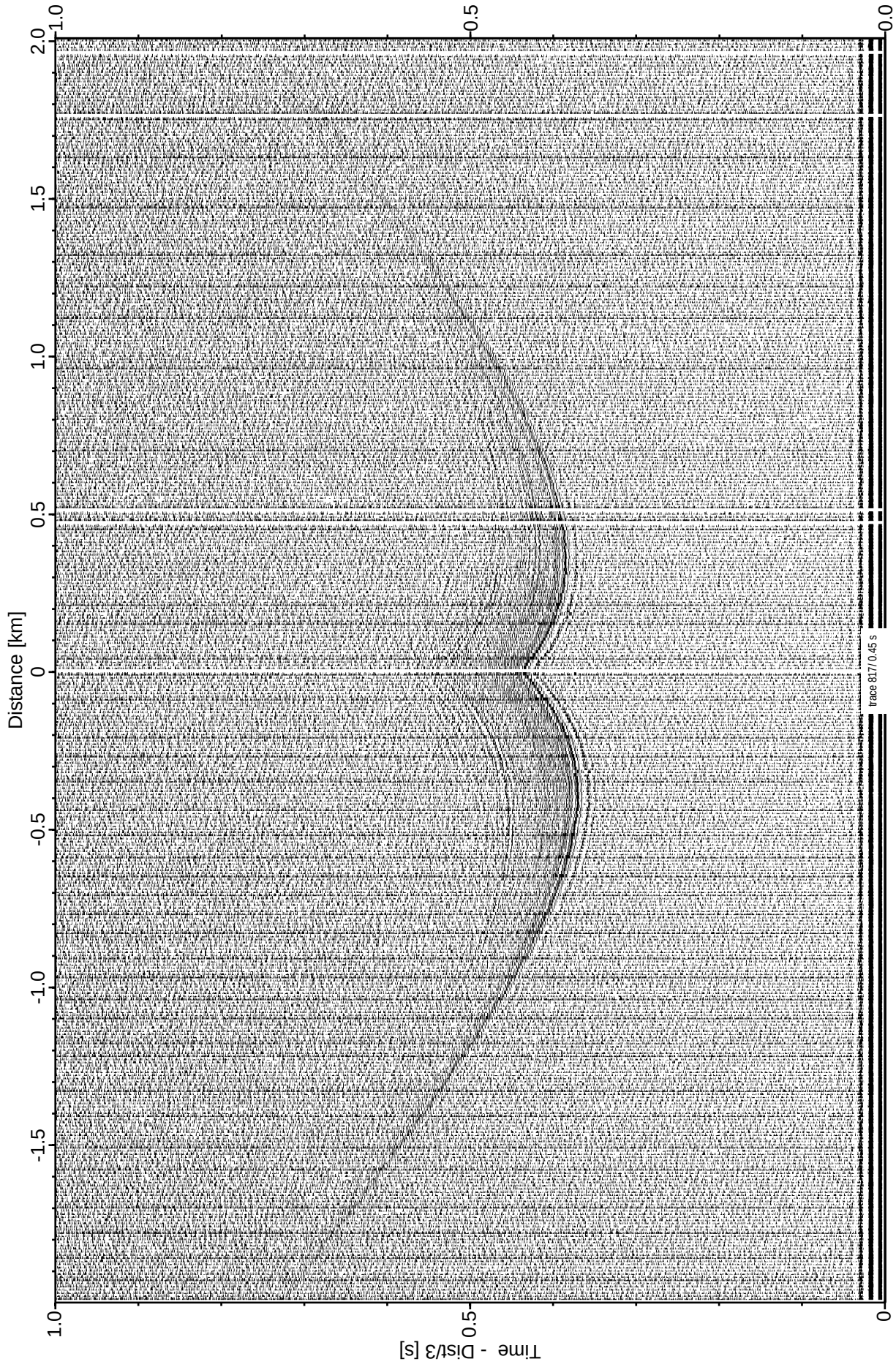

Figure 6.4.10: Record section from obs 49 vertical component, Profile 141.

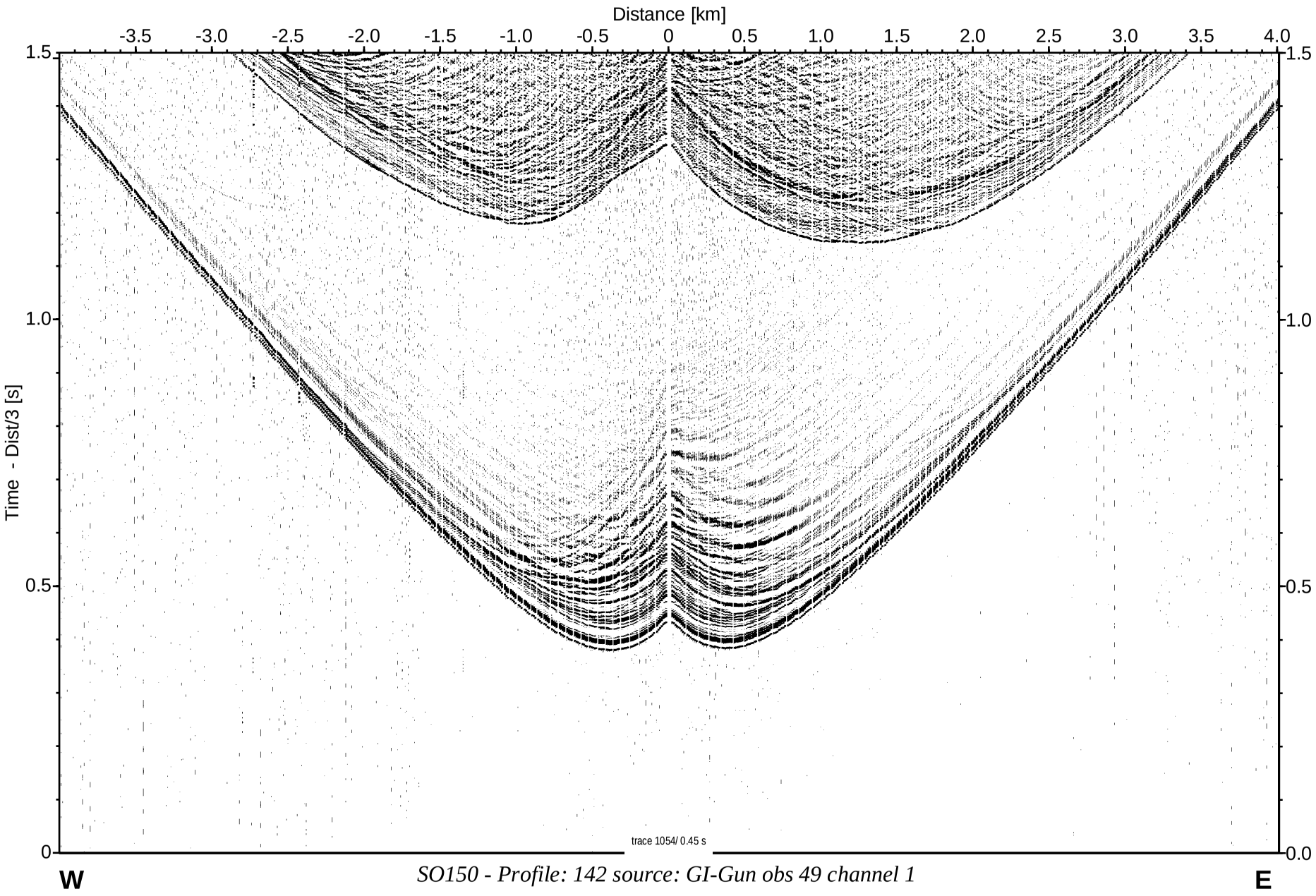

Figure 6.4.11: Record section from obs 49 hydrophone, Profile 142.

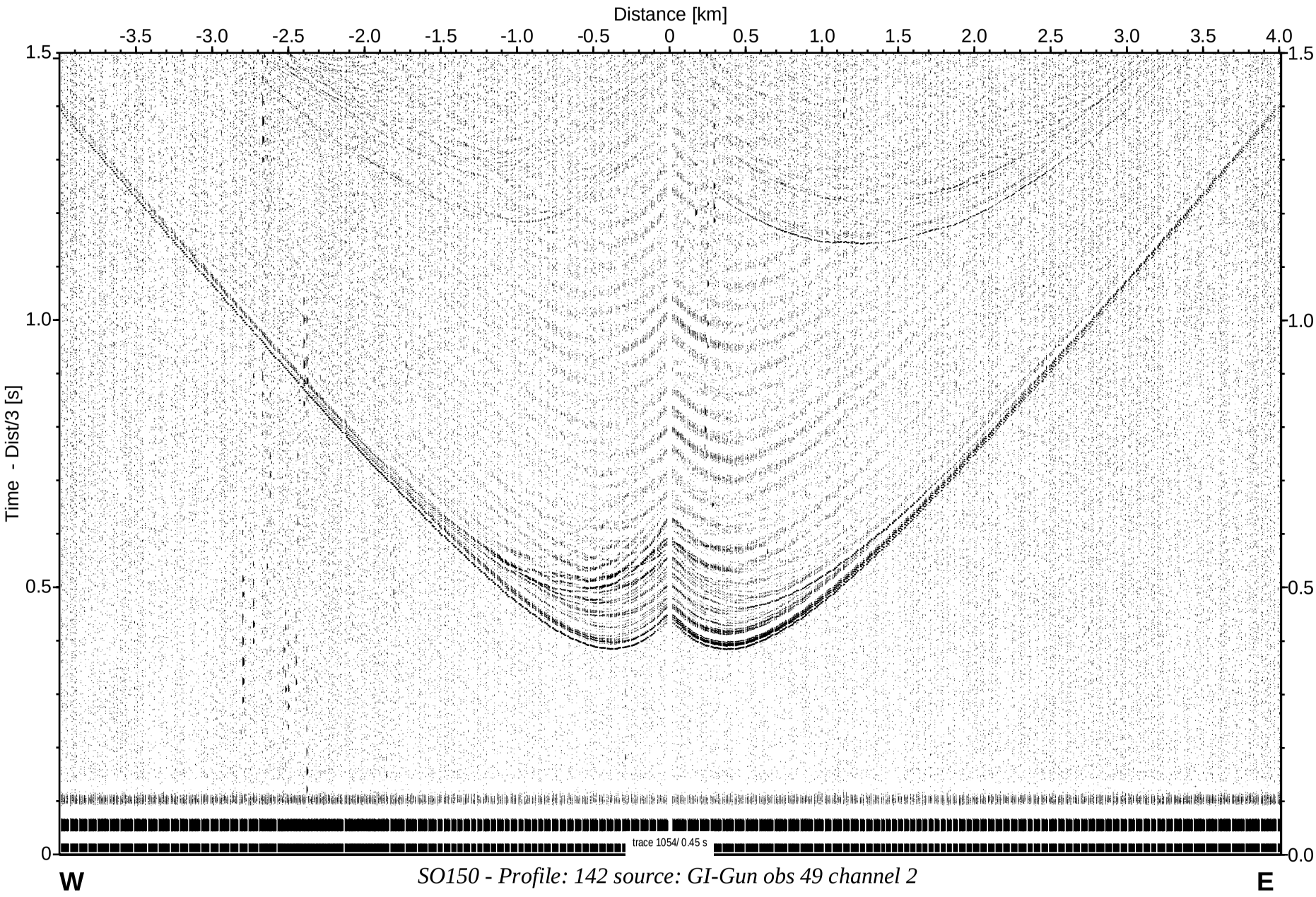

Figure 6.4.12: Record section from obs 49 horizontal component 1, Profile 142.

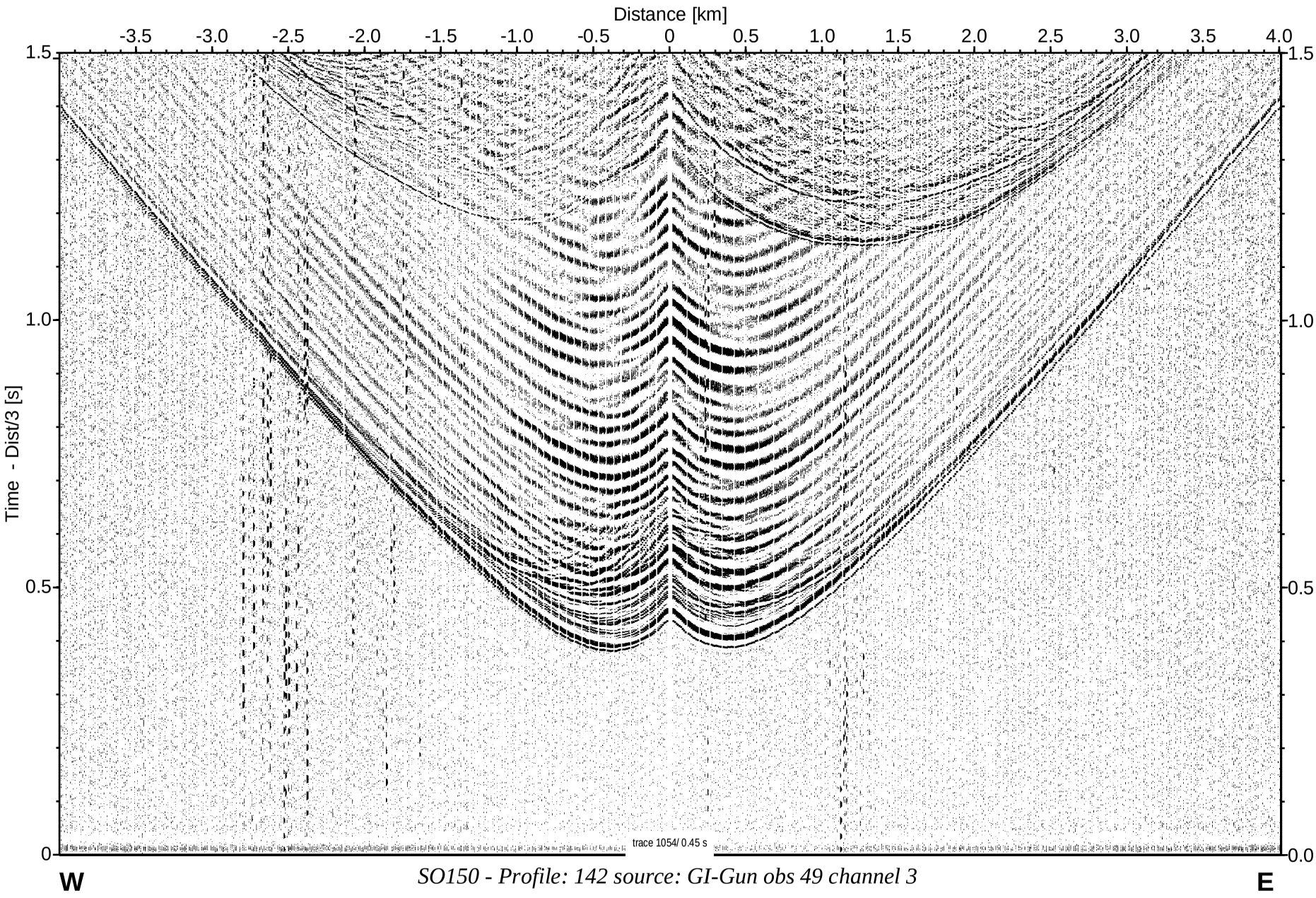

Figure 6.4.13: Record section from obs 49 horizontal component 2, Profile 142.

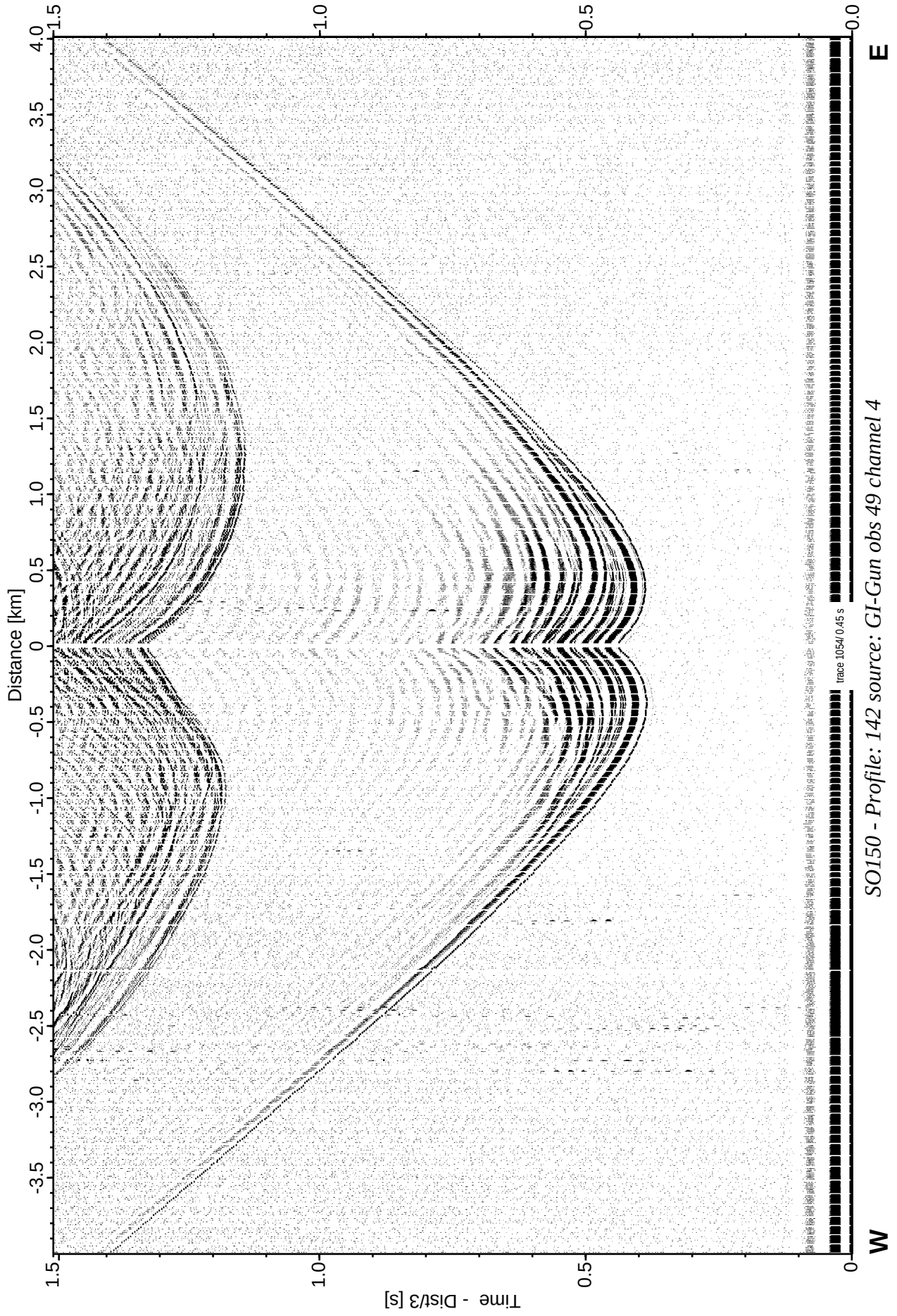

Figure 6.4.14: Record section from obs 49 vertical component, Profile 142.

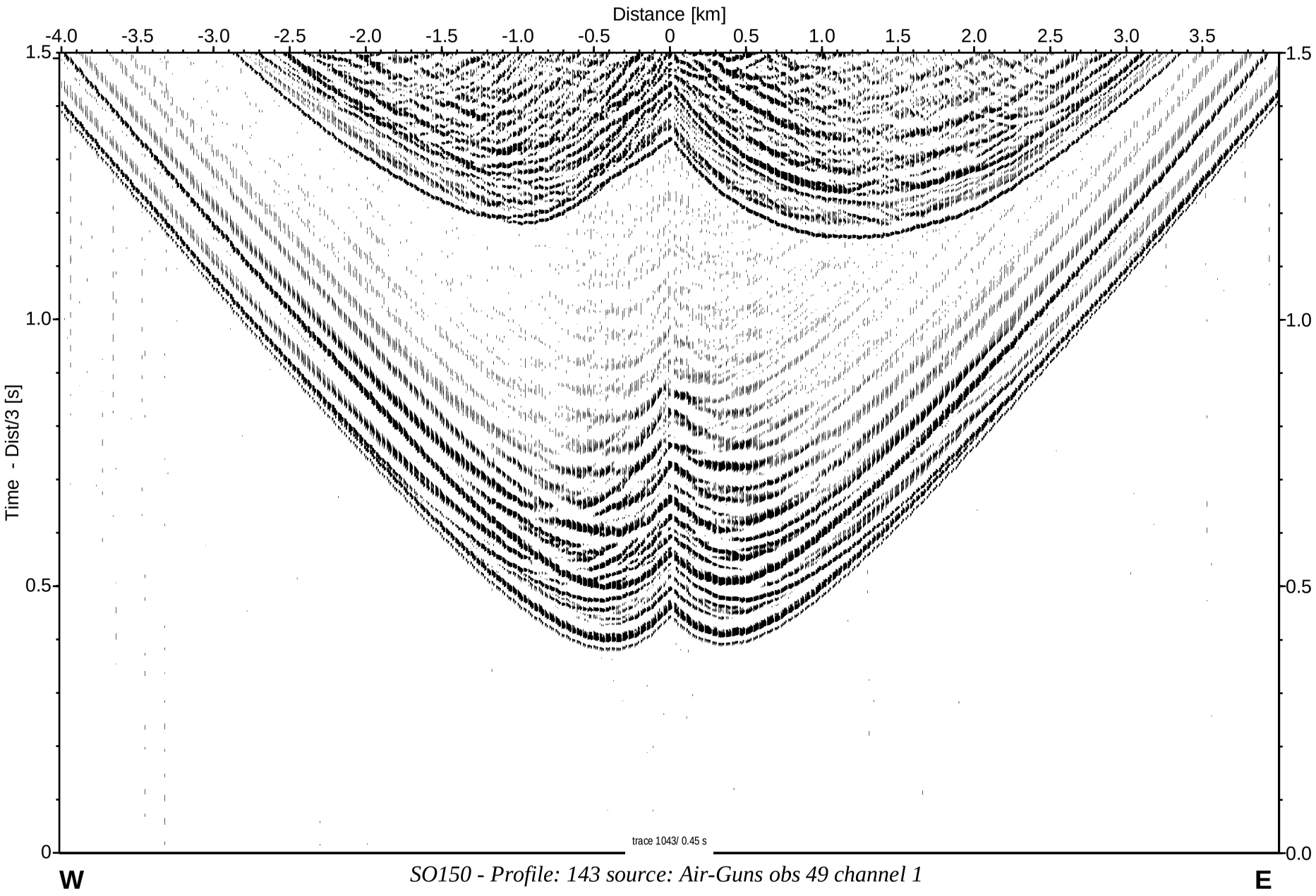

Figure 6.4.15: Record section from obs 49 hydrophone, Profile 143.

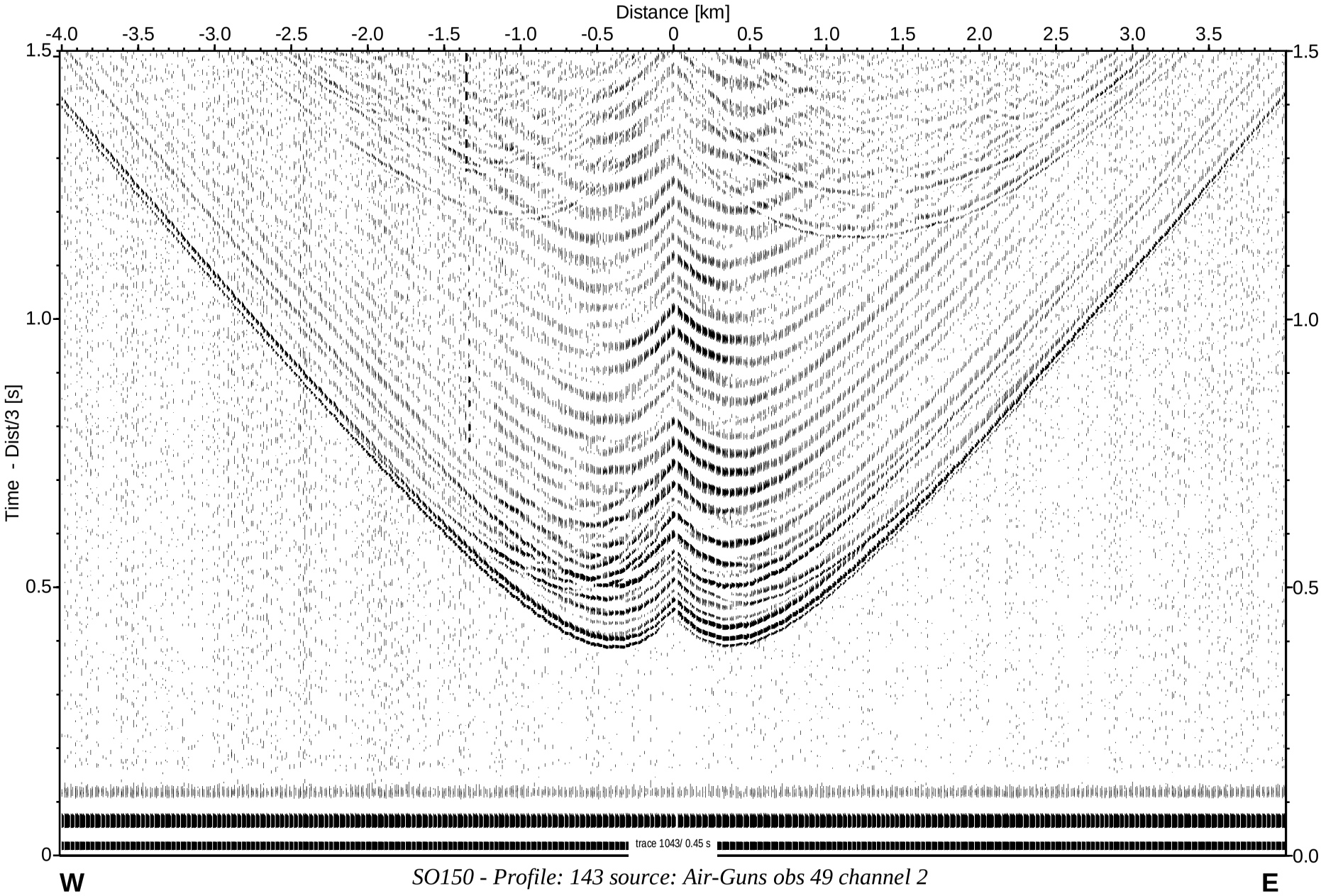

Figure 6.4.16: Record section from obs 49 horizontal component 1, Profile 143.

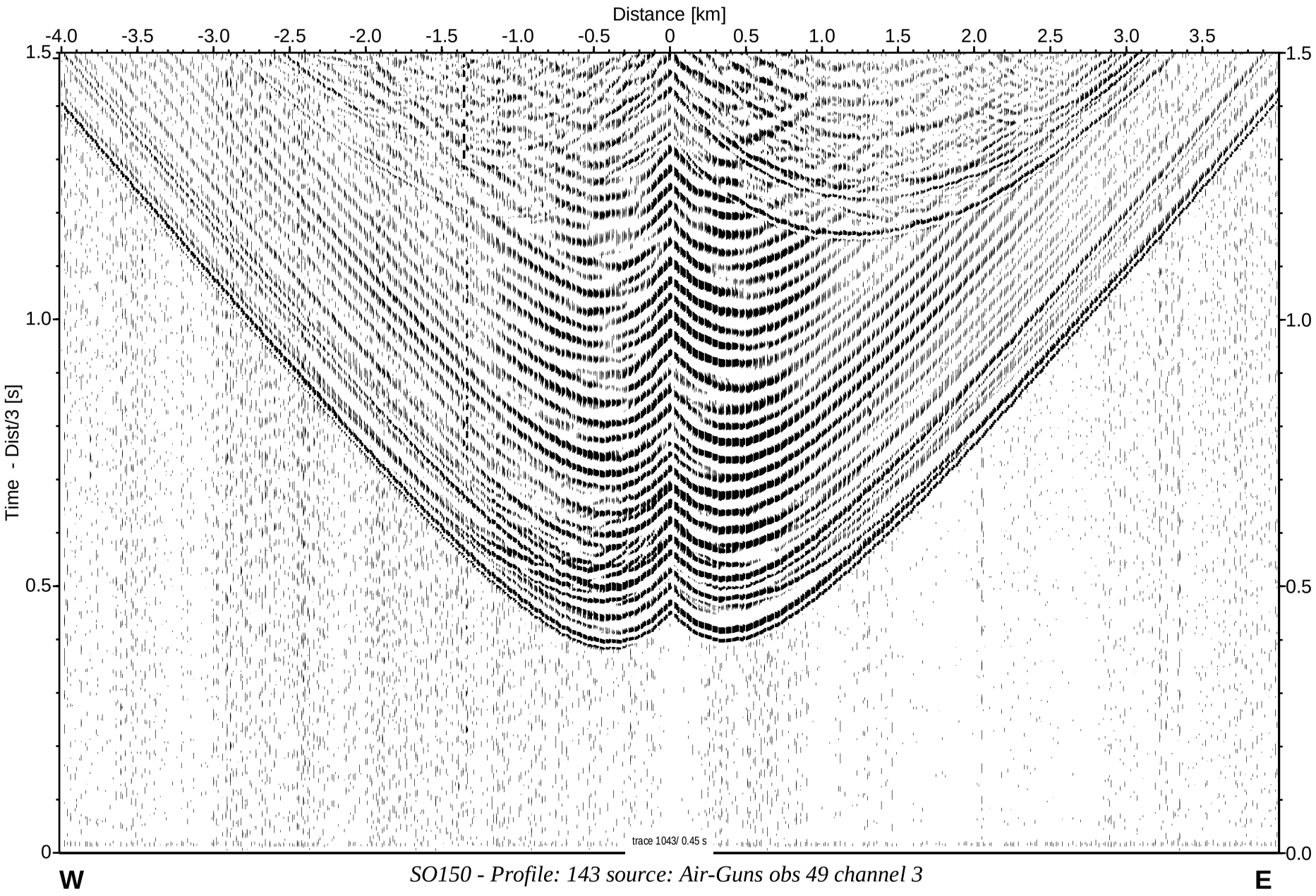

Figure 6.4.17: Record section from obs 49 horizontal component 2, Profile 143.

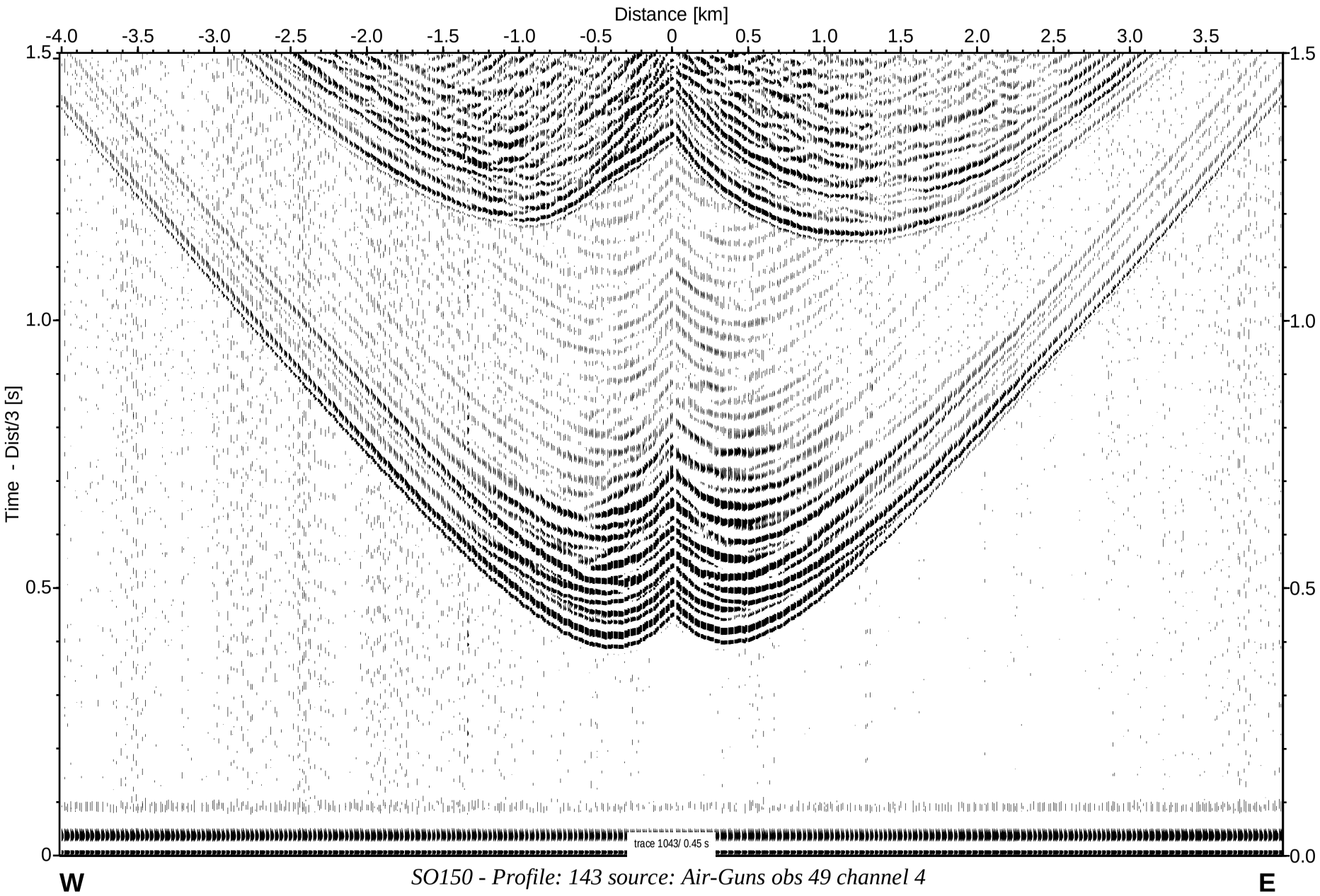

Figure 6.4.18: Record section from obs 49 vertical component, Profile 143.

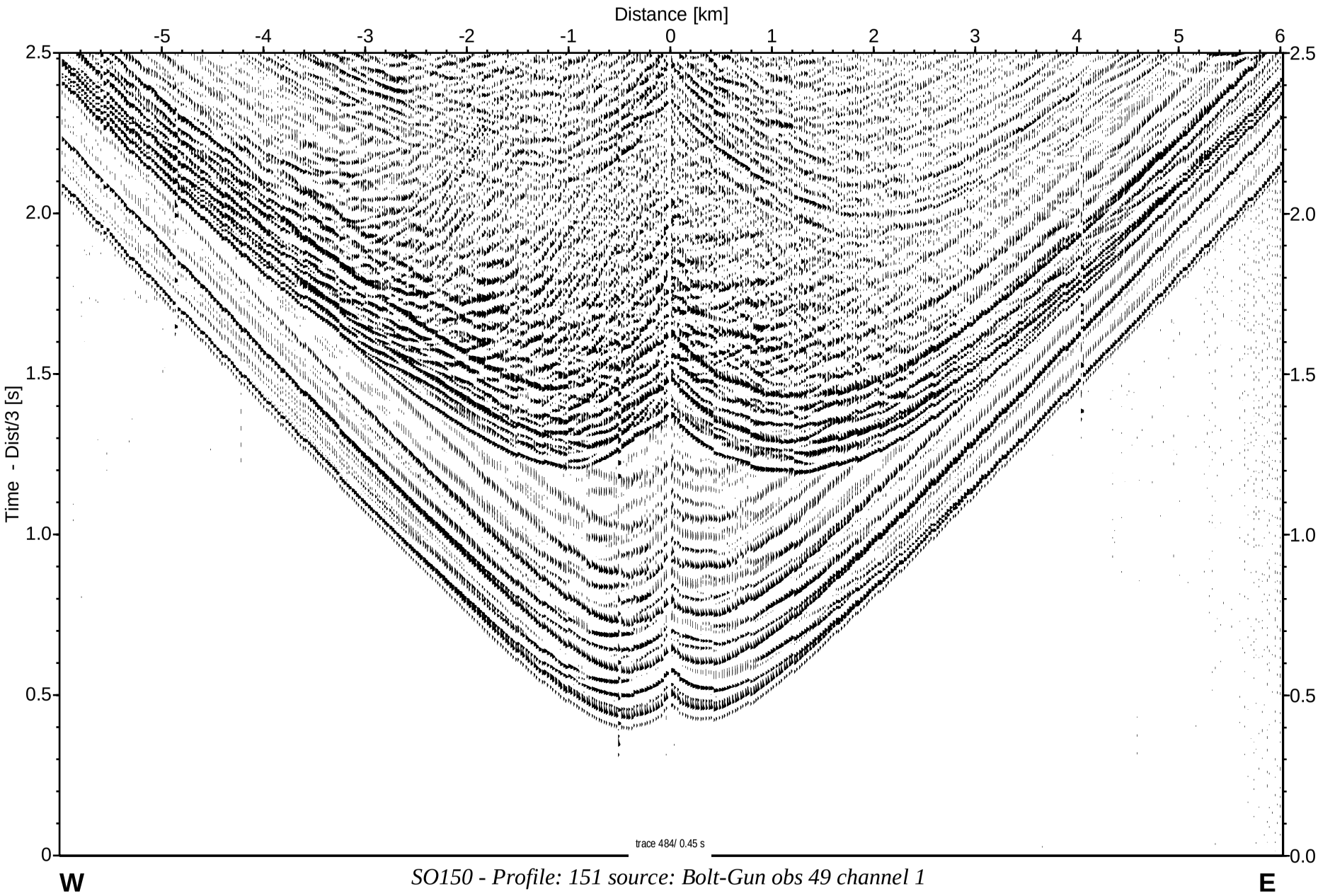

Figure 6.4.19: Record section from obs 49 hydrophone, Profile 151.

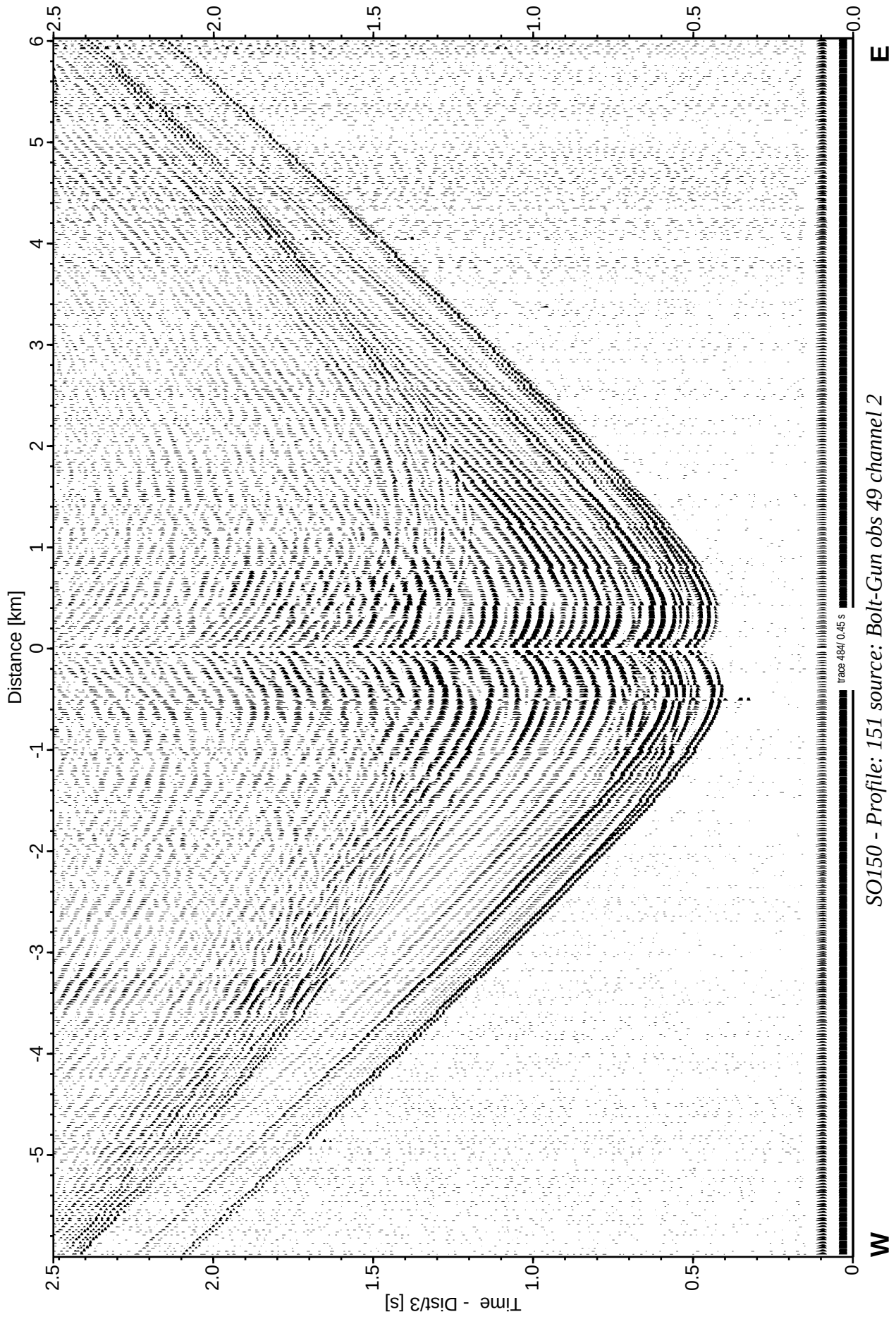

Figure 6.4.20: Record section from obs 49 horizontal component 1, Profile 151.

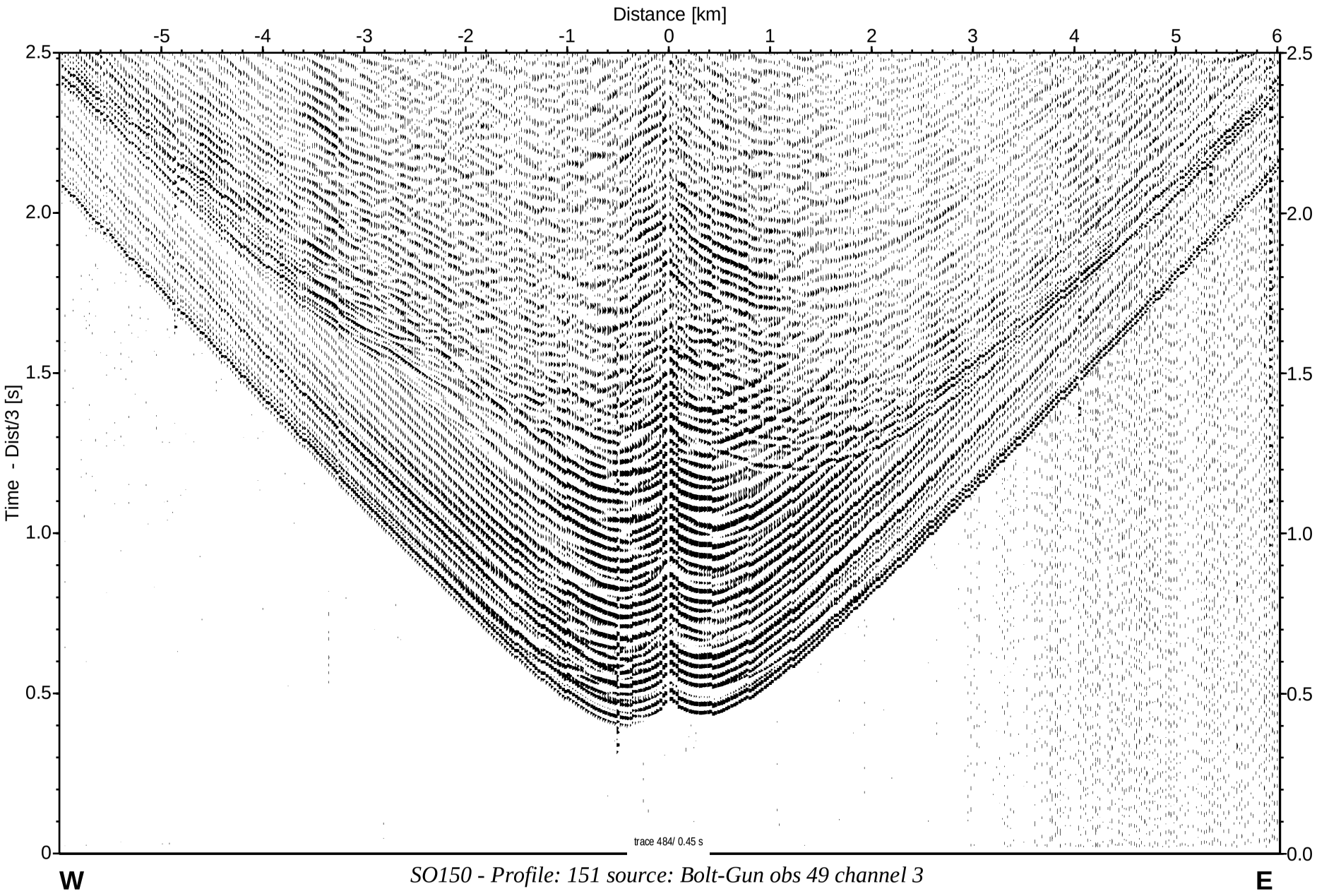

Figure 6.4.21: Record section from obs 49 horizontal component 2, Profile 151.

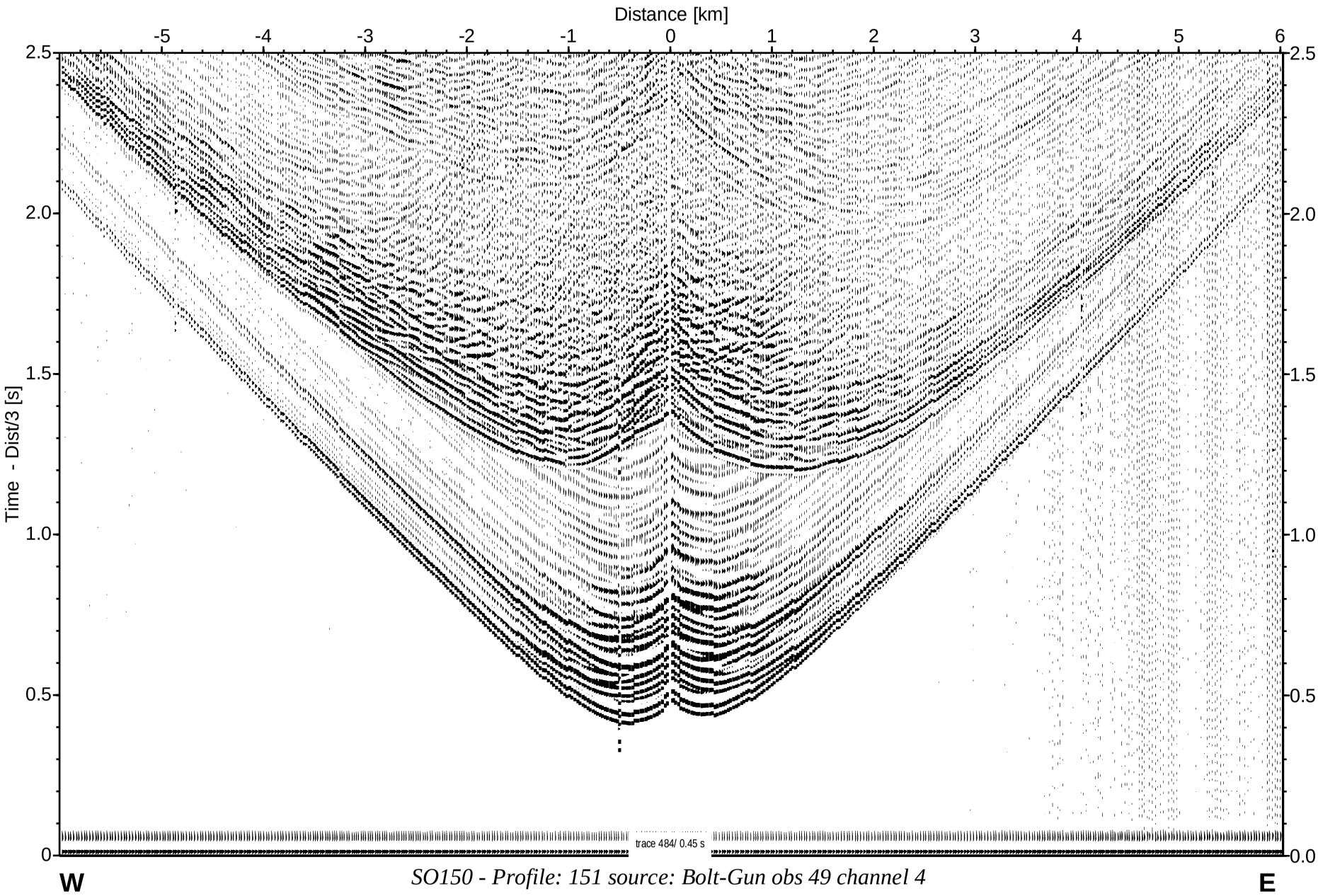

Figure 6.4.22: Record section from obs 49 vertical component, Profile 151.

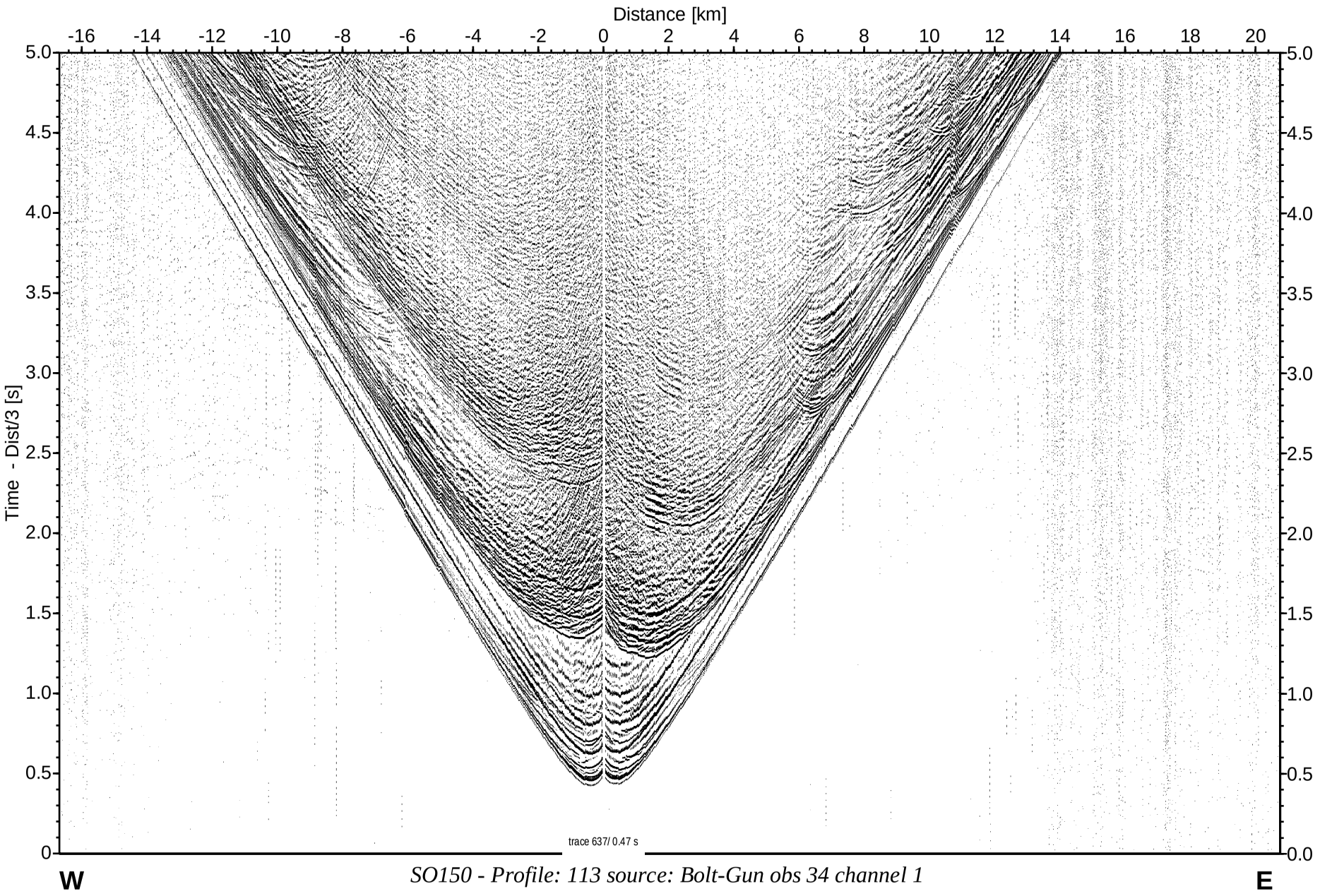

Figure 6.4.23: Record section from obs 34 hydrophone, Profile 113.

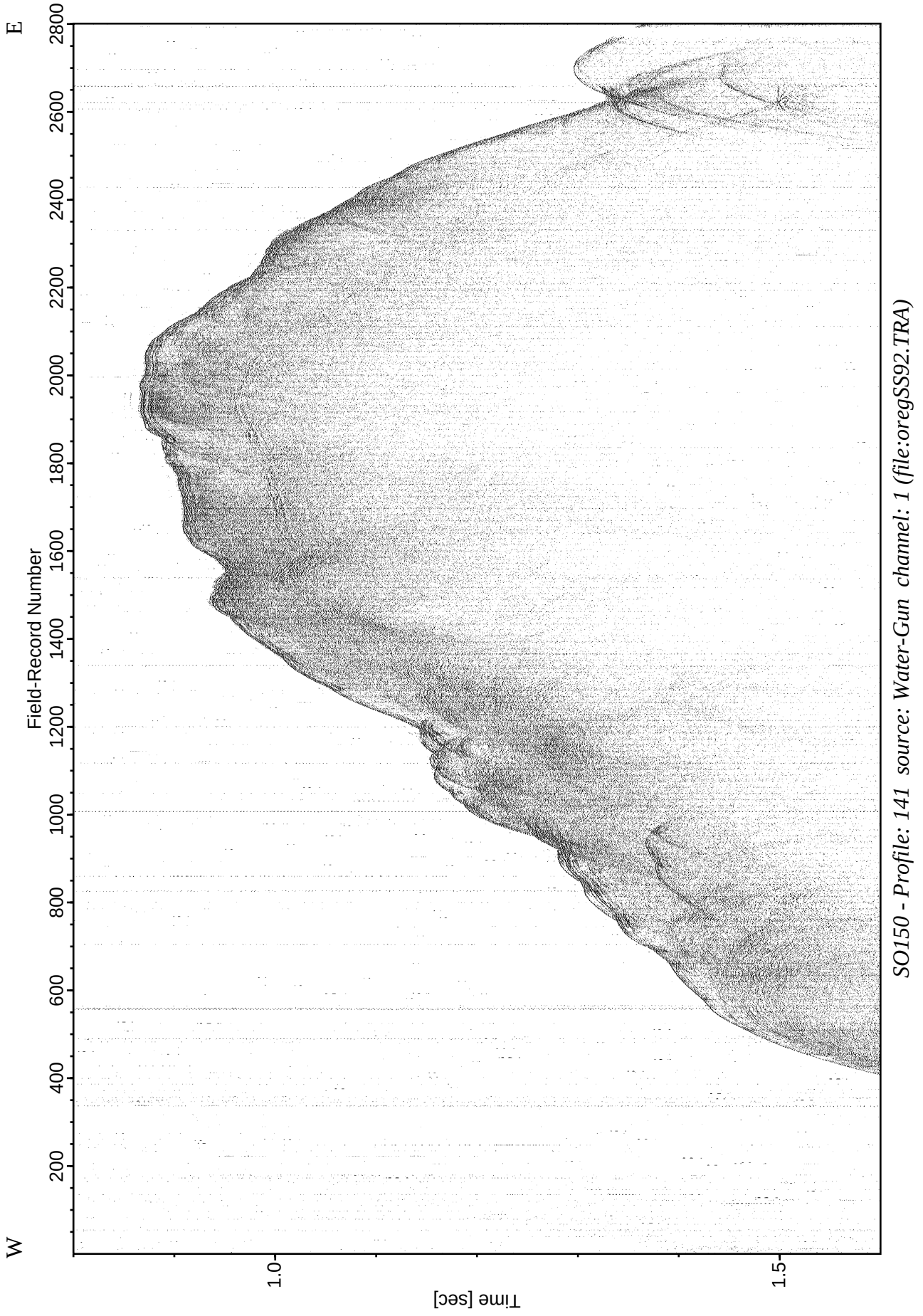

Figure 6.4.24: Record section with source Water-Gun, Profile 141.

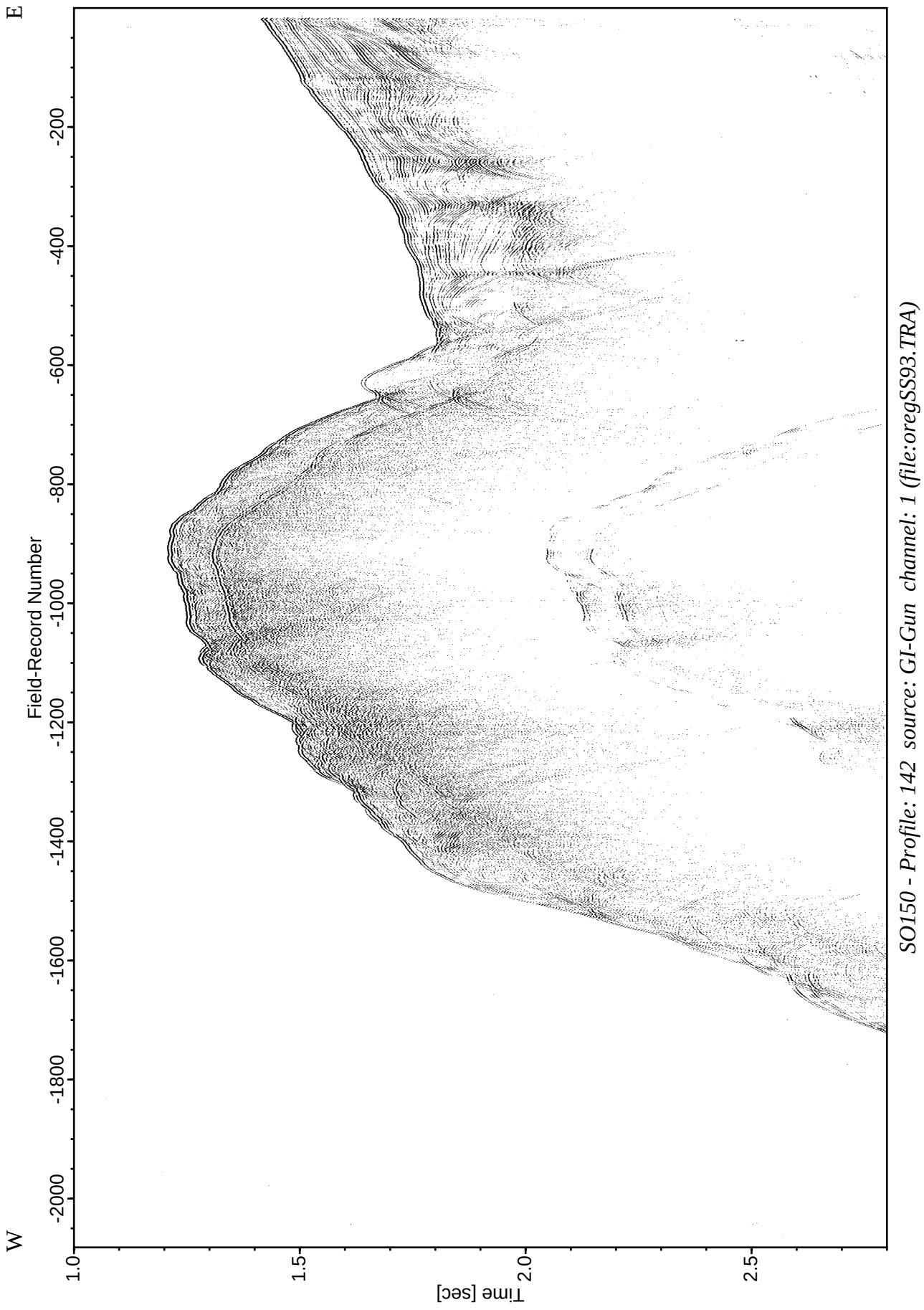

Figure 6.4.25: Record section with source GI-Gun, Profile 142.

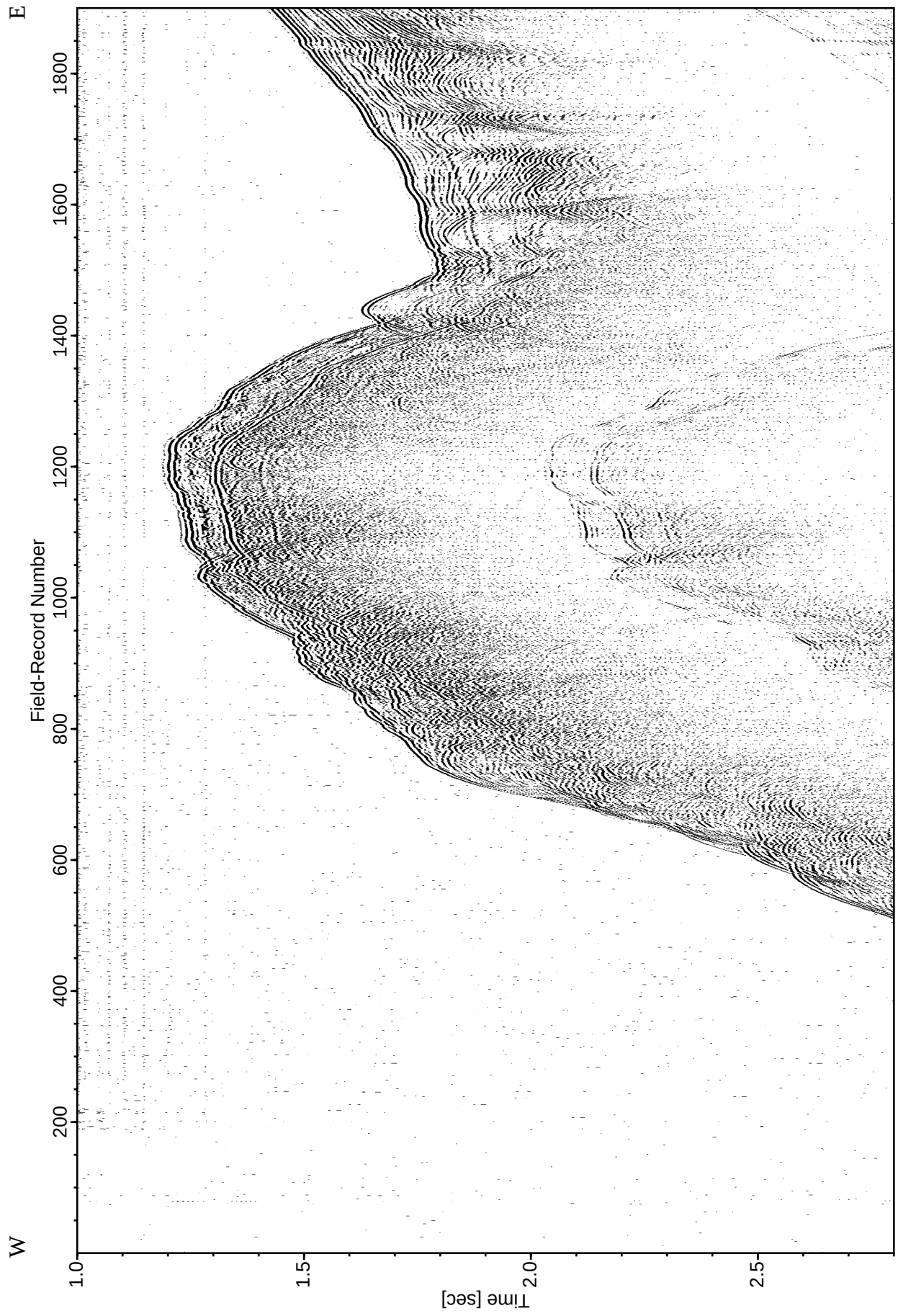

Figure 6.4.26: Record section with source Air-Gun Array, Profile 143.

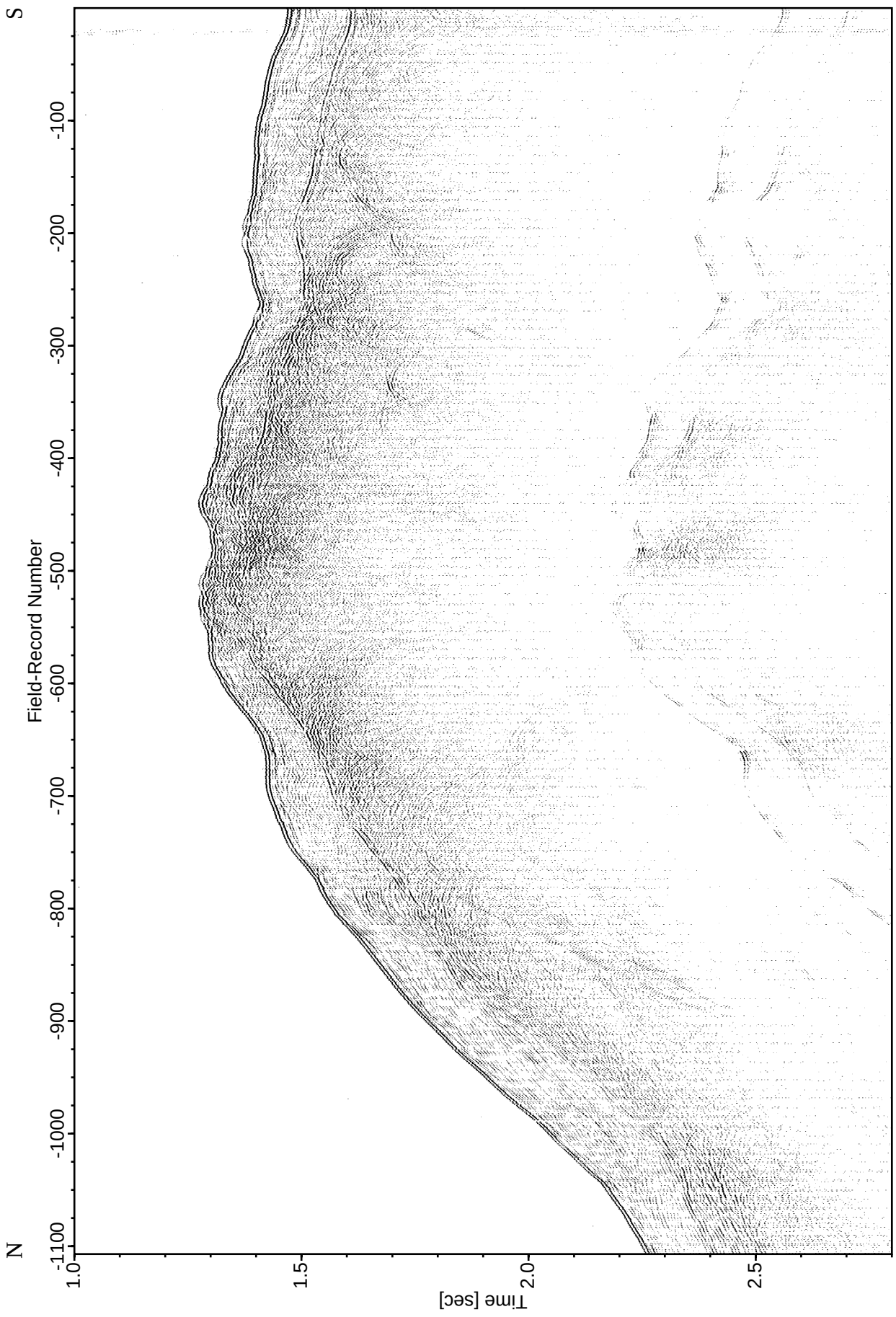

Figure 6.4.27: Record section with source GI-Gun, Profile 110.

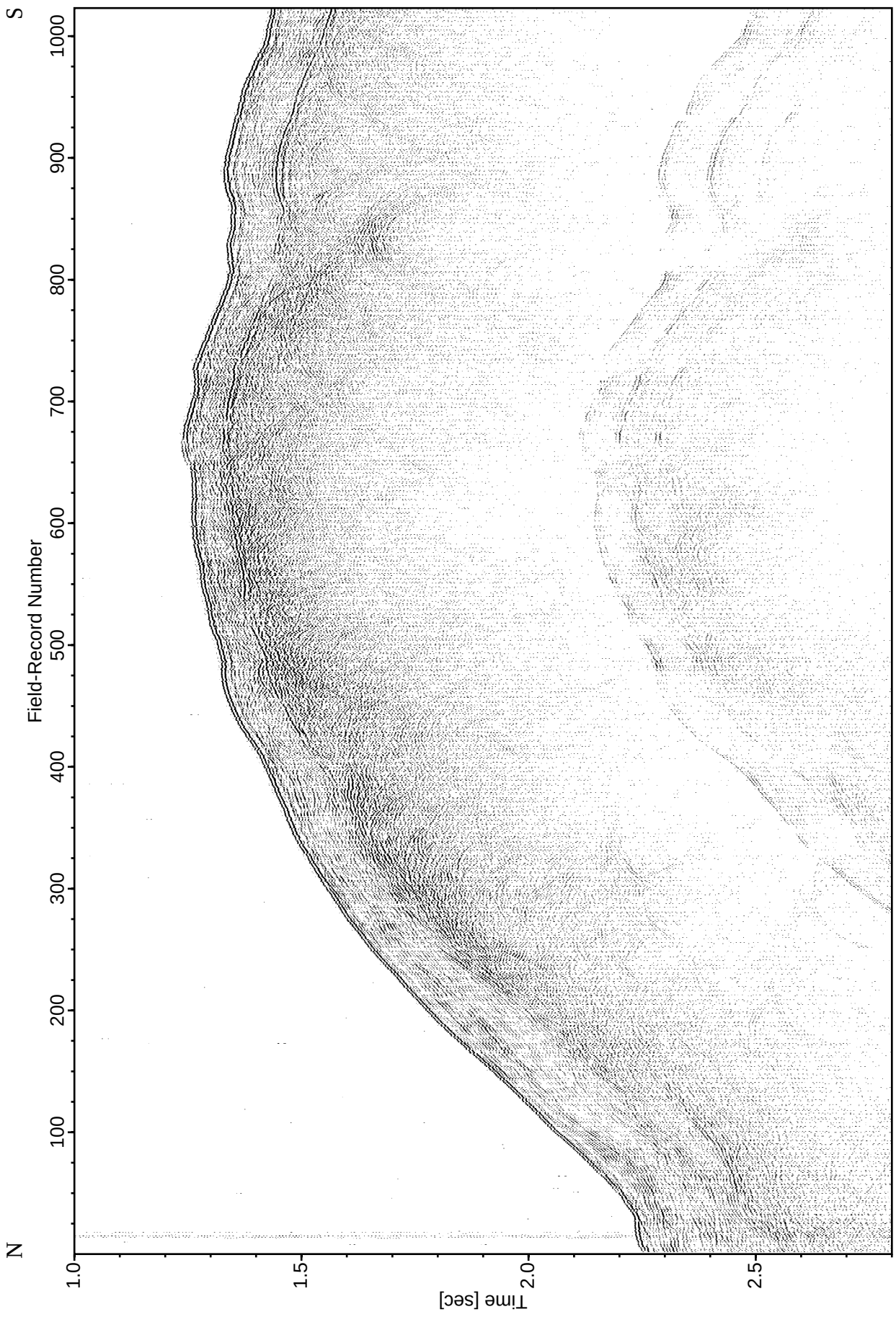

Figure 6.4.28: Record section with source GI-Gun, Profile 107.

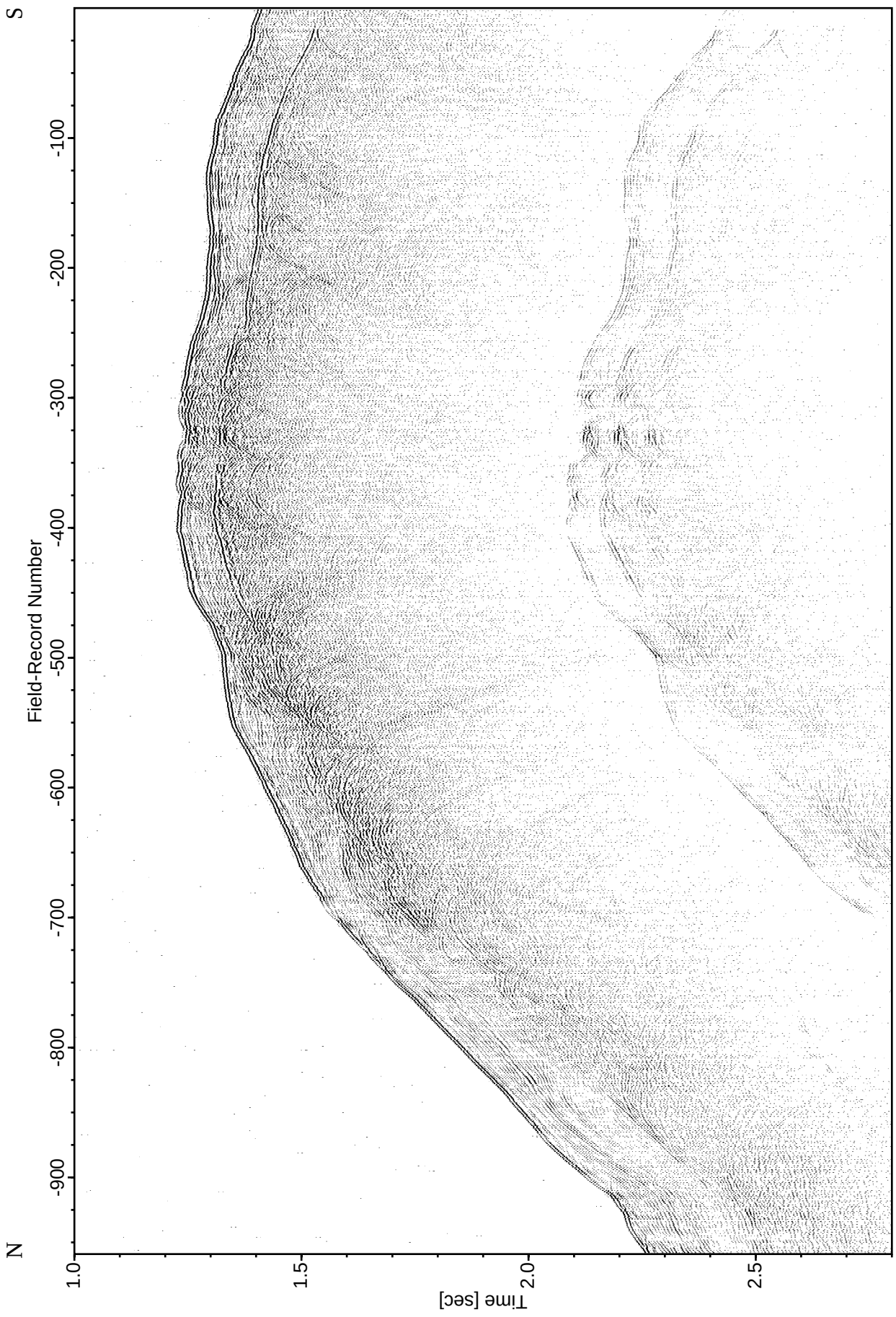

Figure 6.4.29: Record section with source GI-Gun, Profile 108.

6.5 EXPERIMENT ODP Leg 204, LOCATION HR3

(D. Klaeschen, D. Könitz, P. Liersch, J. Petersen, G. Klein)

The refraction and wide-angle reflection seismic experiments along Line OR89-2 of the old reflection seismic survey were meant to provide supplementary data for future ODP drilling. In fact, two tentatively chosen sites, HR1 and HR3 are situated along this profile across the southern summit of Hydrate Ridge. The experiments undertaken during the HYDGAS cruise were at first separated into two deployments at both HR1 and HR3. A third deployment at the end of the cruise was designated to fill data gaps and narrow the spacing between the stations and cross lines. Figure 6.5.1 shows the entire track chart of the lines acquired. Figure 6.5.2 shows a reflection profile along line OR89-2 which illustrates structure of the accretionary margin in this area, and also includes the location of the deployments. It can be seen that the second, upthrusted wedge has a well-developed BSR. Its two sections of interest are the crest (HR3) and the eastern flank (HR1), which gently dips towards a smaller depression with undisturbed, layered sediments (Fig. 6.5.1).

The refraction and wide-angle reflection seismic experiment across the future ODP drill site HR3 was first shot over an OBH/OBS assembly between 23.09. and 25.09. (Figs. 6.5.1, 6.5.2, and 6.6.1). The main WE-profile, along which the seafloor stations were placed, is the formerly acquired line OR89-02 (see MacKay et al., 1995; Trehu et al., 1999). It cross-cuts the southern summit of the Hydrate Ridge in an EW-direction (Fig. 6.5.1). During the first deployment, a total of 4 OBSs and 10 OBHs were aligned at a 200 m spacing (according to the GPS position of the vessel) in a WE-direction across the crest of the ridge. The recorders of the stations were all synchronized and started with frequencies corresponding to the sources used when shooting the array (Fig. 6.4.1). First, a 10 km long WE-line was shot with the Sparker, followed by a 20 km long line with the airgun array in the opposite direction. After the next tag, the 20 km lines were shot once more with the GI-gun before continuing with five 9-km long NS-cross lines at a 200 m spacing across the central seafloor stations (Figs. 6.5.3. and 6.5.4). All cross lines were shot with the GI-gun and the surface streamer, while for the longer EW-profiles the GEOMAR mini streamer was additionally used for acquisition. After completion of the NS-grid, a long profile (32 km) with the Bolt gun was acquired going east. After recovery of the stations and quality control of the received data, it turned out that all 4 OBSs (stations 9-12) in the centre of the profile (Fig. 6.5.4) had not worked because of a mechanical problem with the release system once hitting the ocean bottom. Station 35 (OBH) gained somewhat lower data quality, while the remaining systems operated nicely.

The results from the first deployment (stations 4-17) were so dissatisfying, that gaps in the central part and the edges of the acquisition had to be filled by a second deployment. Another 4 OBSs and 7 OBHs were brought to the seafloor, 6 of which were dropped in the HR3 area (stations 60-65; Fig. 6.5.4). In addition to the EW-profiles with the watergun, GI-gun, and airgun array after recording of the stations started, another 3 NS-profiles of equal 9 km lengths were shot to complement the previous 5. Again, the second deployment was completed with a 32 km long EW-profile across the OBH/OBS assembly with the Bolt gun. After recovery of the equipment and retrieval of the data, it was found that, no failure of the equipment occurred, and all stations recorded valuable information over the different frequency ranges.

Various data examples of OBH, OBS and streamer data for different sources are displayed in Fig. 6.5.3 to Fig. 6.5.23.

Profiles P11-21 & P171-181 seismic lines

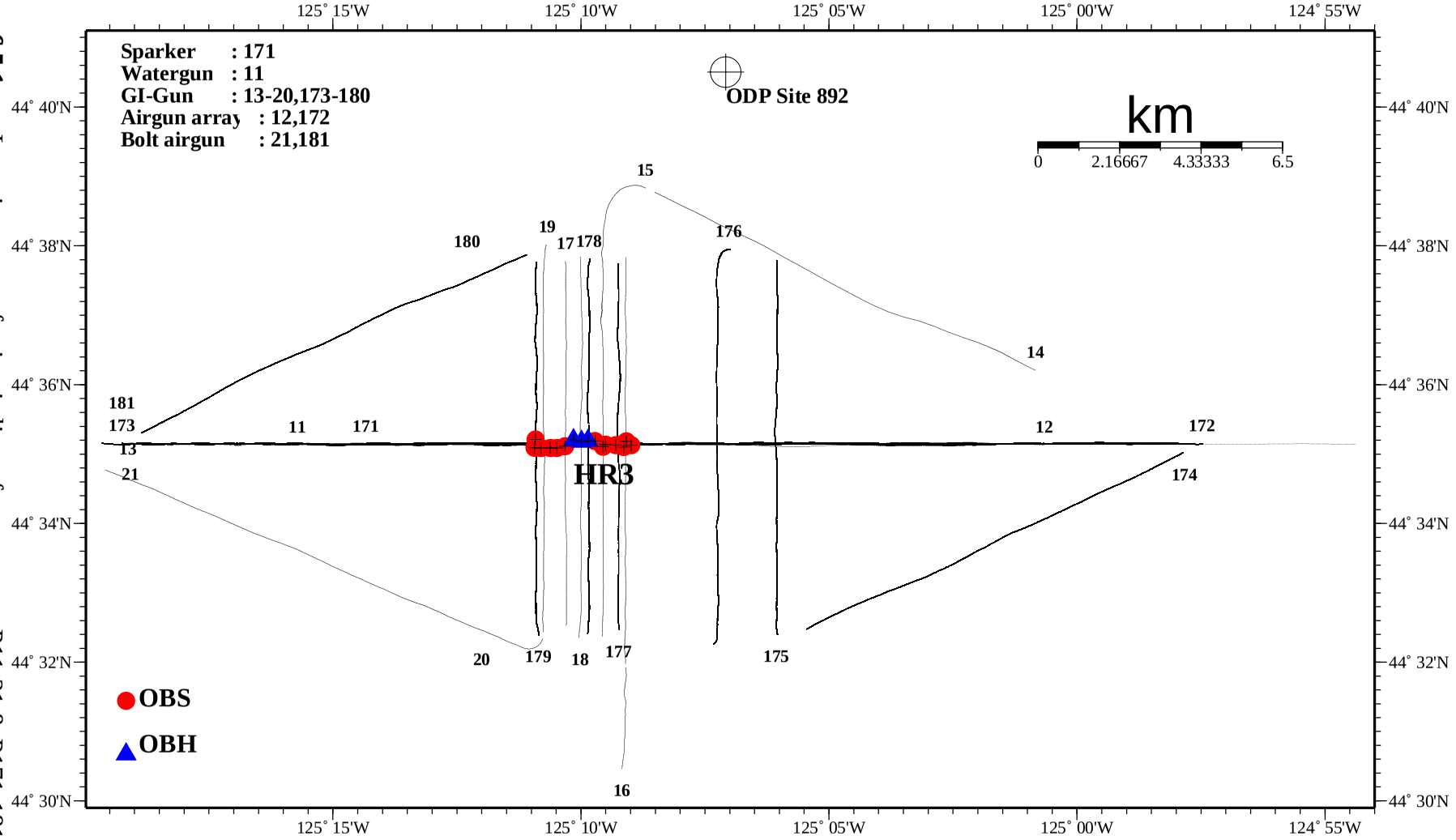

Figure 6.5.1: Location map of seismic line of survey run P11-21 & P171-181.

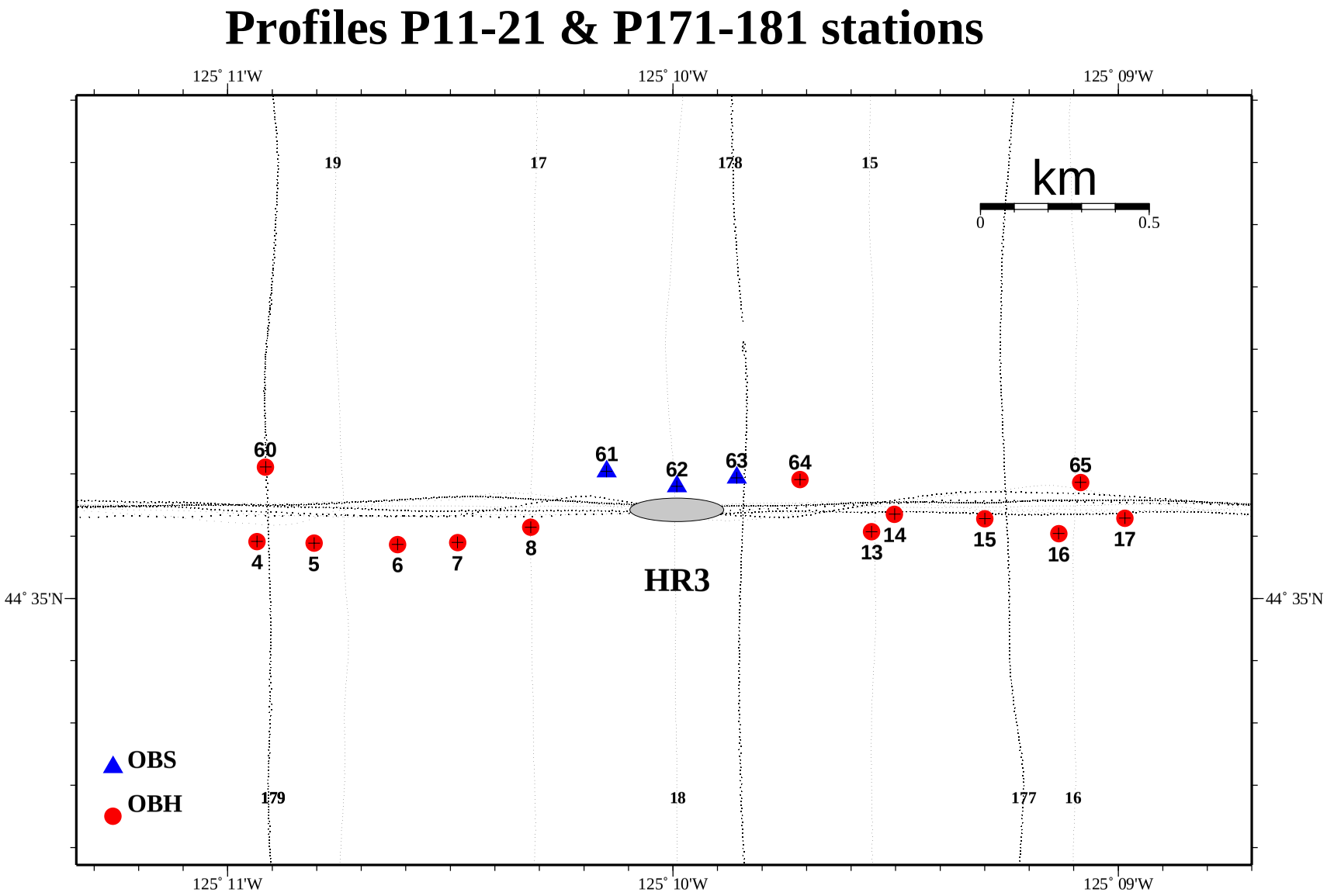

Figure 6.5.2: Location map of OBH/OBS stations for P11-21 & P171-181.

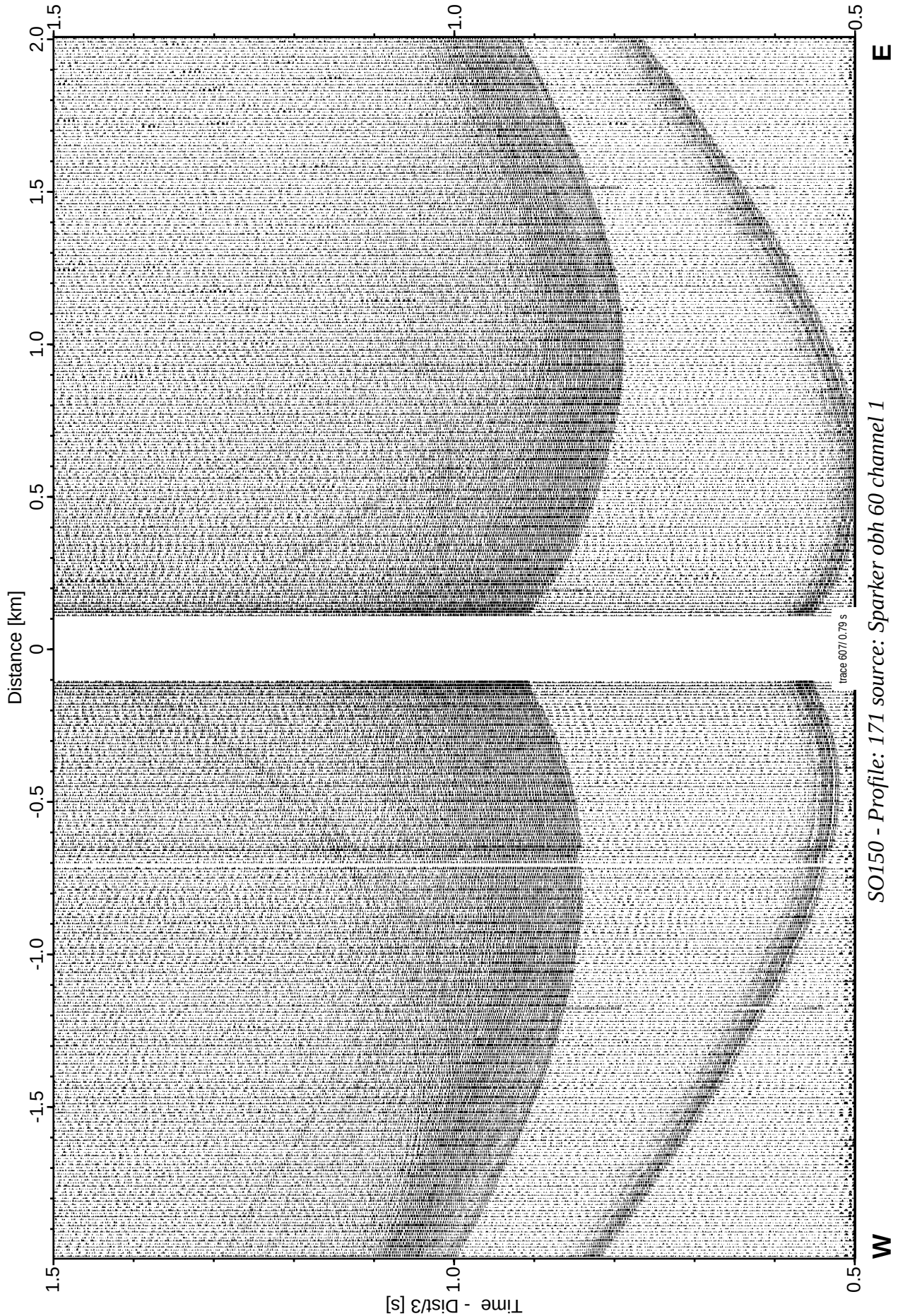

Figure 6.5.3: Record section from obh 60 , Profile 171.

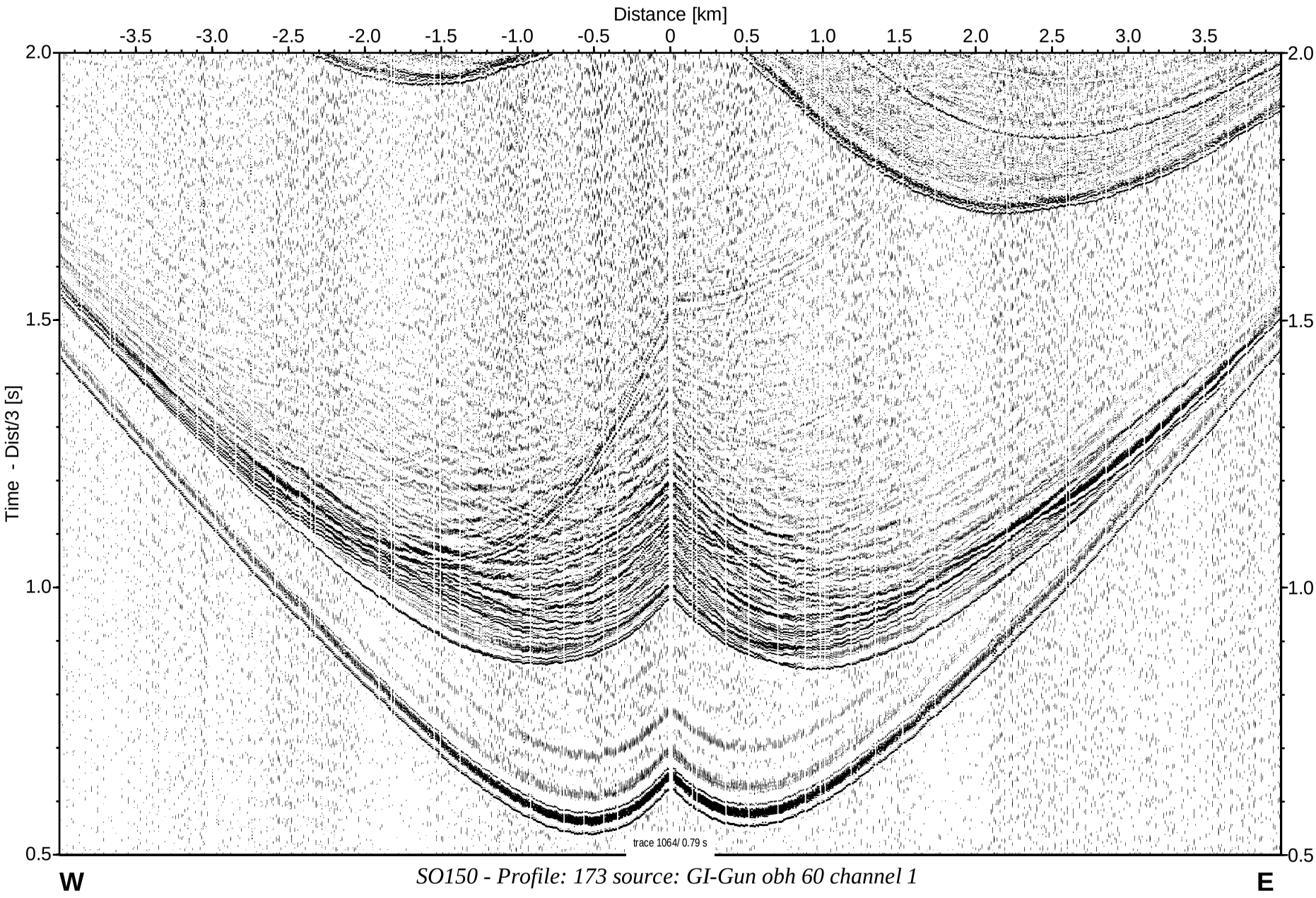

Figure 6.5.4: Record section from obh 60 , Profile 173.

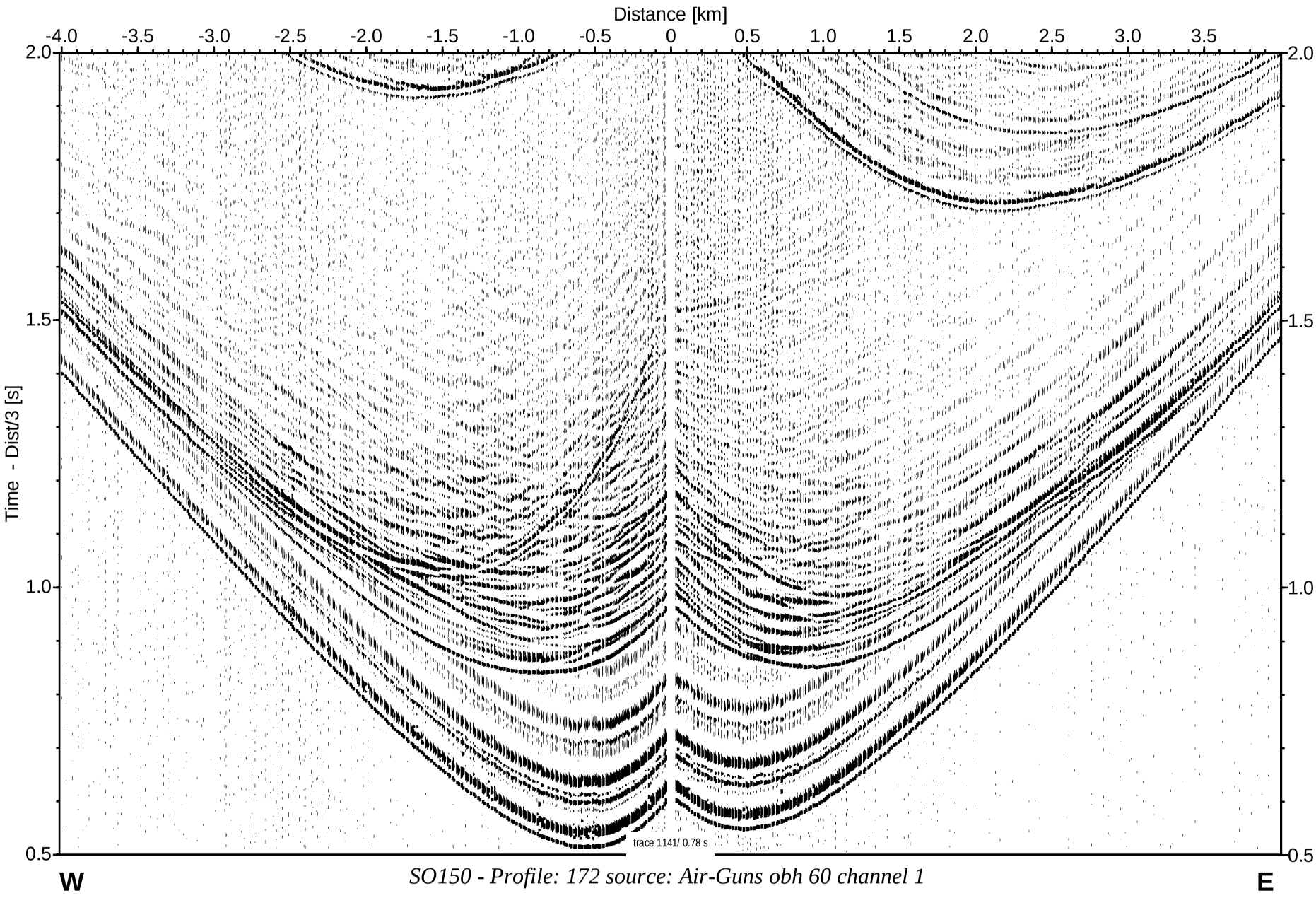

Figure 6.5.5: Record section from obh 60 , Profile 172.

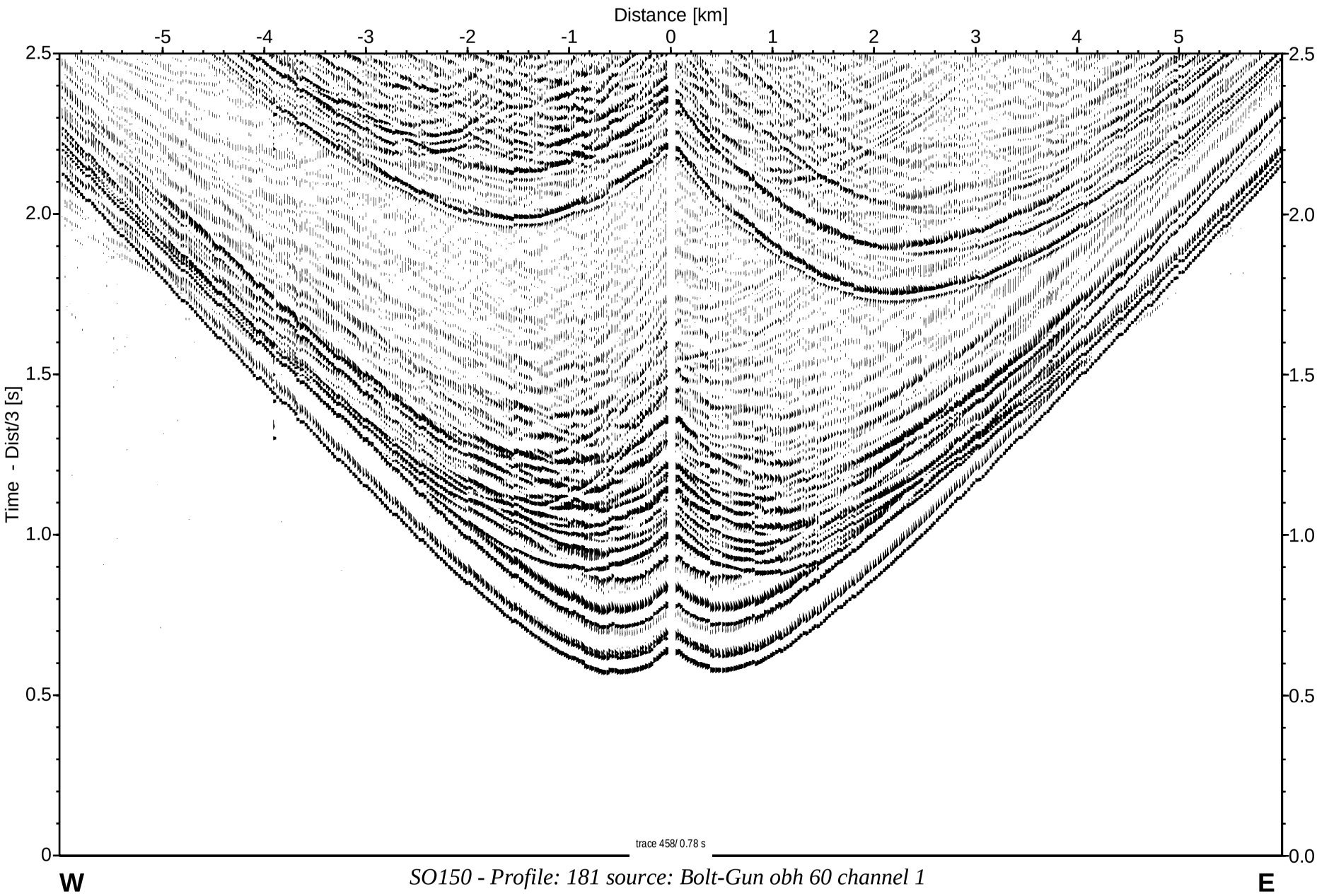

SO150 - Profile: 181 source: Bolt-Gun obh 60 channel 1

Figure 6.5.6: Record section from obh 60 , Profile 181.

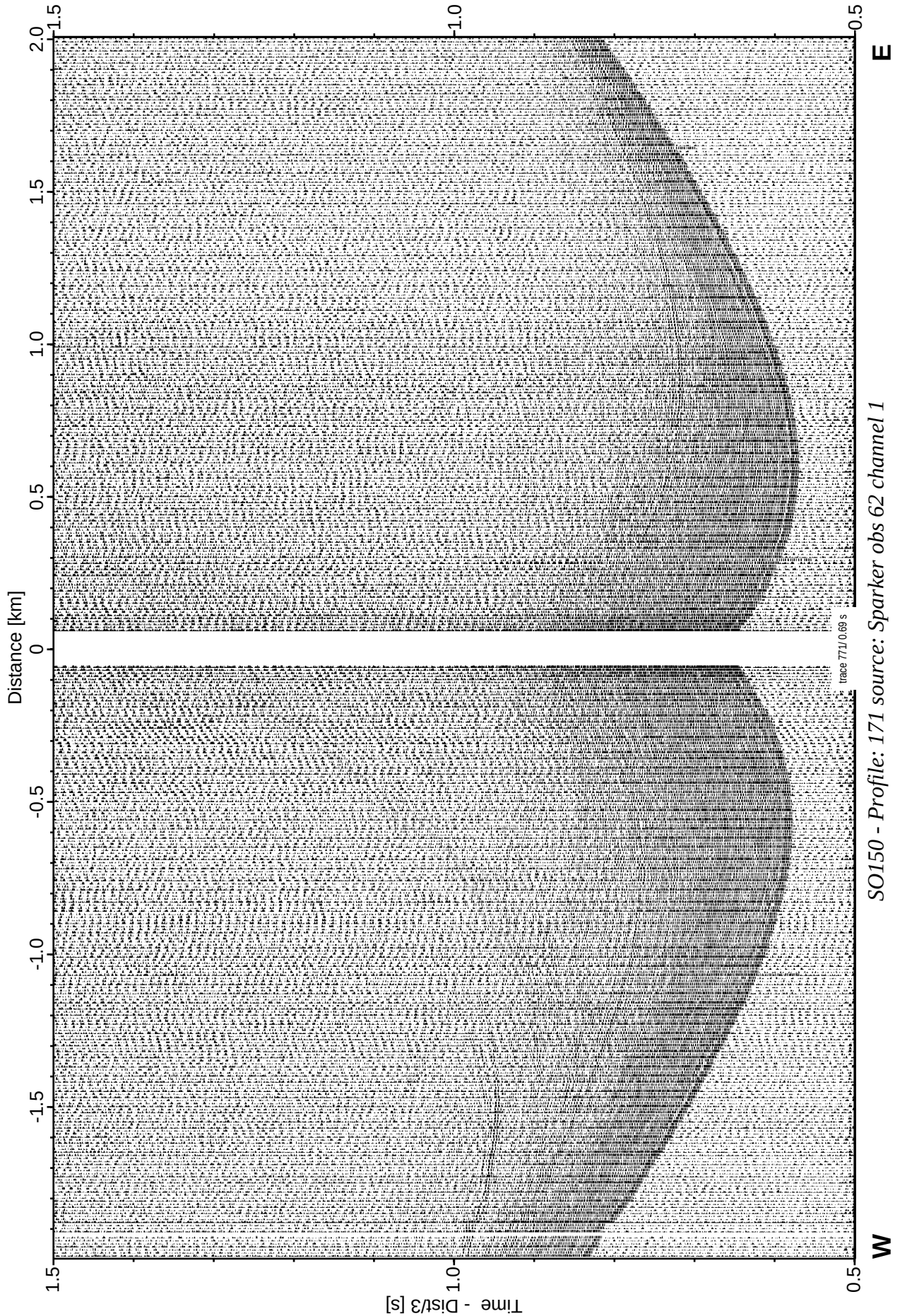

Figure 6.5.7: Record section from obs 62 hydrophone, Profile 171.

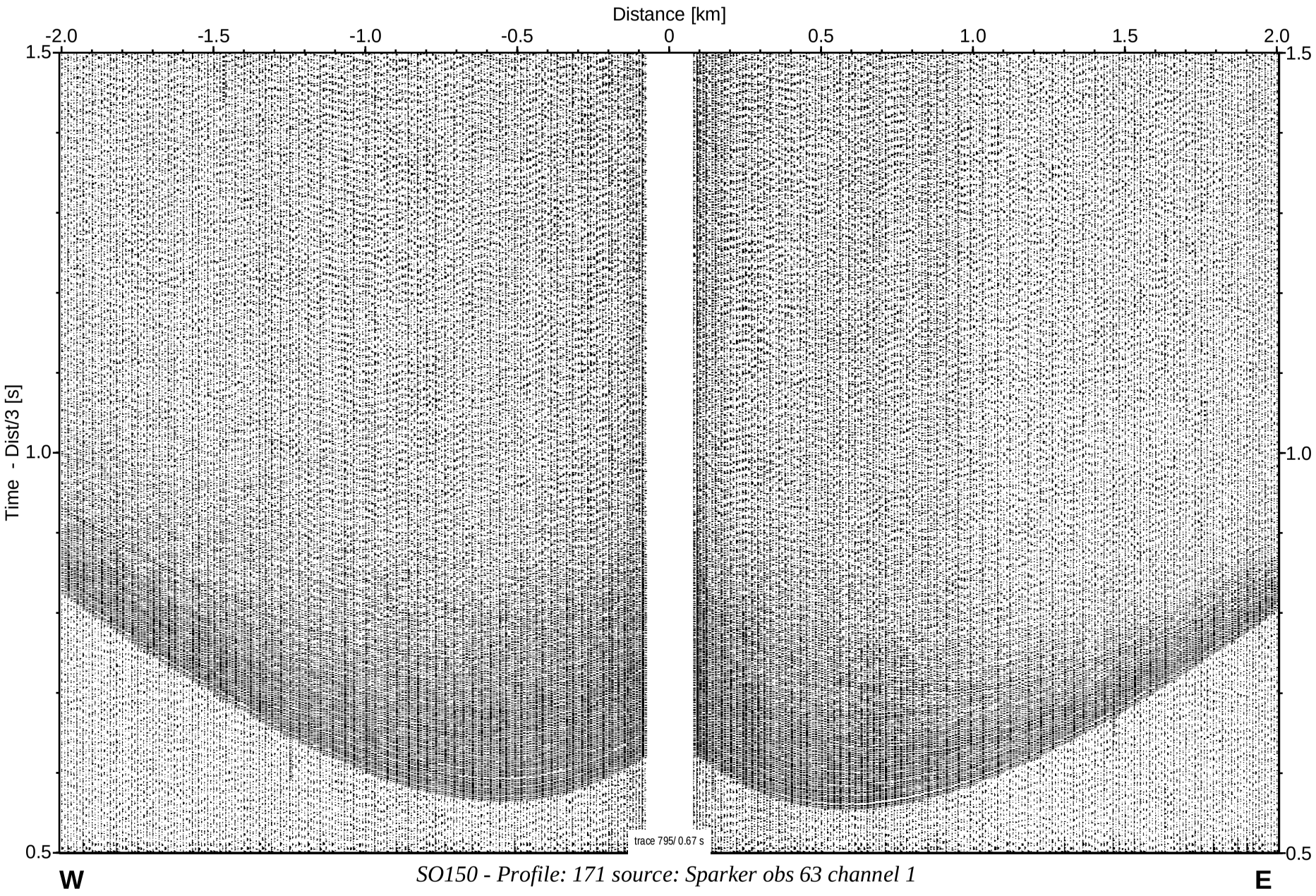

Figure 6.5.8: Record section from obs 63 hydrophone, Profile 171.

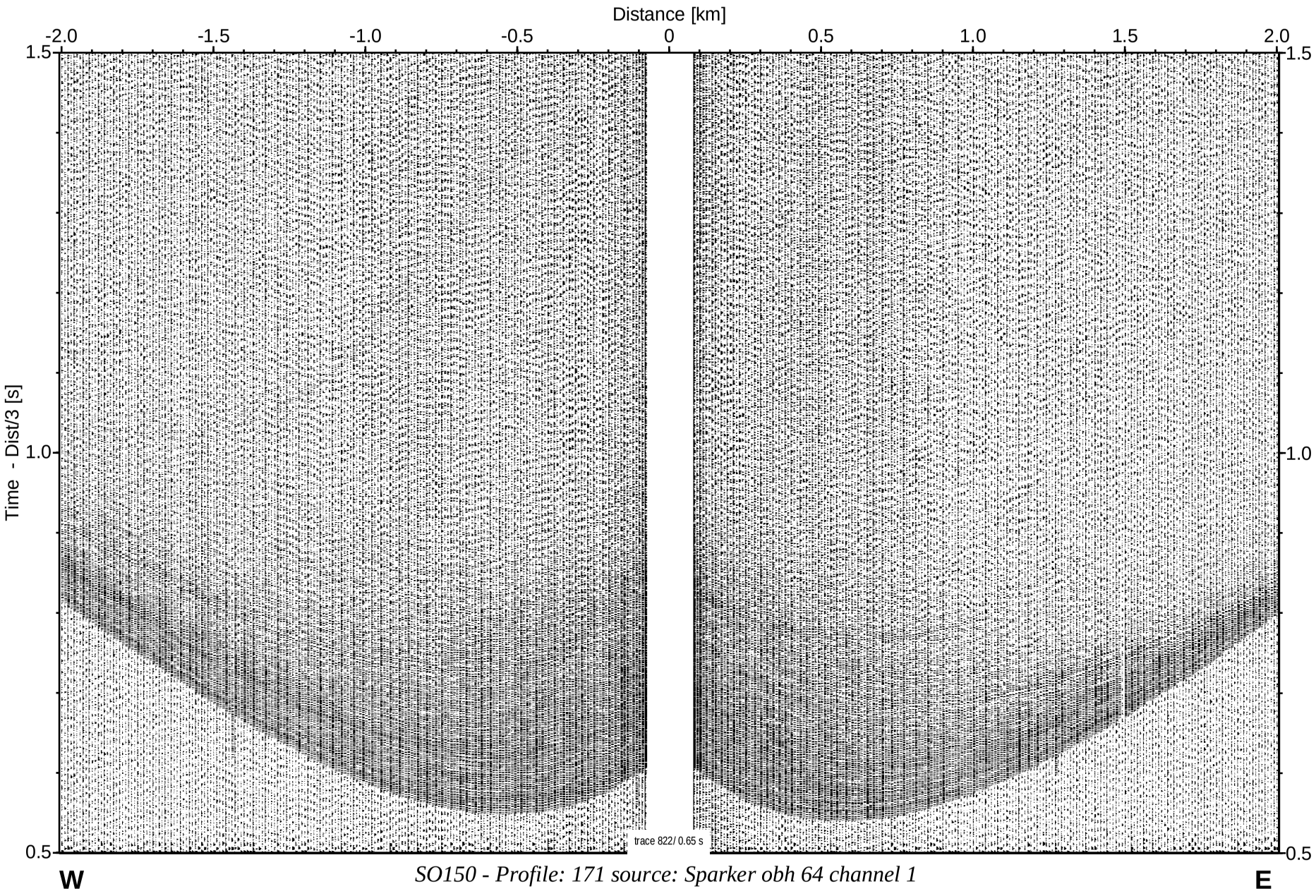

Figure 6.5.9: Record section from obh 64 , Profile 171.

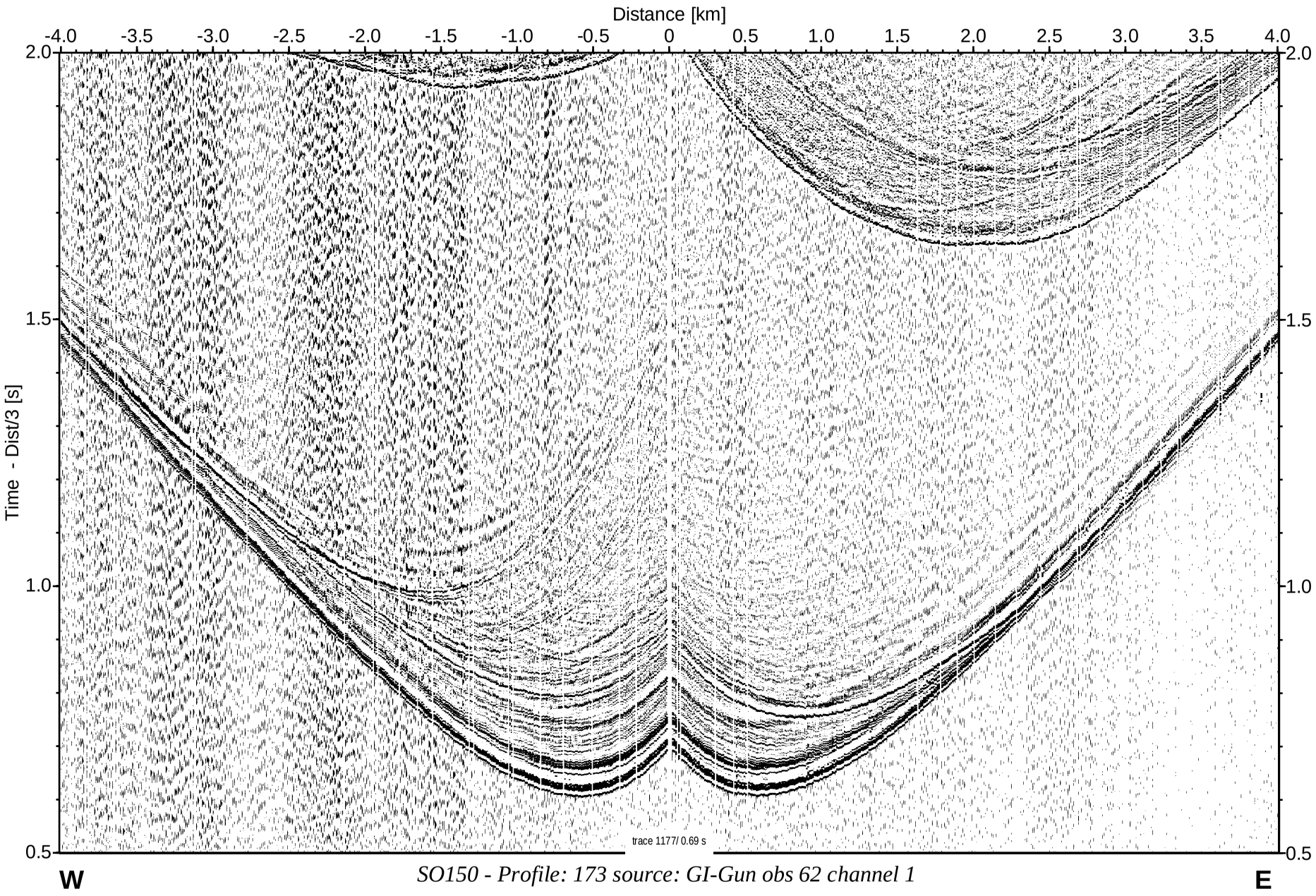

Figure 6.5.10: Record section from obs 62 hydrophone, Profile 173.

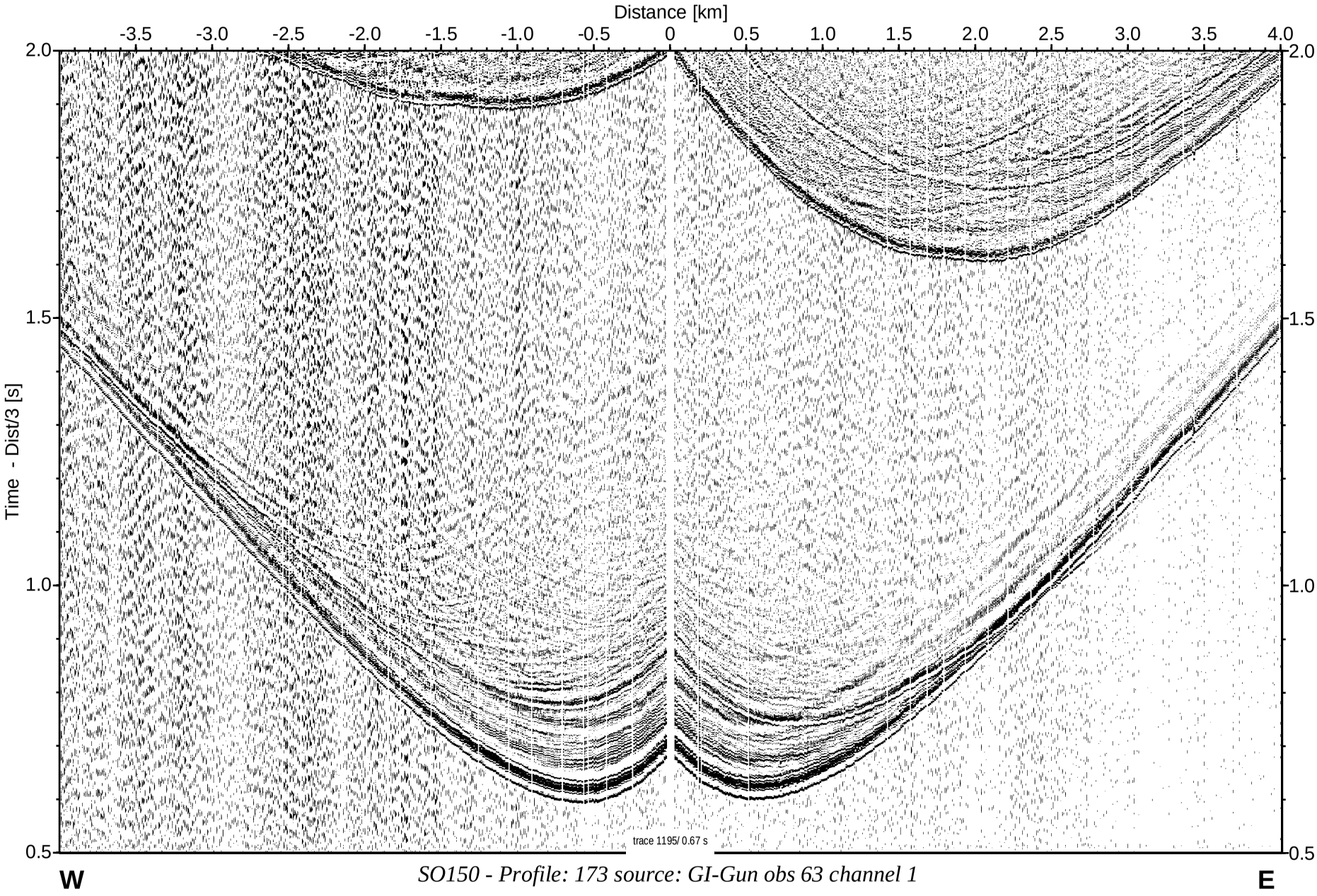

Figure 6.5.11: Record section from obs 63 hydrophone, Profile 173.

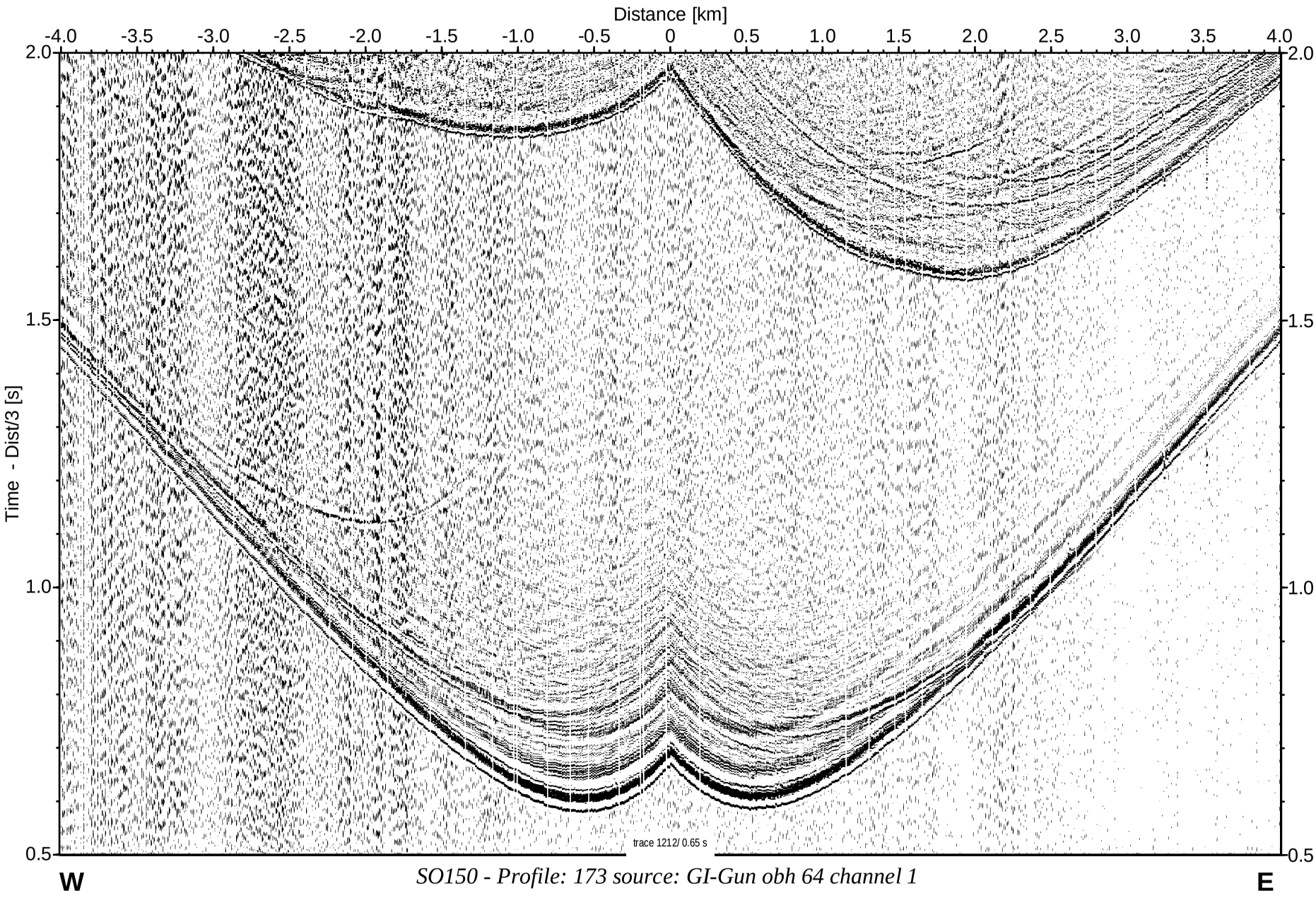

Figure 6.5.12: Record section from obh 64 , Profile 173.

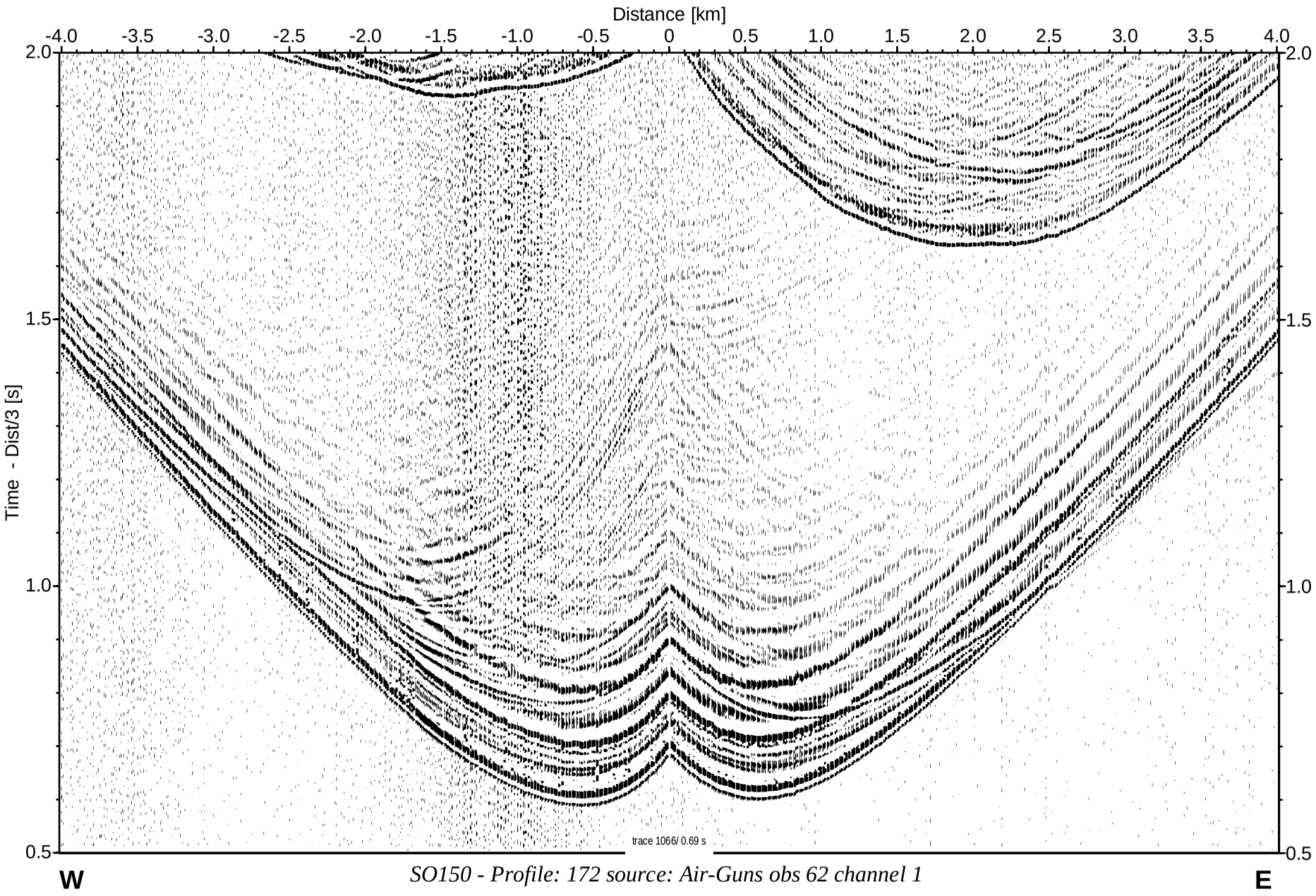

Figure 6.5.13: Record section from obs 62 hydrophone, Profile 172.

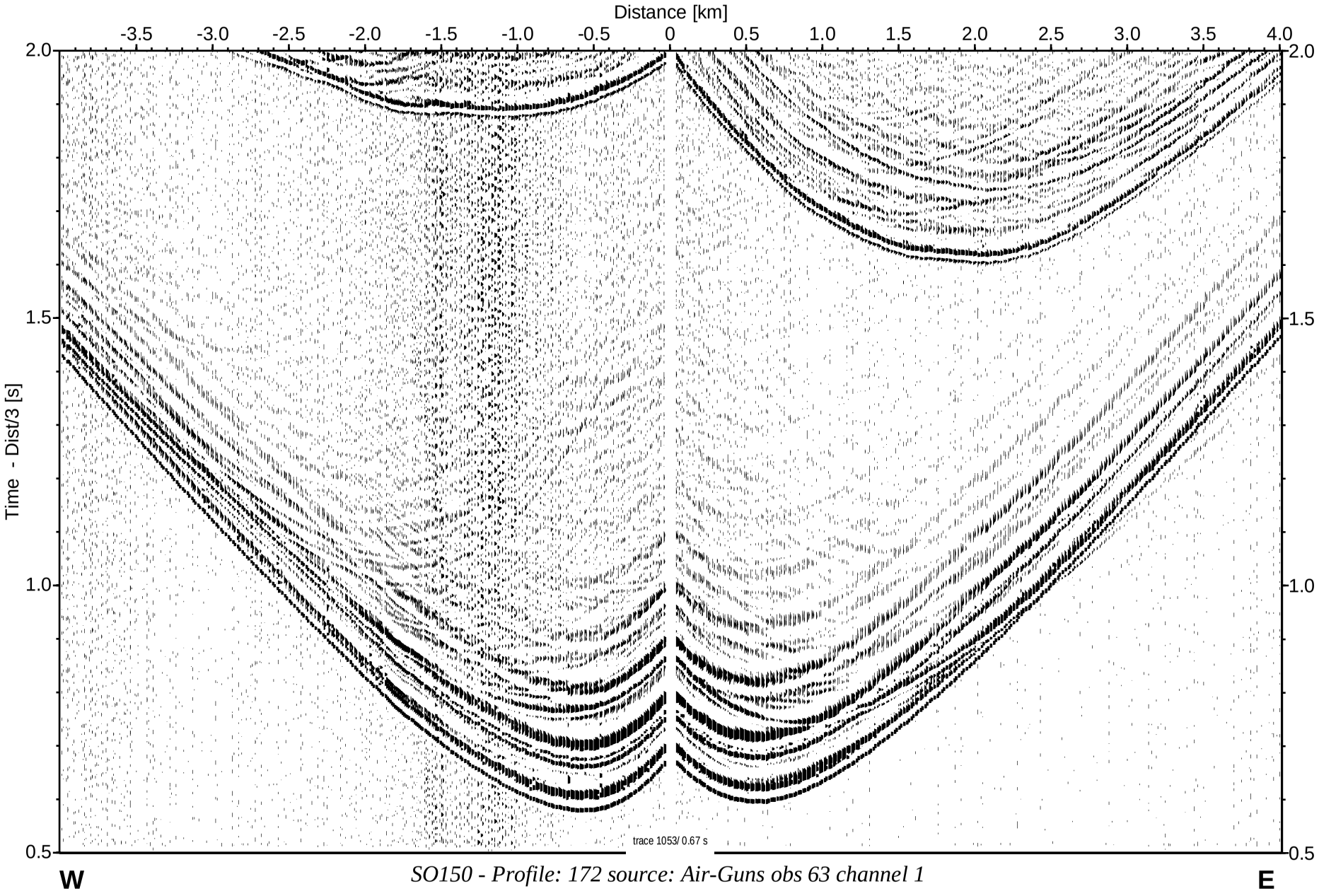

Figure 6.5.14: Record section from obs 63 hydrophone, Profile 172.

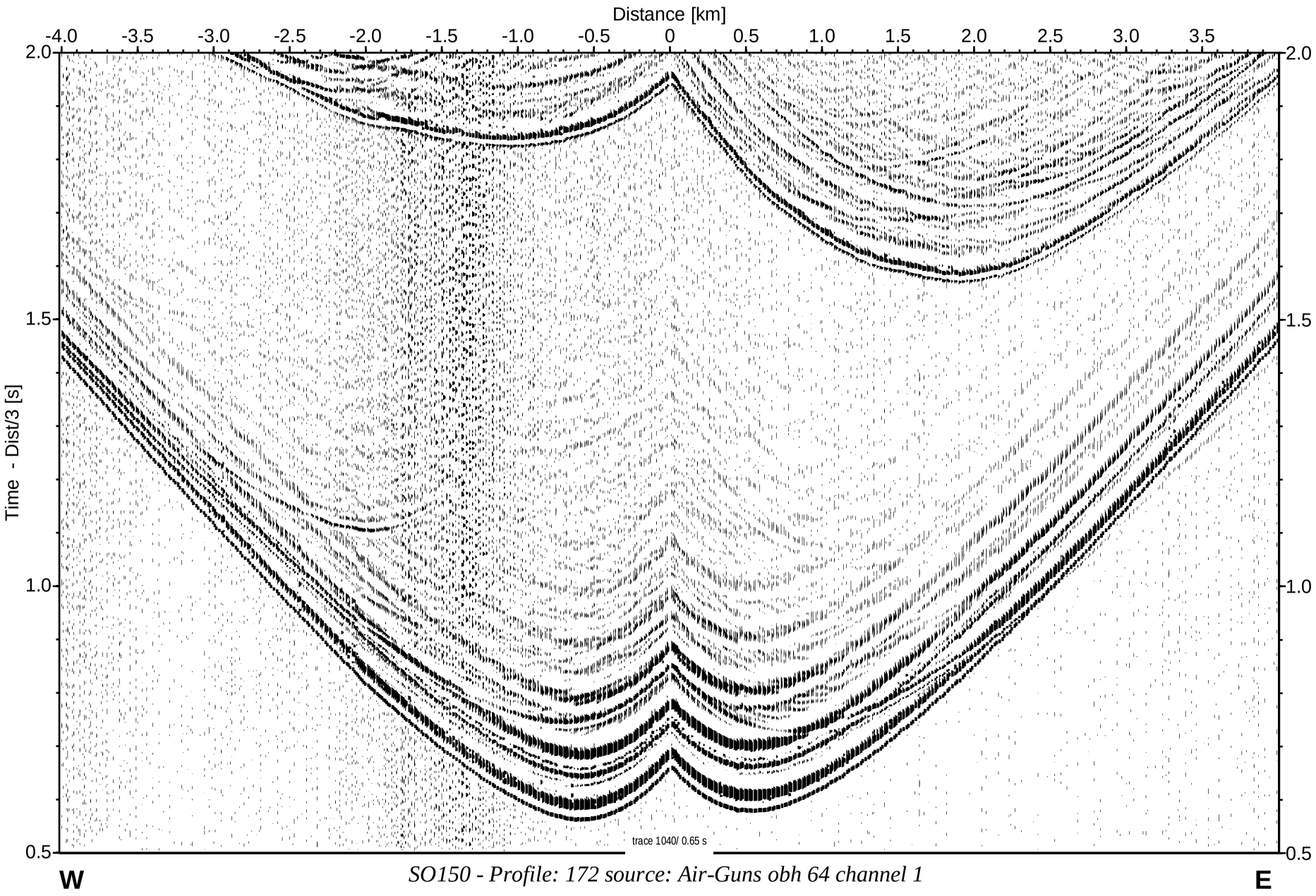

Figure 6.5.15: Record section from obh 64 , Profile 172.

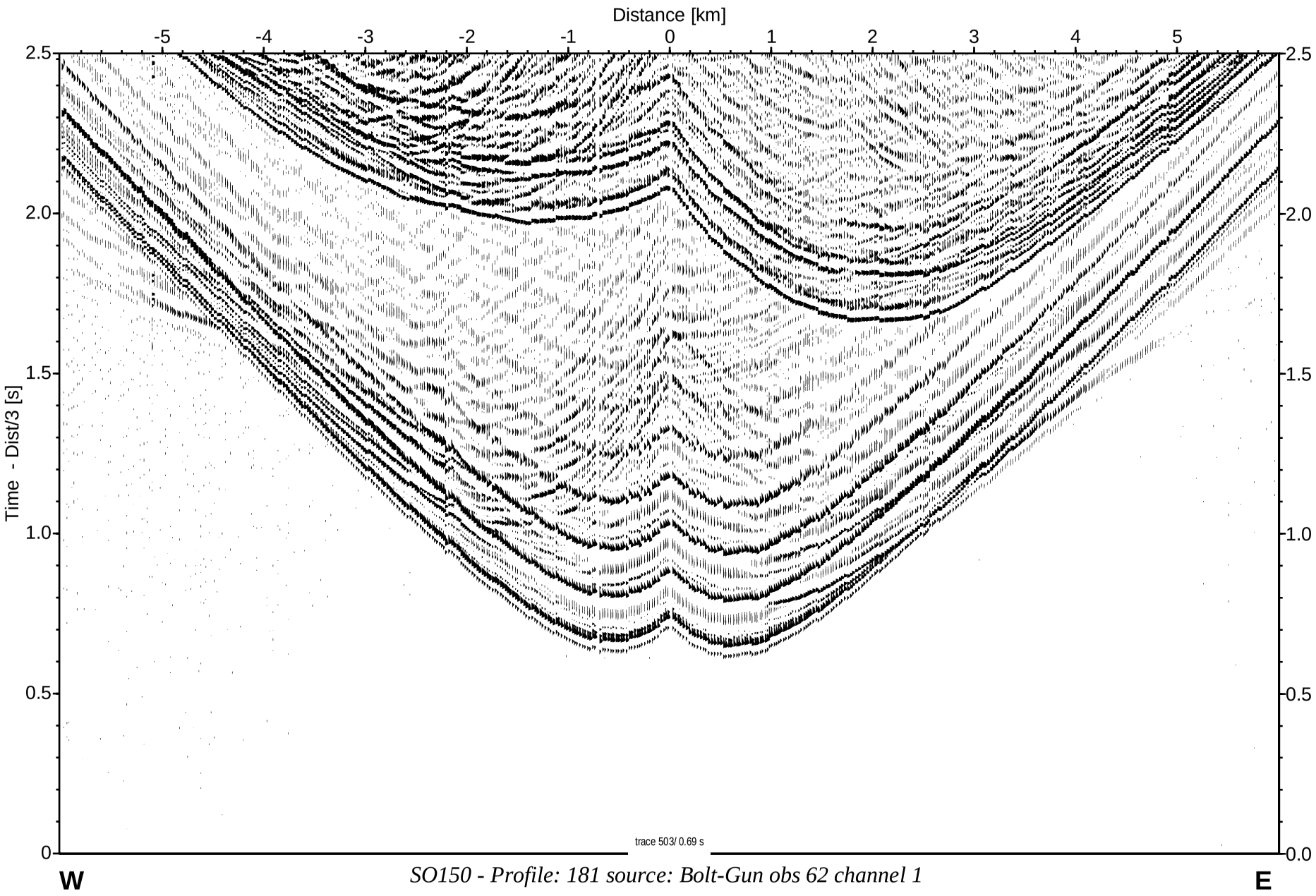

Figure 6.5.16: Record section from obs 62 hydrophone, Profile 181.

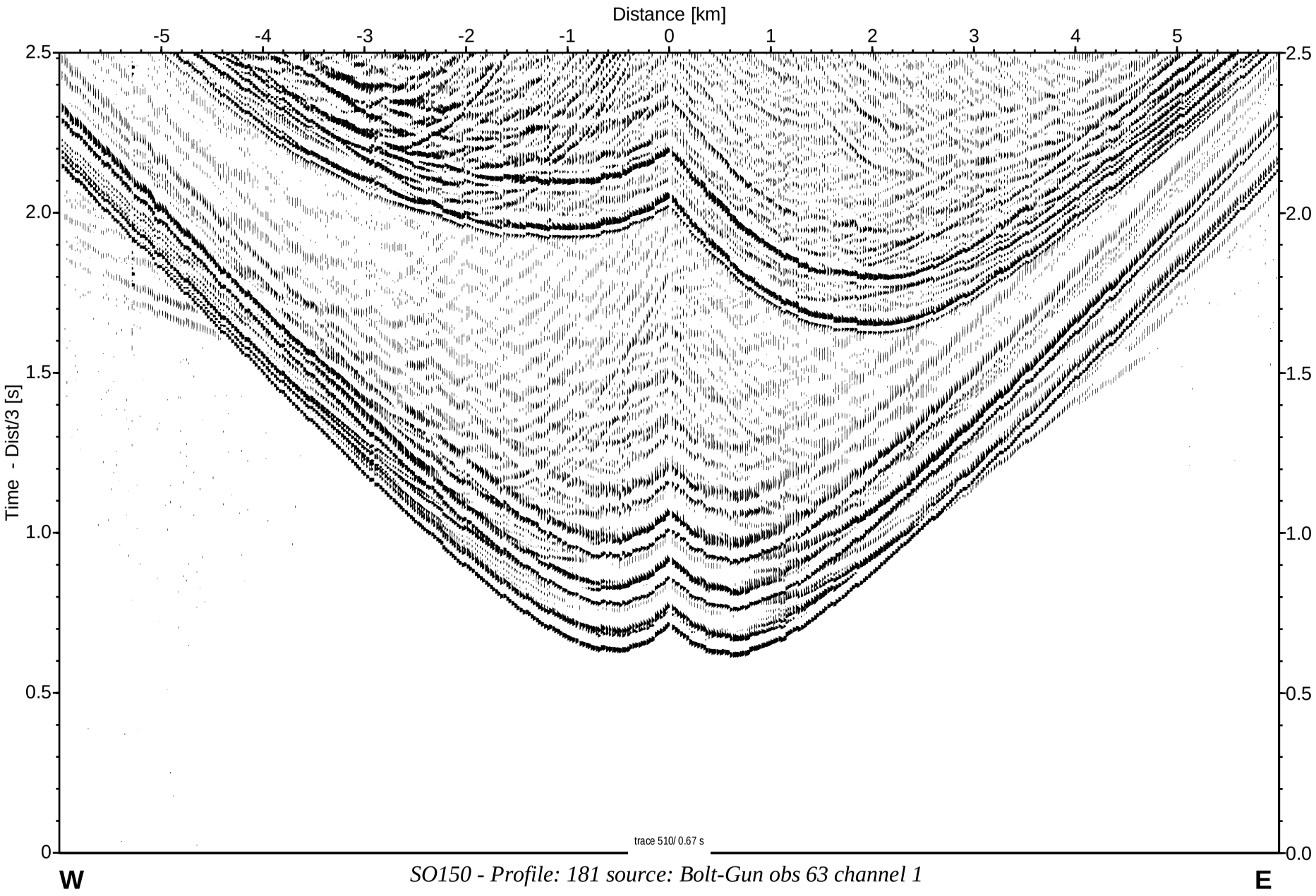

Figure 6.5.17: Record section from obs 63 hydrophone, Profile 181.

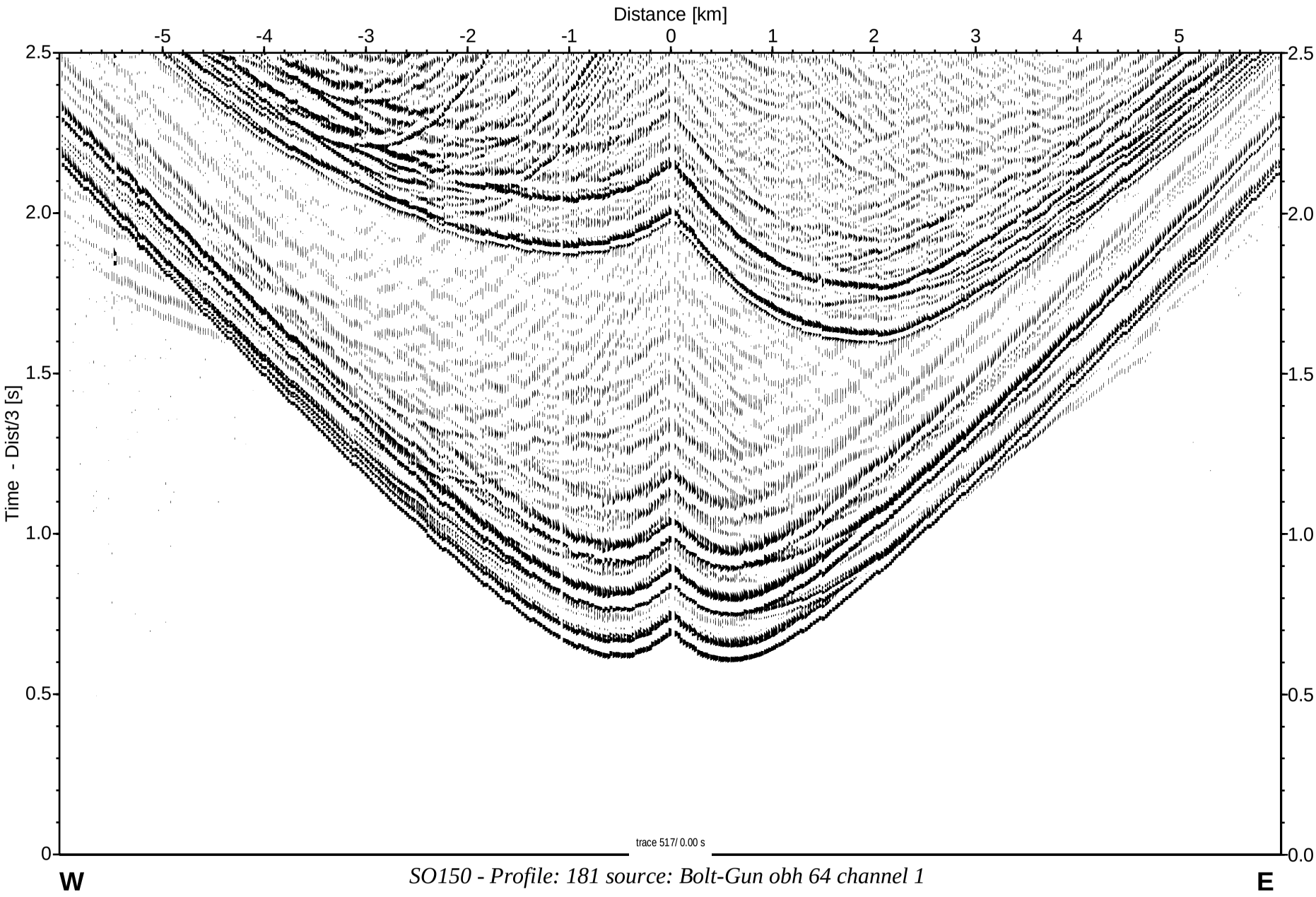

SO150 - Profile: 181 source: Bolt-Gun obh 64 channel 1

Figure 6.5.18: Record section from obh 64 , Profile 181.

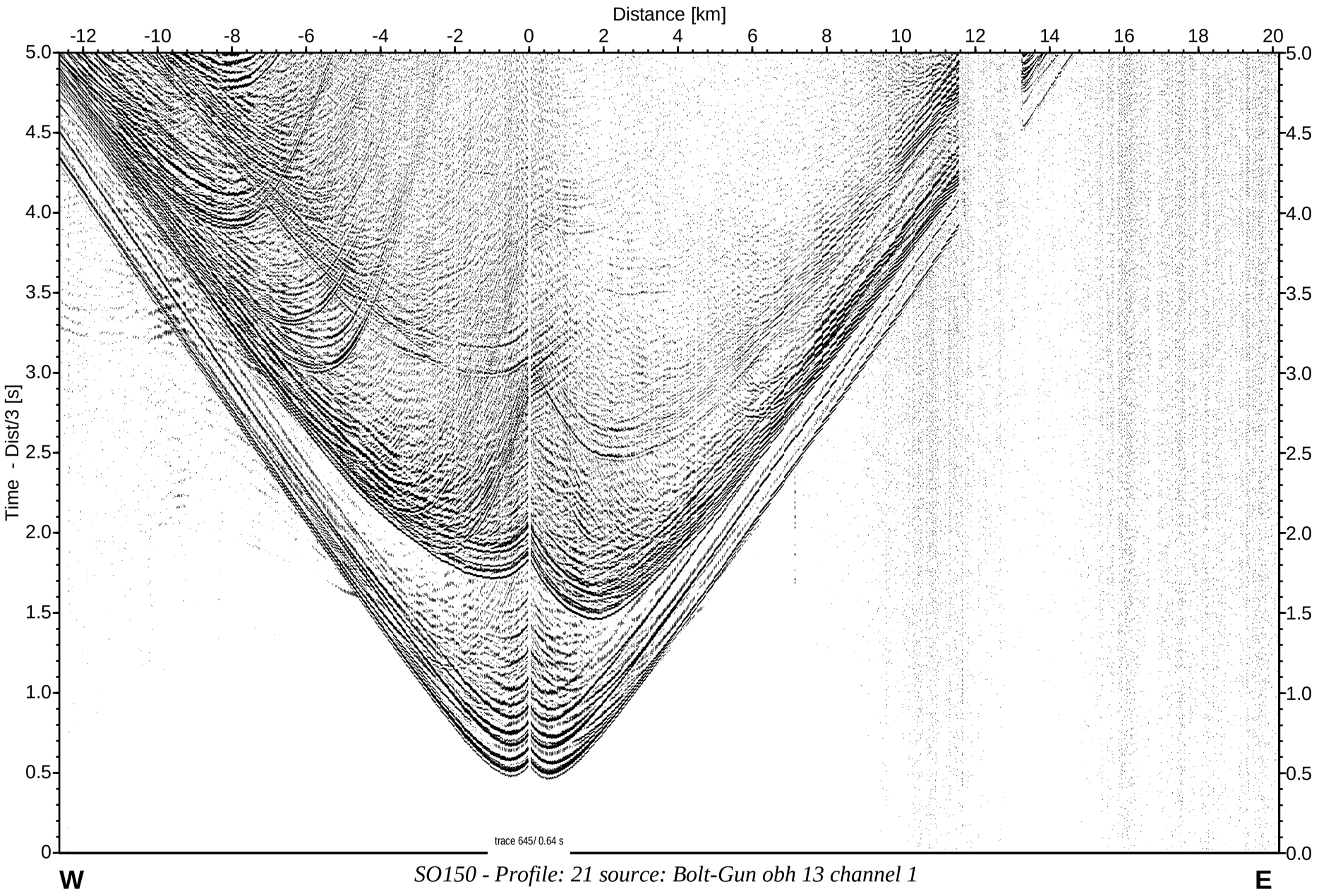

SO150 - Profile: 21 source: Bolt-Gun obh 13 channel 1

Figure 6.5.19: Record section from obh 13 , Profile 21.

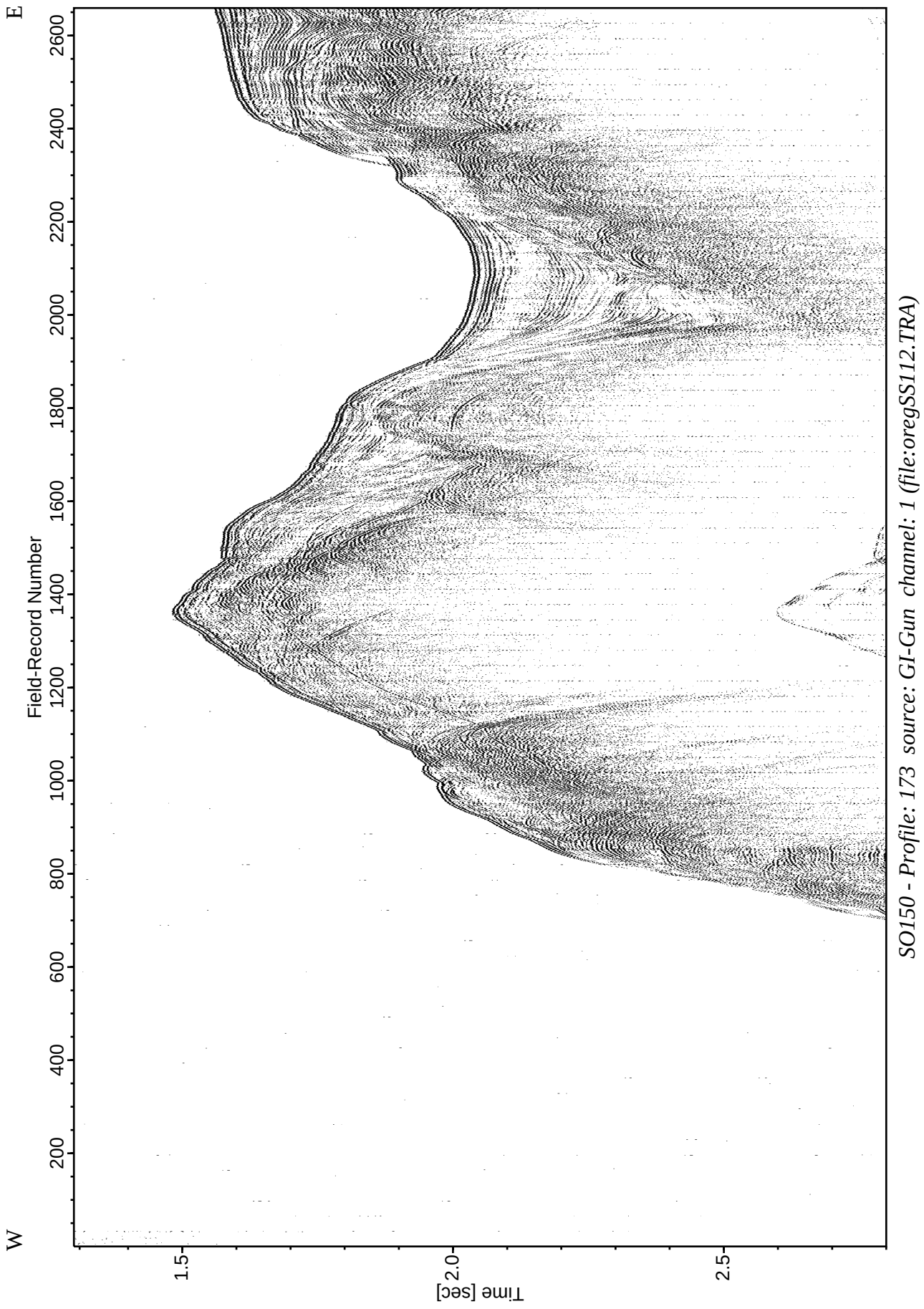

Figure 6.5.20: Record section with source GI-Gun, Profile 173.

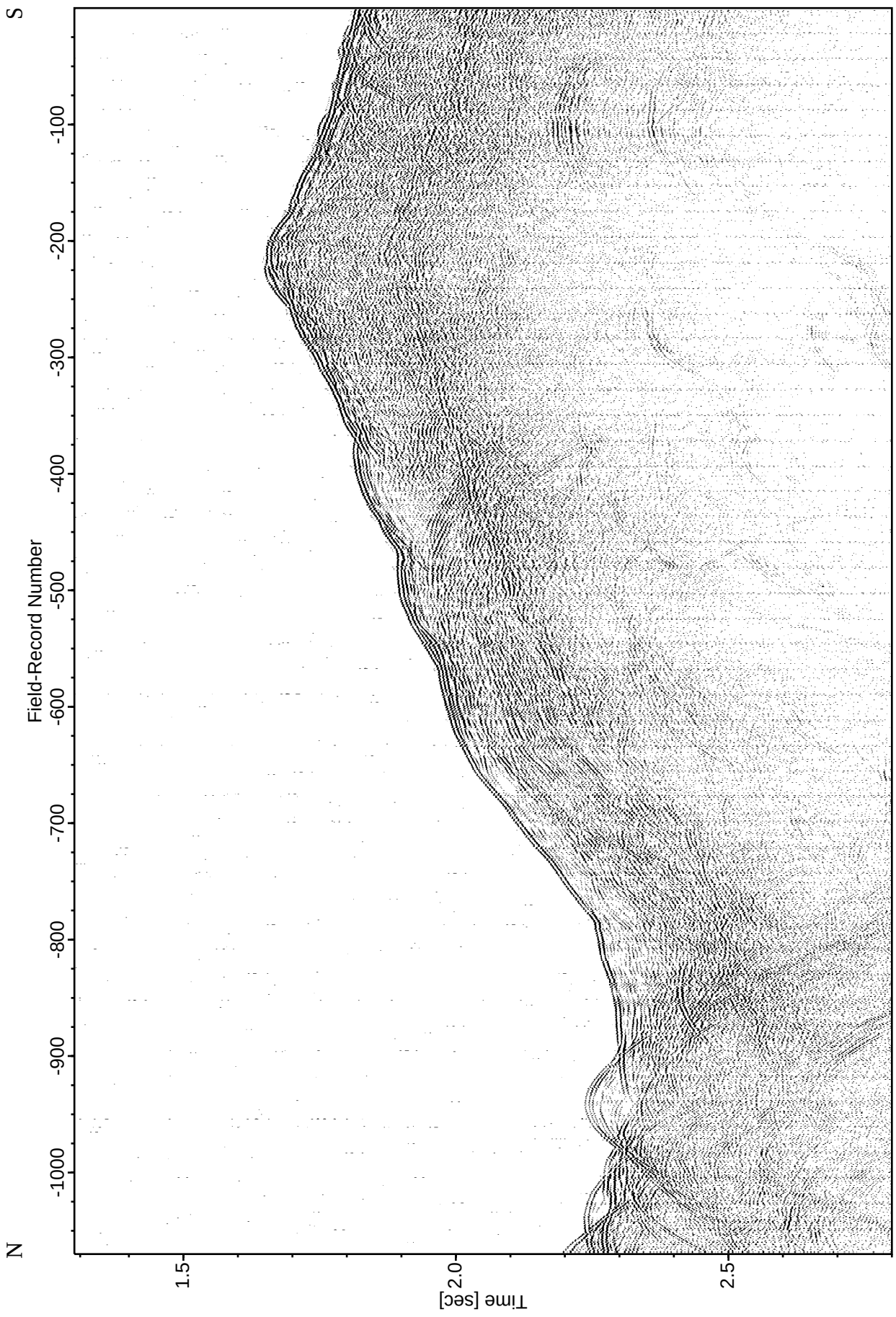

Figure 6.5.21: Record section with source GI-Gun, Profile 179.

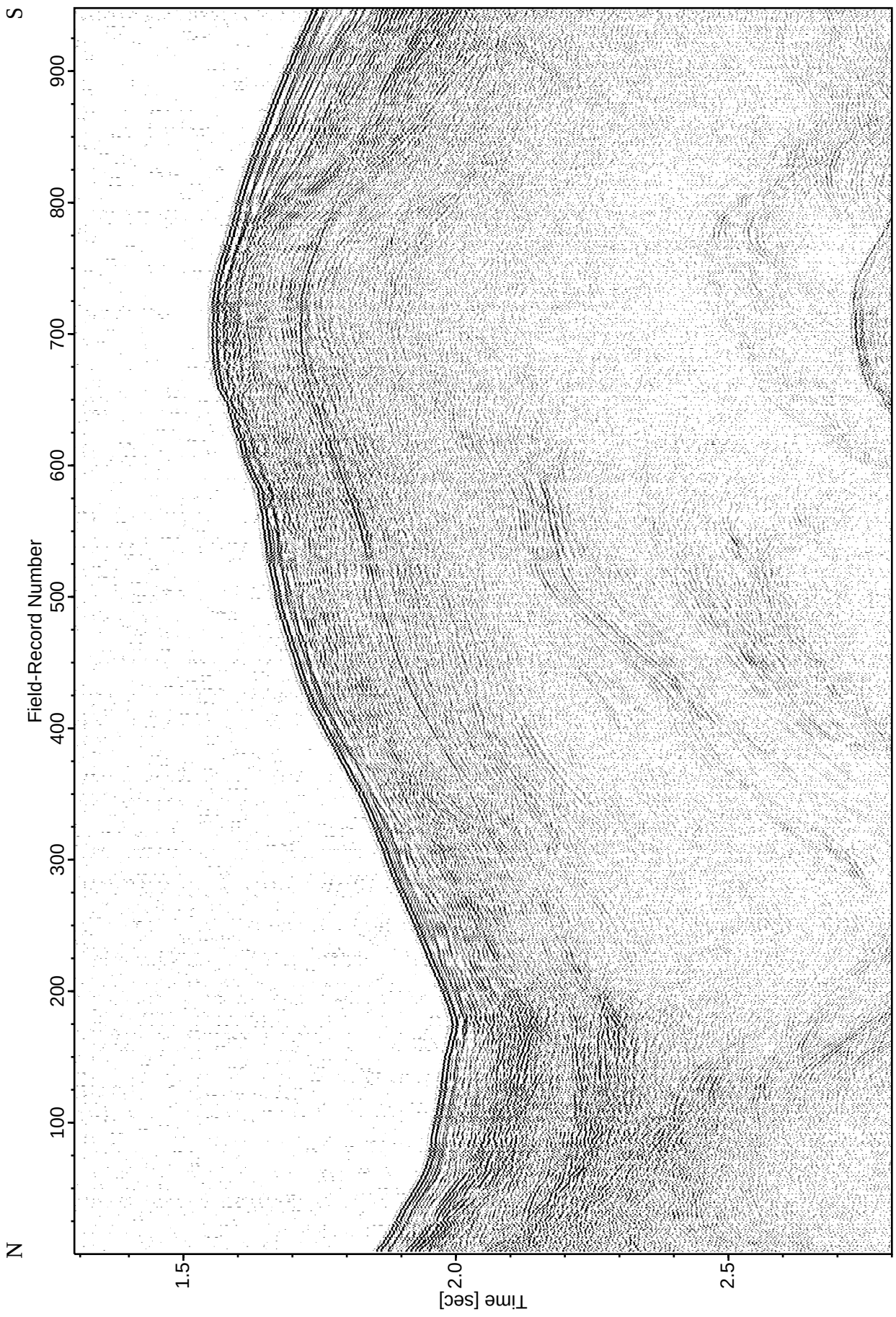

Figure 6.5.22: Record section with source GI-Gun, Profile 178.

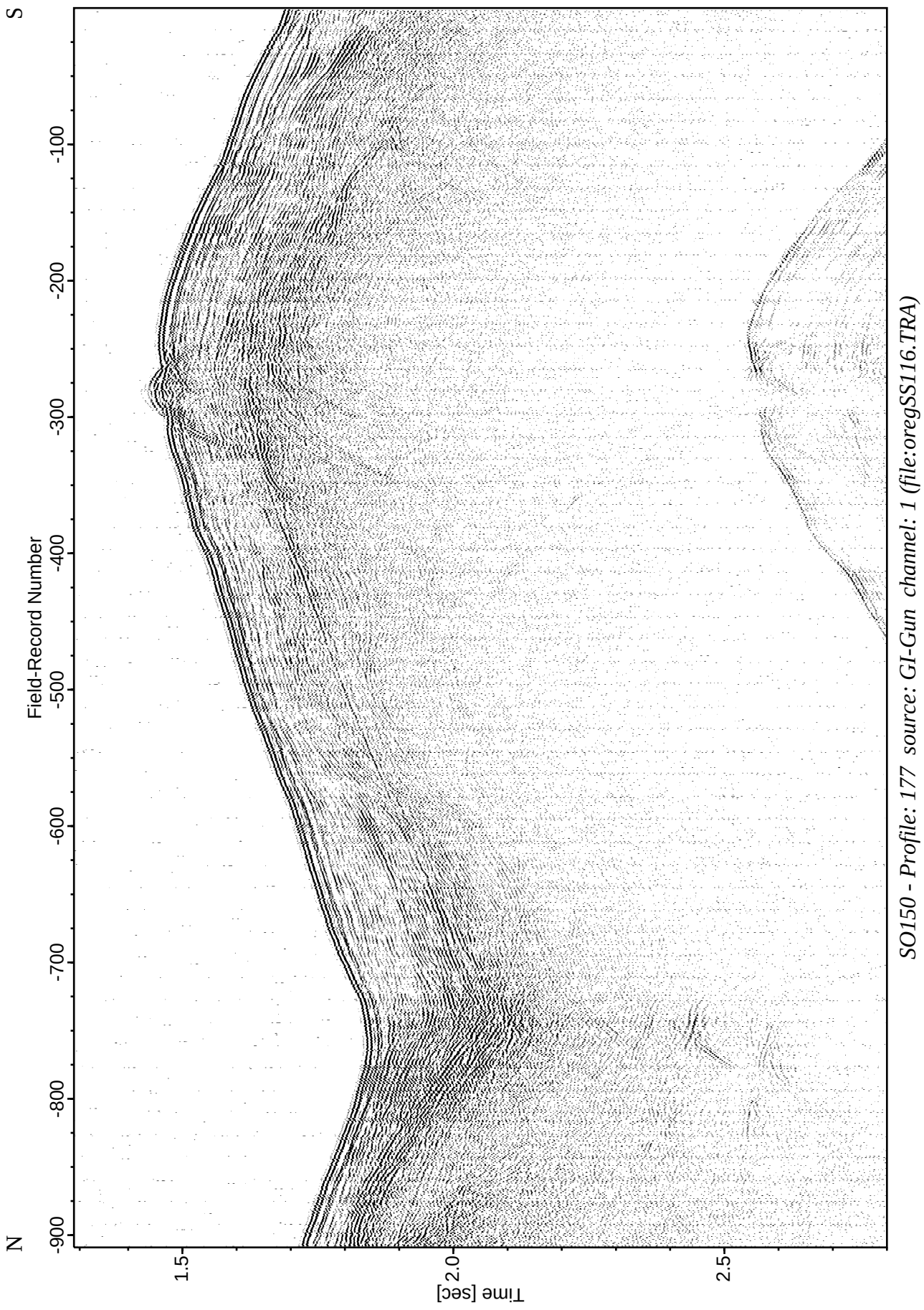

Figure 6.5.23: Record section with source GI-Gun, Profile 177.

6.6 EXPERIMENT ODP Leg 204, LOCATION HR1

(D. Klaeschen, D. Könitz, P. Liersch, J. Petersen, G. Klein)

The proposed drillsite HR1 is located on the landward flank of the second accreted ridge, i.e. the southern summit of the Hydrate Ridge. For the broader area of the experiment, which is located adjacent to Site HR3, see Figure 6.5.1. The first deployment of OBHs and OBSs took place from 27-SEP to 29-SEP. The second deployment, with only 2 cross lines covering the HR1-area, was shot from 08.-10. of October (together with the additions to the HR3 experiment, previous chapter). The main WE-profile is again located at a latitude of 44°35.15 N. It cross-cuts the southern summit of Hydrate Ridge in an EW-direction (Figs. 6.5.1 and 6.6.1). During the first deployment, a total of 4 OBSs and 10 OBHs were aligned in a WE-direction with a desired spacing of 200 m between each device on the seafloor. However, drift of the stations due to currents in the water column caused an irregular spacing, which is shown in Figure 6.6.2. First, a 10 km long WE-line was shot with the watergun, followed by a 20 km long line with the airgun array in the opposite direction. After the next tag, the 20 km line was shot once more with the GI-gun before continuing with five 9-km long NS-crossing lines at a 200 m spacing across the central seafloor stations (Figs. 6.6.1. and 6.6.2). All cross lines were shot with the GI-gun and the surface streamer, while for the longer EW-profiles, the mini streamer was used as a second receiver. After completion of the NS-grid, the 32l Bolt gun was shot as low a frequency source on a 32 km long EW-profile, before the experiment ended and the stations were recovered. Unfortunately, one OBH (station 20) did not work at all, and all 4 OBSs (stations 21, 22, 26, and 27) had no data on their hydrophones. A lower data quality was observed at stations 23 and 30, while the DPGs (stations 18, 19) provided particularly good results.

Because the data from the first deployment showed severe gaps in the profile, such that during the above mentioned acquisition from 08-OCT to 10-OCT, 5 more stations were lowered in the HR1 vicinity (Fig. 6.6.2). With this second deployment covering both the HR1 and HR3 areas, the EW-profiles were shot with the Sparker (15 km length, as compared to 10 km during first deployment), GI-gun, and airgun array (29 km instead of 20 km previously). The length of another 2 NS-profiles was kept to 9 km, and was acquired with the GI-gun. The second deployment was completed with a now (slightly reduced) 29 km long EW-profile across the OBH/OBS assembly with the Bolt gun. After recovery of the equipment and retrieval of the data, it was found that all stations worked comme il faut, so that the resolution off seismic information in the HR1 region was considerably improved.

Various data examples of OBH, OBS and streamer data for different sources are displayed in Fig. 6.6.3 to Fig. 6.6.26.

Profiles P61-71 & P171-181 seismic lines

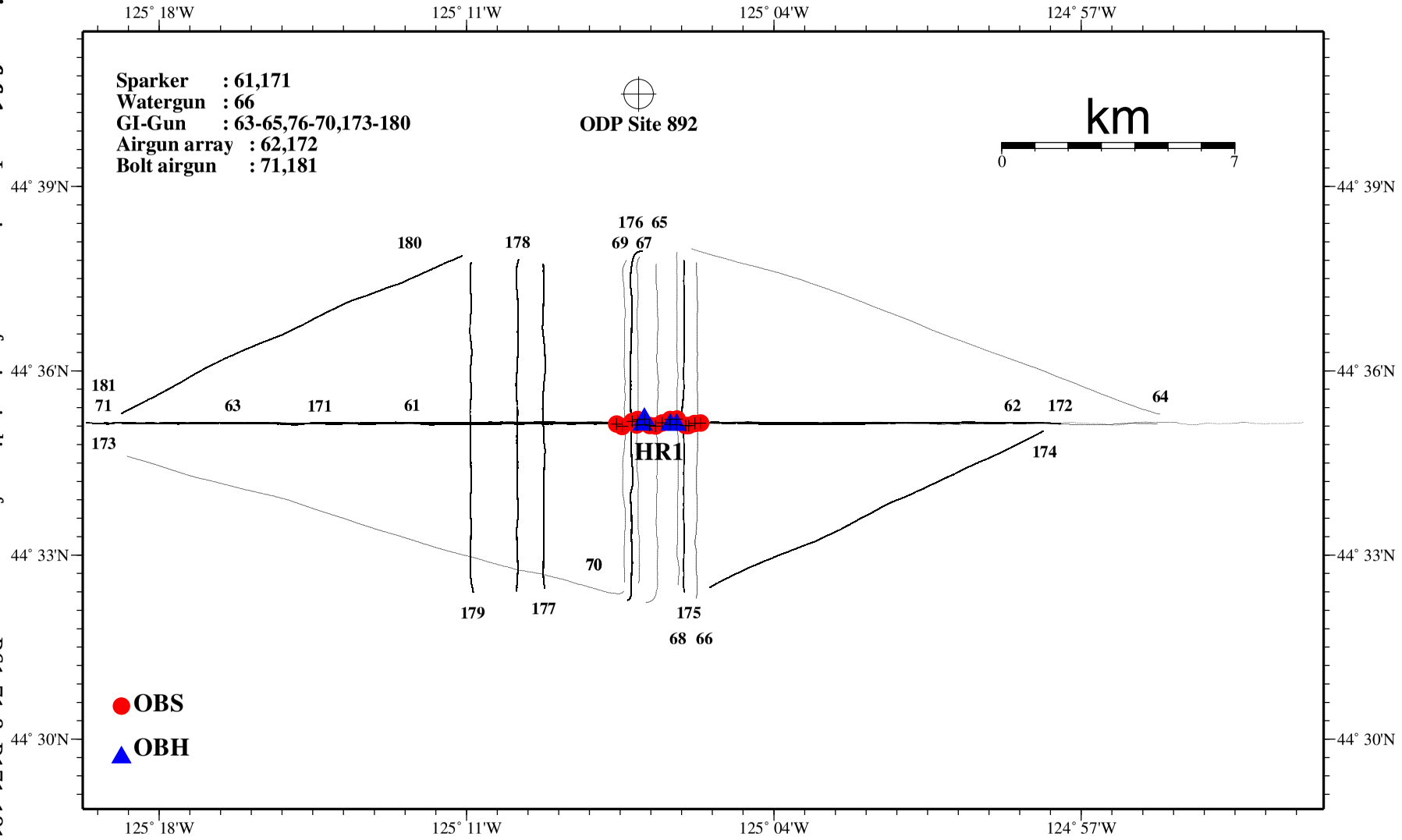

Figure 6.6.1: Location map of seismic line of survey run P61-71 & P171-181.

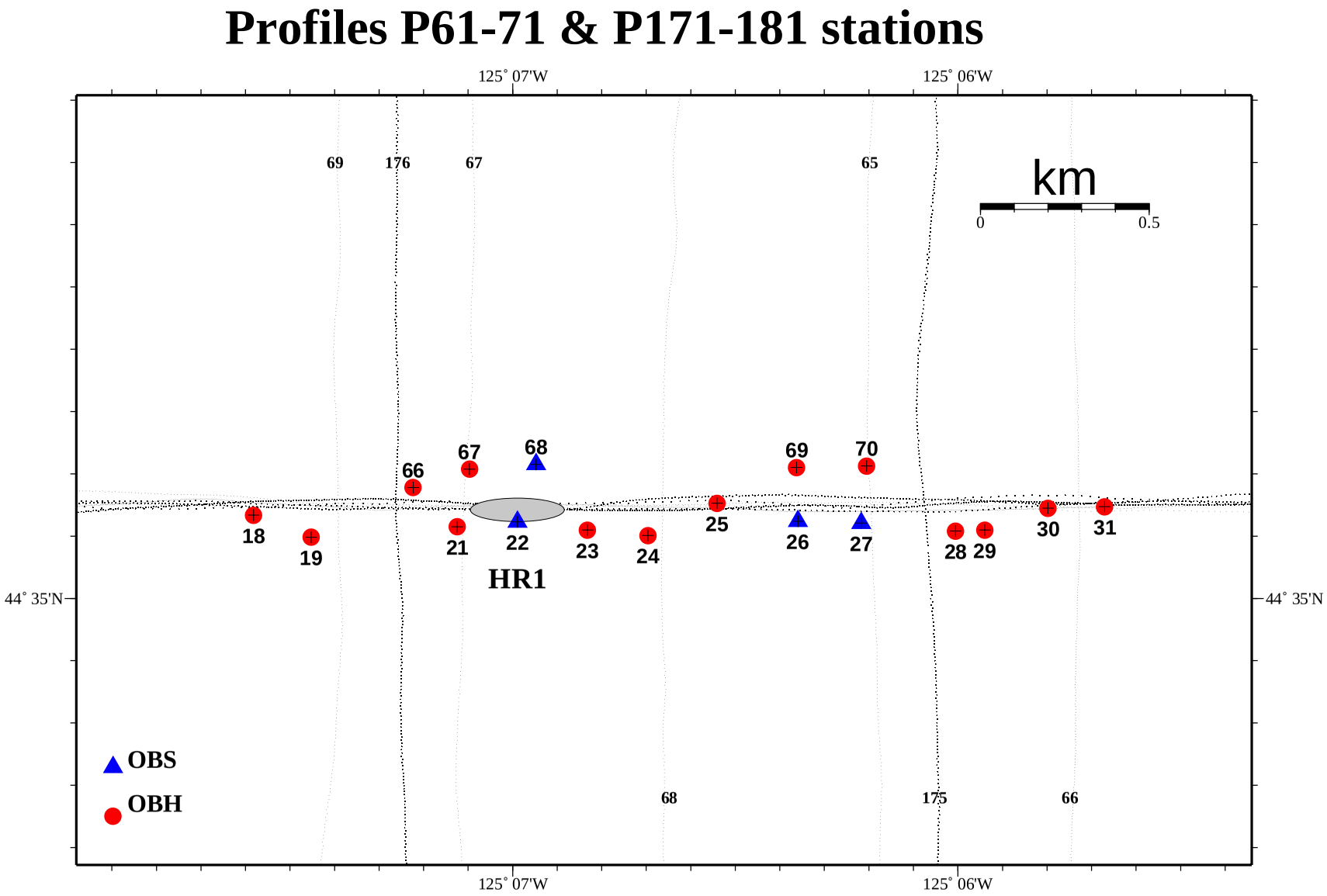

Figure 6.6.2: Location map of OBH/OBS stations for P61-71 & P171-181.

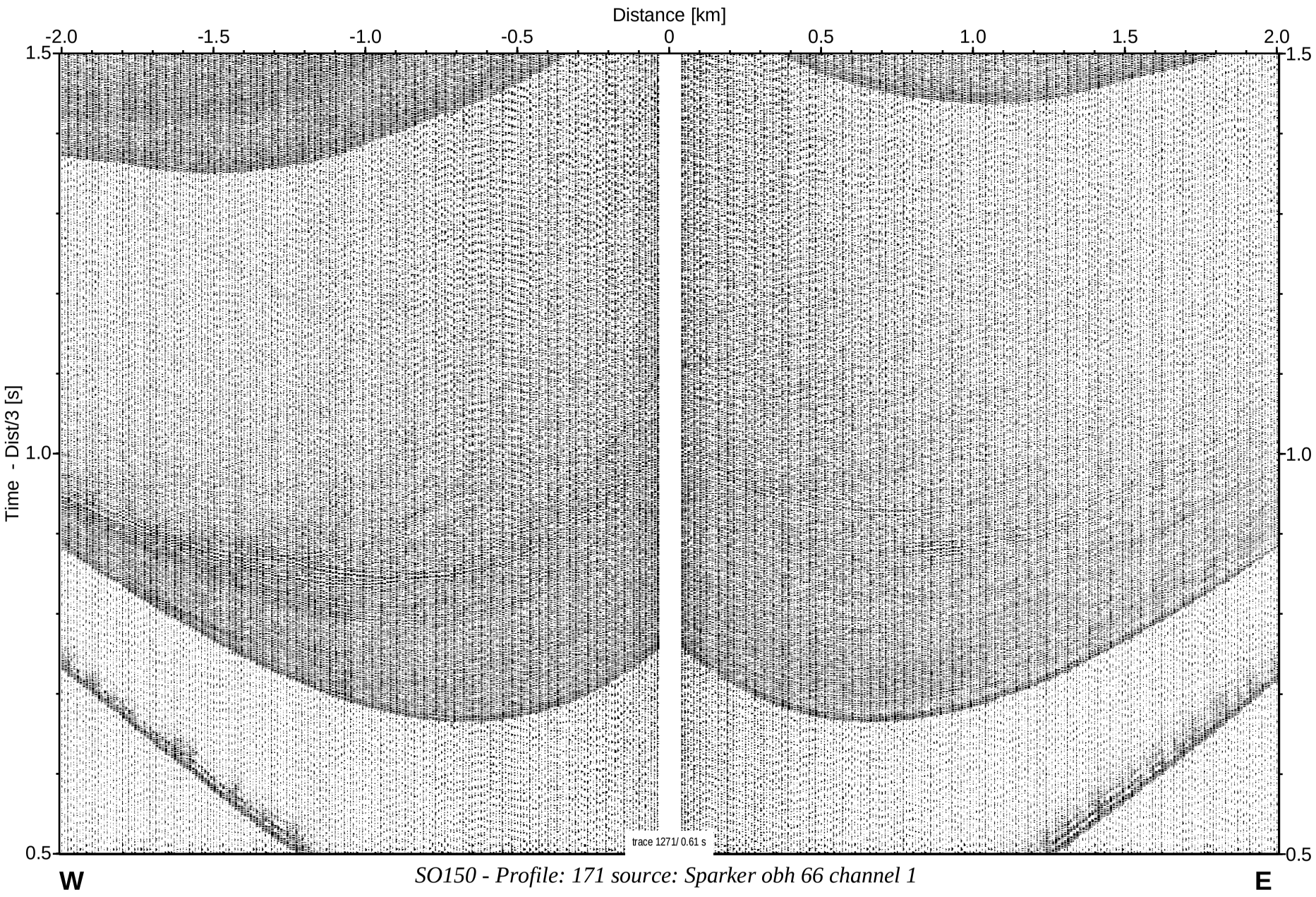

Figure 6.6.3: Record section from obh 66 , Profile 171.

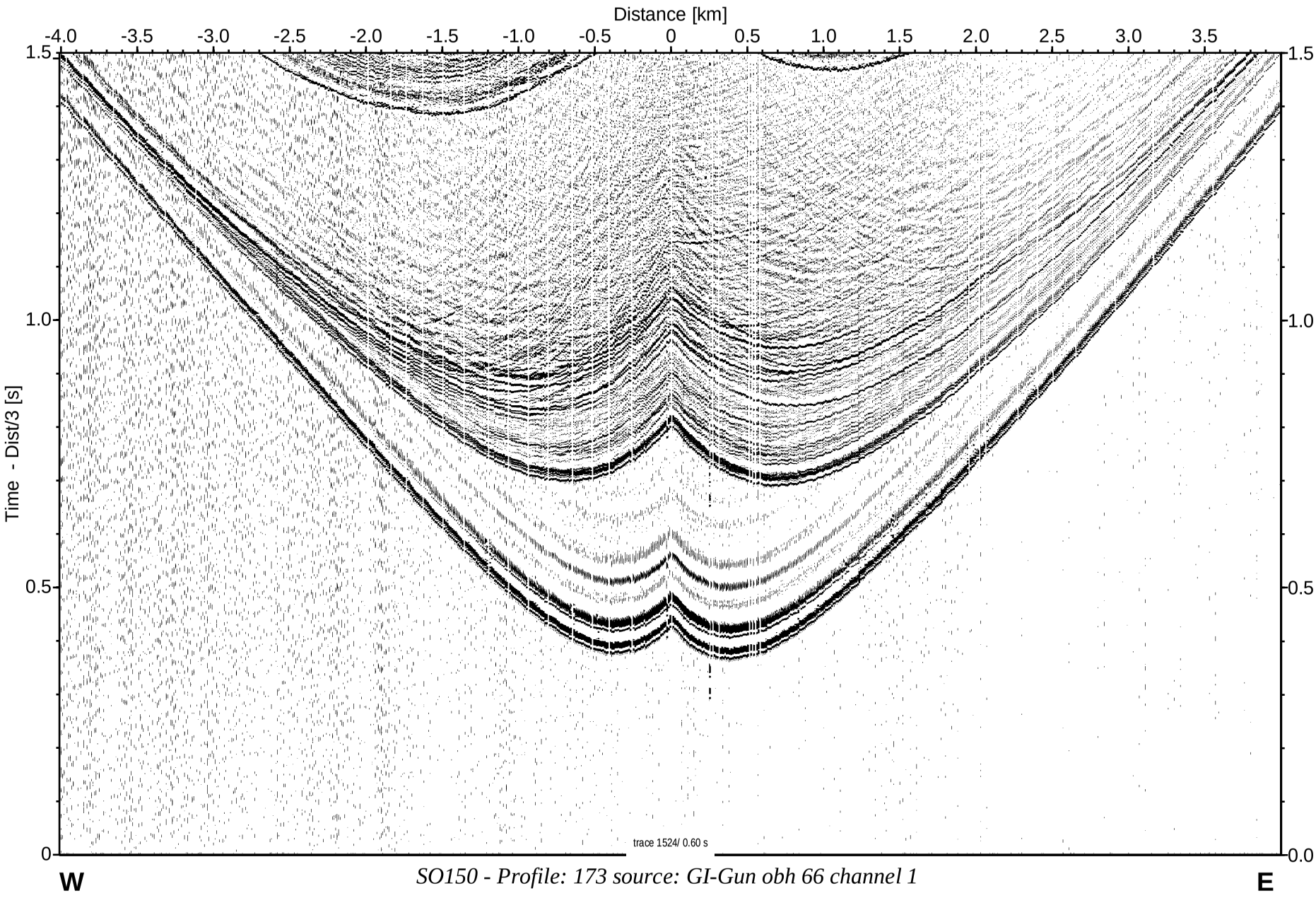

Figure 6.6.4: Record section from obh 66 , Profile 173.

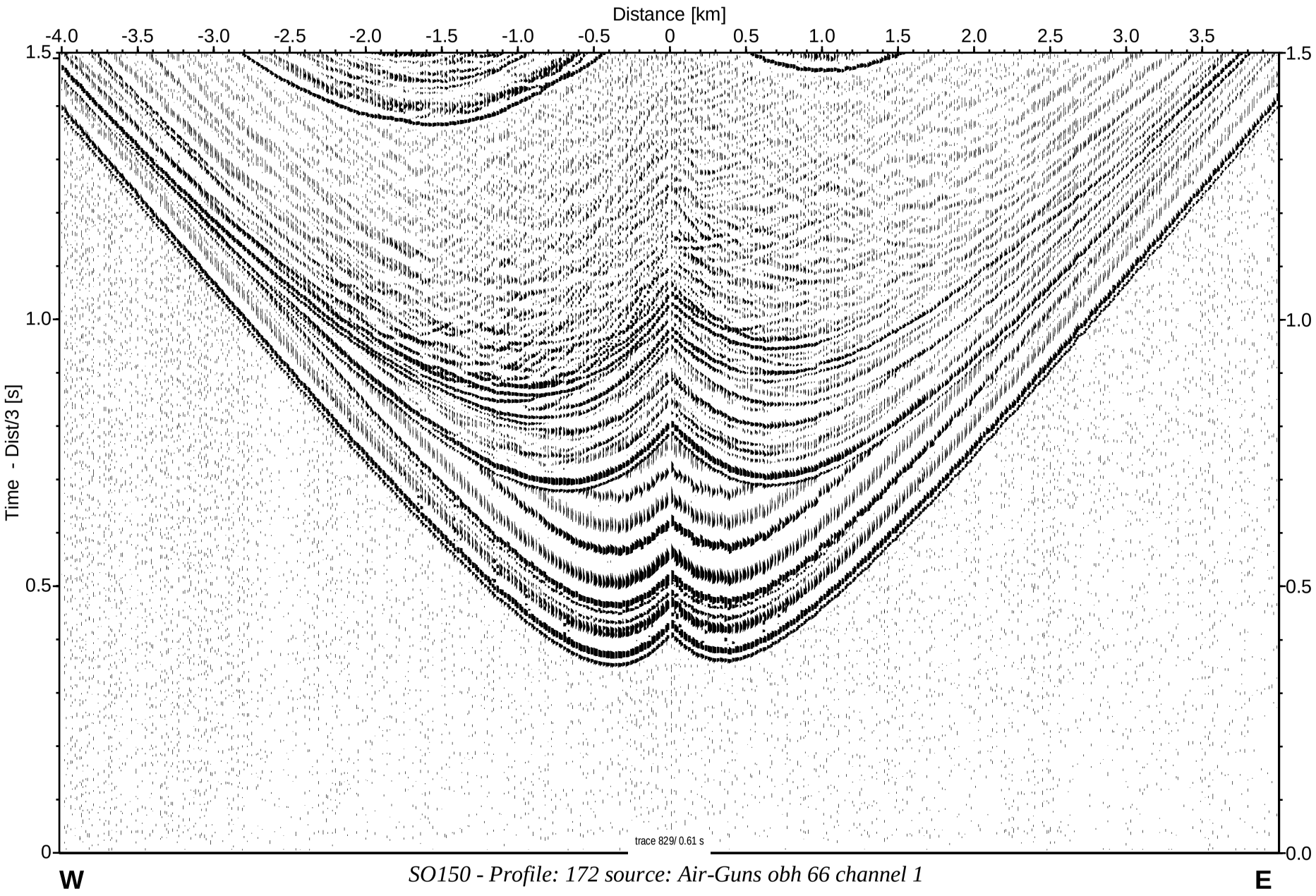

Figure 6.6.5: Record section from obh 66 , Profile 172.

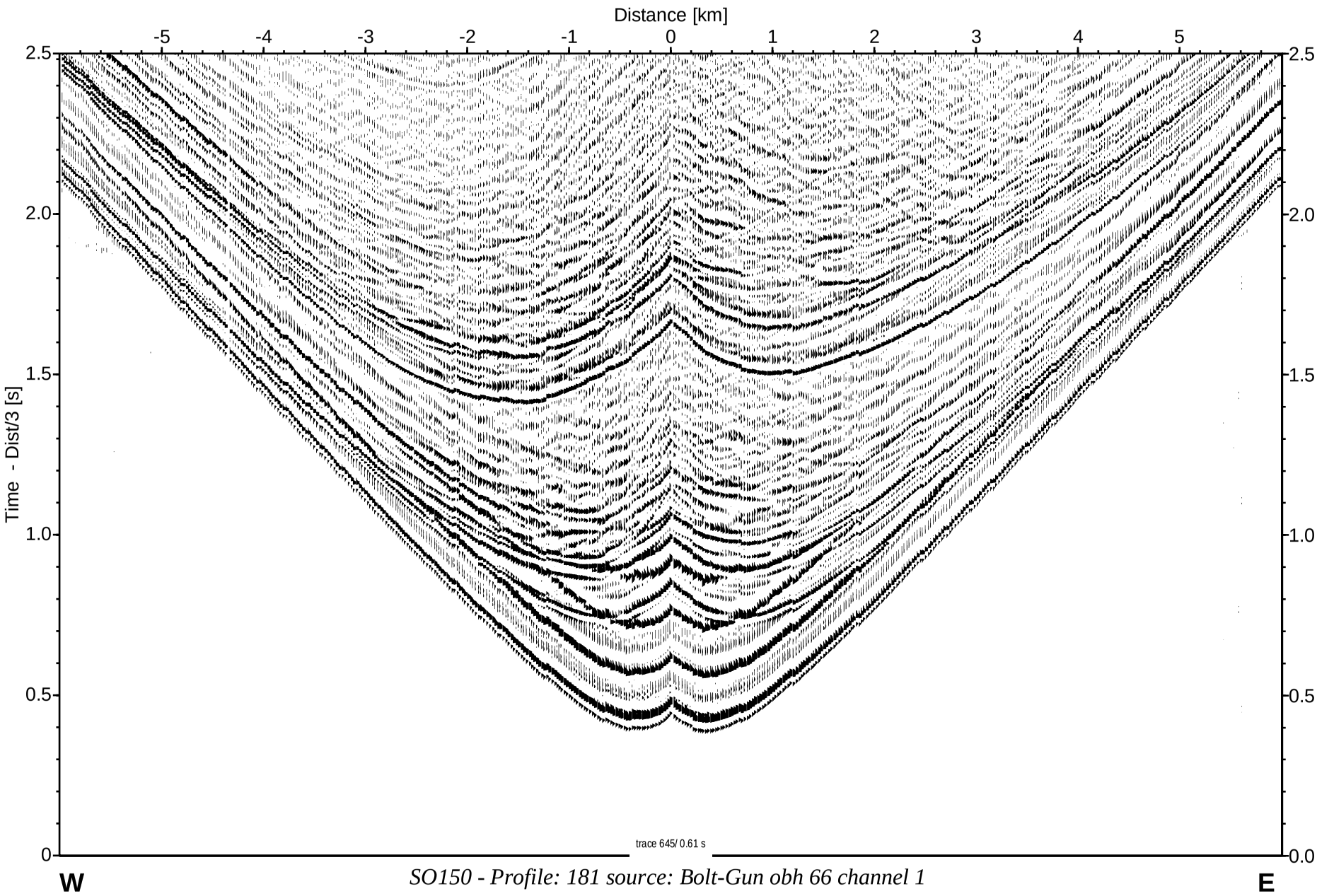

Figure 6.6.6: Record section from obh 66 , Profile 181.

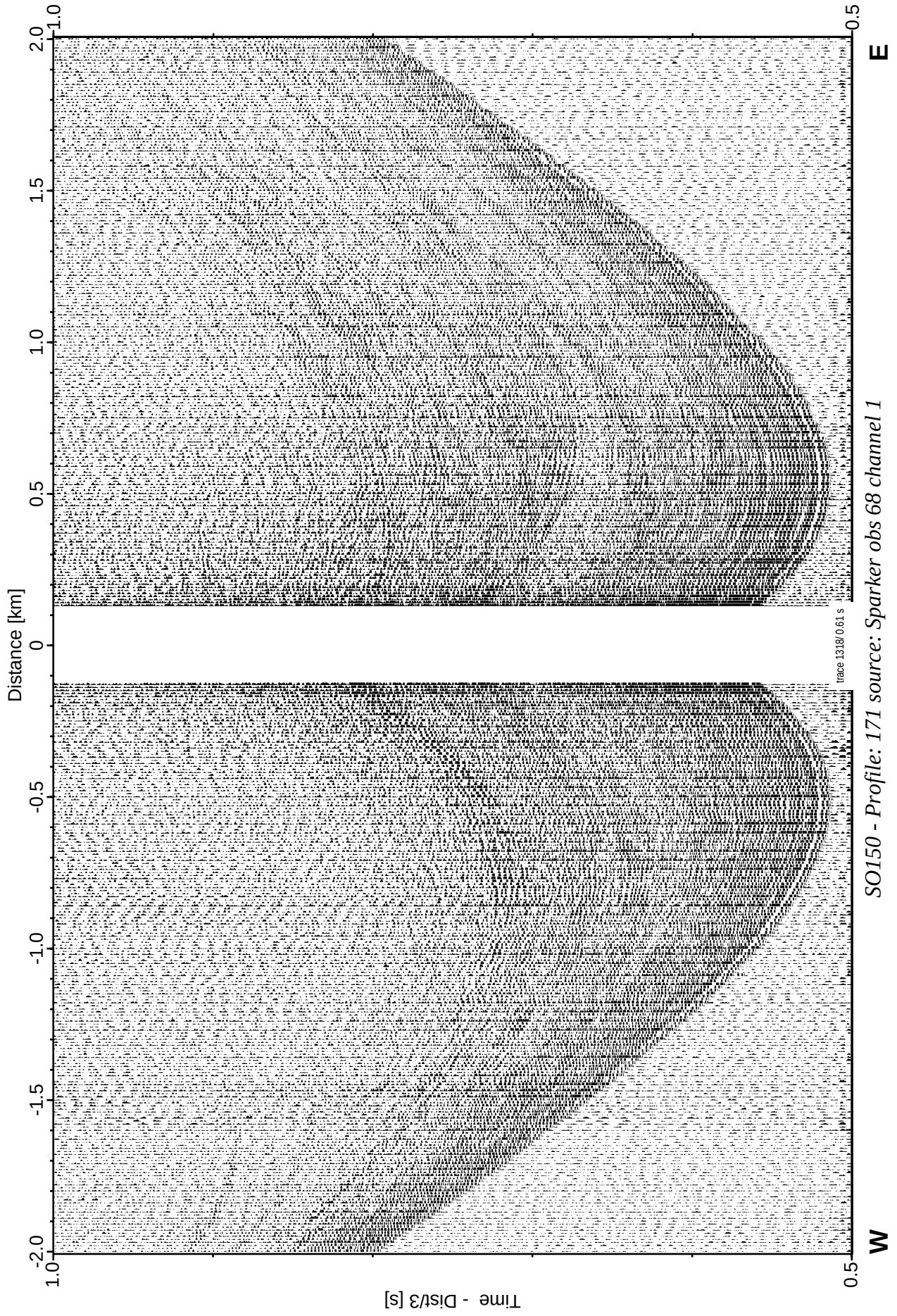

Figure 6.6.7: Record section from obs 68 hydrophone, Profile 171.

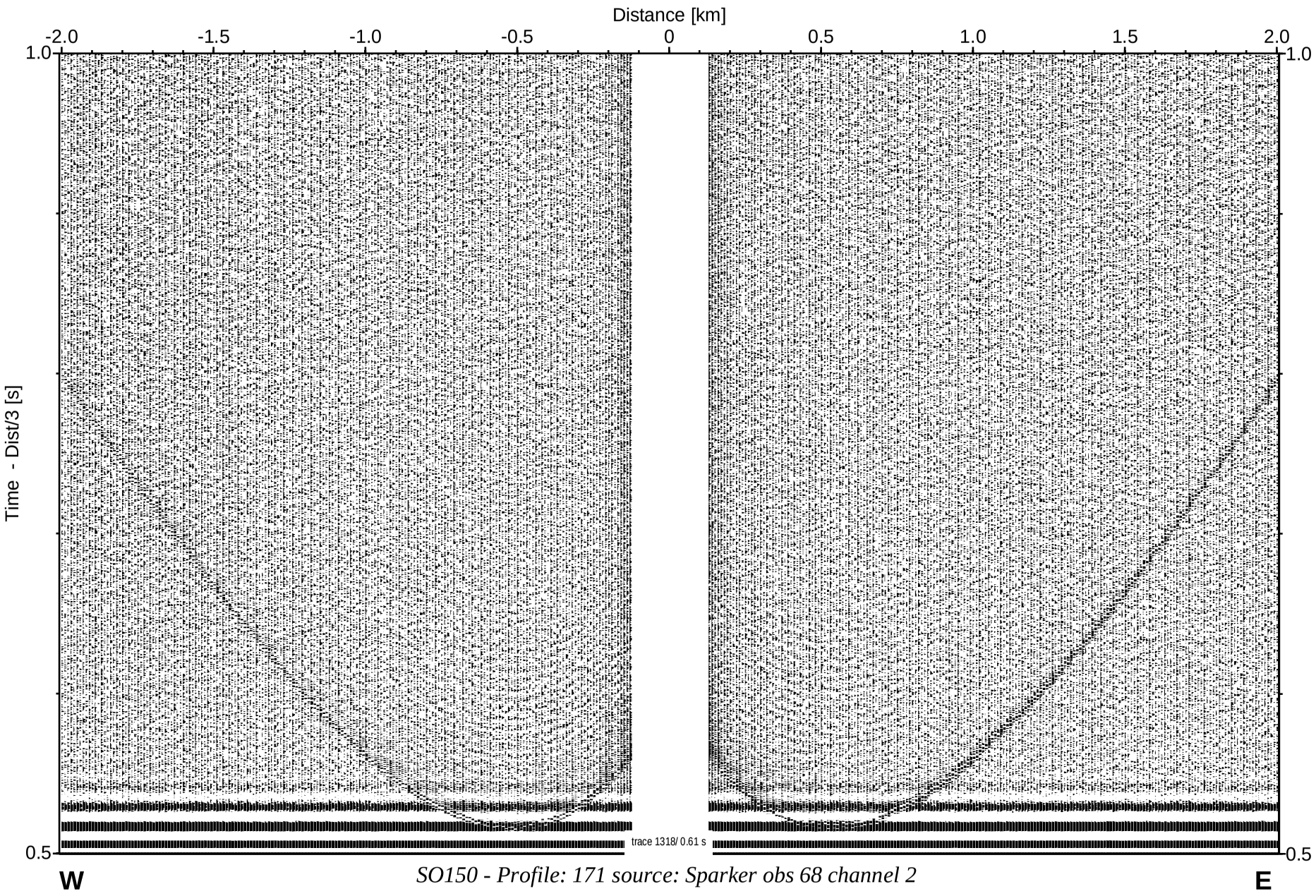

Figure 6.6.8: Record section from obs 68 horizontal component 1, Profile 171.

Figure 6.6.9: Record section from obs 68 horizontal component 2, Profile 171.

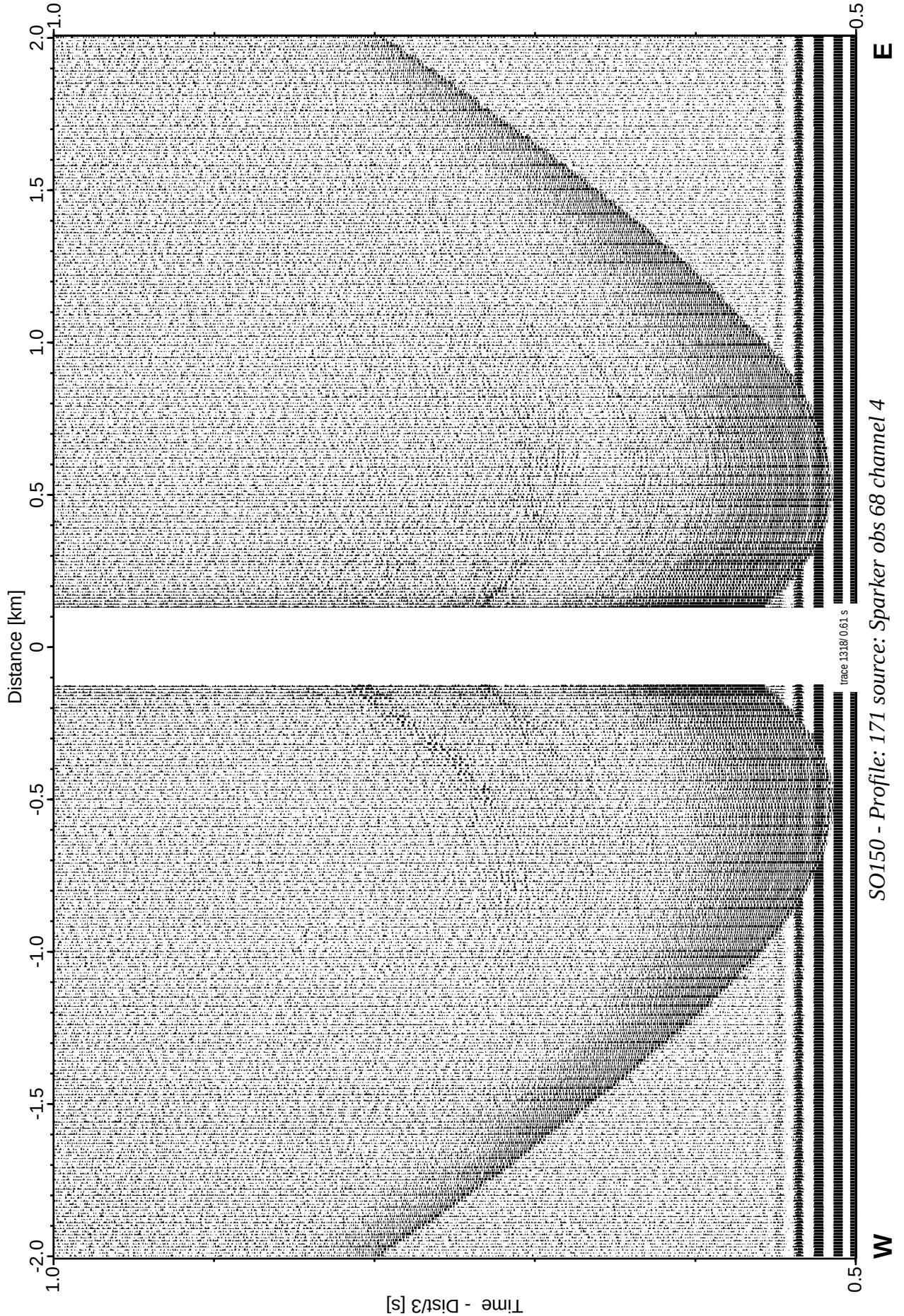

Figure 6.6.10: Record section from obs 68 vertical component, Profile 171.

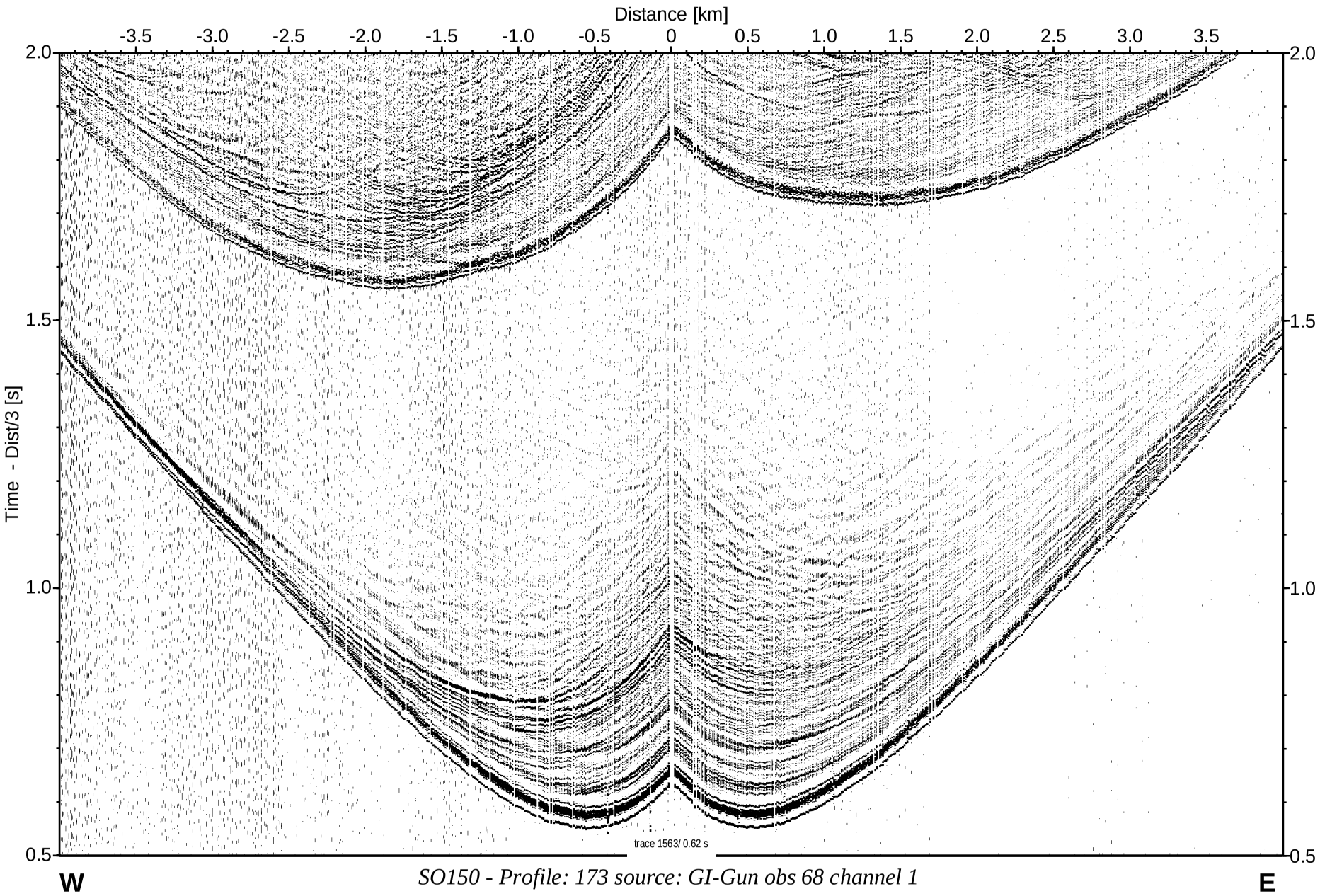

Figure 6.6.11: Record section from obs 68 hydrophone, Profile 173.

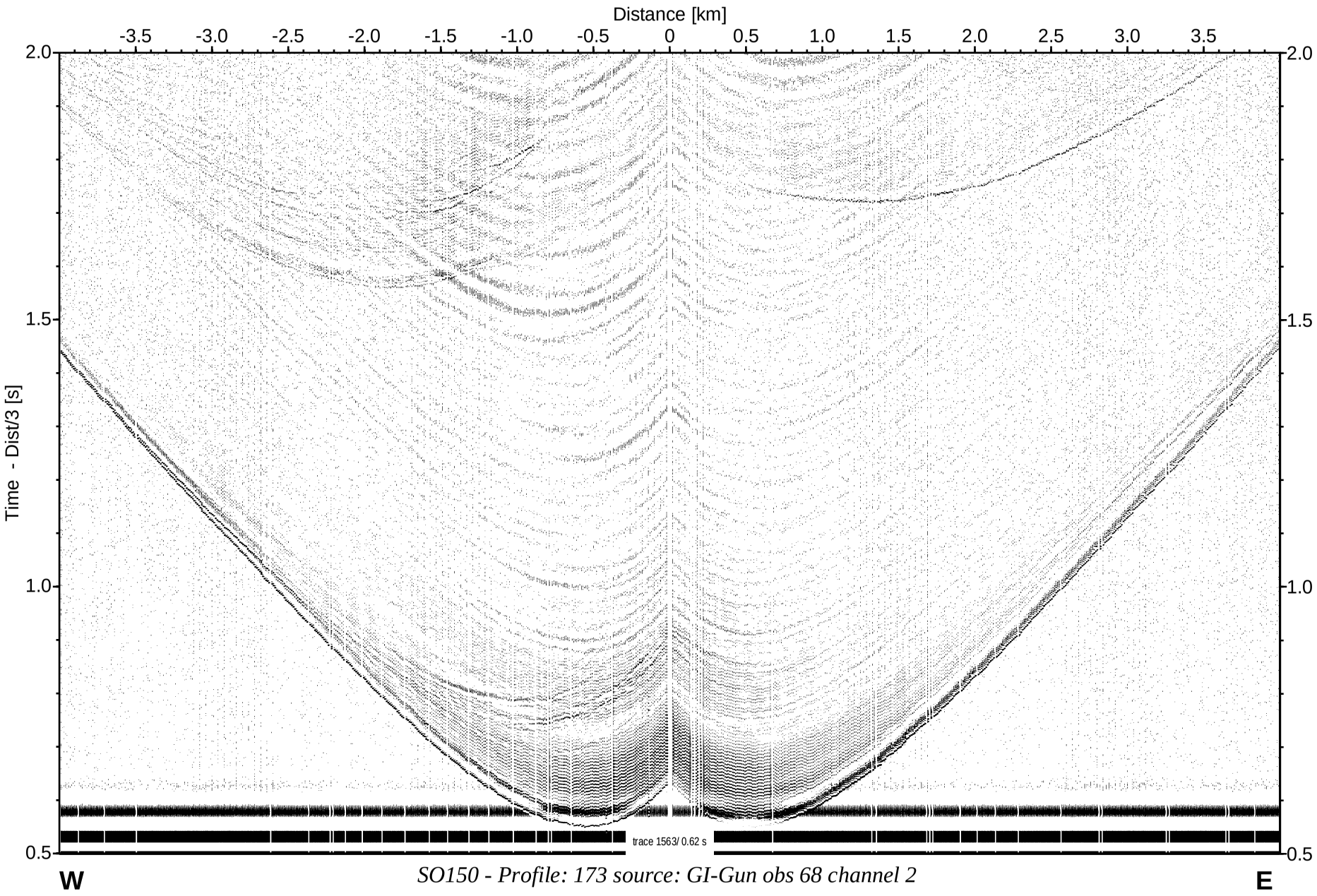

Figure 6.6.12: Record section from obs 68 horizontal component 1, Profile 173.

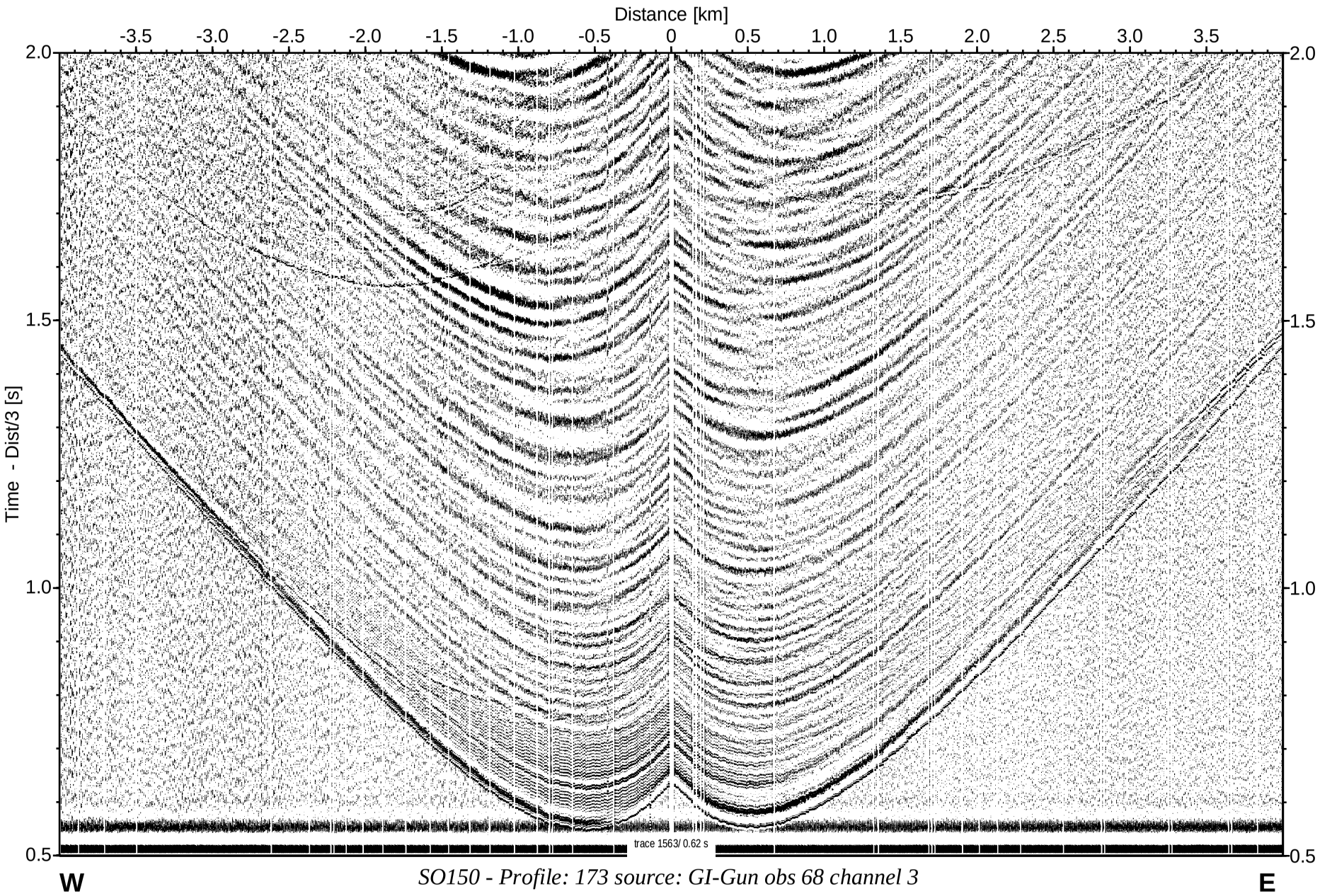

Figure 6.6.13: Record section from obs 68 horizontal component 2, Profile 173.

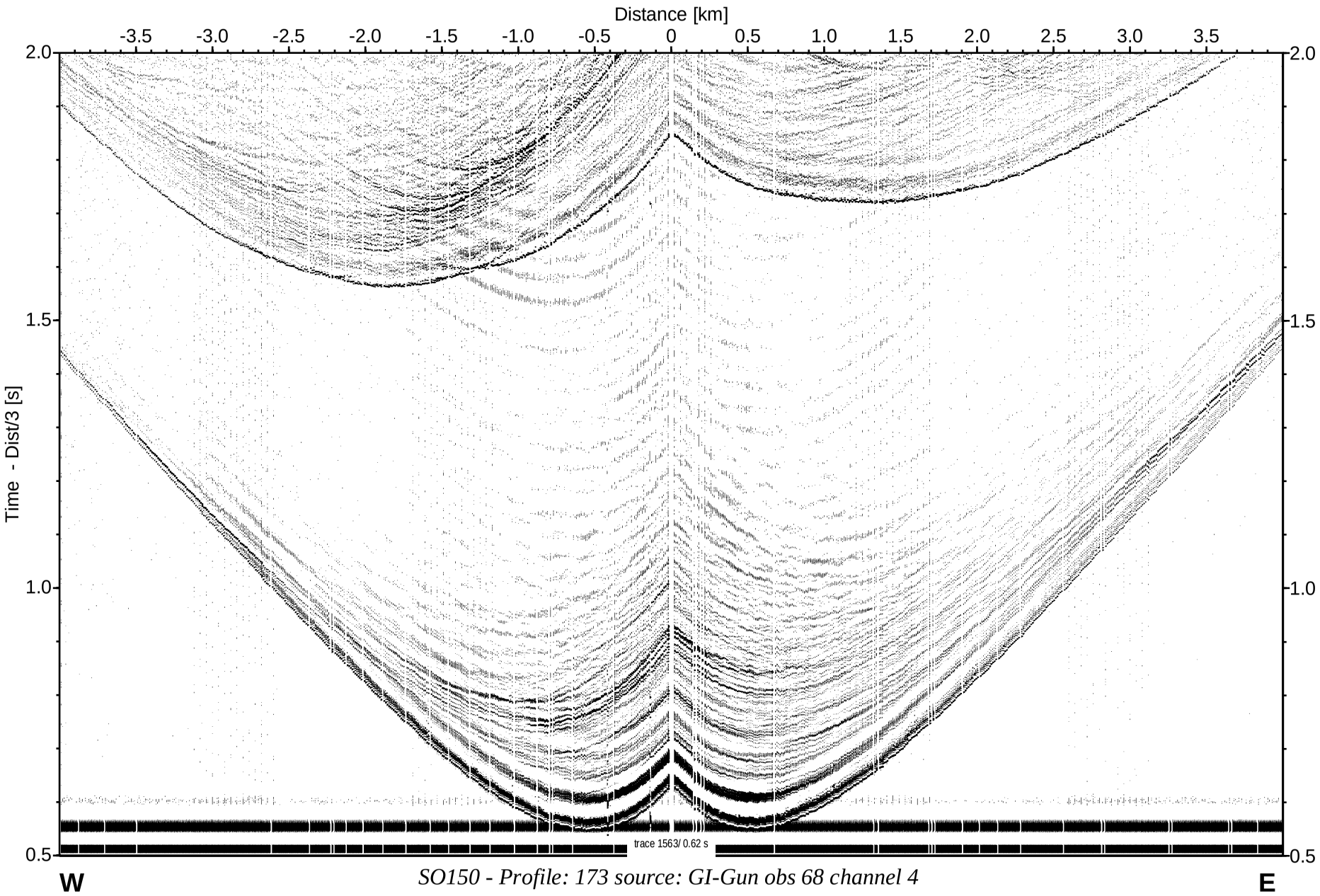

Figure 6.6.14: Record section from obs 68 vertical component, Profile 173.

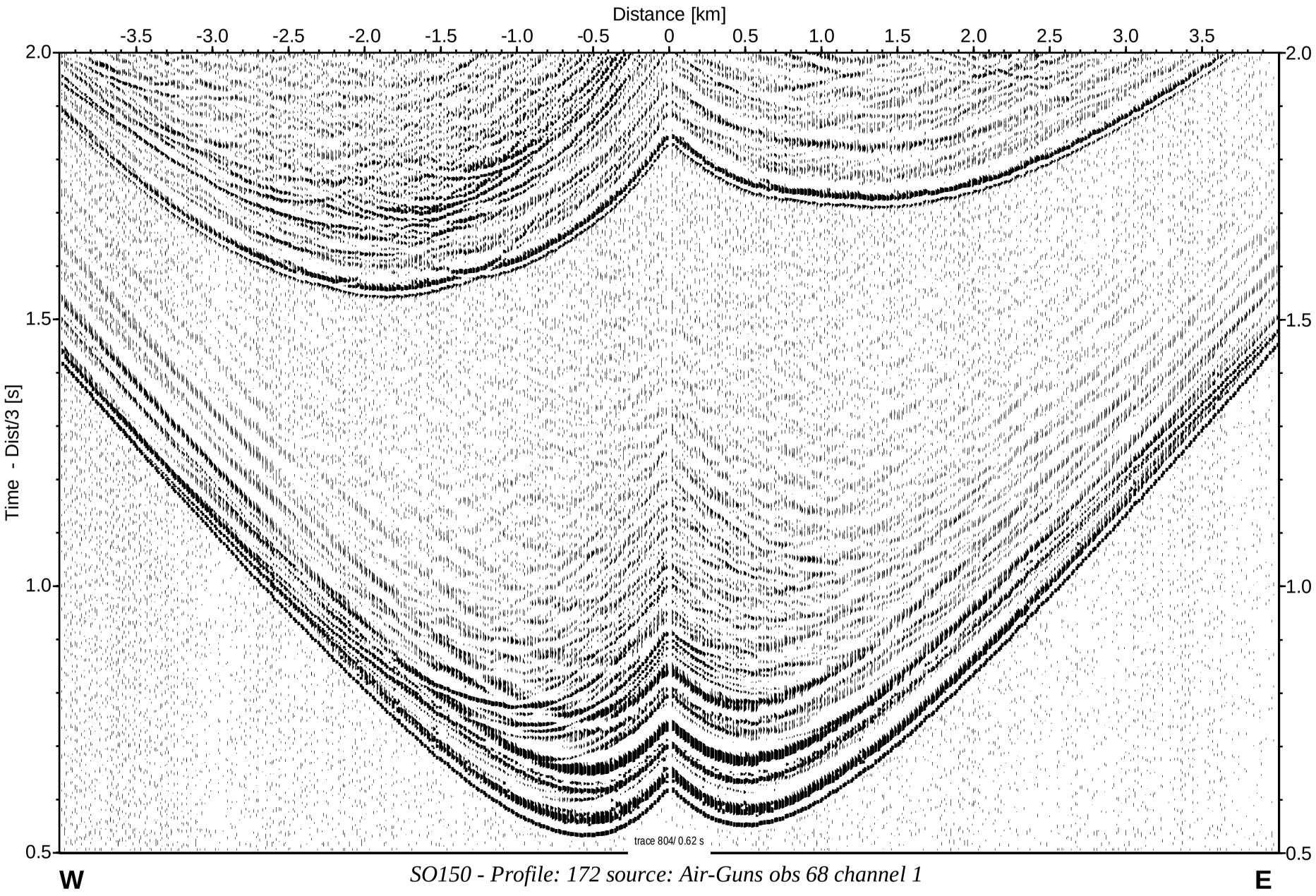

Figure 6.6.15: Record section from obs 68 hydrophone, Profile 172.

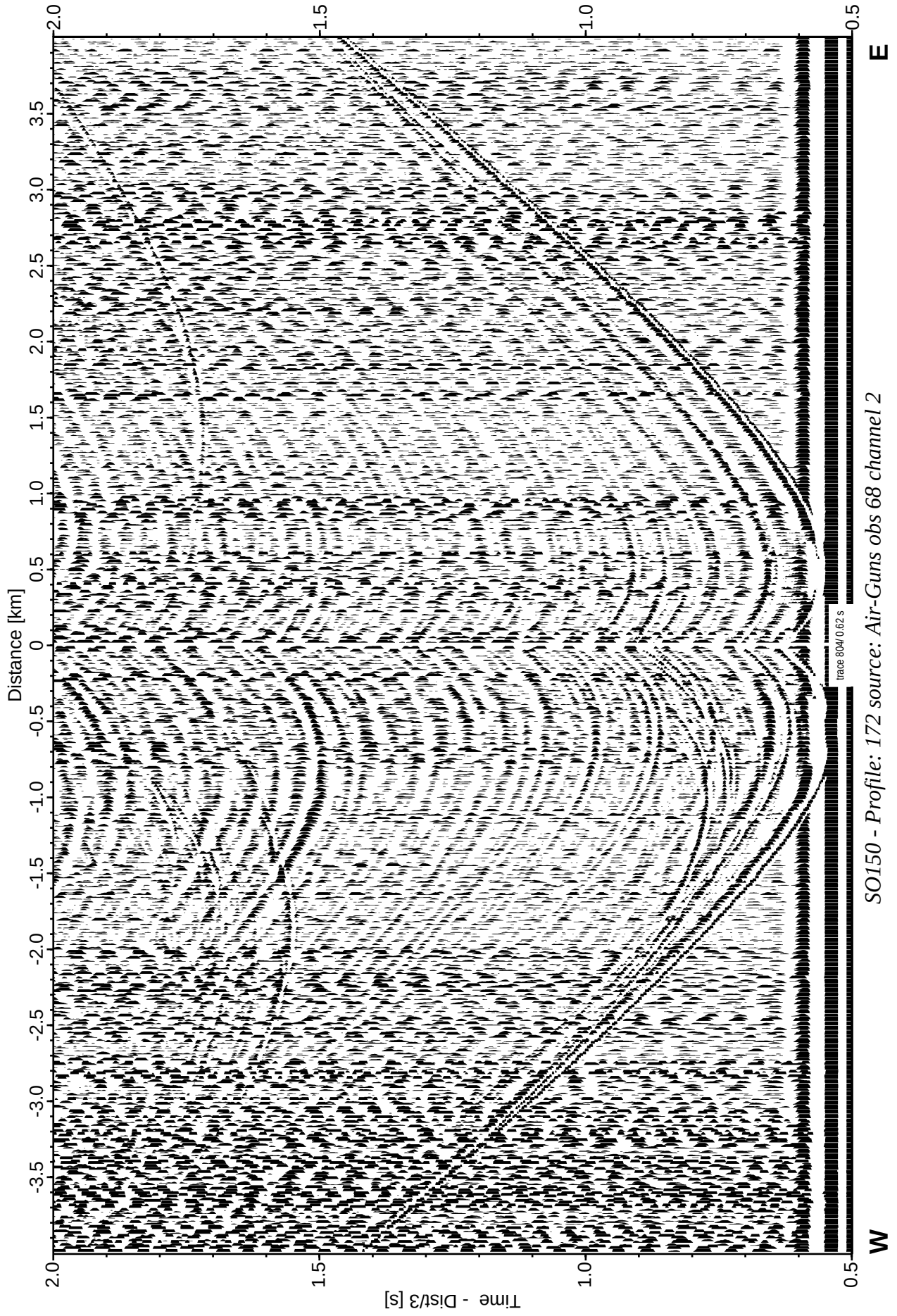

Figure 6.6.16: Record section from obs 68 horizontal component 1, Profile 172.

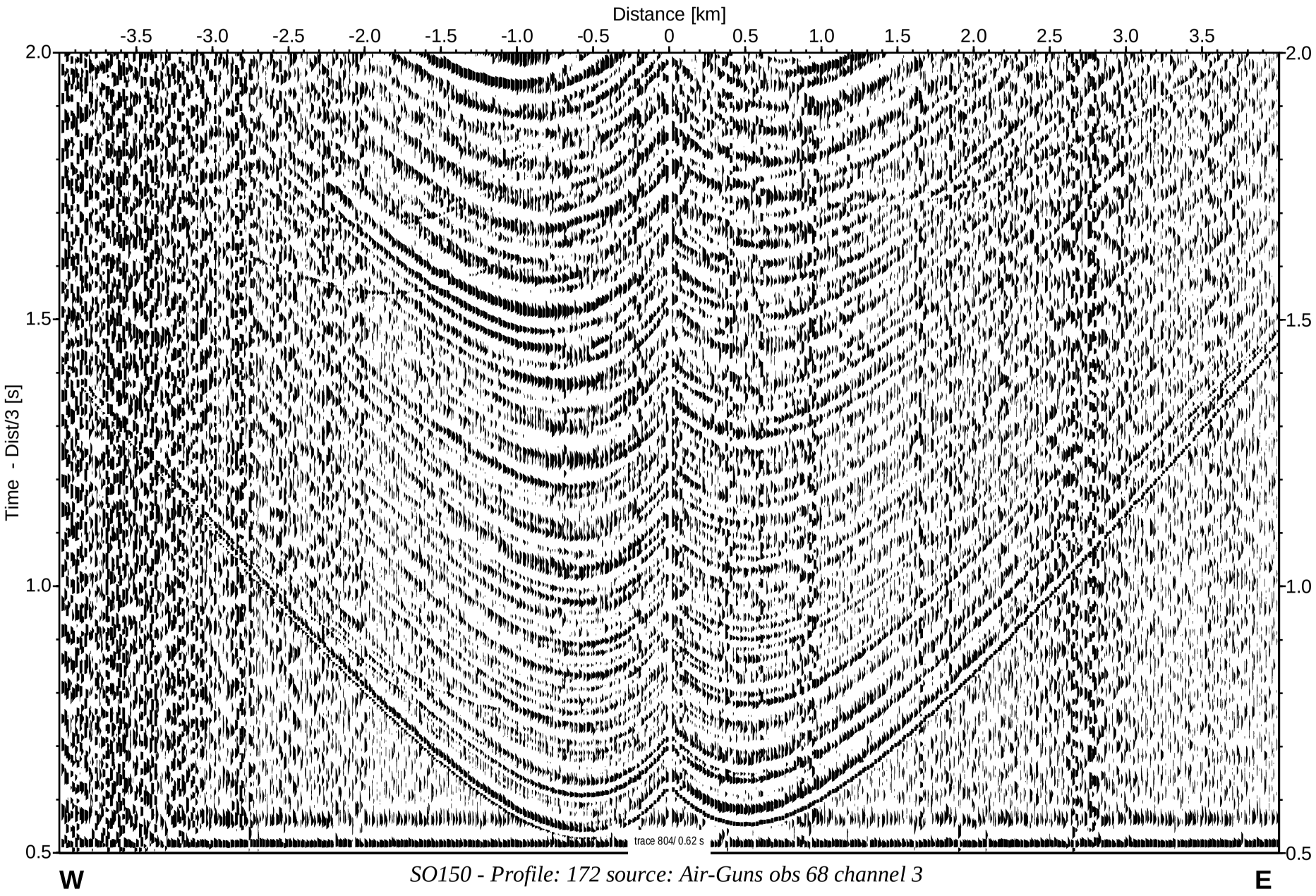

Figure 6.6.17: Record section from obs 68 horizontal component 2, Profile 172.

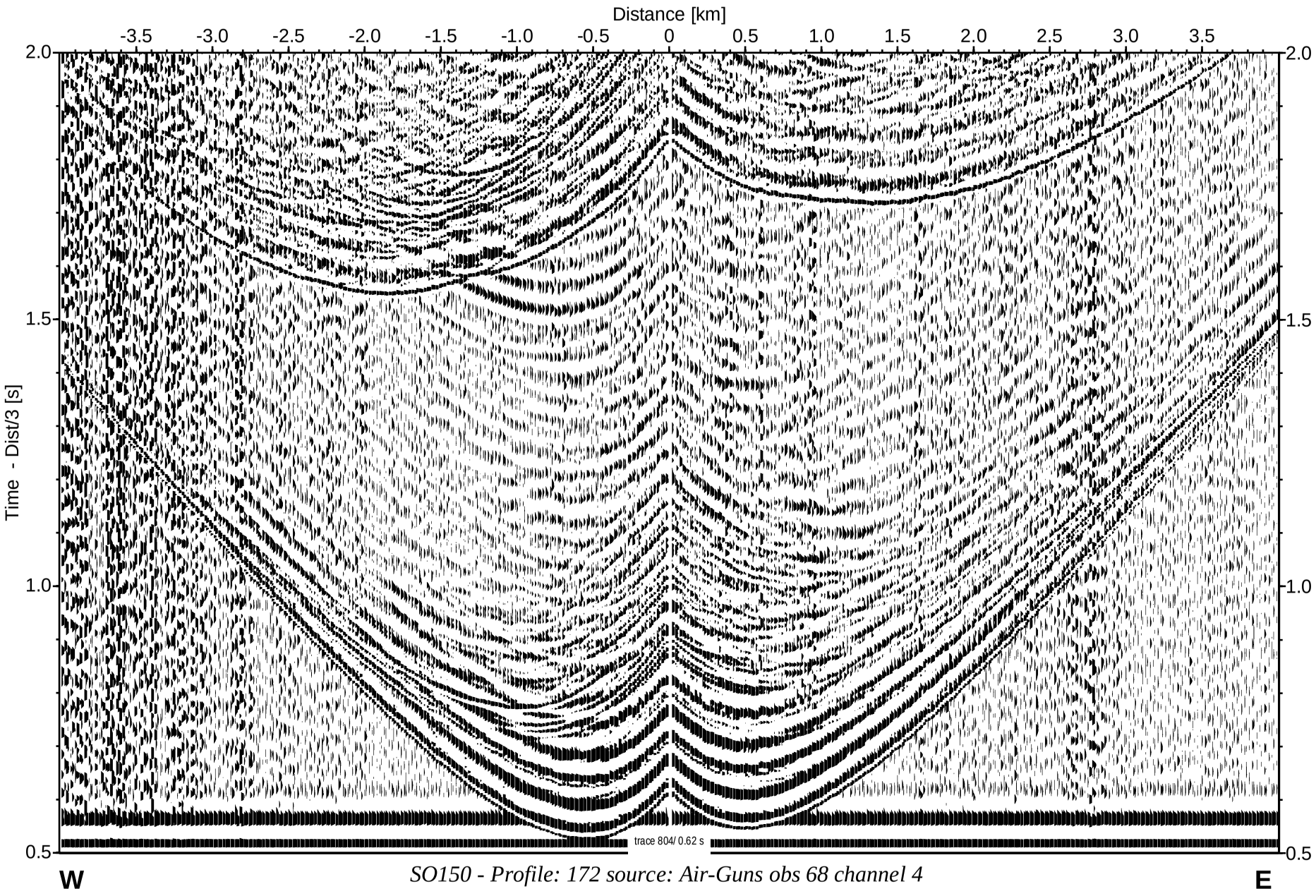

Figure 6.6.18: Record section from obs 68 vertical component, Profile 172.

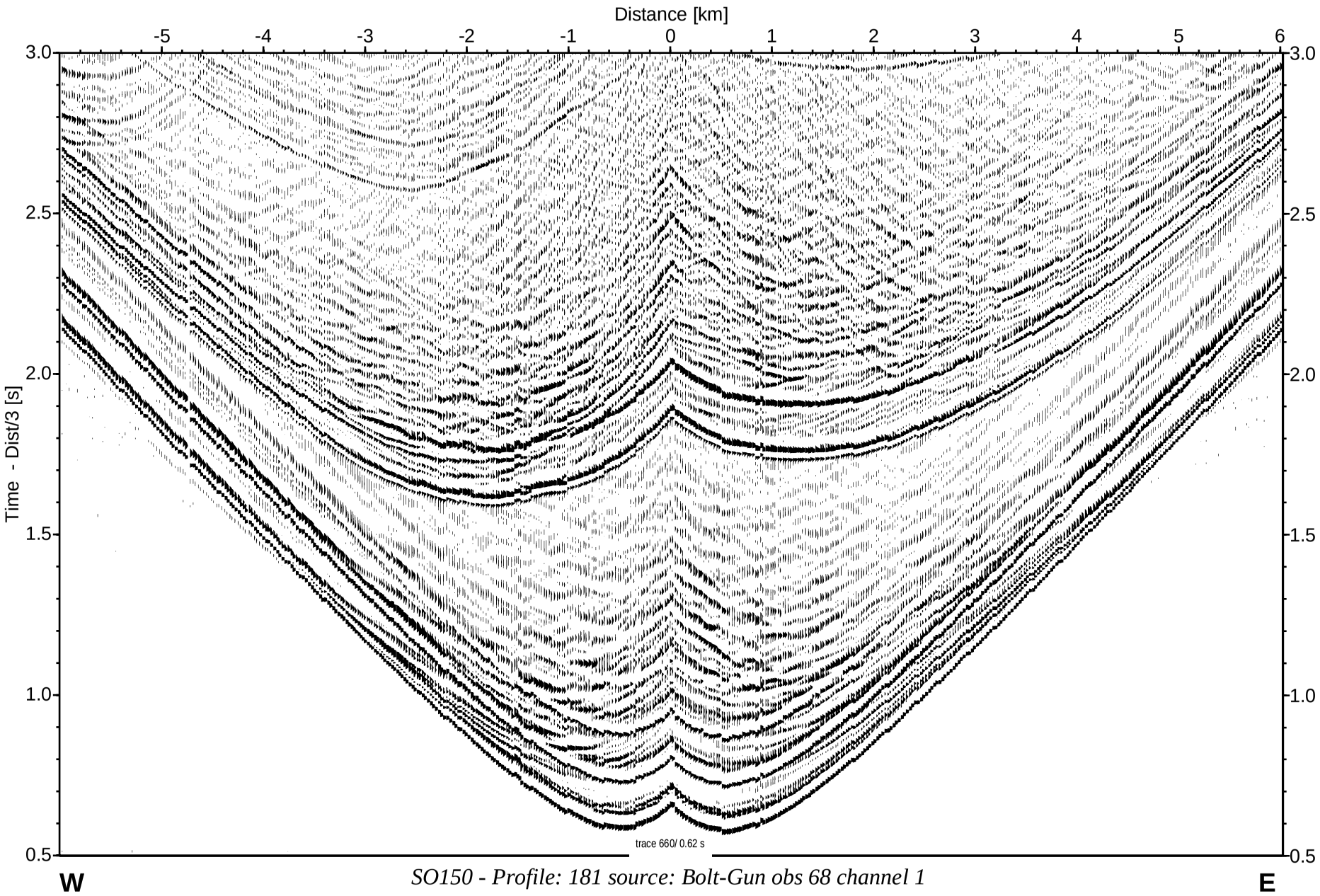

Figure 6.6.19: Record section from obs 68 hydrophone, Profile 181.

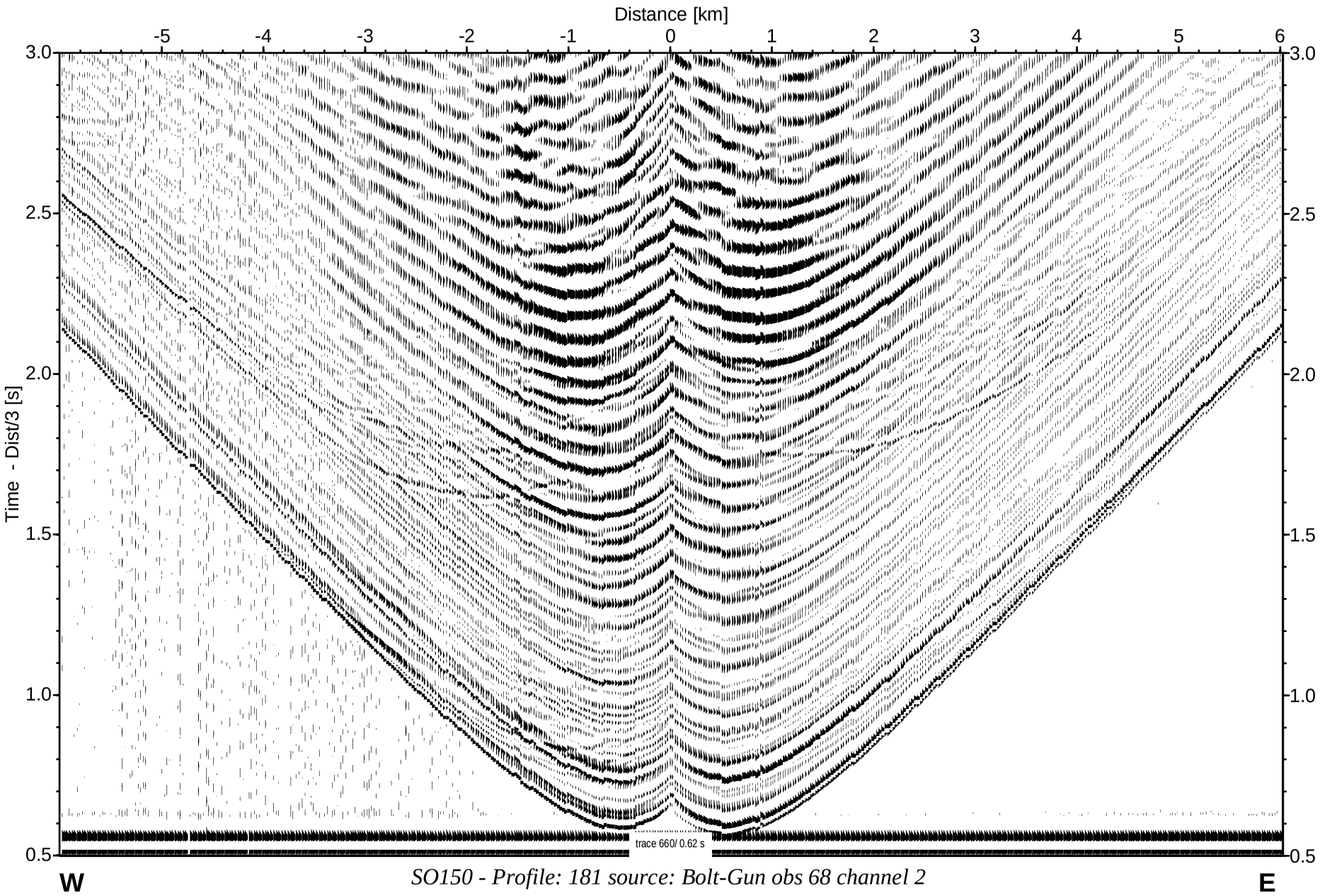

Figure 6.6.20: Record section from obs 68 horizontal component 1, Profile 181.

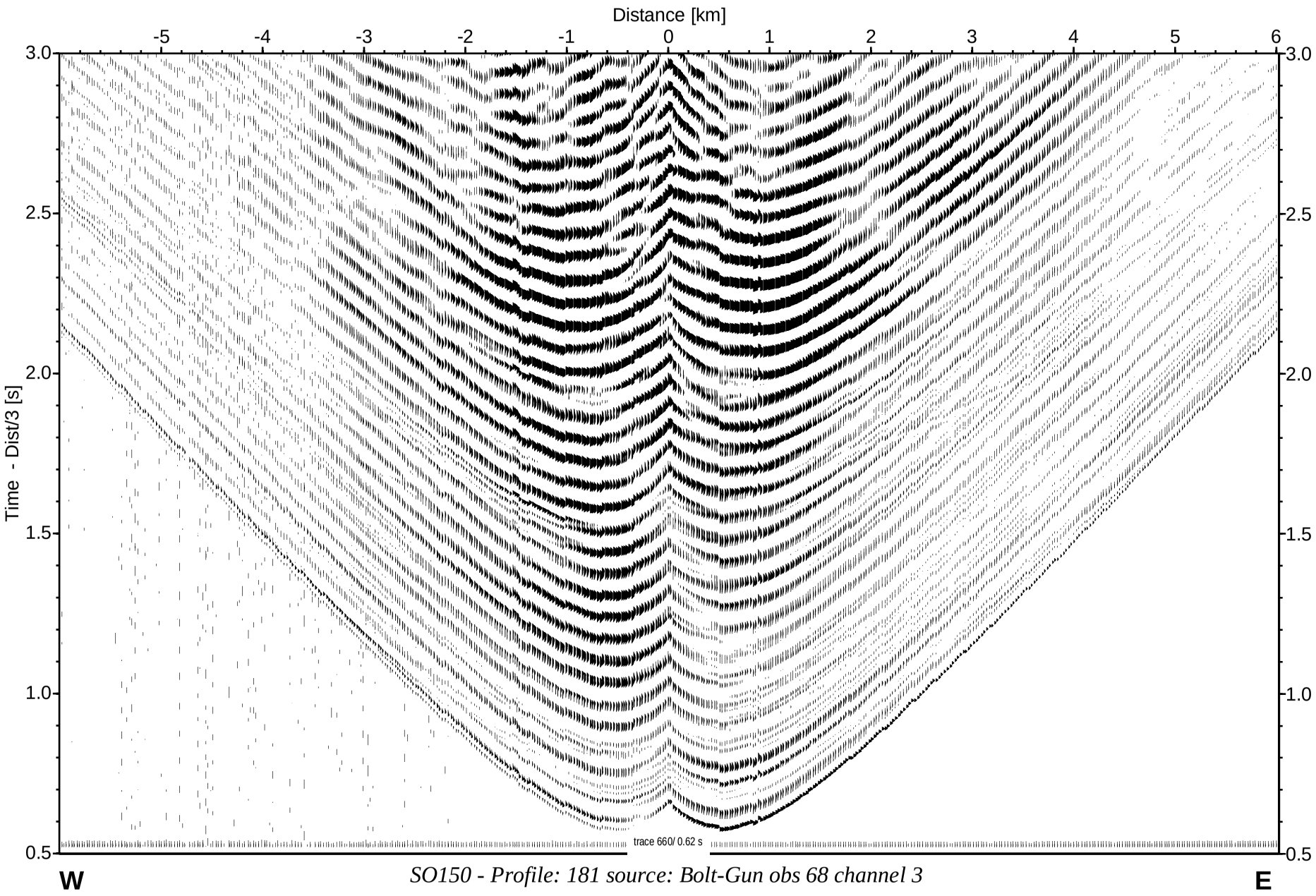

Figure 6.6.21: Record section from obs 68 horizontal component 2, Profile 181.

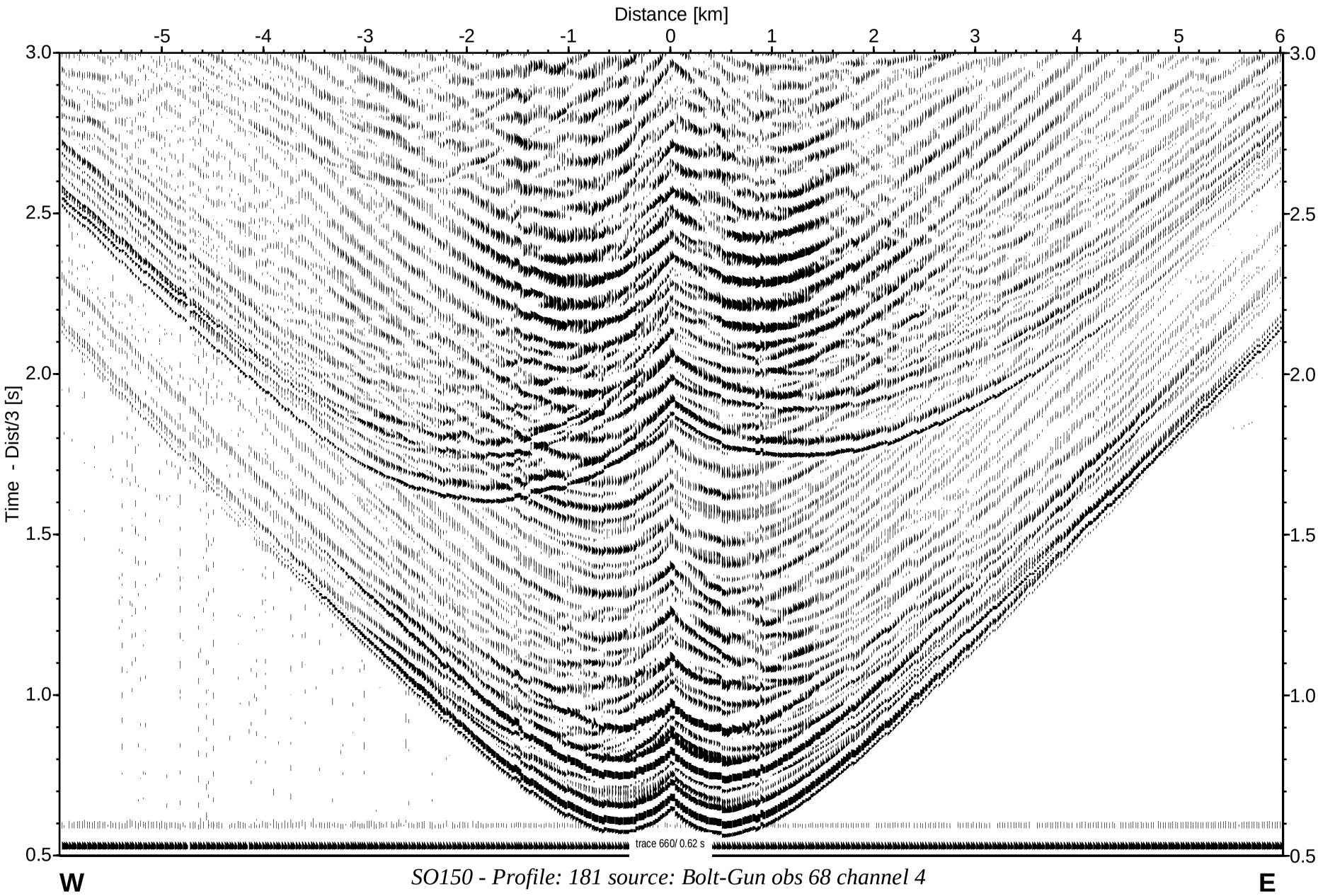

Figure 6.6.22: Record section from obs 68 vertical component, Profile 181.

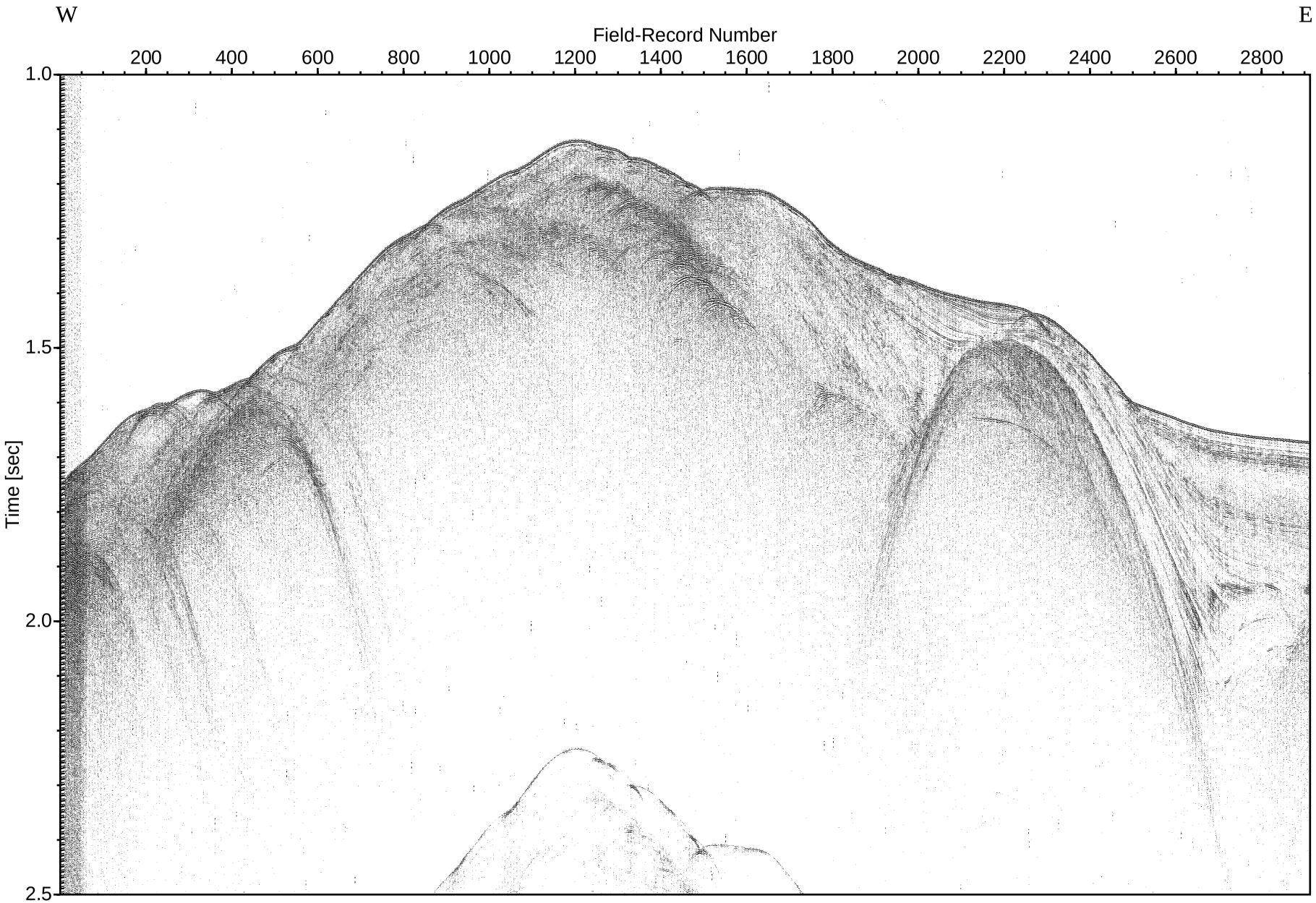

Figure 6.6.23: Record section with source Sparker, Profile 61.

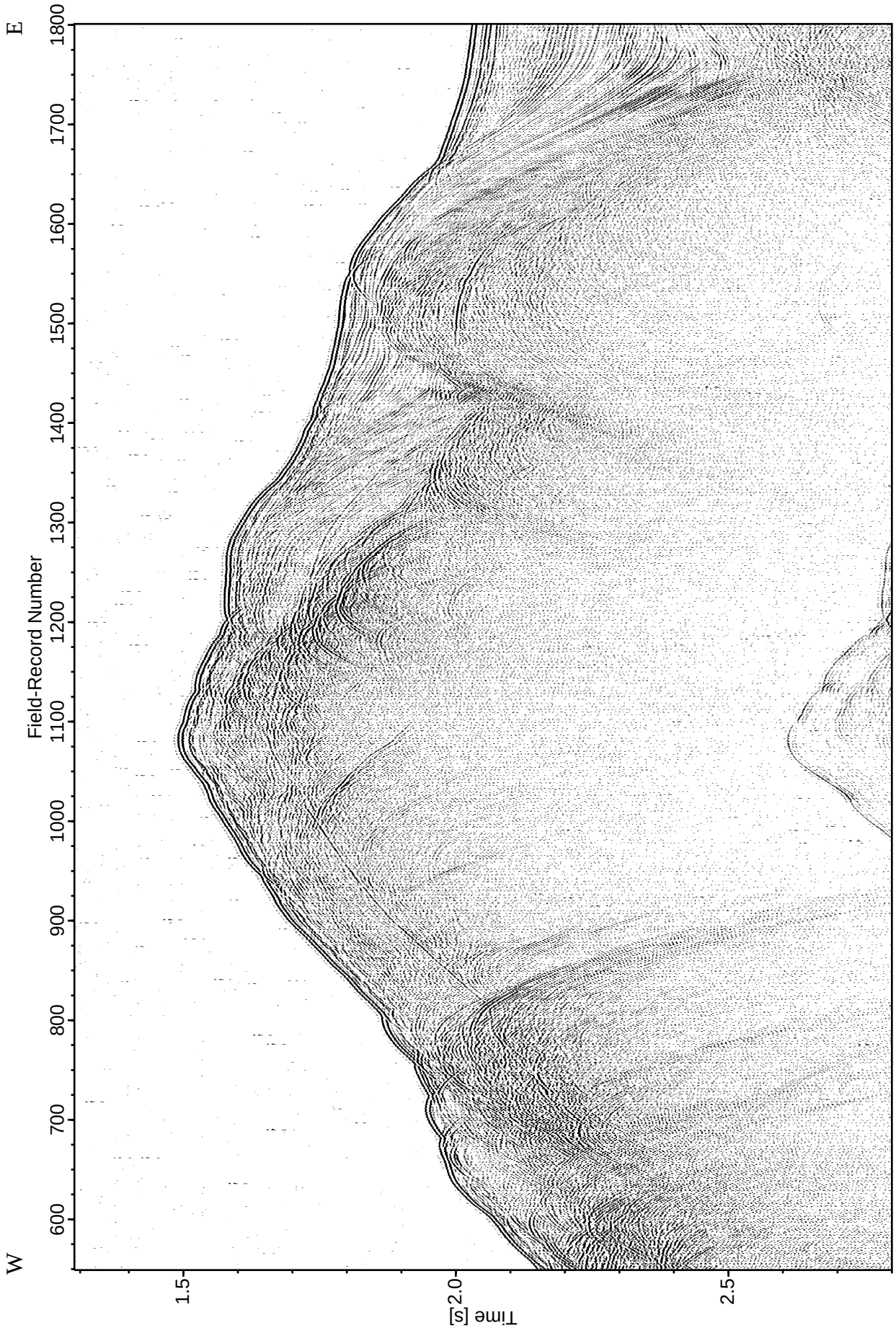

Figure 6.6.24: Record section with source GI-Gun, Profile 63.

Figure 6.6.25: Record section with source GI-Gun, Profile 176.

Figure 6.6.26: Record section with source GI-Gun, Profile 175.

6.7 EXPERIMENT USING THE DROP WEIGHT

(T. Bohlen)

The main objective of the drop weight experiment was to test if seismic waves, especially Scholte waves, can principally be excited by such a source. Previous experiments with explosive and vibrator sources at the seafloor showed clear onsets of Scholte waves on ocean bottom seismic recordings (OBS). A seismic modeling study for the typical subsurface structure around the ODP site 892 indicated that Scholte waves are anticipated on seismograms of displacement (or particle velocity), i.e. on OBS recordings (whereas the energy on the hydrophone components (OBH) in the water column is generally quite low).

In our experiment, the drop weight (3t) hit the seafloor with approximately 1.5 m/s. It was applied at 11 locations in the vicinity of ODP site 892 where one OBH, one OBS, and one DPG were deployed . The minimum distance between source and receiver was approximately 100m, the maximum offset 2500 m.

The UTC-time at which the weight hit the seafloor was used to select the time-windows in which Scholte waves should be recorded. We applied various gains and bandpass filters to these time windows. Even at the nearest locations (100 m and 350 m distance from the OBS), no evidence of seismic waves could be found in the recordings. This suggests that a drop weight of 3t lowered with 1.5 m/s is insufficient to excite seismic waves at the generally unconsolidated seafloor sediment. Better results may be achieved with higher descent speeds since the source energy is proportional to the square velocity.

Additionally an EW and reverse WE profile was shot with two 32l Bolt guns. The profile was extended further to the coast to get deeper refracted events compared to main deployment on ODP Leg 146, Site 892 in Chapter 6.4. Three data examples of this acquisition is shown in Fig. 6.7.1 to 6.7.3.

6.8 MAGNETIC DATA AND HYDROSWEEP ON TRANSIT CRUISE

(D. Könitz, P. Liersch, I. Bode)

During the transit from Los Angeles to Barbados (16.OCT.-01.NOV.2000) 417sml of magnetic and Hydrosweep data were acquired. On the 23.OCT., 12:00h a CTD was performed offshore Nicaragua for callibration purposes of the Hydrosweep system. At 15:00h the Hydrosweep and magnetic recording started. A total of 11 profiles of Hydrosweep and magnetic data were continously acquired offshore Costa Rica and Panama (Fig. 6.8.1) until the measurements stopped on the 25.OCT. 2000.

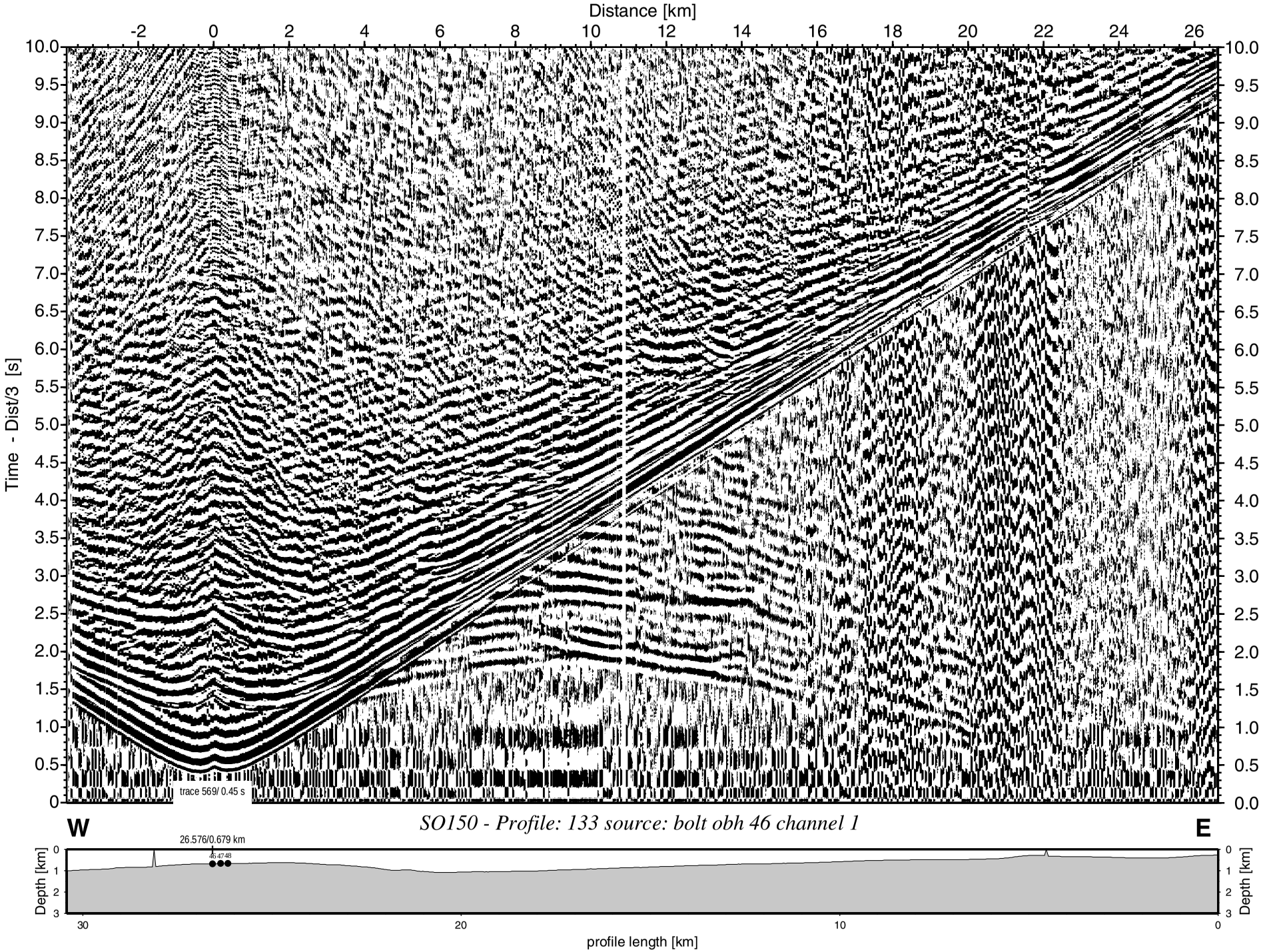

Figure 6.7.1: Record section from obh 46, Profile 133.

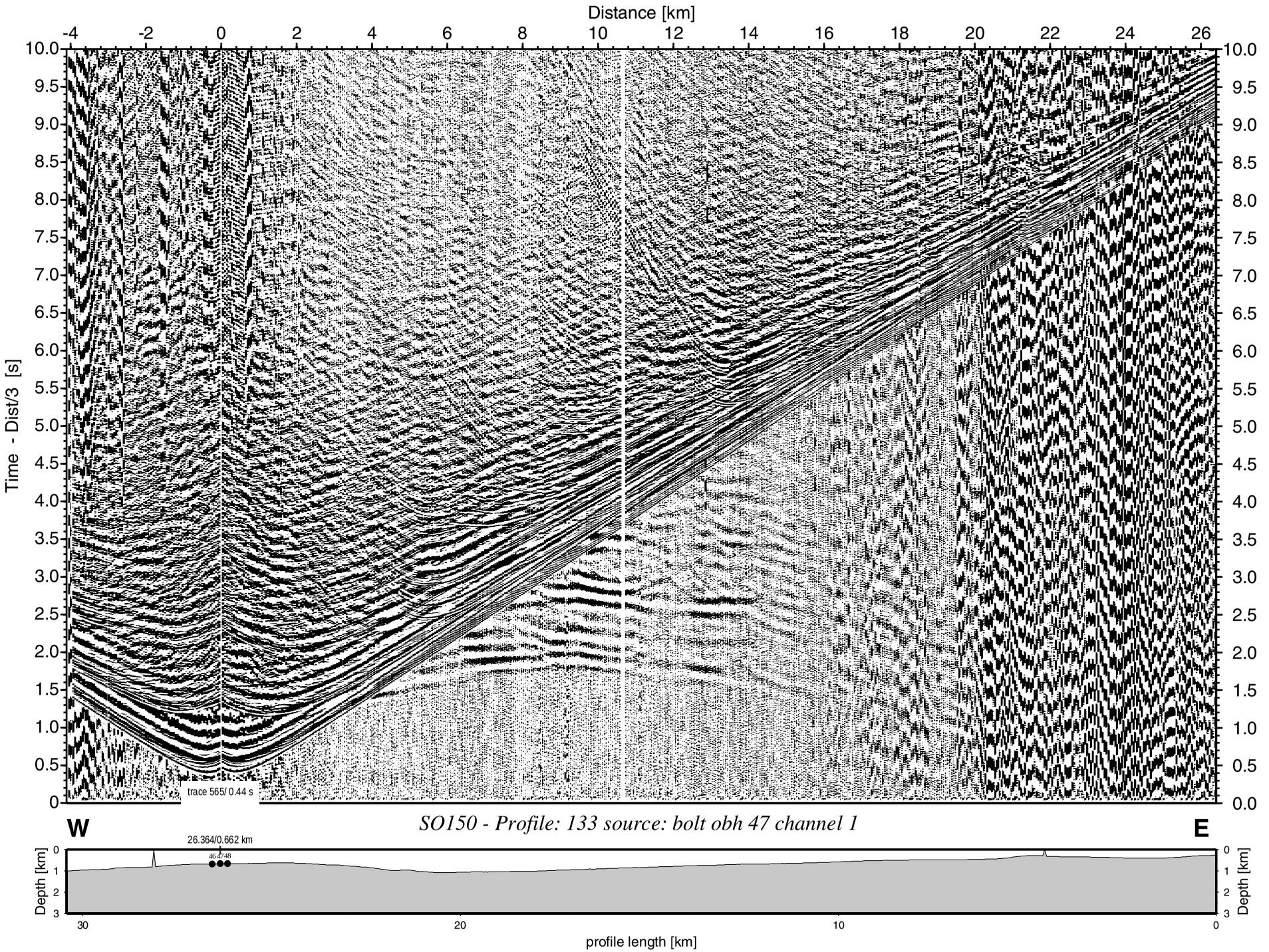

Figure 6.7.2: Record section from obh 47, Profile 133.

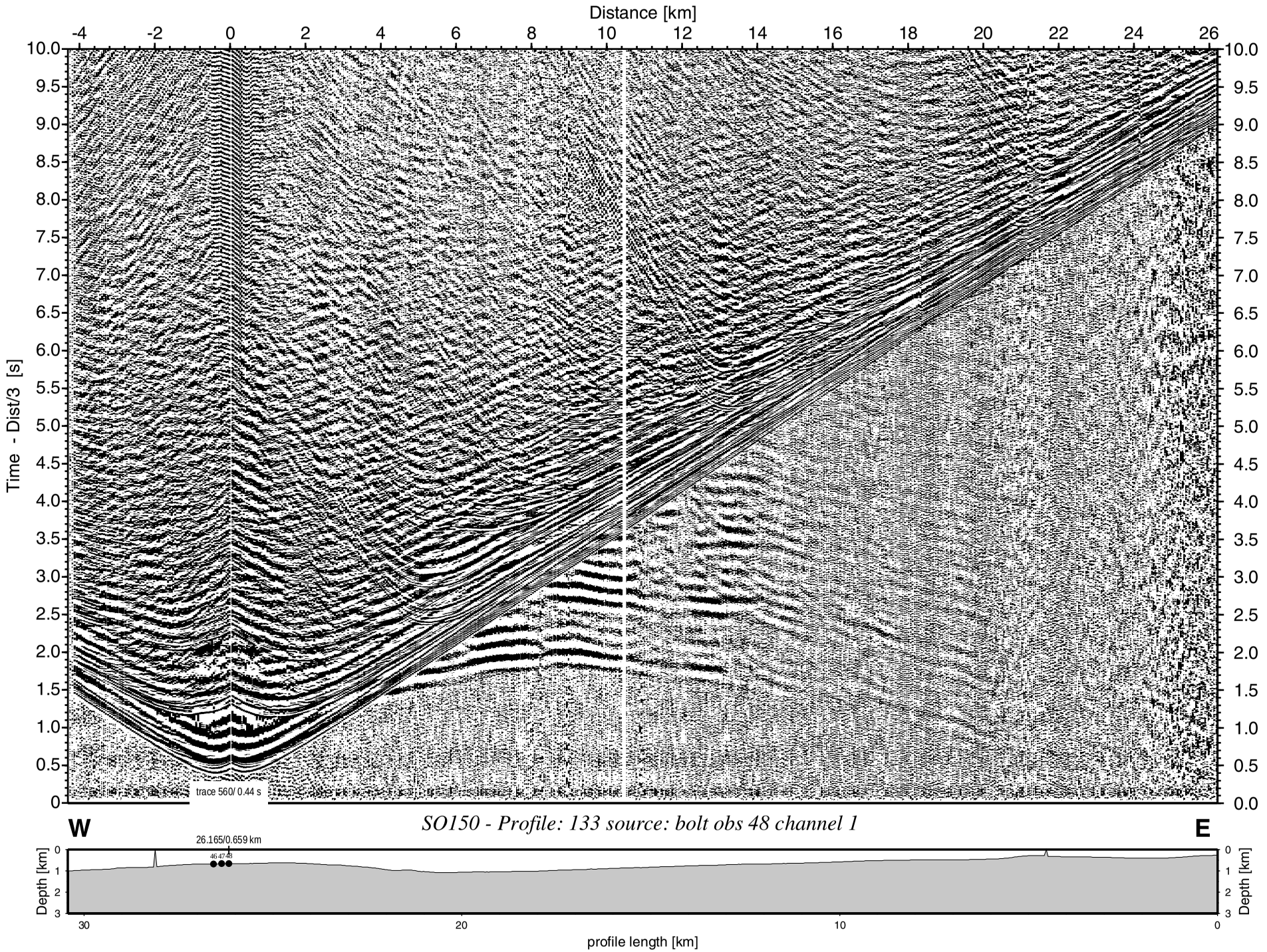

Figure 6.7.3: Record section from obs 48 hydrophone, Profile 133.

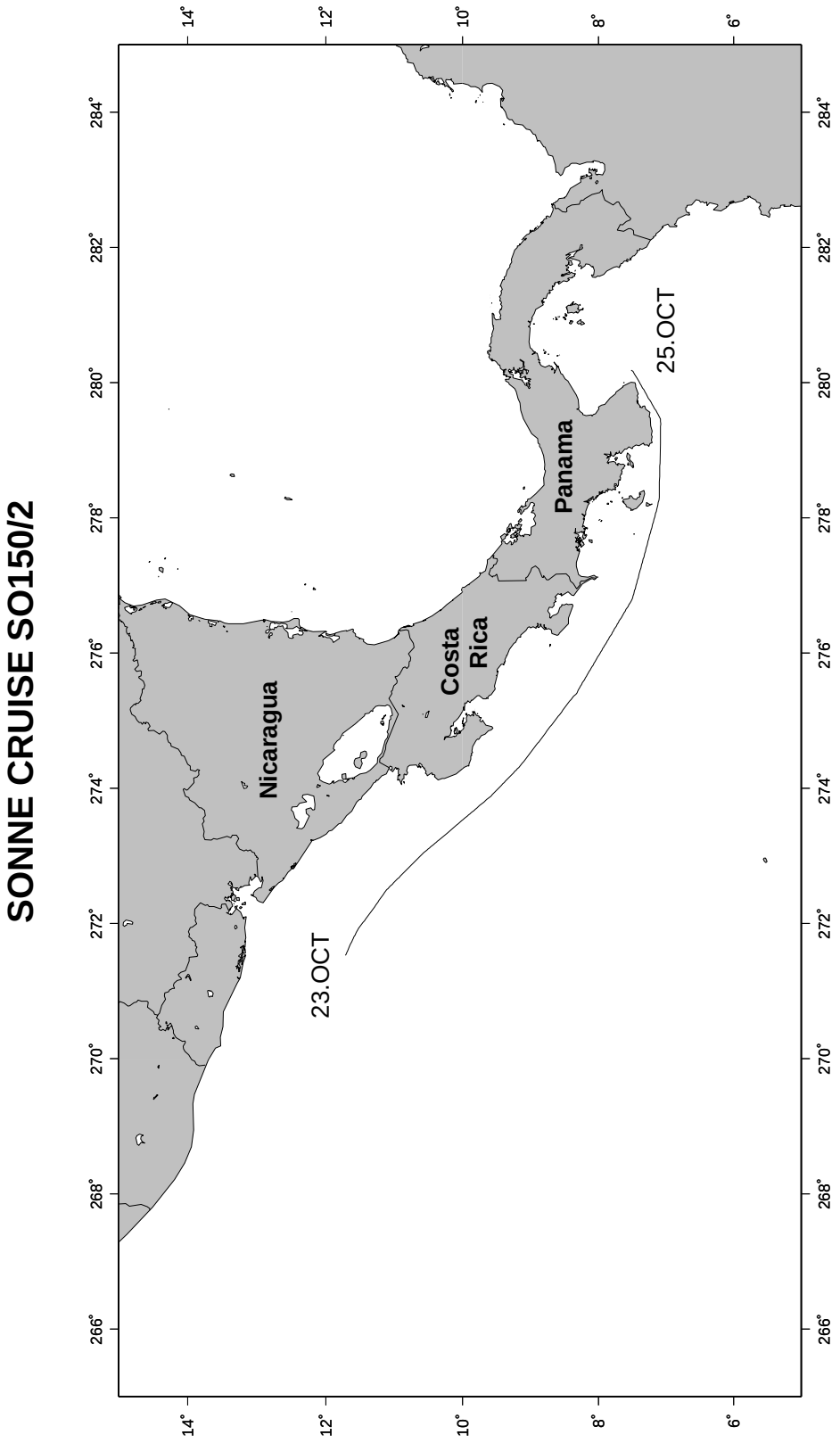

Figure 6.8.1: Location map of magnetic and Hydrosweep data collection on transit cruise.

7. ACKNOWLEDGEMENTS

Cruise SO150 was funded by the German Ministery of Education, Research, Science, and Technology (BMBF) under project No. 03G0150A to GEOMAR within the continued and generous most commendable support for marine sciences with R/V SONNE.

We most warmly thank master H. Papenhagen and his crew for their excellent support in all work done and for the splendid and efficient working atmosphere throughout the entire highly ambitious working program.

8. REFERENCES

Bialas J, Flueh ER (1999): Ocean Bottom Seismometers; Sea Technology, 40, 4, 41-46.

Blondel P, Murton BJ (1997): Handbook of Seafloor Sonar Imagery, John Wiley and Sons, Chichester, 314.

Bohlen T, Klein G, Duveneck E, Milkereit B, Franke D (1999): Analysis of dispersive seismic surface waves in submarine permafrost, EAGE Abstract, Helsinki, pp. 4.

Bohrmann G, Greinert J, Suess E, Torres M (1998): Authigenic carbonates from the Cascadia subduction zone and their relation to gas hydrate stability, Geology, v. 26, p. 647-650.

Bohrman G, Linke P, Suess E, Pfannkuche O (1999): FS Sonne Fahrtbericht/Cruise Report SO143 TECFLUX, Geomar Report 93, ISSN 0936-5788, 243pp

Brandon MT, Roden-Tice MK, Garver JI (1998): Late Cenozoic exhumation of the Cascadia accretionary wedge in the Olympic Mountains, northwest Washington State, GSA Bulletin, v. 110, 985-1009.

Brown, K.M (1990): The nature and hydrogeologic significance of mud diapirs and diatremes for accretionary systems. J. Geophys. Res. 95, 8969-8982.

Carcione JM, Tinivella U (2000): Bottom-simulating reflectors: Seismic velocities and AVO effects, Geophysics, v. 65, no. 1, 54-67.

Caress DW, Chayes DN (1996): Improved processing of Hydrosweep DS Multibeam Data on the R/V Marice Ewing. Mar. Geophys. Res., 18: 631-650.

Claypool GE, Kaplan IR (1974): The origin and distribution of methane in marine sediments. In: Kaplan, I.R. (Ed.), Natural Gases in Marine Sediments, New York (Plenum), 99–139.

Clennell MB, Hovland M, Booth JS, Henry P, and Winters WJ (1999): Formation of natural gas hydrates in marine sediments. Part 1: Conceptual model of gas hydrate growth conditioned by host sediment properties. J. Geophys. Res., 104, 22985-23003

Deyhle, A., Kopf, A., and Eisenhauer, A., in press. Boron systematics of authigenic carbonates: A new approach to identify fluid processes in accretionary prisms. Earth Planet. Sci. Letts.

Dickens GR, Quinby-Hunt MS (1997): Methane hydrate stability in pore water: A simple theoretical approch for geophysical applications. J. Geophys. Res. 102, p.773-785.

Dillon WP, Paull CK (1983): Marine gas-hydrates: II Geophysical evidence. In: Cox JL (eds) Natural gas hydrates, properties, occurrence and recovery, p.73-90.

Duncan RA, Kulm LD (1989): Plate tectonic evolution of the Cascades arc-subduction complex. In: Winterer EL, Hussong DM, Decker RW (eds). The Eastern Pacific Ocean and Hawaii. Geol. Soc. Am., p. 413-438.

Ecker C (1998): Seismic characterisation of methane hydrate structures, Ph.D thesis, Stanford University.

Ecker C, Dvorkin J, Nur AM (2000): Estimating the amount of gas hydrate and free gas from marine seismic data, Geophysics 65,2,565-573.

Erickson SN, Jarrard RD (1998): Velocity-porosity relationships for water-saturated siliciclastic sediments, J. Geophys. Res., v. 103, no. B12, p. 30385-30406.

Flueh ER (1995): Cruise Report SO103, Condor 1B; Geomar Report 41, Kiel, 140 pp.

Flueh ER, Bialas J (1996): A digital, high data capacity ocean bottom recorder for seismic investigations; Int. Underwater Sytems Design, 18(3), 18-20.

Flueh ER, Fisher MA (1996): FS-Sonne-FAhrtbrricht/Cruise Report SO108 ORWELL; GEOMAR Report 49, 252pp.

Gerdom M, Trehu AM, Flüh ER, Klaeschen D (2000): The continental margin off Oregon from seismic investigations, Tectonophysics, in press.

Goldfinger C (1994): Active deformation of the Cascadia forearc: Implications for great earthquake potential in Oregon and Washington, Ph.D. thesis, Oreg. State Univ., Corvallis.

Goldfinger C, Kulm LD, Yeats RS, Applegate B, MacKay M, Cochrane GR (1996): Active strike-slip faulting and folding of the Cascadia plate boundary and forearc in central and northern Oregon, in Assessing and Reducing Earthquake Hazards in the Pacific Northwest, edited by AM rodgers, TJ Walsh, WJ Kockelman, and G. Priest, U.S. Geol. Surv. Prof. Pap., 1560, 223-256.

Goldfinger C, Kulm LD, Yeats RS, Hummon C, Huftile GJ, Niem AR, Fox CG, McNeill LC (1997): Oblique strike-slip faulting of the Cascadia submarine forearc: The Daisy Bank fault zone off central Oregon, in Bebout GE, Scholl DW, Kirby SH, Platt JP, eds., Subduction top to bottom: American Geophysical Union, Geophysical Monograph 96, 65-74.

Greinert J, Bohrmann G, Suess E (2000): Gas Hydrate-Associated Carbonates and Methane-Venting at Hydrate Ridge: Classification, Distribution, and Origin of Authigenic Lithologies, edited by Paull CK and Dillon W, Distribution, and Dynamics, American Geophysical Union, Monograph Series, Washington.

Henry P, Thomas M, and Clennell MB (1999): Formation of natural gas hydrates in marine sediments. Part 2: Thermodynamic calculations. J. Geophys. Res., 104, 23005-23022

Herzig P, Suess E, Linke P (1997): Cruise Report SO109: Hydrotrace; GEOMAR Report 58, 249pp.

Hesse R, Lebel J, and Gieskes JM (1985): Interstitial water chelmistry of gas-hydrate-bearing sections on the middle America trench slope. In: , Proc. DSDP, 84, Washington DC (US Govt. Printing Office), 727-737.

Hobro JW, Minshull TA, Singh SC (1998): Tomographic seismic studies of the methane hydrate stability zone in Cascadia Margin. In: Henriet JP & Minert J (eds) Gas Hydrates: Revevance to World Margin Stability and Climate Change. Geological Society, London, Special Publications, 137, 133-140.

Hojka AM (1998): Zweidimensionale und dreidimensionale refraktionsseismische Untersuchungen an der chilenischen Subduktionszone bei 32° S, Dissertation, GEOMAR-Universität Kiel, pp. 124.

Holbrook WS, Hoskins H, Wood WT, Stephen RA, Lizarralde D (1996): Methane hydrate and free gas on the Blake ridge from vertical seismic profiling, Science 273, p. 1840-1843.

Hovland M, Judd A (1988): Seabed Pockmarks and Seepages, New York (Trottman).

Hyndman RD, Davis EE (1992): A mechanism for the formation of methane hydrate and seafloor bottom simulating reflectors by vertical fluid expulsion. Jour. Geophys. Res. 97 (B5), p. 7025-7041.

Klaeschen D, Adam J, Kukowski N, Flüh ER (1999): Seismische Methoden für die Untersuchung von Akkretionskeilen und deren Deformationsverhalten am Beispiel der Cascadia-Subduktionszone. Statusseminar 1999, Meeresforschung mit FS Sonne, Freiberg, Tagungsband, p. 59-61.

Knickmeyer ET (1996): Hochgenaues Differential-GPS, Proc. 11th Annual Meeting of the German Hydrographic Society, Glücksburg, 3.-5.6.

Kopf A, Deyhle A, and Zuleger E (2000): Evidence for deep fluid circulation and gas hydrate dissociation using boron and boron isotopes in forearc sediments from Costa Rica (ODP Leg 170). Marine Geology 167, p. 1-28.

Kvenvolden KA (1988): Methane hydrate - a major reservoir of carbon in he shallow geosphere?, Chem. Geol., 71, 41-51.

Kvenvolden KA (1993): Gas hydrates, Geological perspective and global change, Rev., Geophys., 31, 173 -183.

Lee MW, Hutchinson DR, Miller JJ, Agena WF, Swift BA (1993): Method of estimating the amount of in situ gas hydrates in deep marine sediments. Marine and Petroleum Geology 10, p. 493-506.

Lee MW, Hutchinson DR, Collet TS, Dillon WP (1996): Seismic velocities for hydrate-beating sediments using weighted equation. Jour. Geophys. Res. 101 (B9), p. 20347-20358.

Lelgemann H, Kläschen D, IMERSE Working Group (1999): AVA analysis in the eastern Mediterranean, Physics and Chemistry of the Earth (A), Vol. 24, No. 5, p. 467-474.

Linke P, Pfannkuche O, Torres ME, Collier RW, Witte U, McManus J, Hammond DE, Brown KM, Tryon MD, Nakamura K (1999): Variability of Benthic Flux and Discharge Rates at Vent Sites Determined by in Situ Instruments, AGU Fall Meeting 1999 in San Francisco, Poster OS21B-01.

MacKay ME (1995): Structural variation and landward vergence at the toe of Oregon accretionary prism, Tectonics, 14, p. 1309-1320.

MacKay ME, Moore GF, Cochrane GR, Moore JC, Kulm LD (1992): Landward vergence and oblique structural trends in the Oregon margin accretionary prism: Implications for fluid flow, Earth Planet, Sci. Lett., v. 109, p. 477-491.

MacKay ME, Jarrad RD, Westbrook GK, Hyndman RD, and the Shipboard Scientific Party of ODP leg 146 (1994): Origin of bottom simulating reflectors: geophysical evidence from the Cascadia accretionary prism, Geology, V. 22, p. 459-462.

Murphy WF, III (1984): Acustic measures of partial gas saturation in tight sandstones, Jour. Geophys. Res., v. 89, p.11,549-11,559.

Orange, DL (1990): Criteria helpful in recognizing shear-zone and diapiric mélanges: Examples from the Hoh accretionary complex, Olympic Peninsula, Washington. GSA Bull., 102: 935-951.

Pearson CF, Halleck PM, McGulre PL, Hermes R, Mathews M (1983): Natural gas hydrates; a review of in situ properties, J. Phys. Chem. 87, 4180-4185.

Pecher IA, Minshull TA, Singh SC, von Huene R (1996): Velocity structure of a bottom simulating reflector offshore Peru: Results from full waveform inversion, Earth and Planetary Science Letters, V. 139, p. 459-469.

Pecher IA, Ranero CR, von Huene R, Minshull TA, Singh SC (1998): The nature and distribution of bottom simulating reflectors at the Costa Rica convergent margin. Geophys. J. Int., 133, 219-229.

Riddihough RP (1984): Recent movements of the Juan de Fuca plate system. Jour. Geophys. Res., 89, p. 6980-6994.

Sample JC, Kopf A (1995): Geochemistry of syntectonic carbonate cements and veins from the Oregon margin (ODP Leg 146), Implications for hydrogeologic evolution of the accretionary wedge. In: B. Carson, G.K Westbrook, R.J. Musgrave, et al., Proc. ODP, Sci. Results, 146, College Station, TX (Ocean Drilling Program), 137-148

Schreiber R, Schencke HW (1990): Efficient hydrographic surveying of EEZ with new multibeam echosounder technology for shallow and deep water, Ocean resources, 1, 73-87.

Seeber G (1996): Stand und Einsetzungsmöglichkeiten von GPS – ein Überblick, Proc. 11th Annual Meeting of the German Hydrographic Society, Glückburg, 3.-5.6.

Seely DR (1977): The significance of landward vergence and oblique structural trends on trench inner slopes, in Island arcs, deep sea trenches and back-arc basins, Talwani M (ed), AGU, Washington, D.C.

Shipboard Scientific Party, Site 892 (1994): in G.K. Westbrook, B. Carson, R. J. Musgrove, et al., Proc. Ocean Drill. Program, Initial Rep., part 1, 146: College Station, TX (Ocean Drilling Program), 234-300.

Shipley TH, Houston MH, Buffler RT, Shaub FJ, McMillen KJ, Ladd JW, Worzel JL (1979): Seismic evidence for widespread possible gas hydrate horizons on continental slope and rises. Am.Assoc. Petrol. Geol. Bull. 63, p. 2204-2213.

Sloan ED (1990, a): Hydrate nucleation from ice: Proceedings of the 69th Annual Gas Proceedings Conference, Phoenix, AZ,8.

Sloan ED (1990, b): Clathrate Hydrates of Natural Gases, New York (Marcel Decker), 641pp

Stoll RD, Bryan GM (1979): Physical Properties of Sediments Containing Gas Hydrates. Journal of Geophysical Research 84(B4), 1629-1634.

Suess E, Bohrmann G (1997): RV SONNE - Cruise Report SO110; GEOMAR Report 59, 181pp.

Tréhu AM, Bangs N (2000): Report of Cruise TNN112 R/V Thomas Thompson June 19 - July 2, 2000, Oregon State University Data Report.

Tréhu AM, Lin G, Maxwell E, Goldfinger C (1995): A seismic reflection profile across the Cascadia subduction zone offshore central Oregon: new constraints on the deep crustal structure and or the distribution of methane in the accretionary prism. Jour. Geophys. Res. 100, p. 15101-15116.

Tréhu AM, Torres M, Moore G, Suess E, Bohrmann G (1999): Dissociation of gas hydrates in response to slumping and folding on the Oregon continental margin. Geology 27, p. 939-942.

von Huene R, Flueh ER (1994): A review of geophysical studies along the Middle America Trench off Costa Rica and the problematic seaward terminus of continental crust; In: H. Seyfried and W. Hellmann (Eds.): Geology of an Evolving Island Arc - The Isthmus of Southern Nicaragua, Costa Rica, and Western Panama., Profil 7, Stuttgart, 143-159.

Wallon Pizarro HU (1997): Bearbeitung eines reflexionsseismischen Profils am aktiven Kontinentalrand vor Oregon, USA, Diplomarbeit, GEOMAR- Universität Kiel.

Weinrebe W (1997): Fahrtbericht SO-112 HIRESBAT, GEOMAR-Report 64, GEOMAR-Kiel.

Wessel P, Smith WHF (1995): New Version of the Generic Mapping Tools (GMT) released. EOS Trans. AGU, 76: 329.

Westbrook GK, Carson B, Musgrave RJ et al. (1994): Site 892 in: Proceedings of the Ocean Drilling Program, Initial Reports, Vol. 146 (Part 1), p. 301-376.

Yuan T, Hyndeman R, Spence G, Desmons B (1996): Seismic velocity increase and deep-sea gas hydrate concentration above a bottom-simulating reflector on the Northern Cascadia continental slope. J. Geophys. Res., 101, 13655-13671.

Zhang W, Durham WB, Stern LA, Kirby SH (1999): Experimental deformation of methane hydrate. EOS Trans. AGU, 80/47 (Supplement): S338.

9. APPENDICES

9.1 DETAILS OF OBH/S DEPLOYMENTS

HYDGAS SO-150: Profile 1-5:

INSTRUMENT	LAT (N)	LON (W)	DIST. TO	DEPTH	RELEASER-	ANT.	RECORDER	SKEW	REMARKS
	D:M	D:M	NEXT (nm)	(m)	CODE	CH.	NUMBER	(ms)	
OBH01	44 : 40,601	125 : 07,109		680	d629	D	991202	-1	140 MB
OBS02	44 : 40,499	125 : 07,098		677	c444	C	971202	0	1 GB
OBH/DPG03	44 : 40,399	125 : 07,110		673	c679	C	000711	0	18 MB

HYDGAS SO-150: Profile 11-21:

INSTRUMENT	LAT (N)	LON (W)	DIST. TO	DEPTH	RELEASER-	ANT.	RECORDER	SKEW	REMARKS
	D:M	D:M	NEXT (nm)	(m)	CODE	CH.	NUMBER	(ms)	
OBH/DPG4	44 : 35,141	125 : 10,918		1179	d629	C	000711	1	DPG; no recording
OBH5	44 : 35,141	125 : 10,780	0,11	1167	C679	D	980902	2	ok
OBH6	44 : 35,142	125 : 10,617	0,11	1134	4949	C	980901	19	ok
OBH7	44 : 35,137	125 : 10,473	0,11	1122	C459	D	980906	-88	single window 1kHz; ok
OBH8	44 : 35,141	125 : 10,300	0,11	1090	6969	C	980904	-220	50m above seabottom; only profile11recorded
OBS9	44 : 35,142	125 : 10,147	0,11	1056	C444	D	000612	10	no coupling with seabottom
OBS10	44 : 35,147	125 : 10,075	0,11	1037	4979	C	971202	1	no coupling with seabottom
OBS11	44 : 35,139	125 : 09,848	0,11	998	4A49 ModeB	D	000610	8	no coupling with seabottom
OBS12	44 : 35,138	125 : 09,710	0,11	977	d654	C	980401	-8	battery low; otherwise ok
OBH13	44 : 35,150	125 : 09,553	0,11	961	5924	D	000614	6	50m above seabottom; ok
OBH14	44 : 35,151	125 : 09,427	0,11	941	B495	C	000613	12	ok
OBH15	44 : 35,160	125 : 09,273	0,11	921,7	6A24	D	991202	-2	ok
OBH/DPG16	44 : 35,146	125 : 09,119	0,11	901	5929	C	000708	-6	DPG; ok
OBH/DPG17	44 : 35,148	125 : 08,951	0,11	878,3	6959	C	000709	-1	DPG; ok

HYDGAS SO-150: Profile 61-71:

INSTRUMENT	LAT (N)	LON (W)	DIST. TO	DEPTH	RELEASER-	ANT.	RECORDER	SKEW	REMARKS
	D:M	D:M	NEXT (nm)	(m)	CODE	CH.	NUMBER	(ms)	
OBH/DPG18	44 : 35,144	125 : 07,557	0,11	905	D629	D	000709	-6695	message resume recording
OBH19	44 : 35,139	125 : 07,410	0,11	904	C679	C	991202	-3	ok
OBH20	44 : 35,143	125 : 07,260	0,11	905	4949	D	990712		50m rope ; no connection to recorder
OBS21	44 : 35,145	125 : 07,097	0,11	909	4979	C	971202	0	ok
OBS22	44 : 35,147	125 : 06,941	0,11	924	4A49 ModeB	D	980401	-6	ok
OBH23	44 : 35,148	125 : 06,798	0,11	946	C459	C	980902	1	resuming recording during skew
OBH24	44 : 35,147	125 : 06,642	0,11	974	6969	D	000614	5	o.k.
OBH25	44 : 35,147	125 : 06,500	0,11	991	5924	C	980901	16	o.k.
OBS26	44 : 35,145	125 : 06,360	0,11	1008	C444	D	000612	8	o.k.
OBS27	44 : 35,140	125 : 06,180	0,11	1022	d654	C	000610	8	o.k.
OBH28	44 : 35,144	125 : 06,050	0,11	1030	B495	D	000613	10	50m rope
OBH29	44 : 35,139	125 : 05,900	0,11	1040	6A24	C	991292	-1	ok
OBH/DPG30	44 : 35,150	125 : 05,746	0,11	1048	5929	C	000711	1	DPG; ok
OBH/DPG31	44 : 35,146	125 : 05,605	0,11	1055	6959	C	000708	-6	DPG; ok

HYDGAS SO-150: Profile 101-113:

INSTRUMENT	LAT (N)	LON (W)	DIST. TO	DEPTH	RELEASER-	ANT.	RECORDER	SKEW	REMARKS
	D:M	D:M	NEXT (nm)	(m)	CODE	CH.	NUMBER	(ms)	
OBH/DPG32	44 : 40,518	125 : 08,016		755	d629	C	000711	0	42 MB
OBH33	44 : 40,497	125 : 07,853	0,11	729	C679	D	980902	3	297 MB
OBS34	44 : 40,502	125 : 07,092	0,11	705	4A49 ModeB	C	000612	9	846 MB
OBS35	44 : 40,490	125 : 07,550	0,11	692	4979	C	000610	10	3k not released; 846 MB
OBH36	44 : 40,500	125 : 07,410	0,11	683	4949	D	991292	-1	Rec.-LED not flashing; rec. program not started
OBH37	44 : 40,500	125 : 07,260	0,11	688	C459	C	980901	17	273 MB
OBH38	44 : 40,490	125 : 07,110	0,11	681	6969	D	991202	1	Rec.-LED not flshng.; rec. Prog. not started;50m rope
OBH39	44 : 40,500	125 : 06,960	0,11	664	5924	C	000614	6	307 MB
OBH40	44 : 40,500	125 : 06,800	0,11	659	B495	D	990712	1	Rec.-LED not flashing; rec. program not started
OBS41	44 : 40,490	125 : 06,640	0,11	657	C444	C	980401	-7	873 MB
OBS42	44 : 40,510	125 : 06,490	0,11	658	D654	D	971202	1	876 MB; 30Hz Geophon
OBH43	44 : 40,500	125 : 06,340	0,11	648	6A24	D	000613	11	326 MB
OBH/DPG44	44 : 40,500	125 : 06,210	0,11	644	5929	C	000708	-7	42 MB
OBH/DPG45	44 : 40,490	125 : 06,060	0,11		6959	C	000709	-4	42 MB

HYDGAS SO-150: Profile 131-133:

INSTRUMENT	LAT (N)	LON (W)	DIST. TO	DEPTH	RELEASER-	ANT.	RECORDER	SKEW	REMARKS
	D:M	D:M	NEXT (nm)	(m)	CODE	CH.	NUMBER	(ms)	
OBH/DPG46	44 : 40,500	125 : 07,110		650	6959	C	000708	-3	DPG; ok
OBH/DPG47	44 : 40,500	125 : 06,950	0,11	662	6969	C	980902	1	DPG; ok
OBS48	44 : 40,490	125 : 06,800	0,32	657	C444	D	980401	-2	ok

HYDGAS SO-150: Profile 141-151:

INSTRUMENT	LAT (N)	LON (W)	DIST. TO	DEPTH	RELEASER-	ANT.	RECORDER	SKEW	REMARKS
	D:M	D:M	NEXT (nm)	(m)	CODE	CH.	NUMBER	(ms)	
OBS49	44 : 40,425	125 : 07,026		669,6	d654	D	000612	8	868 MB; 30 Hz sensor
OBS50	44 : 40,493	125 : 07,173	0,21	688	C444	C	971202	1	LED not flashing; main started on PC connect; 0 MB
OBS51	44 : 40,696	125 : 07,094	0,40	696	4A49 ModeB	D	000610	9	882 MB
OBS52	44 : 40,304	125 : 07,112	0,26	671	4979	C	980401	-6	848 MB
OBH53	44 : 40,500	125 : 07,330	0,11	683	146-16	D	000616	-3	294 MB
OBH54	44 : 40,497	125 : 07,478	0,43	687	146-14	C	980902	2	message resume rec.; 226 MB
OBH55	44 : 40,493	125 : 06,880	0,11	658	4949	D	000613	10	282 MB
OBH56	44 : 40,490	125 : 06,719	0,37	658,4	C679	C	991292	-1	LED not flashing; main started on PC connect; 0 MB
OBH57	44 : 40,495	125 : 06,205	0,11	643	6A24	C	980901	14	270 MB
OBH58	44 : 40,501	125 : 06,053	1,39	632	B495	C	991202	-1	287 MB
OBH59	44 : 40,509	125 : 08,003	2,32	751	5.924	C	000614	6	267 MB

HYDGAS SO-150: Profile 171-181:

INSTRUMENT	LAT (N)	LON (W)	DIST. TO	DEPTH	RELEASER-	ANT.	RECORDER	SKEW	REMARKS
	D:M	D:M	NEXT (nm)	(m)	CODE	CH.	NUMBER	(ms)	
OBH60	44 : 35,157	125 : 10,894		1181	5924	D	000614	4	217 MB; 250 m Seil
OBS61	44 : 35,165	125 : 10,139	0,54	1064	C444	C	971202	1	709 MB
OBS62	44 : 35,148	125 : 09,990	0,11	1032	d654	D	000610	7	738 MB; 30 Hz sensor
OBS63	44 : 35,152	125 : 09,848	0,11	1005	4979	C	980401	-5	723 MB
OBH64	44 : 35,140	125 : 09,708	0,11	982	6969	D	000616	-3	225 MB
OBH65	44 : 35,138	125 : 09,081	0,43	900	c459	C	980902	2	180 MB; 250 m Seil
OBH66	44 : 35,148	125 : 07,244	1,32	907	4949	D	991202	-2	226 MB; 250 m Seil
OBH67	44 : 35,156	125 : 07,096	0,11	910	C679	C	980904	-169	400 MB; nur HF (Gent)
OBS68	44 : 35,153	125 : 06,949	0,11	924	4A49 (B)	D	000610	8	753 MB
OBH69	44 : 35,151	125 : 06,349	0,43	1007	6A24	C	000613	9	246 MB
OBH70	44 : 35,144	125 : 06,208	0,11	1019	B495	C	980901	14	B

9.2 DETAILS OF SOURCES, RECEIVERS, AND PROFILE NUMBERS

Profile name	Source	Receiver	Geomar profile	Shoot. rate (sec)	Start time	End time	DATE	Shot number
OREG0001	Watergun	OBH, DT (meth)	Profile 1	5	06:17	10:16	21	?
OREG0002	Gun array	OBH, DT (meth)	Profile 2	10	10:55	13:34	21	?
OREG0003	GI-gun	OBH, DT (meth), Geo SS	Profile 3	10	14:13	17:40	21	?
OREG0004	GI-gun	OBH, DT (meth), Geo SS	Profile 4	10	20:09	20:31	21	?
OREG0005	Airgun	OBH, DT(meth), SIG-SS	Profile 5	10 then 30	00:06:21	02:00:05	22	229
OREGSS06	GI-gun	DT (meth), SIG-SS		10	00:33:50	01:32:50	23	355
OREGSS06a	GI-gun	DT (meth), SIG-SS		10	01:34:40	02:13:30	23	234
OREGSS07	Watergun	OBH, DT (meth), SIG-SS, Geo SS	Profile 11	10	18:34:50	21:30:31	23	1057
OREGSS08	Gun array	OBH, DT (meth), SIG-SS, Geo SS	Profile 12	10	23:37:00	03:48:50	24	1512
OREGSS09	GI-gun	OBH, DT (meth), SIG-SS, Geo SS	Profile 13	7	05:04:55	09:53:54	24	2478
OREGSS10	GI-gun	OBH, DT (meth), SIG-SS, Geo SS	loop	7	09:55:40	10:32:44	24	319
OREGSS11	GI-gun	OBH, DT (meth), SIG-SS, Geo SS	Profile 14	7	10:34:12	12:38:04	24	1062
OREGSS12	GI-gun	OBH, DT (meth), SIG-SS, Geo SS	Profile 15	7	12:41:26	15:06:06	24	1241
OREGSS13	GI-gun	OBH, SIG-SS, Geo SS	Profile 16	7	18:35:43	20:56:06	24	1205
OREGSS15	GI-gun	OBH, SIG-SS, Geo SS	Profile 17	7	21:25	23:08	24	896
OREGSS16	GI-gun	OBH, DT (test), SIG-SS, Geo SS	Profile 18	7	23:27	01:18	24-25	951
OREGSS17	GI-gun	OBH, SIG-SS, Geo SS	Profile 19	7	01:33	03:28	25	987
OREGSS18	GI-gun	OBH, SIG-SS, Geo SS	Profile 20	7	03:36	05:51	25	1163
OREGSS19	Bolt Gun	OBH, SIG-SS, Geo SS	Profile 21	17	07:10:24	13:53:02	25	1446-64
OREGSS20	Sparker	SIG-SS, Geo SS	Profile 31	3	21:22:53	00:32:26	25-26	3792
OREGSS20B	Sparker	SIG-SS, Geo SS	Profile 31	5	00:41:47	01:43:14	26	734
OREGSS21	Sparker	DT (test), SIG-SS, Geo SS	Profile 32	5	01:59:47	02:41:59	26	507
OREGSS21B	Sparker	DT (test), SIG-SS, Geo SS	Profile 32	5	03:38:24	04:44:54	26	799
OREGSS22	Sparker	SIG-SS, Geo SS	Profile 33	3	04:47:27	05:48:59	26	1232
OREGSS23	Sparker	SIG-SS, Geo SS	Profile 34	3	05:50:36	06:48:47	26	1164
OREGSS24	Sparker	SIG-SS, Geo SS	Profile 35	3	06:50:07	08:05:32	26	1509
OREGSS25	Sparker	SIG-SS, Geo SS	Profile 36	3	08:07:11	09:03:50	26	1134
OREGSS26	Sparker	SIG-SS, Geo SS	Profile 37	3	09:04:59	09:55:53	26	1019
OREGSS27	Sparker	SIG-SS, Geo SS	Profile 38	3	09:57:18	10:43:41	26	928
OREGSS28	Sparker	SIG-SS, Geo SS	Profile 39	3	10:44:44	11:51:32	26	1337
OREGSS29	Sparker	SIG-SS, Geo SS	Profile 40	3	11:54:28	12:48:13	26	1076
OREGSS30	Sparker	SIG-SS, Geo SS	Profile 41	3	12:51:56	14:02:26	26	1411
OREGSS31	Sparker	SIG-SS, Geo SS	Profile 42	3	14:07:16	14:53:59	26	935
OREGSS32	Sparker	SIG-SS, Geo SS	Profile 43	3	15:13:28	18:09:59	26	3531
OREGSS33	Sparker	SIG-SS, Geo SS	Profile 44	3	18:11:07	19:47:44	26	1933
OREGSS34	Sparker	SIG-SS, Geo SS	Profile 45	3	19:58:03	20:35:20	26	747
-	Sparker	Geo SS	Profile 46	3	?	?	26	?
OREGSS35	Sparker	SIG-SS, Geo SS	Profile 47	3	21:48:04	01:04:14	26-27	3924
OREGSS36	Sparker	DT (test), SIG-SS, Geo SS	Profile 50	3	01:58:46	03:59:47	27	2421
OREGSS37	Sparker	DT (test), SIG-SS, Geo SS	Profile 51	3	04:43:52	05:07:44	27	478
OREGSS37B	Sparker	DT (test), SIG-SS, Geo SS	Profile 51	3	05:08:28	05:16:17	27	157
OREGSS37C	Sparker	DT (test), SIG-SS, Geo SS	Profile 51	3	05:18:12	07:27:20	27	2583
OREGSS38	Sparker	SIG-SS, Geo SS	Profile 52	3	08:08:09	09:55:23	27	2145
OREGSS39	Sparker	SIG-SS, Geo SS	Profile 53	3	10:05:19	10:43:21	27	762
OREGSS40	Sparker	SIG-SS	Profile 54	3	14:21:23	15:18:56	27	1152

OREGSS41	Sparker	SIG-SS	Profile 55	3	15:20:27	16:11:08	27	1014
OREGSS42	Sparker	SIG-SS	Profile 56	3	16:12:27	17:47:17	27	1897
OREGSS43	Sparker	SIG-SS	Profile 57	3	17:48:22	18:35:27	27	942
OREGSS44	Sparker	SIG-SS	Profile 58	3	18:46:19	19:35:03	27	975
OREGSS45	Sparker	OBH, SIG-SS, Geo SS	Profile 61	3	20:42:18	23:07:53	27	2912
OREGSS46	Gun array	OBH, DT, SIG-SS, Geo SS	Profile 62	10	00:41:20	00:43:40	28	15
OREGSS46B	Gun array	OBH, DT, SIG-SS, Geo SS	Profile 62	10	00:44:26	00:57:40	28	80
OREGSS46C	Gun array	OBH, DT, SIG-SS, Geo SS	Profile 62	10	00:58:24	04:59:00	28	1444
OREGSS47	GI-gun	OBH, DT, SIG-SS, Geo SS	Profile 63	7	05:50	11:30	28	2920
OREGSS48	GI-gun	OBH, SIG-SS, Geo SS	Profile 64	7	11:38:16	14:00:30	28	1221
OREGSS49	GI-gun	OBH, SIG-SS, Geo SS	Profile 65	7	14:08:36	14:12:36	28	35
OREGSS49B	GI-gun	OBH, SIG-SS, Geo SS	Profile 65	7	14:14	15:55	28	870
-	Watergun	OBH, Geo SS	Profile 66	5	?	?	28	?
-	GI-gun	OBH, Geo SS	Profile 67	7	?	?	28	?
OREGSS50	GI-gun	OBH, SIG-SS, Geo SS	Profile 68	7	20:53:56	22:55:23	28	1042
OREGSS51	GI-gun	OBH, SIG-SS, Geo SS	Profile 69	7	23:09:44	00:56:10	28-29	914
OREGSS52	GI-gun	OBH, SIG-SS, Geo SS	Profile 70	7	00:57:45	03:32:55	29	1331
OREGSS53	Bolt Gun	OBH, DT, SIG-SS, Geo SS	Profile 71	17	04:22:50	11:39:27	29	1542
OREGSS54	GI Gun	DT, SIG-SS, Geo SS	Profile 81	7	19:12:59	20:16:10	29	542
OREGSS55	GI-gun	DT, SIG-SS, Geo SS	Profile 82	7	21:41:44	00:21:08	29-30	1367
OREGSS56	GI-gun	DT, SIG-SS, Geo SS	Profile 83	7	01:36:34	04:06:27	30	1285
OREGSS57	GI-gun	DT, SIG-SS	Profile 84	7	04:50:04	07:57:48	30	1610
OREGSS58	GI-gun	DT, SIG-SS	Profile 85	7	10:15:48	11:41:18	30	1027
OREGSS59	GI-gun	DT, SIG-SS	Profile 86	7	12:41:45	14:25:48	30	893
OREGSS60	GI-gun	SIG-SS	Profile 87	7	15:14:29	16:14:47	30	518
OREGSS61	GI-gun	SIG-SS	Profile 88	7	16:36:36	17:40:04	30	545
OREGSS62	GI-gun	SIG-SS	Profile 89	7	18:09:28	19:05:56	30	485
OREGSS63	GI-gun	SIG-SS	Profile 90	7	19:33:27	20:29:56	30	485
OREGSS64	GI-gun	SIG-SS	Profile 91	7	00:09:10	02:14:49	1	1078
OREGSS65	GI-gun	SIG-SS	Profile 92	7	02:45:37	03:50:08	1	554
OREGSS66	GI-gun	SIG-SS	Profile 93	7	03:52:07	05:03:44	1	615
OREGSS67	GI-gun	SIG-SS	Profile 94	7	05:05:15	06:21:13	1	652
OREGSS68	Watergun	OBH, SIG-SS, Geo SS	Profile 101	5	07:43:02	07:44:41	1	34
OREGSS69	Watergun	OBH, SIG-SS, Geo SS	Profile 101	5	07:45:26	07:48:17	1	58
OREGSS70	Watergun	OBH, SIG-SS, Geo SS	Profile 101	5	07:48:59	08:19:11	1	605
OREGSS71	Watergun	OBH, SIG-SS, Geo SS	Profile 101	5	08:19:49	09:57:15	1	1950
OREGSS72	Gun array	OBH, DT, SIG-SS, Geo SS	Profile 102	7	11:21	11:58	1	310
OREGSS72A	Gun array	OBH, DT, SIG-SS, Geo SS	Profile 102	7	12:00	13:02	1	543
OREGSS72B	Gun array	OBH, DT, SIG-SS, Geo SS	Profile 102	7	13:03:51	15:42:44	1	1362
OREGSS73	GI-gun	OBH, DT, SIG-SS, Geo SS	Profile 103	7	15:46:42	21:16:03	1	2824
OREGSS74	GI-gun	OBH, SIG-SS, Geo SS	Profile 104	7	22:19:09	00:37:17	1-2	1185
OREGSS75	GI-gun	OBH, SIG-SS	Profile 105	7	00:44:02	02:32:06	2	927
OREGSS76	GI-gun	OBH, SIG-SS	Profile 106	7	02:48:47	04:49:04	2	1032
OREGSS77	GI-gun	OBH, SIG-SS	Profile 107	7	05:04:09	07:03:20	2	1022
OREGSS78	GI-gun	OBH, SIG-SS	Profile 108	7	07:13:14	09:04:55	2	958
OREGSS79	GI-gun	OBH, SIG-SS	Profile 109	7	09:16:16	11:09:24	2	971
OREGSS80	GI-gun	OBH, SIG-SS	Profile 110	7	11:11:09	13:20:03	2	1106
OREGSS81	GI-gun	OBH, SIG-SS	Profile 111 - 112	7	13:21:13	18:23:59	2	2596
OREGSS82	Bolt Gun	OBH, DT, SIG-SS	Profile 113	17	20:16:45	03:11:49	2-3	1467
OREGSS83	GI-gun	DT, SIG-SS, Geo SS	Profile 121	7	09:48:20	13:37:48	3	1968
OREGSS84	GI-gun	DT, SIG-SS, Geo SS	Profile 122	7	14:55:03	18:10:14	3	1674
OREGSS85	GI-gun	DT, SIG-SS, Geo SS	Profile 123	7	18:50:56	22:08:50	3	1698
OREGSS86	GI-gun	DT, SIG-SS, Geo SS	Profile 124	7	22:48:10	02:25:22	3-4	1862
OREGSS87	GI-gun	DT, SIG-SS, Geo SS	Profile 125	7	03:06:28	07:30:06	4	2260
OREGSS88	GI-gun	DT,Geo SS	Profile 126	7	07:43:03	10:52:52	4	1628
OREGSS88a	GI-gun	DT,Geo SS	Profile 126	7	10:53:55	11:37:26	4	374
OREGSS89	GI-gun	DT,Geo SS	Profile 127	7	12:33:04	16:12:10	4	1880
-	Drop Weigth	OBH, Geo SS	Profile 131		-	-	?	?
OREGSS90	2 Bolt Gun	SIG-SS, Geo SS	Profile 132	30	01:18:22	06:43:21	5	651
OREGSS91	2 Bolt Gun	SIG-SS, Geo SS	Profile 133	30	07:13:37	12:39:22	5	653
OREGSS92	Watergun	SIG-SS	Profile 141	5	18:15:20	20:35:17	5	2800
OREGSS93	GI-gun	OBH, SIG-SS	Profile 142	7	21:46:30	01:49:13	5-6	2081
OREGSS94	Gun array	OBH, SIG-SS, Geo SS	Profile 143	10	01:50:23	07:05:20	6	1899
OREGSS95	GI-gun	OBH, SIG-SS, Geo SS	Profile 144	7	07:24:11	09:30:18	6	1082
OREGSS96	GI-gun	OBH, SIG-SS, Geo SS	Profile 145	7	09:35:54	11:36:18	6	1033
OREGSS97	GI-gun	OBH, SIG-SS, Geo SS	Profile 146	7	11:52:10	13:41:14	6	936
OREGSS98	GI-gun	OBH, SIG-SS, Geo SS	Profile 147	7	13:53:22	16:09:03	6	1164
OREGSS99	GI-gun	OBH, SIG-SS, Geo SS	Profile 148	7	16:27:45	18:21:22	6	975
OREGSS100	GI-gun	OBH, SIG-SS, Geo SS	Profile 149	7	18:36:24	20:36:09	6	1028
OREGSS101	GI-gun	OBH, SIG-SS, Geo SS	Profile 150	7	20:42:22	22:48:21	6	1081
OREGSS102	Bolt Gun	OBH, SIG-SS, Geo SS	Profile 151	17	23:08:21	03:33:09	6-7	396
OREGSS103	Sparker	(OBH), SIG-SS, Geo SS	Profile 161	3	05:00:52	07:01:08	7	2406
OREGSS104	Sparker	(OBH), SIG-SS, DT, Geo SS	Profile 162	3	08:13:32	08:45:56	7	649
OREGSS105	Sparker	(OBH), SIG-SS, DT, Geo SS	Profile 162	3	08:47:52	09:00:33	7	153
OREGSS105a	Sparker	(OBH), SIG-SS, DT, Geo SS	Profile 162	5	09:01:18	09:16:33	7	184

OREGSS105b	Sparker	(OBH), SIG-SS, DT, Geo SS	Profile 162	5	09:17:38	09:18:48	7	15
OREGSS105c	Sparker	(OBH), SIG-SS, DT, Geo SS	Profile 162	5	09:19:43	13:08:44	7	2749
OREGSS106	GI-gun	(OBH), SIG-SS, DT, Geo SS	Profile 163	7	13:28:29	14:30:23	7	531
OREGSS107	GI-gun	SIG-SS, DT	Profile 164	7	19:42	00:37	7-8	2527
OREGSS108	GI-gun	SIG-SS, DT	Profile 165	7	0:40	04:33	8	1997
OREGSS109	GI-gun	SIG-SS,DT	Profile 166	7	5:13	09:31	8	2208
OREGSS110	Sparker	OBH, SIG-SS, Geo SS	Profile 171	5	16:41:59	19:46:09	8	2211
OREGSS111	Gun array (6)	OBH, SIG-SS, Geo SS	Profile 172	10	21:16:17	02:32:10	8-9	1896
OREGSS112	GI-gun	OBH, SIG-SS, Geo SS	Profile 173	7	02:54:46	08:04:42	9	2658
OREGSS113	GI-gun	OBH, SIG-SS, Geo SS	Profile 174	7	08:13:27	10:15:22	9	1046
OREGSS114	GI-gun	OBH, SIG-SS, Geo SS	Profile 175	7	10:24:42	12:15:32	9	951
OREGSS115	GI-gun	OBH, SIG-SS, Geo SS	Profile 176	7	12:33:58	14:39:38	9	1078
OREGSS116	GI-gun	OBH, SIG-SS, Geo SS	Profile 177	7	15:12:21	16:58:14	9	908
OREGSS117	GI-gun	OBH, SIG-SS, Geo SS	Profile 178	7	17:12:21	19:02:43	9	947
OREGSS118	GI-gun	OBH, SIG-SS, Geo SS	Profile 179	7	19:21:41	21:26:17	9	1069
OREGSS119	GI-gun	OBH, SIG-SS, Geo SS	Profile 180	7	21:31:43	23:29:52	9	1013
OREGSS120	Bolt Gun	OBH, SIG-SS	Profile 181	17	23:54:48	05:13:34	9-10	1126
OREGSS121a	GI-gun	SIG-SS, DT	Profile 191	7	11:40:47	13:09:42	10	763
OREGSS121a	GI-gun	SIG-SS, DT	Profile 192	7	13:30:46	13:39:20	10	74
OREGSS122	GI-gun	SIG-SS, DT	Profile 193	7	14:03:37	15:02:14	10	504
OREGSS123	GI-gun	SIG-SS, DT	Profile 194	7	15:42:01	16:50:30	10	588

DT : Deeptow streamer (single channel – RCMG Gent) **Geo SS** : Multichannel surface streamer (3 channels – GEOMAR)
SIG-SS : Surface streamer (single channel – RCMG Gent) **OBH** : Ocean bottom hydrophone and seismometer (GEOMAR)

9.3 MAPVIEW OF PROFILES WITH DIFFERENT SOURCES

A map overview of the profiles shot with the different sources during the cruise SO-150 is displayed in Figures 9.3.1-9.3.5.

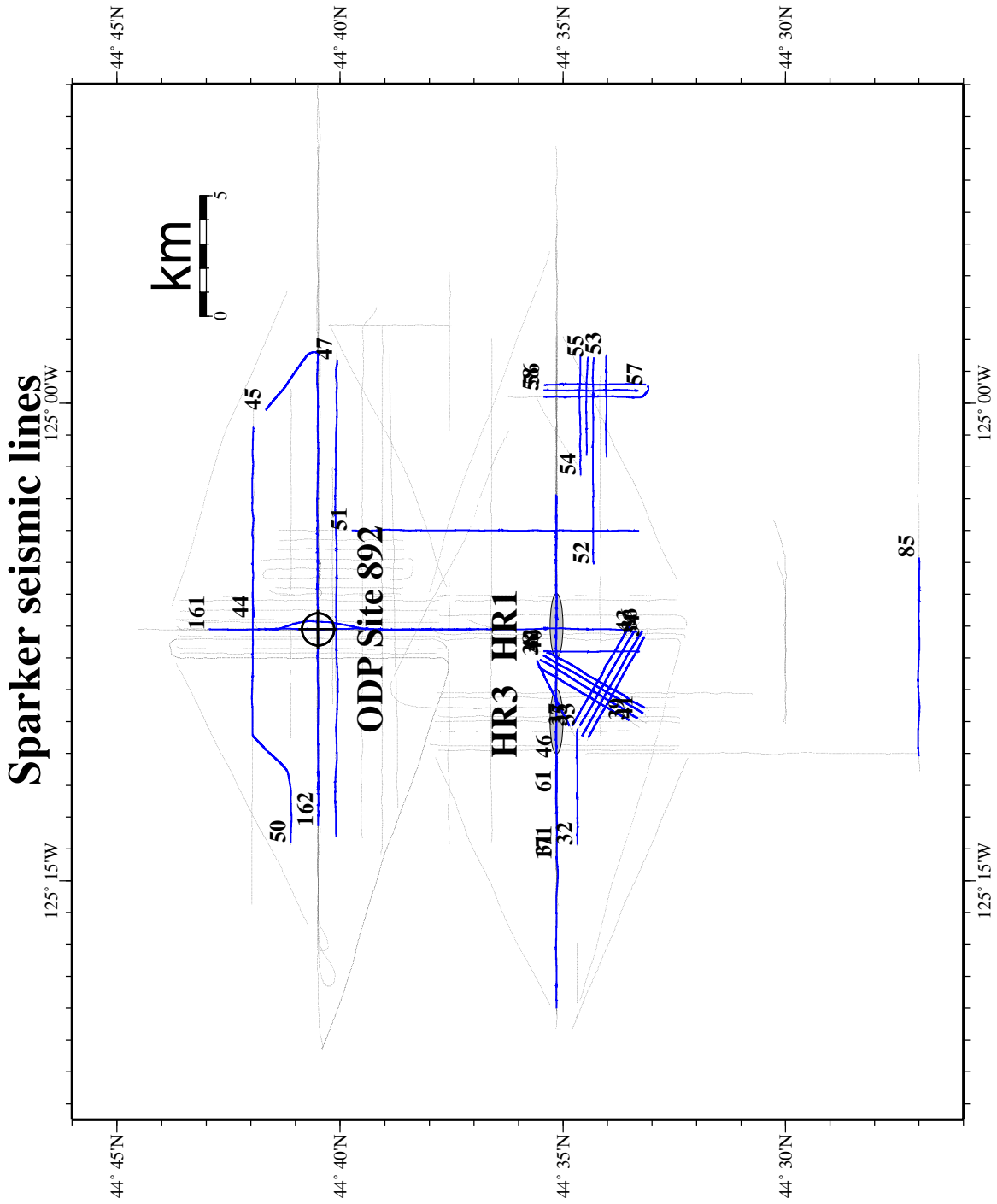

Figure 9.3.1: Location map of seismic lines shot with the Sparker.

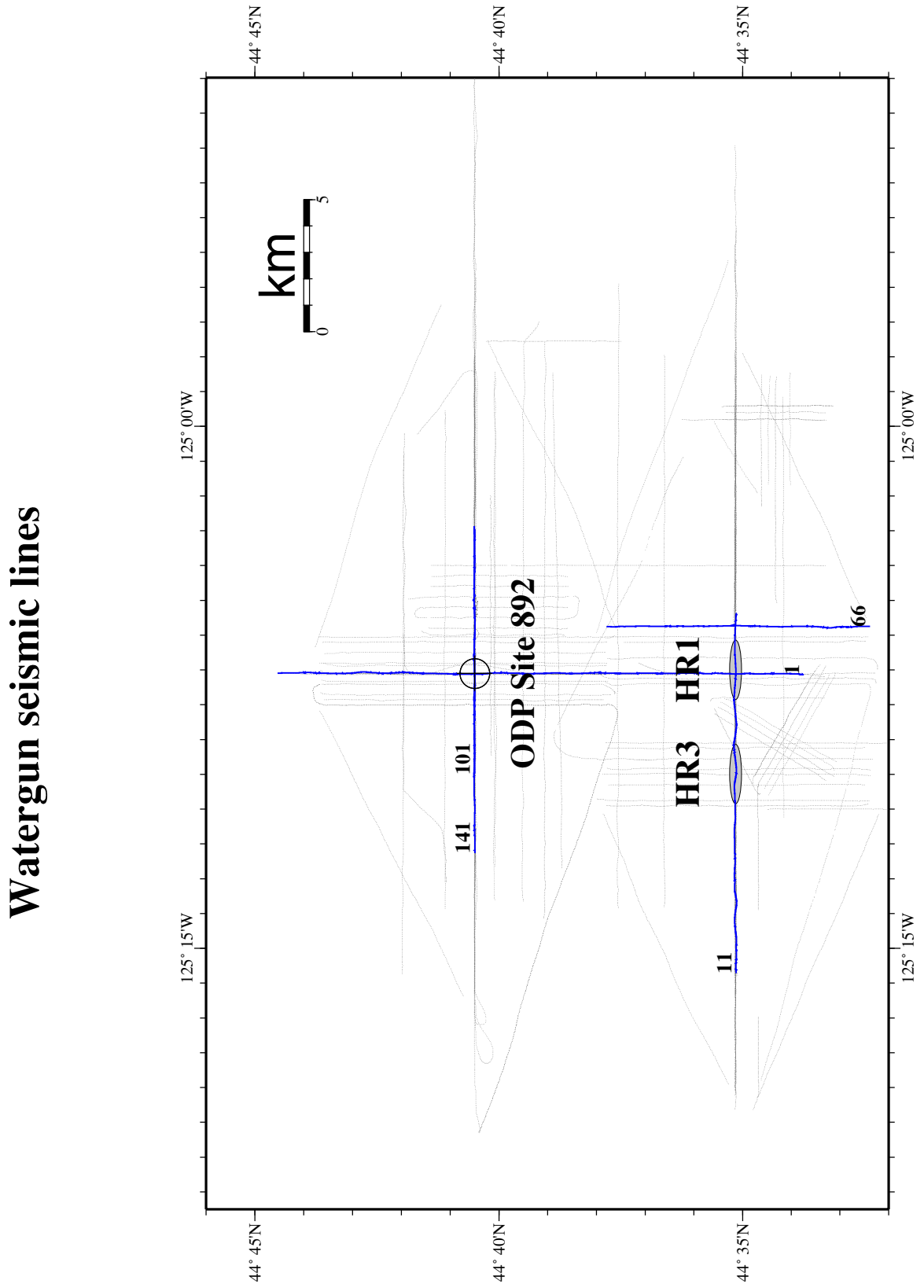

Figure 9.3.2: Location map of seismic lines shot with the Watergun.

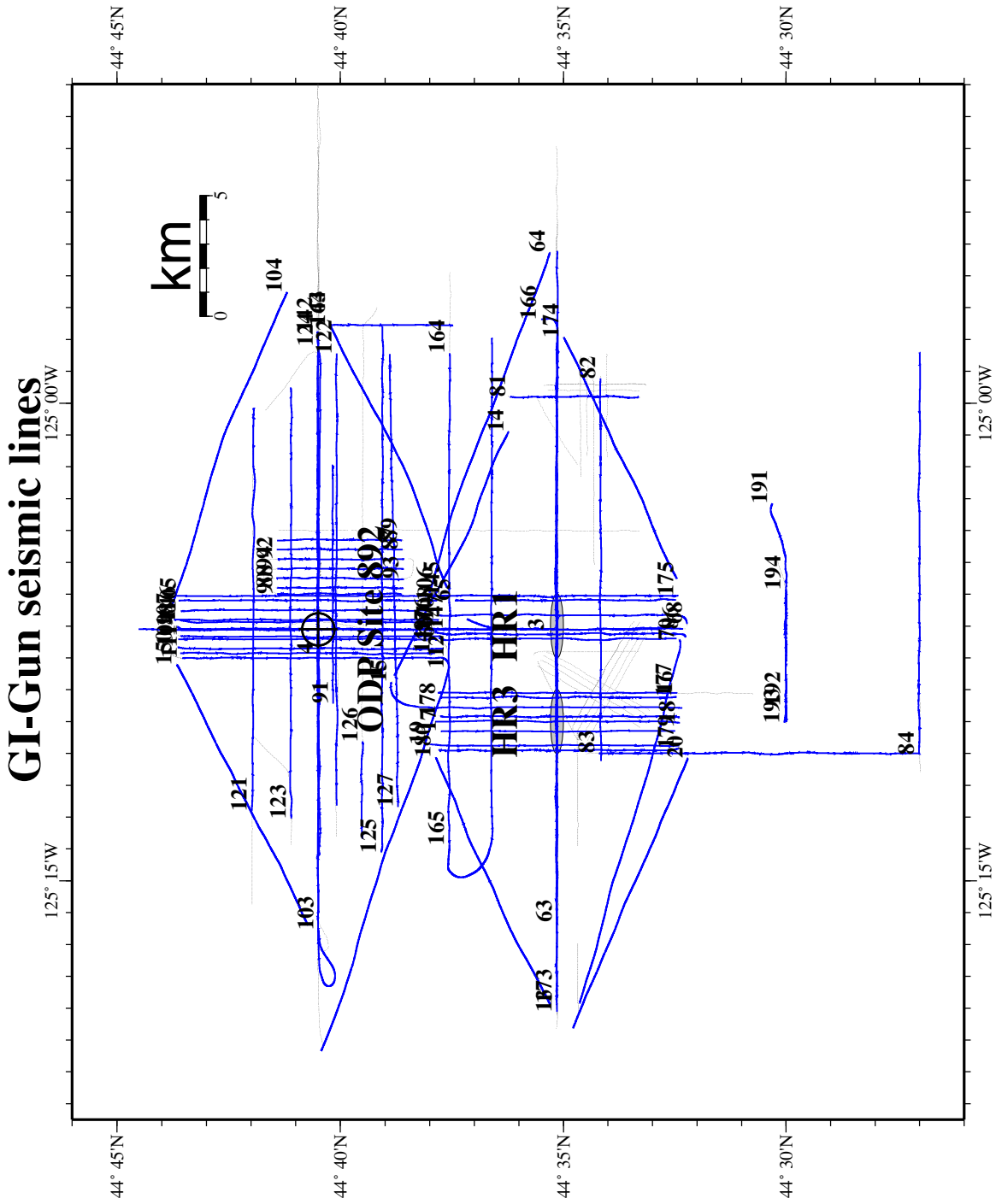

Figure 9.3.3: Location map of seismic lines shot with the GI-Gun.

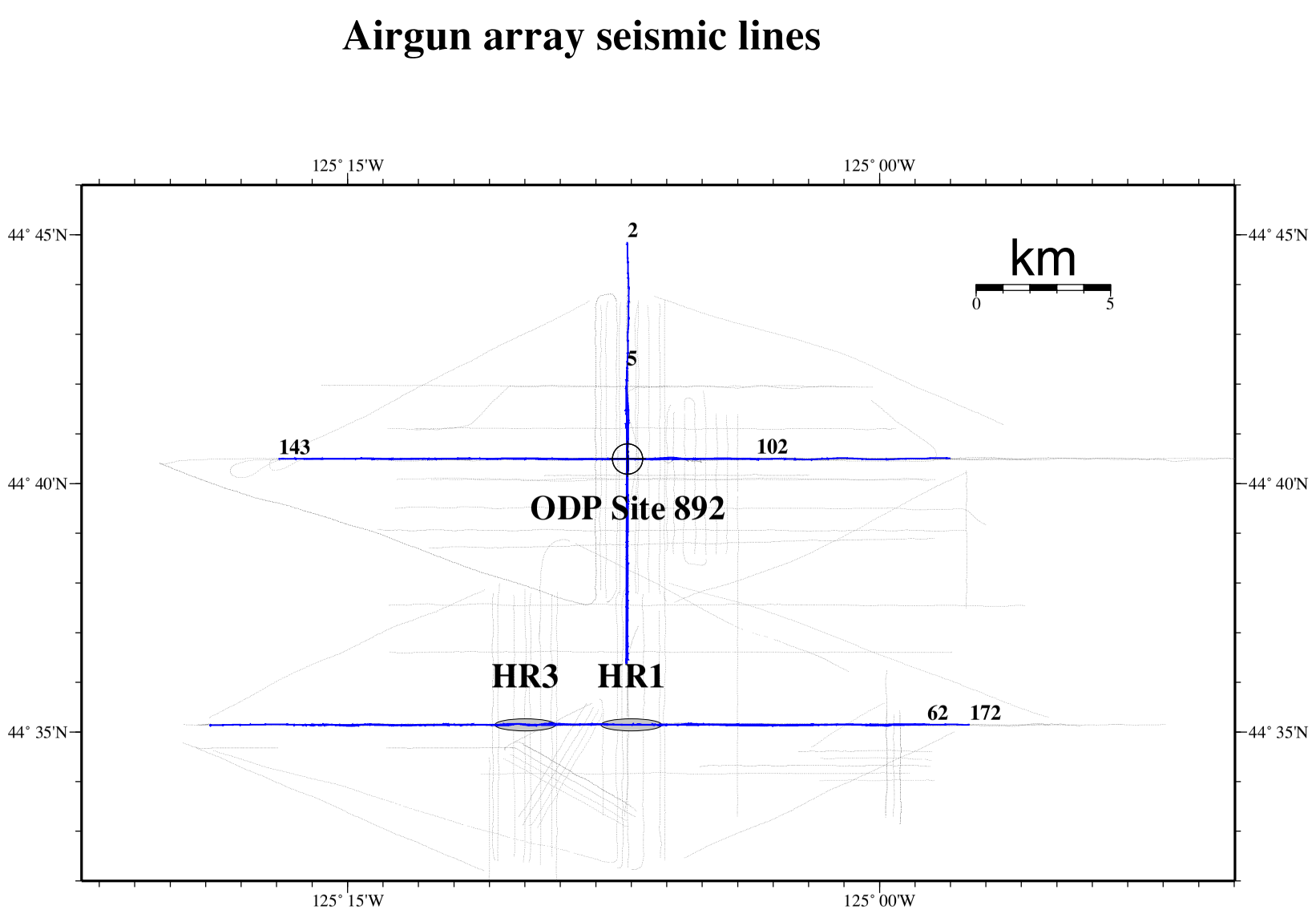

Figure 9.3.4: Location map of seismic lines shot with the Airgun array.

Bolt gun seismic lines

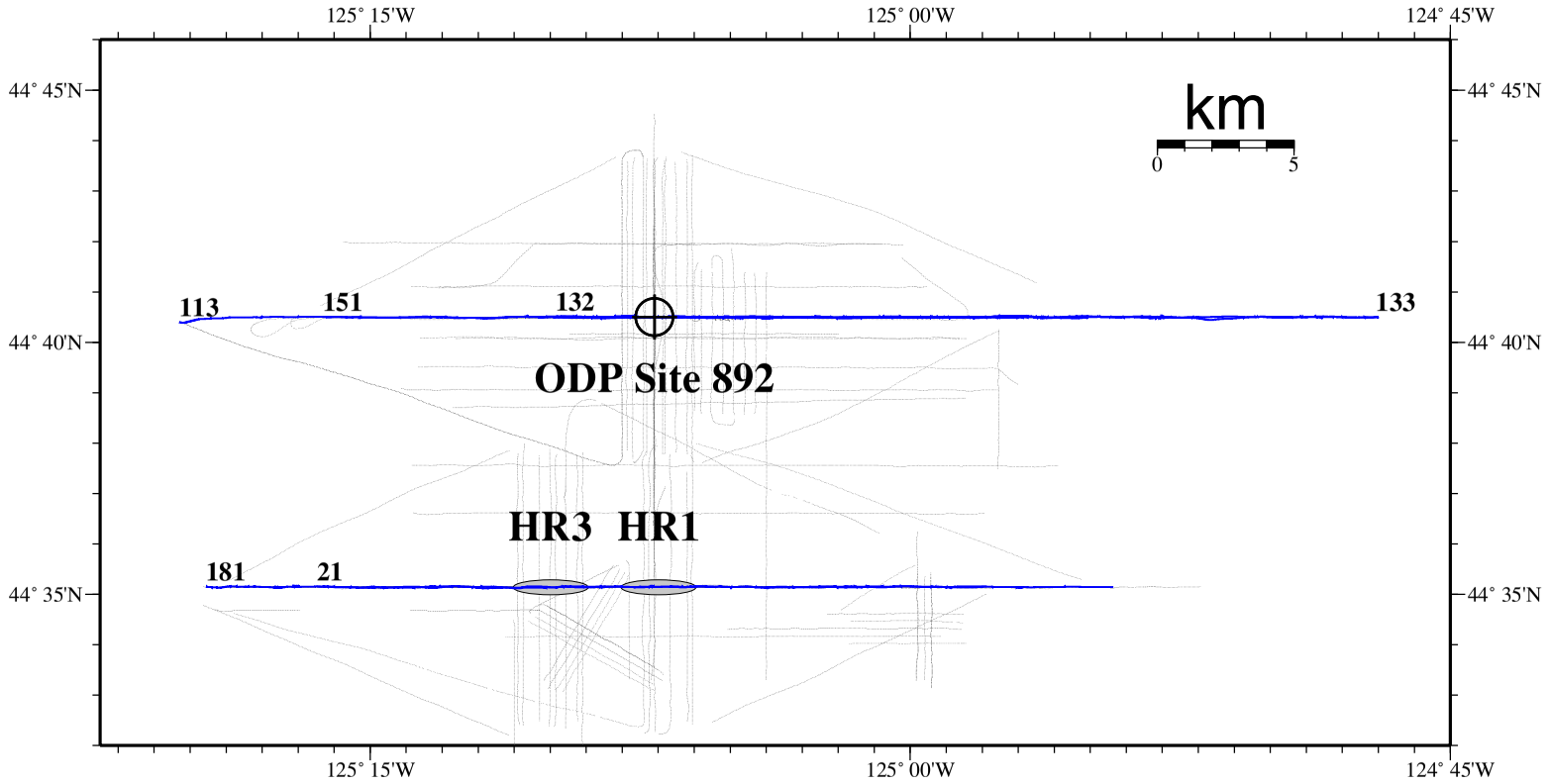

Figure 9.3.5: Location map of seismic lines shot with the Bolt gun.

9.4 CAPTAIN'S REPORT

Stationsprotokoll F.S. "S O N N E" Reise SO 150

Eingesetzte Geräte			**Einsätze / Seemeilen**
OBH	Ocean Bottom Hydrofons	OBH/OBS	70
OBS	Ocean Bottom Seismographs		
GI	GI-air-gun	01,50 Liter	
WG	Water-air-gun	00,25 Liter	
BG	Bolt-air-gun	32,00 Liter	
PA	Prakla-airgun-array	05,16 Liter	
D-T-S	Deeptow-Streamer	1 Kanal und 8 Kanäle	
MS	Multichannel-Streamer	3 Kanäle	
MiS	Ministreamer	1 Kanal	
SP	Sparker		
CTD	CTD-Sonde		01
HS	Hydrosweep		
PS	Parasound		

Seismik-Profile	677 sml
Sparker-Profile	128 sml
Hydrosweep-Profile	491 sml

Eingesetzte Winden :

Winde	D/M .	Typ	RF-Nr	SO 150 Einsatz	Gesamt Einsatz	SO 150 S`länge	Gesamt S`länge	Zust.
W 1	18,2	LWL	816233	008 h	1249 h	10516 m	59359 m	3
W 2	18,2	LWL	810001	071	0155	13000	043097	2
W 4	11,0	NSW	817141	000	0222	00000	139383	3
W 5	11,0	NSW	817164	002	0079	02918	074234	3
W 6	18,2	DRAKO	814150	006	0987	05684	772764	3

Winde	SO 150 gefierte max.Länge	jemals gefierte max.Länge
W 1	6050 m	6474 m
W 2	3000	3000
W 4	0000	6100
W 5	2918	5200
W 6	2684	7900

Geräteverluste : keine

Abkürzungen im Stationsprotokoll:

z.W.	zu Wasser
a.D.	an Deck
Boko	Bodenkontakt
Bosi	Bodensicht
SL(max.)	(maximale)Seillänge
LT	Lottiefe nach Hydrosweep
Wx	eingesetzte Winde
HS	Hydrosweep
PS	Parasound
XPNDR	Transponder

Zeit : UTC - 07 Stunden

20.09.2000

Station 01	Releasertest W 6		
0600	Beginn Station	LT = 1596 m	45 13,70 N 125 06,32 W
0610	Korb mit 8 Releasern z.W.		
0643	Slmax = 1000 m		

0643 – 0648 Auslösetest
0712 Gerät a.D. ; Ende Station

Deep Tow Streamer Test W 2

1050	Streamer z.W.	v = 3,0 kn		44 32,2 N 125 19,7 W
1110	SL = 1126 m	DTS = 500 m	LT = 2928 m	
1204	hieven ein			
1257	Streamer a.D	Ende Test		

1304 – 1427 Test Bb – airgun-arry
1435 – 1500 Test GI-gun

Station 02 CTD W 5

1518	Beginn Station	LT = 2950 m	44 27,00 N 125 21,00 W
1525	CTD z.W.		
1623	Slmax = 2918 m	LT = 2951 m	
1750	CTD a.D.		44 27,01 N 125 21,00 W
1751	Ende Station		

Station 03 Releaser-Test W 6

1800	Beginn Station	LT = 2950 m	44 27,01 N 125 2101 W
1801	8 Releaser z.W.		
1826	SL = 1000 m	LT = 2949 m	
1834	Test beendet, hieven ein		
1859	Releaser a.D. Ende Station		

Auslegung OBH/OBS

2103	OBH 01	z.W.	LT = 0686 m	44 40,60 N 125 07,10 W
2142	OBS 02	z.W.	LT = 0678 m	44 40,49 N 125 07,10 W
2201	OBH 03	z.W.	LT = 0673 m	44 40,39 N 125 07,10 W

Seismik-Profil 01 W 02 Kurs = 360 Grad v = 3,0 kn

2252 – 2337	fieren Deep-Tow-Streamer auf SL = 1069 m	T = 500 m		LT = 909 m
2306	Stb-water-gun z.W.			
21.09.00				
0019	Beginn Profil 01		44 36,43 N 125 07,10 W	
0306	hieven streamer auf SL = 800 m			
0315	Ende Profil 01		44 44,57 N 125 07,10 W	08 sml
0321	airgun a.D.			

Seismik-Profil , 02 W 02 Kurs = 180 Grad v = 3,0 kn

0348 - 0354	Bb-airgun-array z.W.		
0355	Streamer auf SL = 1069 m		
0359	Beginn Profil 02	44 44,57 N 125 07,10 W	
0407	Streamer auf SL = 1069 m		
0620	Beginn hieven Streamer auf SL = 900 m		
0634	Ende Profil	44 36,43 N 125 07,10 W	08 sml
0644	Bb-airgun-array a.D.		
0644	hieven Streamer auf SL = 850 m		

Profil 03 W 02 Kurs = 360 Grad v = 3,0 kn

0718	Bb-GI-gun z.W.		
0734	Mini-Streamer MS z.W. , fieren Deep-Tow-Stremer auf SL 900 m		
0736	Beginn Profil	44 36,43 N 125 07,10 W	
0743	Deap-Tow-Streamer auf SL = 1069 m		
1026 – 1034	hieven Deeptow-Streamer auf SL = 850 m		
1041	Ende Profil	44 44,57 N 125 07,10 W	08 sml
1048	Mini-Streamer MS a.D.		
1054	Bb-GI-gun a.D.		

Profil 04 W 02 Kurs = 90 Grad v = 3,0 kn

1246 Stb-GI-gun z.W.

1256 Deeptow-Streamer auf SL = 1069 m
1257 Mini-Streamer MS z.W.
1308 Beginn Profil 44 40,50 N 125 09,86 W
1331 Ende Profil 44 40,50 N 125 06,34 W 01 sml
1331 – 1340 hieven Deeptow-streamer auf SL = 850 m
1350 Mini-Streamer MS a.D.
1354 Stb-GI-gun a.D.

Profil 05 W 02 Kurs = 180 Grad v = 3,0 kn

1603 Stb-Bolt-gun z.W.
1605 Beginn Profil 44 45,25 N 125 07,07 W
1616 Deeptow-Streamer SL = 1069 m
1619 Mini-Streamer Bb z.W.
1858 hieven Deeptow-Streamer ein
1900 Ende Profil 44 36,43 N 125 07,11 W 09 sml
1906 Mini-Streamer a.D.
1513 Bolt-airgun Stb a.D.
1936 Deeptow-Streamer a.D.

Aufnahme OBH 01 bis 03

2008 OBH 03 ausgelöst 2018 gesichtet 2028 a.D. 44 40,29 N 125 07,15 W
2030 OBH 02 2041 2109 44 40,47 N 125 07,16 W
2057 OBH 01 2100 2109 44 40,47 N 125 07,16 W

22.09.00

HS/PS-Profile 01 bis 06 v = 10,0 kn

0008 Beginn Profil 01 090 Grad 44 26,40 N 125 21,00 W
0244 Ende Profil 01 44 26,40 N 124 45,00 W 26 sml
0249 Beginn Profil 02 270 Grad 44 25,20 N 124 45,00 W
0521 Ende Profil 02 44 25,20 N 125 21,00 W 26 sml
0527 Beginn Profil 03 090 Grad 44 24,00 N 125 21,00 W
0804 Ende Profil 03 44 24,00 N 124 45,00 W 26 sml
0811 Beginn Profil 04 270 Grad 44 22,80 N 124 45,00 W
1040 Ende Profil 04 44 22,80 N 125 21,00 W 26 sml
1048 Beginn Profil 05 090 Grad 44 21,60 N 125 21,00 W
1322 Ende Profil 05 44 21,60 N 124 45,00 W 26 sml
1327 Beginn Profil 06 270 Grad 44 20,40 N 124 45,00 W
1601 Ende Profil 06 44 20,40 N 125 21,00 W 26 sml

Station 04 Releaser-Test W 6

1601 Beginn Station LT = 2978 m 44 20,5 N 125 21,3 W
1606 Releaser z.W.
1625 Slmax = 1000 m Test
1627 hieven ein
1646 Releaser a.D. Ende Station

Streamer - Test

1650 Beginn Test LT = 2980 m 44 20,5 N 125 21,4 W
v = 3,0 kn Kurs = 40 Grad
1708 Ministreamer MS z.W.
1711 GI-gun z.W.
1715 Mini-Streamer Bb z.W.
1813 Deep-Tow-Streamer auf SL = 1069 m
1827 hieven Deeptow-Streamer ein
1910 Deeptow a.D.
1918 GI-gun a.D.
1925 Streamer MS a.D.
1927 Mini-streamer Bb a.D. 44 26,38 N 125 17,04 W

HS/PS-Profil 07 v = 10,0 kn Kurs = 90 Grad

2016 Beginn Profil 44 19,20 N 125 21,00 W

2251	Ende Profil	44 19,20 N	124 45,00 W	26 sml

23.09.00

Auslegung OBH/OBS 04 bis 18

0111	OBH 04 z.W.	LT = 1168 m	44 35,14 N 125 10,91 W	
0127	OBH 05 z.W.	LT = 1166 m	44 35,14 N 125 10,75 W	
0144	OBH 06 z.W.	LT = 1139 m	44 35,14 N 125 10,60 W	
0159	OBH 07 z.W.	LT = 1121 m	44 35,14 N 125 10,45 W	
0210	OBH 08 z.W.	LT = 1094 m	44 35,14 N 125 10,30 W	50 m Seil
0226	OBH 09 z.W.	LT = 1064 m	44 35,14 N 125 10,15 W	
0234	OBH 10 z.W.	LT = 1037 m	44 35,14 N 125 10,00 W	
0243	OBH 11 z.W.	LT = 1001 m	44 35,14 N 125 09,85 W	
0255	OBH 12 z.W.	LT = 0977 m	44 35,14 N 125 09,70 W	
0305	OBH 13 z.W.	LT = 0961 m	44 35,14 N 125 09,55 W	50 m Seil
0324	OBH 14 z.W.	LT = 0938 m	44 35,14 N 125 09,40 W	
0334	OBH 15 z.W.	LT = 0921 m	44 35,14 N 125 09,25 W	
0359	OBH 16 z.W.	LT = 0902 m	44 35,14 N 125 09,10 W	
0413	OBH 17 z.W.	LT = 0881 m	44 35,14 N 125 08,95 W	

HS/PS-Profil 08 Kurs 270 Grad v = 10,0 kn

0630	Beginn Profil	44 18,00 N	124 45,00 W
0800	Ende Profil	44 18,00 N	125 06,29 W 15 sml

Seismik- Profile 11 bis 21 W 02 v = 3,0 kn

1000	Erreichen Aussetzposition		44 35,10 N 125 22,25 W	
1003	Water-gun Stb z.W.			
1010	Streamer MS z.W.			
1012	Mini-Streamer Bb z.W.			
1024	Beginn fieren Deeptow-Streamer			
1122	Mini-Streamer a.D.			
1128	Deeptow SL = 1152 m			
1131	Ministreamer Bb z.W. (Magnetikauslege)			
1200	Beginn Profil 11	Kurs = 90 Grad	44 35,14 N 125 14,00 W	
1429	Ende Profil 11		44 35,14 N 125 05,50 W	06 sml
1434	Watergun a.D.			
1436	Ministreamer Bb a.D.			
1439	Deeptow SL = 900 m			
1444	Streamer MS a.D.			
1633			44 35,06 N 124 59,67 W	
1628	Bb-airgun-array z.W.			
	Deeptow-Streamer bleibt bei SL = 900 m			
1633	Ministreamer Bb z.W.			
1637	Beginn Profil 12		44 35,13 N 125 00,73 W	
1658	Streamer Stb über Ausleger z.W.			
2048	Ende Profil 12		44 35,14 N 125 18,93 W	13 sml
2058	Streamer Stb a.D.			
2104	Bb-airgun-array a.D.			
2142	fieren Deeptow-Streamer			
2151	SL = 1069 m			
2200	GI-gun Stb z.W.			
2208	Beginn Profil 13		44 35,14 N 125 18,93 W	

24.09.00

0250	Ende Profil 13	44 35,14 N 125 00,75 W	13 sml
0300	Deeptow-Streamer SL = 900 m		
0319	Beginn Profil 14	44 35,93 N 125 00,11 W	
0341	D-T-S SL = 1069 m		
0538	Ende Profil 14	44 38,70 N 125 08,60 W	07 sml
0611	Beginn Profil 15	44 37,77 N 125 09,55 W	
0753	hieven D-T-S ein		
0803	Ende Profil 15	44 32,44 N 125 09,57 W	05 sml
0811	GI-gun a.D.		
0815	Ministreamer a.D.		

0825	D-T-S a.D.			
1130	Stb-GI-gun z.W.			
1135	Ministreamer Bb z.W.			
1143	Streamer MS z.W.			
1210	Beginn Profil 16	44 32,47 N	125 09,10 W	
1355	Ende Profil 16	44 37,77 N	125 09,10 W	05 sml
1423	Beginn Profil 17	44 37,77 N	125 10,30 W	
1608	Ende Profil 17	44 32,48 N	125 10,30 W	05 sml
1629	Beginn Profil 18	44 32,47 N	125 10,03 W	
1635 – 1658	D-T-S z.W. SL = 5 m			
1816	Ende Profil 18	44 37,77 N	125 10,00 W	05 sml
1837	Beginn Profil 19	44 37,77 N	125 10,75 W	
2026	Ende Profil 19	44 32,47 N	125 10,75 W	05 sml
2036	Beginn Profil 20	44 32,21 N	125 11,17 W	
2252	Ende Profil 20	44 34,81 N	125 19,75 W	07 sml
2259	GI-gun a.D.			
2312	Stb-Bolt-gun z.W.			
2325	Beginn Profil 21	44 35,14 N	125 18,93 W	
25.09.00				
0531	Bb-Bolt-gun z.W.			
0647	Ende Profil 21	44 35,14 N	124 54,73 W	17 sml
0653	Streamer MS a.D.			
0702	Bb-Bolt-gun a.D.			
0704	Stb-Bolt-gun a.D.			
0713	Ministreamer Bb a.D.			

Aufnahme OBH/OBS 17 bis 04

0809	OBH 17 ausgelöst	0820	gesichtet	0826 a.D.	44 35,15 N	125 09,12 W
0828	OBH 16	0837		0843	44 35,12 N	125 09,21 W
0844	OBH 15	0854		0900	44 35,16 N	125 09,43 W
0900	OBH 14	0908		0913	44 35,14 N	125 09,25 W
0914	OBH 13	0924		0929	44 35,14 N	125 09,65 W
0929	OBH 12	0945		0951	44 35,14 N	125 09,82 W
0952	OBH 11	1001		1007	44 35,14 N	125 09,04 W
1007	OBH 10	1024		1031	44 35,14 N	125 10,14 W
1031	OBH 09	1049		1054	44 35,14 N	125 10,19 W
1055	OBH 08	1109		1115	44 35,12 N	125 10,38 W
1115	OBH 07	1129		1134	44 35,13 N	125 10,53 W
1135	OBH 06	1150		1200	44 35,11 N	125 10,66 W
1200	OBH 05	1212		1219	44 35,10 N	125 10,86 W
1219	OBH 04	1236		1242	44 35,05 N	125 10,99 W

Sparkerprofile 31 bis xx

1350	Erdungskabel z.W.			
1355	Sparker z.W.			
1400	Streamer MS z.W.			
1405	Beginn Profil 31	44 35,14 N	124 57,68 W	
1407	Ministreamer Bb z.W.			
1842	Ende Profil 31	44 35,14 N	125 18,93 W	15 sml
1905	Beginn Profil 32	44 34,68 N	125 18,93 W	
1910	D-T-S z.W.			
1923	SL = 295 m			
1936	hieven ein			
2046	D-T-S a.D.			
2144	Profilwechsel 32 / 33	44 34,68 N	125 10,28 W	06,5 sml
2248	Ende Profil 33	44 33,42 N	125 07,20 W	02,5 sml
2304	Beginn Profil 34	44 33,20 N	125 07,40 W	
2348	Ende Profil 34	44 34,42 N	125 10,46 W	02,5 sml
26.09.00				
0006	Beginn Profil 35	44 34,80 N	125 10,15 W	
0104	Ende Profil 35	44 33,55 N	125 07,10 W	02,5 sml

0117	Beginn Profil 36	44 33,30 N 125 07,30 W	
0202	Profilwechsel 36 / 37	44 34,54 N 125 10,36 W	02,5 sml
0256	Profilwechsel 37 / 38	44 35,57 N 125 08,01 W	02,5 sml
0343	Ende Profil 38	44 33,25 N 125 09,70 W	02,5 sml
0356	Beginn Profil 39	44 33,40 N 125 10,05 W	
0450	Ende Profil 39	44 35,52 N 125 08,32 W	02,5 sml
0503	Beginn Profil 40	44 35,32 N 125 07,82 W	
0548	Ende Profil 40	44 35,32 N 125 07,82 W	02,5 sml
0604	Beginn Profil 41	44 33,35 N 125 09,87 W	
0700	Ende Profil 41	44 35,42 N 125 08,12 W	02,5 sml
0712	Beginn Profil 42	44 35,42 N 125 07,80 W	
0753	Ende Profil 42	44 33,30 N 125 07,80 W	02,0 sml
0813	Beginn Profil 43	44 33,29 N 125 07,19 W	
1027	weichen bis auf 350 m vom Profil ab, Fischer sitzt fest auf ODP-Position		
1110	Ende Profil 43	44 41,67 N 125 07,10 W	09,0 sml
1119	Beginn Profil 44	44 41,96 N 125 06,70 W	
1246	Profilwechsel 44 / 45	44 41,94 N 125 00.80 W	04,0 sml
1246 – 1254	Sparker a.D. für Wartung		
1333	Profilwechsel 45 / 46	44 40,45 N 124 58,47 W	02,5 sml
1355	Abbruch Profil 46	44 40,45 N 125 00,00 W	01,0 sml
1445	Beginn Profil 47	44 40,08 N 124 58,33 W	
1809	Profilwechsel 47 / 48	44 40,09 N 125 13,89 W	12,0 sml
1845	Profilwechsel 48 / 49	44 41,10 N 125 14,70 W	01,5 sml
1902	D-T-S SL = 100 m		
1920	Abbruch Profil 49	44 41,10 N 125 12,22 W	02,0 sml
1931	D-T-S a.D.		
1954	Beginn Profil 50	44 41,96 N 125 10,45 W	
2059	Ende Profil 50	44 41,96 N 125 06,00 W	03,0 sml
2131	Beginn Profil 51	44 41,96 N 125 04,00 W	
2244	D-T-S SL = 500 m		
2332	hieven D-T-S		
2355	D-T-S a.D.		
27.09.00			
0027	Ende Profil 51	44 33,30 N 125 04,00 W	09,0 sml
0109	Beginn Profil 52	44 34,32 N 125 05,00 W	
0255	Ende Profil 52	44 34,32 N 124 58,60 W	04,5 sml
0307	Beginn Profil 53	44 34,03 N 124 58,60 W	
0342	Ende Profil 53	44 34,03 N 125 01,60 W	02,0 sml
0345	Sparker a.D.		
0354	MS-Streamer a.D.		
0357	Bb-Streamer a.D.		

Auslegung OBH/OBS 18 bis 31

0429	OBH 18 z.W.	LT =	0906 m	44 35,14 N	125 07,55 W
0442	OBH 19		0904 m	35,14 N	07,40 W
0454	OBH 20 50 m Leine		0907 m	35,14 N	07,25 W
0504	OBH 21		0909 m	35,14 N	07,10 W
0513	OBH 22		0924 m	35,14 N	06,95 W
0522	OBH 23		0943 m	35,14 N	06,80 W
0531	OBH 24		0974 m	35,14 N	06,65 W
0540	OBH 25		0994 m	35,14 N	06,50 W
0557	OBH 26		1009 m	35,14 N	06,35 W
0610	OBH 27		1022 m	35,14 N	06,19 W
0622	OBH 28 50 m Leine		1030 m	35,14 N	06,05 W
0631	OBH 29		1039 m	35,14 N	05,90 W
0640	OBH 30		1047 m	35,14 N	05,75 W
0649	OBH 31		1055 m	35,14 N	05,60 W

Sparker-Profile 54 bis 59

0713	Sparker z.W.	
0719	Bb-Streamer z.W.	
0733	Beginn Profil 54	44 34,60 N 125 02,36 W

0817	Ende Profil 54	44 34,61 N 124 58,60 W	02,0 sml
0830	Beginn Profil 55	44 34,47 N 124 58,60 W	
0910	Ende Profil 55	44 34,47 N 125 01,60 W	02,0 sml
0959	Beginn Profil 56	44 35,40 N 124 59,43 W	
1044	Ende Profil 56	44 33,30 N 124 59,40 W	02,0 sml
1056	Beginn Profil 57	44 33,30 N 124 59,80 W	
1135	Ende Profil 57	44 35,40 N 124 59,80 W	02,0 sml
1148	Beginn Profil 58	44 35,40 N 124 59,60 W	
1235	Ende Profil 58	44 33,30 N 124 59,60 W	02,0 sml
1237	Sparker a.D.		
1237	Bb-Streamer a.D.		

Seismik-Profile 61 bis XX v = 3,0 kn W 06

1332	Sparker z.W.		
1335	Bb-Streamer z.W.		
1337	MS-Streamer z.W.		
1400	Beginn Profil 61	44 35,14 N 125 11,25 W	
1607	Ende Profil 61	44 35,15 N 125 02,91 W	06 sml
1610	Sparker a.D.		
1612	Bb-Streamer a.D.		
1619	MS-Streamer a.D.		
1655		44 35,10 N 124 53,77 W	
1654	Bb-airgun-array z.W.		
1702	D-T-S z.W.		
1730	Streamer BB z.W.		
1735	Streamer MS z.W.		
1735	D-T-S SL = 500 m		
1750	Beginn Profil 62	44 35,14 N 124 57,98 W	
2157	Ende Profil 62	44 35,14 N 125 16,18 W	13,0 sml
2205	Bb-airgun-array a.D.		
2213	MS-Streamer a.D.		
2247	GI-gun Stb z.W.		
2252	Beginn Profil 63	44 35,14 N 125 16,18 W	
2258	MS-Steamer z.W.		
2308	D-T-S SL = 1000 m		
28.09.00			
0347	Ende Profil 63	44 35,15 N 124 57,98 W	13,0 sml
0430	D-T-S a.D.		
0430	Beginn Profil 64	44 35,15 N 124 55,19 W	
0700	Ende Profil 64	44 38,00 N 125 05,91 W	08,0 sml
0707	Beginn Profil 65	44 37,77 N 125 06,20 W	
0855	Ende Profil 65	44 32,48 N 125 06,20 W	05,3 sml
0908	Beginn Profil 66	44 32,47 N 125 05,78 W	
0914	Abbruch Profil 66 GI-gun defekt		
0915	GI-gun a.D.		
0916 – 0946	Schleife über Bb		
0941	Watergun Bb z.W.		
0946	Neubeginn Profil 66	44 32,47 N 125 05,75 W	
1124	Ende Profil 66	44 37,77 N 125 05,75 W	05,3 sml
1130	Stb watergun a.D.		
1140	Stb GI-gun z.W.		
1200	Beginn Profil 67	44 37,77 N 125 17,10 W	
1345	Ende Profil 67	44 32,47 N 125 07,10 W	05,3 sml
1400	Beginn Profil 68	44 32,47 N 125 06,65 W	
1555	Ende Profil 68	44 37,78 N 125 06,65 W	05,3 sml
1610	Beginn Profil 69	44 37,78 N 125 07,37 W	
1755	Profilwechsel 69 / 70	44 32,47 N 125 07,40 W	05,5 sml
2049	Ende Profil 70	44 34,85 N 125 20,00 W	09,0 sml
2052	Stb-GI-gun a.D.		
2103	D-T-S z.W.		
2118	Bb Boltgun z.W.		
2135	SL = 434 m hieven D-T-S ein		

2208	Beginn Profil 71	44 35,14 N	125 16,18 W
2214	D-T-S z.W.		
2253	SL = 500 m		

29.09.00

0438	Ende Profil 71	44 35,14 N	124 51,98 W	17,5 sml
0447	Bolt-gun a.D.			
0450	hieven D-T-S			
0452	Bb Streamer a.D.			
0456	MS Streamer a.D.			
0510	D-T-S a.D.			

Aufnahme OBH/OBS 31 bis 18

0607	OBH 31 ausgelöst	0619	gesichtet	0653	a.D.	44 34,88 N	125 05,93 W
0653	OBH 30	0705		0710		35,10 N	05,84 W
0710	OBH 29	0722		0728		35,08 N	06,07 W
0728	OBH 28	0737		0741		35,12 N	06,20 W
0740	OBS 27	0759		0806		35,10 N	06,40 W
0806	OBS 26	0822		0830		35,14 N	06,42 W
0830	OBH 25	0839		0847		35,18 N	06,66 W
0847	OBH 24	0857		0907		35,13 N	06,82 W
0903	OBH 23	0916		0925		35,16 N	06,95 W
0923	OBS 22	0931		0939		35,15 N	07,07 W
0939	OBS 21	0953		1002		35,16 N	07,22 W
1002	OBH 20	1013		1019		35,14 N	07,35 W
1019	OBH 19	1030		1035		35,15 N	07,52 W
1034	OBH 18	1048		1055		35,15 N	07,64 W

Seismik-Profile 81 bis 90

1154	D-T-S z.W.			
1205	STb-GI-gun z.W.			
1213	MS-Streamer z.W.			
1215	Stb Streamer z.W.			
1228	Beginn Profil 81	44 35,40 N	124 59,80 W	
1241	D-T-S SL = 1000 m			
1316	Ende Profil 81	44 33,30 N	124 59,80 W	02,0 sml
1321	Bb Streamer a.D.			
1326	GI-gun a.D.			
1332	MS Streamer a.D.			
1345	D-T-S SL = 500 m			
1431	Beginn Profil 82	44 34,17 N	124 58,60 W	
1435	Stb GI-gun z.W.			
1440	Bb Streamer z.W.			
1442	MS Streamer z.W.			
1719	Ende Profil 82	44 34,17 N	125 11,00 W	09,0 sml
1724	Bb Streamer a.D.			
1729	Stb GI-gun a.D.			
1737	D-T-S SL = 500 m			
1830	Stb GI-gun z.W.			
1840	Bb-Streamer z.W.			
1842	Beginn Profil 83	44 34,17 N	125 11,00 W	
1859	D-T-S SL = 1000 m			
2106	Ende Profil 83	44 27,00 N	125 11,00 W	07,0 sml
2113 – 2151	GI-gun vorgehievt			
2123	D-T-S SL = 500 m			
2159	Beginn Profil 84	44 27,00 N	125 11,00 W	
2208	D-T-S SL = 1000 m			

30.09.00

0057	Ende Profil 84	44 27,00 N	124 58,00W	09,0 sml

0103	D-T-S SL = 500 m		
0109	GI-gun a.D.		
0133	Sparker z.W.		
0146	Beginn Profil 85	44 27,00 N 124 58,00 W	
0300	D-T-S a.D.		
0440	Ende Profil 85	44 27,00 N 125 11,00 W	09,0 sml
454	Sparker und Streamer a.D.		
0522	D-T-S z.W.		
0528	Stb GI-gun z.W.		
0535	D-T-S SL 0 100 m		
0546	Bb Streamer z.W.		
0600	Beginn Profil 86	44 33,30 N 125 07,10 W	
0619	D-T-S SL = 500 m		
0703	Ausfall D-T-S hieven ein		
	Abbruch Profil 86	44 36,30 N 125 07,10 W	03,0 sml
0735	D-T-S a.D.		
0814	Beginn Profil 87	44 33,60 N 125 04,60 W	
0914	Ende Profil 87	44 41,40 N 125 04,60 W	02,8 sml
0936	Beginn Profil 88	44 41,40 N 125 05,80 W	
1040	Ende Profil 88	44 38,60 N 125 05,80 W	02,8 sml
1109	Beginn Profil 89	44 38,60 N 125 04,30 W	
1205	Ende Profil 89	44 41,40 N 125 04,30 W	02,8 sml
1235	Beginn Profil 90	44 41,40 N 125 06,00 W	
1329	Ende Profil 90	44 38,00 N 125 06,00 W	03,4 sml
1333	GI-gun a.D.		
1337	Bb Streamer a.D.		

Auslegung OBH/OBS 32 bis 45

1409	OBH 32 z.W.	LT =	757 m	44	40,50 N	125	08,00 W
1421	OBH 33		729		40,49 N		07,85 W
1429	OBH 34		712		40,49 N		07,70 W
1435	OBH 35		694		40,49 N		07,55 W
1442	OBH 36		683		40,50 N		07,40 W
1453	OBH 37		686		40,50 N		07,25 W
1503	OBH 38 50 m Seil		682		40,49 N		07,11 W
1519	OBH 39		664		40,50 N		06,96 W
1531	OBH 40		660		40,50 N		06,80 W
1543	OBH 41		657		40,49 N		06,65 W
1551	OBH 42		653		40,50 N		06,51 W
1601	OBH 43		649		40,50 N		06,34 W
1617	OBH 44		645		40,50 N		06,21 W
1626	OBH 45		634		40,49 N		06,06 W

Seismik-Profile 91 bis XXX

1654		44 40,14 N 125 10,45 W	
1657	Stb GI-gun z.W.		
1659	Bb Streamer z.W.		
1715	Beginn Profil 91	44 40,17 N 125 09,00 W	
1914	Ende Profil 91	44 40,17 N 125 02,00 W	05,0 sml
1919	Stb GI-gun a.D.		
1921	Bb Streamer a.D.		
1945	Stb GI-gun az.W.		
1948	Bb Streamer z.W.		
1954	Beginn Profil 92	44 41,40 N 125 04,90 W	
2050	Ende Profil 92	44 38,60 N 125 04,90 W	02,8 sml
2106	Beginn Profil 93	44 38,60 N 125 05,50 W	
2203	Ende Profil 93	44 41,40 N 125 05,50 W	02,8 sml
2219	Beginn Profil 94	44 41,60 N 125 05,20 W	
2321	Ende Profil 94	44 38,60 N 125 05,20 W	03,0 sml
2328	Stb GI-gun a.D.		
2330	Bb Streamer a.D.		

01.10.00

0028	Stb Watergun z.W.			
0034	MS Streamer z.W.			
0040	Bb Streamer z.W.			
0100	Beginn Profil 101	44 40,50 N	125 12,25 W	
0300	Ende Profil 101	44 40,50 N	125 02,91 W	06,0 sml
0301	Bb Streamer a.D.			
0308	MS Streamer a.D.			
0312	Stb watergun a.D.			
0348	D-T-S z.W.			
0355	Bb airgun-array z.W.			
0406	Bb Streamer z.W.			
0408	MS Streamer z.W.			
0425	DTS KL = 836 m			
0450	Beginn Profil 102	44 40,50 N	124 57,98 W	
0842	Ende Profil 102	44 40,50 N	125 16,18 W	09,0 sml
0846	Bb airgun-array a.D.			
0849	Bb Streamer a.D.			
0856	MS Streamer a.D.			
0929	Stb GI-gun z.W.			
0935	MS Streamer z.W.			
0937	Bb Streamer z.W.			
0943	Beginn Profil 103	44 40,50 N	125 16,18 W	
0944	DTS KL = 1003 m			
1416	Ende Profil 103	44 40,50 N	124 57,90 W	13,0 sml
1424	MS Streamer a.D.			
1453	D-T-S a.D.			
1453	Beginn Profil 104	44 40,66 N	124 55,09 W	
1740	Profilwechsel 104 / 105	44 43,74 N	125 06,41 W	09,0 sml
1932	Ende Profil 105	44 37,83 N	125 06,50 W	06,0 sml
1949	Beginn Profil 106	44 37,83 N	125 06,20 W	
2149	Ende Profil 106	44 43,60 N	125 06,20 W	05,8 sml
2206	Beginn Profil 107	44 43,60 N	125 07,10 W	
2400	Ende Profil 107	44 37,83 N	125 07,10 W	05,8 sml
02.10.00				
0014	Beginn Profil 108	44 37,83 N	125 06,80 W	
0203	Ende Profil 108	44 43,60 N	125 06,80 W	05,8 sml
0215	Beginn Profil 109	44 43,60 N	125 07,70 W	
0406	Ende Profil 109	44 37,83 N	125 07,70 W	05,8 sml
0419	Beginn Profil 110	44 37,83 N	125 07,40 W	
0620	Ende Profil 110	44 43,60 N	125 07,40 W	05,8 sml
0633	Beginn Profil 111	44 43,60 N	125 08,00 W	
0824	Ende Profil 111	44 37,83 N	125 08,00 W	05,8 sml
0833	Beginn Profil 112	44 37,57 N	125 08,33 W	
1120	Ende Profil 112	44 40,36 N	125 08,33 W	09,0 sml
1127	GI-gun a.D.			
1150 – 1258	Ausfall Tiefseewinde			
1118	Bb Streamer a.D.			
1300	D-T-S z.W.			
1310	Bb boltgun z.W.			
1319	Bb Streamer z.W.			
1343	DTS KL = 1003 m			
1412	Beginn Profil 113	44 40,50 N	125 16,18 W	
1511	Stb boltgun z.W.			
1522	Bb boltgun a.D.			
1939	DTS KL = 800 m			
1958	hieven DTS ein			
2011	Ende Profil 113	44 40,50 N	124 51,98 W	17,0 sml
2020	Stb boltgun a.D.			
2032	DTS a.D.			
2034	Bb Streamer a.D.			

Aufnahme OBH/OBS 32 bis 45

2133	OBH 32 ausgelöst	2144	gesichtet	2155	a.D.	44	40,45 N	125 08,32 W
2155	OBH 33	2204		2212			40,46 N	08,05 W
2212	OBH 34	2219		2228			40,47 N	07,91 W
2228	OBH 35	2242		2249			40,48 N	07,71 W
2249	OBH 36	2258		2304			40,48 N	07,53 W
2304	OBH 37	2312		2319			40,49 N	07,34 W
2319	OBH 38	2327		2332			40,45 N	07,20 W
2332	OBH 39	2342		2347			40,47 N	07,05 W
2346	OBH 40	2353		2400			40,46 N	06,94 W
03.10.00								
0001	OBH 41	0011		0020			40,50 N	06,84 W
0020	OBH 42	0030		0042			40,47 N	06,67 W
0042	OBH 43	0047		0058			40,46 N	06,53 W
0058	OBH 44	0104		0114			40,50 N	06,37 W
0114	OBH 45	0123		0132			40,50 N	06,23 W

Seismik-Profile 121 bis 127

0225	Beginn Aussetzen DTS			
0238	GI-gun Stb z.W.			
0242	MS Streamer z.W.			
0244	Bb Streamer z.W.			
0311	DTS KL = 1001 m			
0332	Beginn Profil 121	44 41,97 N	125 12,56 W	
0647	DTS KL = 500 m			
0639	Ende Profil 121	44 41,94 N	125 00,07 W	10,0 sml
0647	Bb Streamer a.D.			
0755	MS Streamer a.D.			
0702	Stb GI-gun vorgehievt			
0744	MS Streamer z.W.			
0748	Stb GI-gun ausgesteckt			
0754	Beginn Profil 122	44 40,08 N	124 58,38 W	
0757	MS Streamer z.W.			
0802	DTS KL = 1002 m			
1109	Ende Profil 122	44 40,08 N	125 12,57 W	10,0 sml
1117	MS Streamer a.D.			
1158	MS Streamer z.W.			
1200	Beginn Profil 123	44 41,10 N	125 12,56 W	
1508	Ende Profil 123	44 41,11 N	125 59,51 W	09,5 sml
1514	MS Streamer a.D.			
1524	DTS KL = 500 m			
1552	Beginn Profil 124	44 40,47 N	125 58,47 W	
1605	DTS KL = 1003 m			
1925	Ende Profil 124	44 40,45 N	125 14,17 W	06,0 sml
2013	Beginn Profil 125	44 39,05 N	125 13,70 W	
2018	MS Streamer z.W.			
04.10.00				
0018	hieven DTS auf KL = 500 m			
0029	Ende Profil 125	44 39,05 N	124 57,63 W	11,5 sml
0034	MS Streamer a.D.			
0105	Beginn Profil 126	44 39,50 N	124 58,46 W	
0113	DTS KL = 1000 m			
0247	hieven DTS auf KL = 800 m			
0348	Bb Streamer a.D.			
0436	Ende Profil 126	44 39,51 N	125 13,59 W	11,0 sml
	hieven DTS auf KL = 500 m			
0516	Beginn Profil 127	44 38,69 N	125 13,60 W	
0533	DTS KL = 1000 m			
0912	Ende Profil 127	44 38,89 N	124 58,48 W	09,0 sml
0916	Stb GI-gun a.D.			
0949	DTS a.D.			

Auslegung OBH/OBS 46 bis 48

1100	OBH 46 z.W.	LT = 680 m	44 40,49 N	125 07,18 W
1110	OBH 47 z.W.	LT = 662 m	44 40,50 N	125 06,95 W
1120	OBS 48 z.W.	LT = 658 m	44 40,49 N	125 06,80 W

Seismik-Profil 131 W 06 **F**all**G**ewicht = 3 tons

1207	FG z.W.	LT = 705 m	44 40,50 N	125 04,84 W
1238		LT = 705 m	44 40,49 N	125 04,92 W
1254			44 40,49 N	125 05,04 W
1319			44 40,49 N	125 05,14 W
1340			44 40,49 N	125 05,27 W
1359		LT = 636 m	44 40,49 N	125 05,37 W
1422			44 40,49 N	125 05,46 W
1520			44 40,49 N	125 05,70 W
1550			44 40,51 N	125 06,42 W
1615			44 40,49 N	125 06,62 W
1624			44 40,49 N	125 06,67 W

auf jeder Position mehrere Bodenkontakte mit FG
gefiert mit 1,5 m/sec

1629	Ende der FG-Messungen, hieven ein
1647	FG a.D.
1657	Ende des Profils, verholen zum Profil 132

Seismik-Profile 132 bis 133

1727	Beginn aussetzen Geräte	44 40,39 N	125 13,39 W	
1732	Stb boltgun z.W.			
1737	Bb boltgun z.W.			
1740	Bb Streamer z.W.			
1816	Beginn Profil 132	44 40,50 N	125 10,00 W	
2344	Ende Profil 132	44 40,50 N	124 47,00 W	16,5 sml
05.10.00				
0012	Beginn Profil 133	44 40,50 N	124 46,99 W	
0538	Ende Profil 133	44 40,50 N	125 10,00 W	16,0 sml
0547	Stb boltgun a.D.			
0600	Bb boltgun a.D.			
0601	Bb Streamer a.D.			

Aufnahme OBH/OBS 48 - 46

0619	OBS 48 ausgelöst	0630 gesichtet	0637 a.D.	44 40,49 N	125 06,86 W
0636	OBH 47	0646	0662	44 40,48 N	125 07,00 W
0652	OBH 46	0700	0705	44 40,48 N	125 07,15 W

Auslegung OBH/OBS 49 bis 59

0718	OBS 49 z.W.	LT = 671 m	44	40,49 N	125	07,02 W
0731	OBS 50	686 m		40,49 N		07,17 W
0752	OBS 51	695 m		40,69 N		07,09 W
0810	OBS 52	670 m		40,30 N		07,11 W
0823	OBH 53	685 m		40,50 N		07,35 W
0833	OBH 54	687 m		40,50 N		07,48 W
0845	OBH 55	658 m		40,50 N		06,88 W
0853	OBH 56	658 m		40,49 N		06,72 W
0904	OBH 57	643 m		40,50 N		06,21 W
0911	OBH 58	632 m		40,50 N		06,06 W
0942	OBH 59 250 m Seil	751 m		40,50 N		08,00 W

Seismik-Profile 141 bis XXX

1100	Stb watergun z.W.			
1107	MS Streamer z.W.			
1113	Bb Streamer z.W.			
1130	Beginn Profil 141	44 40,50 N	125 11,25 W	
1334	Ende Profil 141	44 40,50 N	125 02,91 W	05,5 sml
1340	Stb water gun a.D.			

1350	Stb GI-gun z.W.			
1450	Beginn Profil 142	44 40,50 N	124 58,00 W	
1849	Ende Profil 142	44 40,50 N	125 16,18 W	13,0 sml
1855	GI-gun a.D.			
1915	Bb airgun-array z.W.			
1922	Beginn Profil 143	44 40,50 N	125 16,18 W	
06.10.00				
0005	Ende Profil 143	44 40,50 N	124 57,98 W	13,0 sml
0015	Bb airgun-array a.D.			
0021	Stb GI-gun z.W.			
0021	Beginn Profil 144	44 40,28 N	124 57,39 W	
0230	Profilwechsel 144 / 145	44 37,61 N	125 05,83 W	07,0 sml
0433	Ende Profil 145	44 43,60 N	125 06,05 W	06,0 sml
0452	Beginn Profil 146	44 43,60 N	125 06,87 W	
0640	Ende Profil 146	44 37,83 N	125 06,87 W	06,0 sml
0658	Beginn Profil 147	44 37,83 N	125 07,10 W	
0908	Ende Profil 147	44 43,60 N	125 07,10 W	06,0 sml
0928	Beginn Profil 148	44 43,59 N	125 07,31 W	
1120	Ende Profil 148	44 37,83 N	125 07,32 W	06,0 sml
1135	Beginn Profil 149	44 37,83 N	125 07,85 W	
1336	Profilwechsel 149 / 150	44 43,60 N	125 07,85 W	06,0 sml
1548	Ende Profil 150	44 40,71 N	125 16,45 W	07,0 sml
1551	GI-gun a.D.			
1605	Bb Boltgun z.W.			
1610	Beginn Profil 151	44 40,50 N	125 16,20W	
2033	Ende Profil 151	44 40,50 N	124 57,98 W	13,0 sml
2042	Bb Boltgun a.D.			
2050	Streamer BB a.D.			
2051	Streamer MS a.D.			

Sparkerprofile 161 bis 162

2146	Sparker z.W.			
2150	Bb Streamer z.W.			
2150	Beginn Profil 161	44 43,50 N	125 07,10 W	
2400	Ende Profil 161	44 37,00 N	125 07,10 W	06,5 sml
07.10.00				
0005	Sparker und Streamer a.D.			
0056	DTS z.W.			
0103	Sparker z.W.			
0105	Streamer Bb z.W.			
0134	DTS KL = 1001 m			
0144	Beginn Profil 162	44 40,50 N	125 15,50 W	
0355	hieven DTS auf KL = 800 m			
0607	Ende Profil 162	44 40,50 N	124 58,47 W	06,0 sml
0610	Sparker a.D.			
0627	Bb GI-gun z.W.			

Seismik-Profil

0628	Beginn Profil 163	44 40,25 N	124 57,55 W	
0728	Ende Profil 163	44 37,58 N	124 57,55 W	03,0 sml
0731	GI-gun a.D.			
0734	MS Streamer a.D.			
0756	DTS a.D.			

Aufnahme OBH/OBS 52 bis 59

0837	OBH 58 ausgelöst	0844 gesichtet	0849 a.D.	44 40,50 N	125	05,98 W
0849	OBH 57	0857	0903	40,50 N		06,12 W
0903	OBH 56	0912	0918	40,49 N		06,67 W
0918	OBH 55	0925	0932	40,53 N		06,77 W
0937	OBH 54	0945	0950	40,48 N		07,45 W
0951	OBH 53	0958	1003	40,50 N		07,32 W
1003	OBS 50	1015	1020	40,50 N		07,11 W

1022	OBS 49	1033	1046	40,40 N	07,20 W
1047	OBS 52	1058	1103	40,38 N	07,18 W
1104	OBS 51	1113	1119	40,71 N	07,12 W
1121	OBH 59	1131	1138	40,47 N	08,19 W

Seismik-Profile 164 bis 16

1236	DTS z.W.			
1240	Stb GI-gun z.W.			
1244	Bb Streamer z.W.			
1305	DTS KL = 800 m			
1317	Beginn Profil 164	44 37,55 N	125 58,46 W	
1709	Ende Profil 164	44 37,55 N	125 14,52 W	11,0 sml
1740	Beginn Profil 165	44 36,61 N	125 13,71 W	
2135	Ende Profil 165	44 36,60 N	124 57,84 W	11,0 sml
2214	Beginn Profil 166	44 35,12 N	124 57,67 W	
08.10.00				
0230	Ende Profil 166	44 35,12 N	125 15,61 W	13,0 sml
0237	Bb Streamer a.D.			
0302	Dtb GI-gun a.D.			
0308	DTS a.D.			

Auslegung OBH/OBS 60 bis 70

0459	OBH 60	z.W. 250 m Seil	LT = 1180 m	44	35,15 N	125	10,89 W
0517	OBH 61		1064		35,15 N		10,14 W
0527	OBH 62		1032		35,15 N		09,99 W
0535	OBH 63		1005		35,15 N		09,85 W
0544	OBH 64		0979		35,15 N		09,70 W
0600	OBH 65	250 m	0898		35,15 N		09,10 W
0631	OBH 66		0907		35,14 N		07,25 W
0641	OBH 67		0910		35,15 N		07,10 W
0653	OBS 68		0925		35,15 N		06,94 W
0713	OBH 69		1007		35,15 N		06,35 W
0722	OBH 70		1020		35,14 N		06,20 W

Seismik-Profile 171 bis XXX

0932		44 35,04 N	125 16,43 W	
0936	Sparker z.W.			
0944	MS Streamer z.W.			
0948	Bb Streamer z.W.			
1000	Beginn Profil 171	44 35,14 N	125 14,32 W	
1245	Ende Profil 171	44 35,14 N	125 02,91 W	
1248	Sparker a.D.			
1406	Bb airgun array z.W.			
1423	Beginn Profil 172	44 35,14 N	124 57,98 W	
1933	Ende Profil 172	44 35,14 N	125 18,93 W	15,0 sml
1942	Bb airgun-array a.D.			
1954	Stb GI-gun z.W.			
1958	Beginn Profil 173	44 35,14 N	125 18,93 W	
09.10.00				
0106	Profilwechsel 173 / 174	44 35,14 N	124 57,98 W	15,0 sml
0322	Profilwechsel 174 / 175	44 42,35 N	125 05,98 W	06,0 sml
0514	Ende Profil 175	44 37,77 N	125 06,05 W	05,3 sml
0536	Beginn Profil 176	44 37,77 N	125 07,25 W	
0734	Ende Profil 176	44 32,47 N	125 07,25 W	05,3 sml
0813	Beginn Profil 177	44 32,48 N	125 09,22 W	
0958	Ende Profil 177	44 37,78 N	125 09,25 W	05,3 sml
1012	Beginn Profil 178	44 37,78 N	125 09,83 W	
1200	Ende Profil 178	44 32,47 N	125 09,85 W	05,3 sml
1223	Beginn Profil 179	44 32,49 N	125 10,87 W	
1426	Profilwechsel 179 / 180	44 37,77 N	125 10,87 W	06,0 sml
1631	Ende Profil 180	44 35,27 N	125 18,95 W	07,0 sml

1634	Stb GI-gun a.D.			
1653	Bb Boltgun z.W.			
1657	Beginn Profil 181	44 35,14 N	125 19,47 W	
2212	Ende Profil 181	44 35,14 N	124 57,98 W	15,0 sml
2223	Bb Boltgun a.D.			
2232	Bb und MS Streamer a.D.			

Aufnahme OBS/OBH 60 - 70

2330	OBH 60 ausgelöst	2342 gesichtet	2352 a.D.	44	35,17 N	125	10,85 W
2352	OBS 61						
10.10.00							
		0011	0021		35,19 N		10,07 W
0021	OBS 62	0039	0047		35,16 N		10,00 W
0047	OBS 63	0103	0111		35,15 N		09,87 W
0111	OBH 64	0122	0129		35,17 N		09,77 W
0139	OBH 65	0146	0152		35,11 N		09,08 W
0208	OBH 66	0217	0223		35,15 N		07,25 W
0223	OBH 67	0234	0241		35,17 N		07,11 W
0242	OBH 68	0251	0258		35,19 N		06,98 W
0304	OBH 69	0314	0320		35,19 N		06,36 W
0322	OBH 70	0333	0347		35,13 N		06,20 W

Seismik-Profile 191 - 193

0428		44 30,01 N	125 03,01 W	
0431	DTS z.W.			
0436	Stb GI-gun z.W.			
0441	Bb Streamer z.W.			
0449	DTS KL = 430 m			
0535	Beginn Profil 191	44 30,00 N	125 07,43 W	
0639	Ende Profil 191	44 30,00 N	125 10,00 W	03,0 sml
0704	Beginn Profil 192	44 30,00 N	125 10,00 W	
0716	DTS KL = 900 m			
0803	Ende Profil 192	44 30,00 N	125 06,00 W	03,0 sml
0842	DTS KL = 1300 m			
0843	Beginn Profil 193	44 30,00 N	125 06,00 W	
0950	Ende Profil 193	44 30,00 N	125 10,02 W	03,0 sml
0953	hieven DTS			
0958	Stb GI-gun a.D.			
1000	Bb Streamer a.D.			
1036	DTS a.D.			

Aufnahme Lander von SO 148

1123	Lander ausgelöst			
1135	Lander aufgetaucht			
1143	Lander a.D.	44 39,94 N	125 06,10 W	

Hydrosweep und Parasound Vermessung v = 8 kn

1310	Beginn Profil 09	Kurs = 090 Grad	44 26,80 N	125 07,00 W	
1503	Ende Profil 09		44 26,80 N	124 45,00 W	15,8 sml
1509	Beginn Profil 10	Kurs = 270	44 26,04 N	124 45,20 W	
1702	Ende Profil 10		44 26,00 N	125 07,00 W	15,8 sml
1724	Beginn Profil 11	090	44 25,60 N	125 07,00 W	
1918	Ende Profil 11		44 25,60 N	124 45,00 W	15,8 sml
1923	Beginn Profil 12	270	44 24,80 N	124 45,00 W	
2124	Ende Profil 12		44 24,80 N	125 07,00 W	15,8 sml
2130	Beginn Profil 13	090	44 24,40 N	125 07,00 W	

2327	Ende Profil 13		44 24,40 N 124 45,00 W	15,8 sml
2332	Beginn Profil 14	270	44 23,60 N 124 45,00 W	
11.10.00				
0135	Ende Profil 14		44 23,60 N 125 07,00 W	15,8 sml
0141	Beginn Profil 15	090	44 23,20 N 125 07,00 W	
0341	Ende Profil 15		44 23,20 N 124 45,00 W	15,8 sml
0349	Beginn Profil 16	270	44 22,40 N 124 45,00 W	
0545	Ende Profil 16		44 22,40 N 125 07,00 W	15,8 sml
0550	Beginn Profil 17	090	44 22,00 N 125 07,00 W	
0747	Ende Profil 17		44 22,00 N 124 45,00 W	15,8 sml
0754	Beginn Profil 18	270	44 21,60 N 124 45,00 W	
1104	Ende Profil 18		44 21,60 N 125 21,00 W	26,0 sml
1112	Beginn Profil 19	090	44 20,40 N 125 21,00 W	
1443	Ende Profil 19		44 20,40 N 124 45,00 W	26,0 sml
1442	Beginn Profil 20	270	44 19,20 N 124 45,00 W	
1750	Ende Profil 20		44 19,20 N 125 21,00 W	26,0 sml
1800	Beginn Profil 21	090	44 18,00 N 125 21,00 W	
2111	Ende Profil 21		44 18,00 N 124 45,00 W	26,0 sml
2117	Beginn Profil 22	270	44 18,40 N 124 45,00 W	
2315	Ende Profil 22		44 18,40 N 125 07,00 W	15,8 sml
2321	Beginn Profil 23	090	44 18,80 N 125 07,00 W	
12.10.00				
0115	Ende Profil 23		44 18,80 N 124 45,00 W	15,8 sml
0125	Beginn Profil 24		44 19,60 N 124 45,00 W	
0319	Ende Profil 24		44 19,60 N 125 07,60 W	15,8 sml

Ende der Stationsarbeiten

Stationsprotokoll F.S. "S O N N E" Reise SO 150/2

Eingesetzte Geräte		**Einsätze / Seemeilen**
CTD	CTD-Sonde	01
MG	Magnetometer	417 sml
HS	Hydrosweep	

Eingesetzte Winden :

Winde	*D/M .*	*Typ*	*RF-Nr*	*SO 150/2 Einsatz*	*Gesamt Einsatz*	*SO 150/2 S`länge*	*Gesamt S`länge*	*Zust.*
W 1	18,2	LWL	816233	0000 h	1249 h	10516 m	359359 m	4
W 2	18,2	LWL	810001	0000	0155	13000	043097	2
W 4	11,0	NSW	817141	0000	0222	00000	139383	3
W 5	11,0	NSW	817164	0003	0082	04000	078234	3
W 6	18,2	DRAKO	814150	0000	0987	05684	772764	3

Winde	*SO 150/2 gefierte max.Länge*	*jemals gefierte max.Länge*
W 1	0000 m	6474 m
W 2	0000	3000
W 4	0000	6100
W 5	4000	5200
W 6	0000	7900

Geräteverluste : keine

Abkürzungen im Stationsprotokoll:

z.W.	zu Wasser
a.D.	an Deck
Boko	Bodenkontakt
Bosi	Bodensicht
SL(max.)	(maximale)Seillänge
LT	Lottiefe nach Hydrosweep
W x	eingesetzte Winde
HS	Hydrosweep
PS	Parasound
XPNDR	Transponder

Zeit : UTC - 05 Stunden

23.10.2000

Station 01 CTD/ROS W 5

1200	Beginn Station	LT = 5353 m	11 43,00 N	88 29,00 W
1201	CTD z.W.			
1320	Slmax = 4000 m			
1512	CTD a.D.		11 43,09 N	88 29,18 W
1513	Ende Station			

Magnetik-Hydrosweep-Profile M 01 bis v = 10,0 kn

1525	Beginn Profil 01	Kurs 114 Grad	11 42,83 N	88 28,62 W	
1709	Profilwechsel 1 / 2	118	11 36,00 N	88 13,00 W	16 sml
1812	Profilwechsel 2 / 3	127	11 31,00 N	88 04,00 W	10 sml
1926	Profilwechsel 3 / 4	126	11 23,50 N	87 54,00 W	12 sml
2219	Profilwechsel 4 / 5	134	11 06,50 N	87 30,00 W	29 sml
24.10.00					
0300	Profilwechsel 5 / 6	139	10 35,00 N	86 58,00 W	28 sml
1119	Profilwechsel 6 / 7	134	09 35,00 N	86 07,00 W	78 sml
1503	Profilwechsel 7 / 8	127	09 09,00 N	85 40,00 W	37 sml
2325	Profilwechsel 8 / 9	120	08		
25.10.00					
0256	Profilwechsel 9 / 10	120	08 00,00 N	84 02,50 W	35 sml
0844	Profilwechsel 10 / 11	105	07 30,00 N	83 12,0 0W	58 sml
1715	Ende Profil 11		07 07,79 N	81 50,22 W	85 sml

Gesamtmeilen : 417 sml

Ende der Stationsarbeiten